KIGAM, 2014

Geometry, kinematics and mechanics of foreland fold-thrust belts (2) : how the basement (and deeper lithospheric levels) may control the structural evolution

Professor Olivier LACOMBE

UPMC SORBONNE UNIVERSITÉS
cnrs
Institut des Sciences de la Terre de Paris ISTeP SORBONNE UNIVERSITÉS

Basement involvement in fold-and-thrust belts : what are the evidence?

The fold-and-thrust belt / foreland system

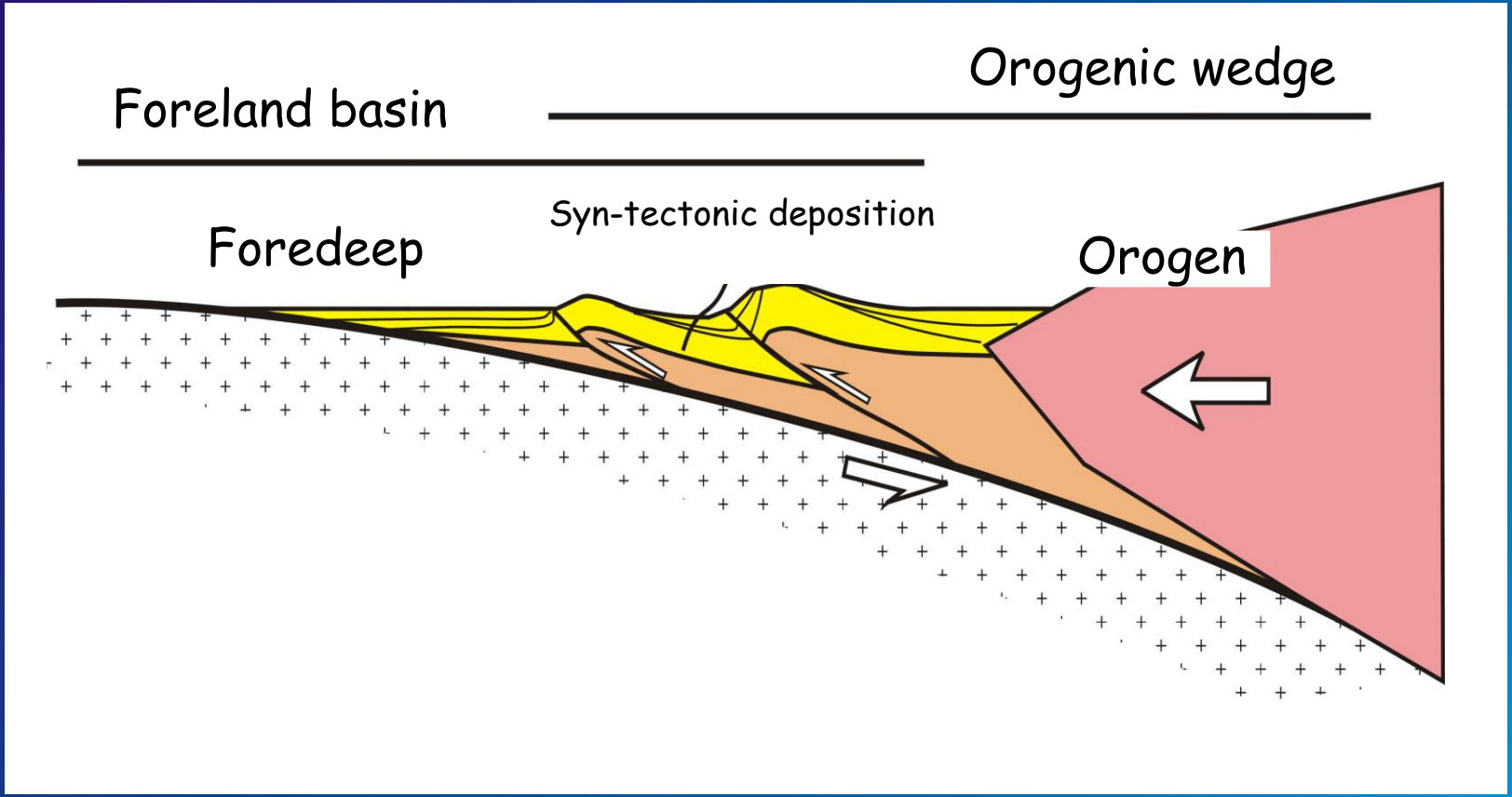

Internal thickening until critical angle α is reached

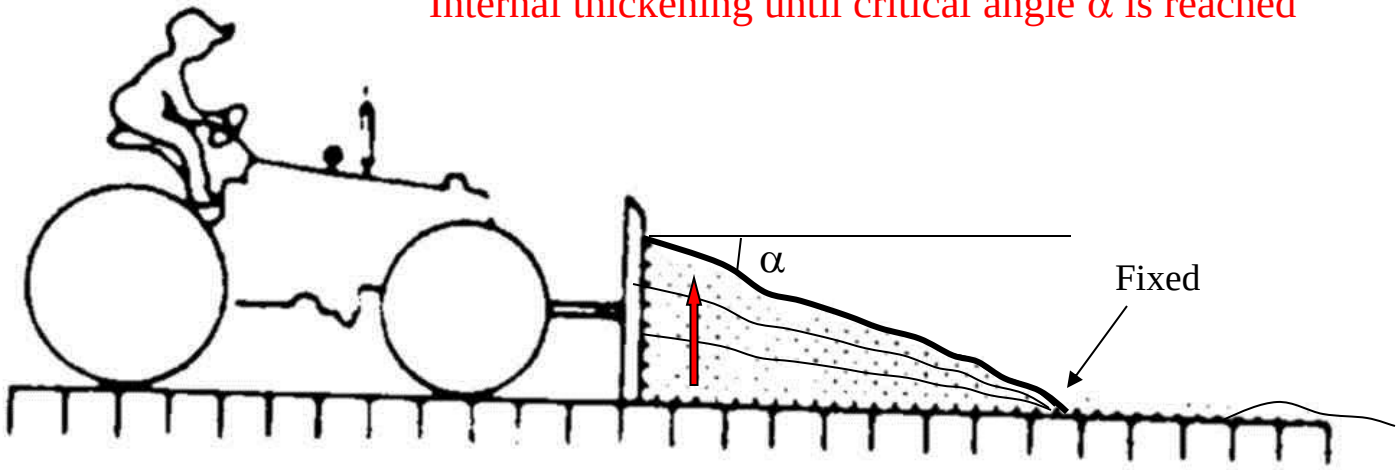

1. Basal sliding without internal thickening, then
2. New snow is incorporated in the wedge, α is lowered, then
3. The wedge will deform internally until α is reached again, and so on

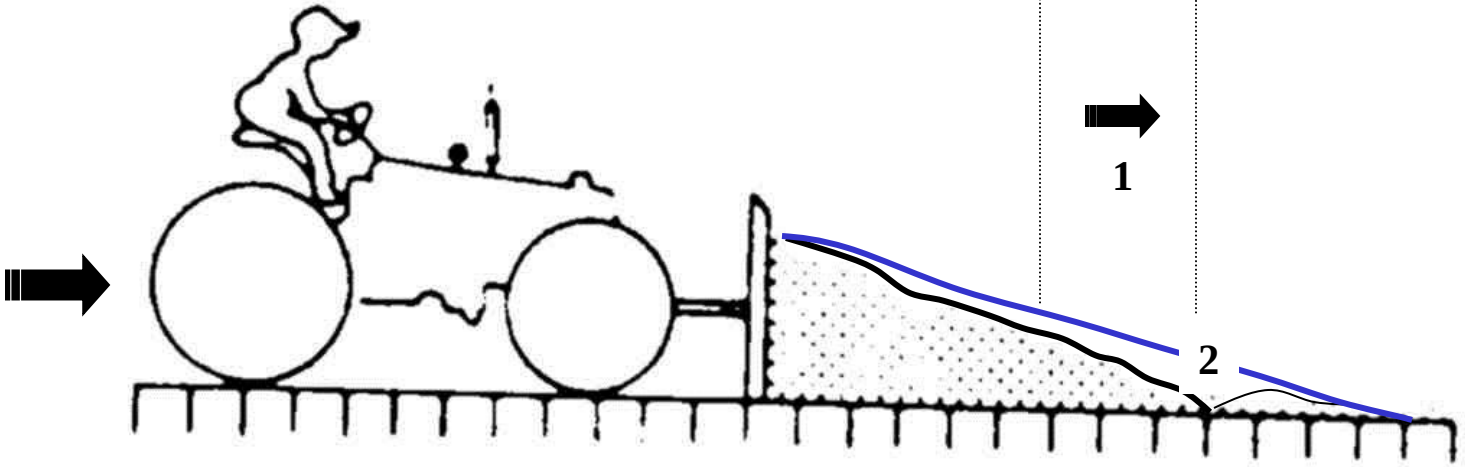

Davis et al. (1983)

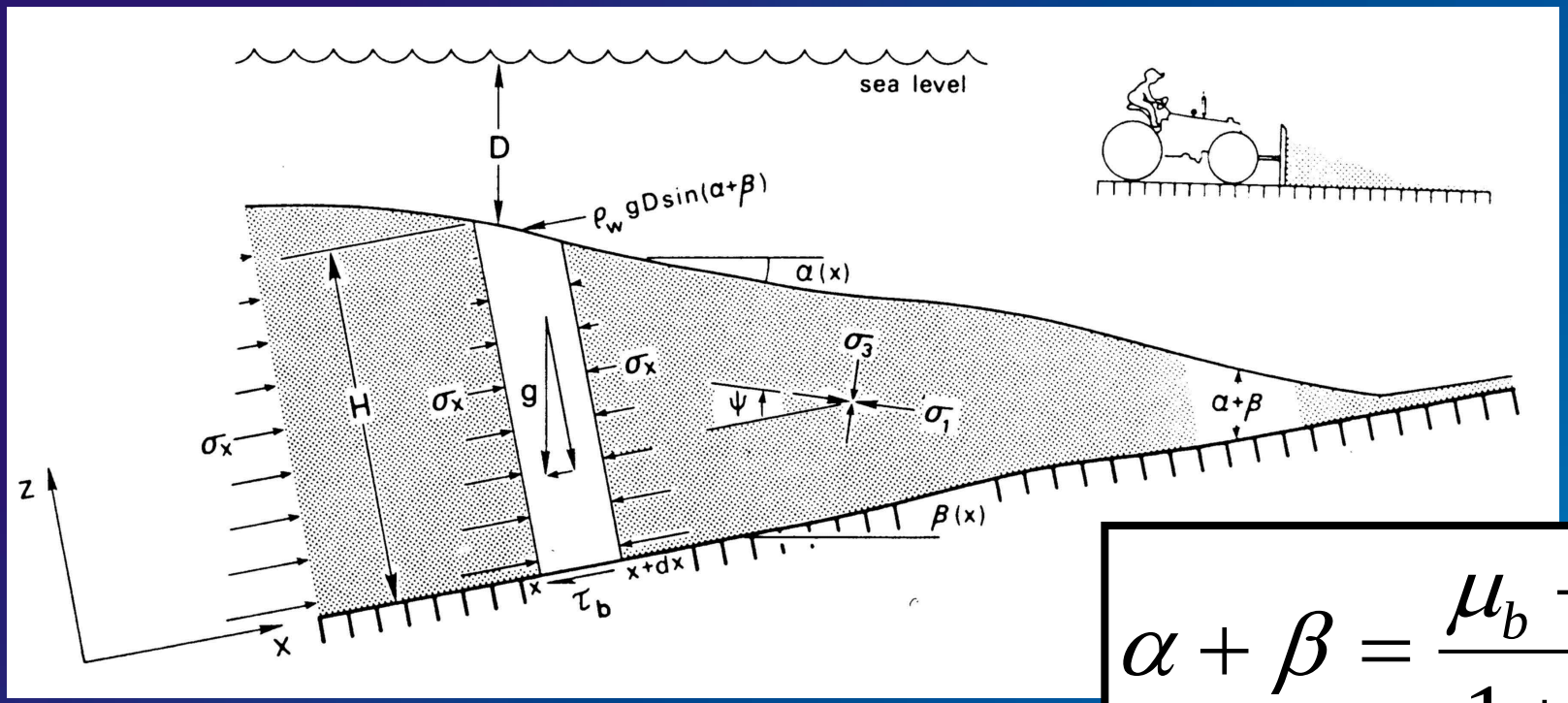

$$\alpha + \beta = \frac{\mu_b + \beta}{1 + K}$$

$$\rho g H \beta + \rho_w g D(\alpha + \beta) + \tau_b + \frac{d}{dx}\int_0^H \sigma_x dz = 0$$

Weight of sedimentary column (lithostatic pressure)

Weight of water column

Basal frictional shear strength)

Sum of lateral push forces

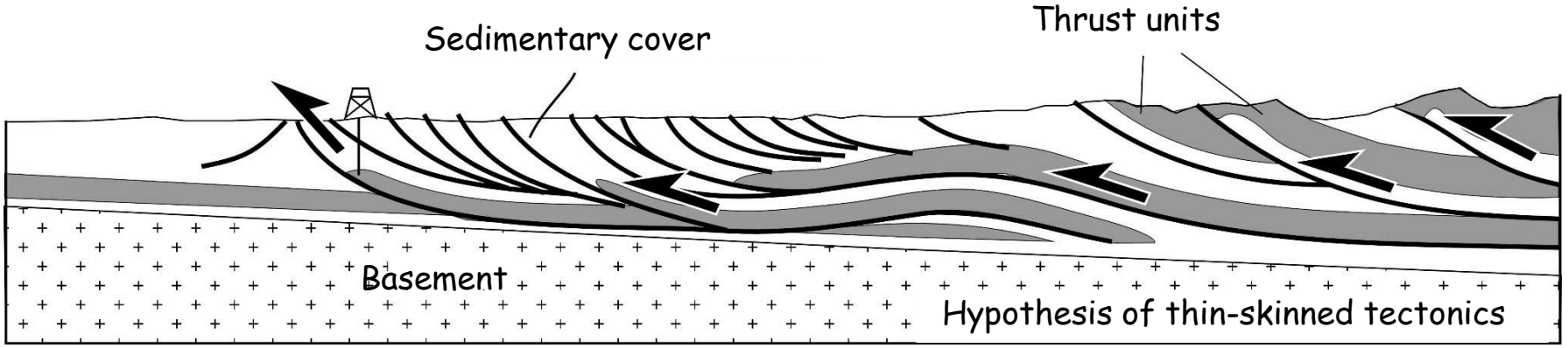

Shortening is accommodated in the upper part of the crust above a basal décollement dipping toward the hinterland

Implicit assumption of « thin-skinned » tectonic style

Topographic slope and dip of basal décollement define the orogenic wedge

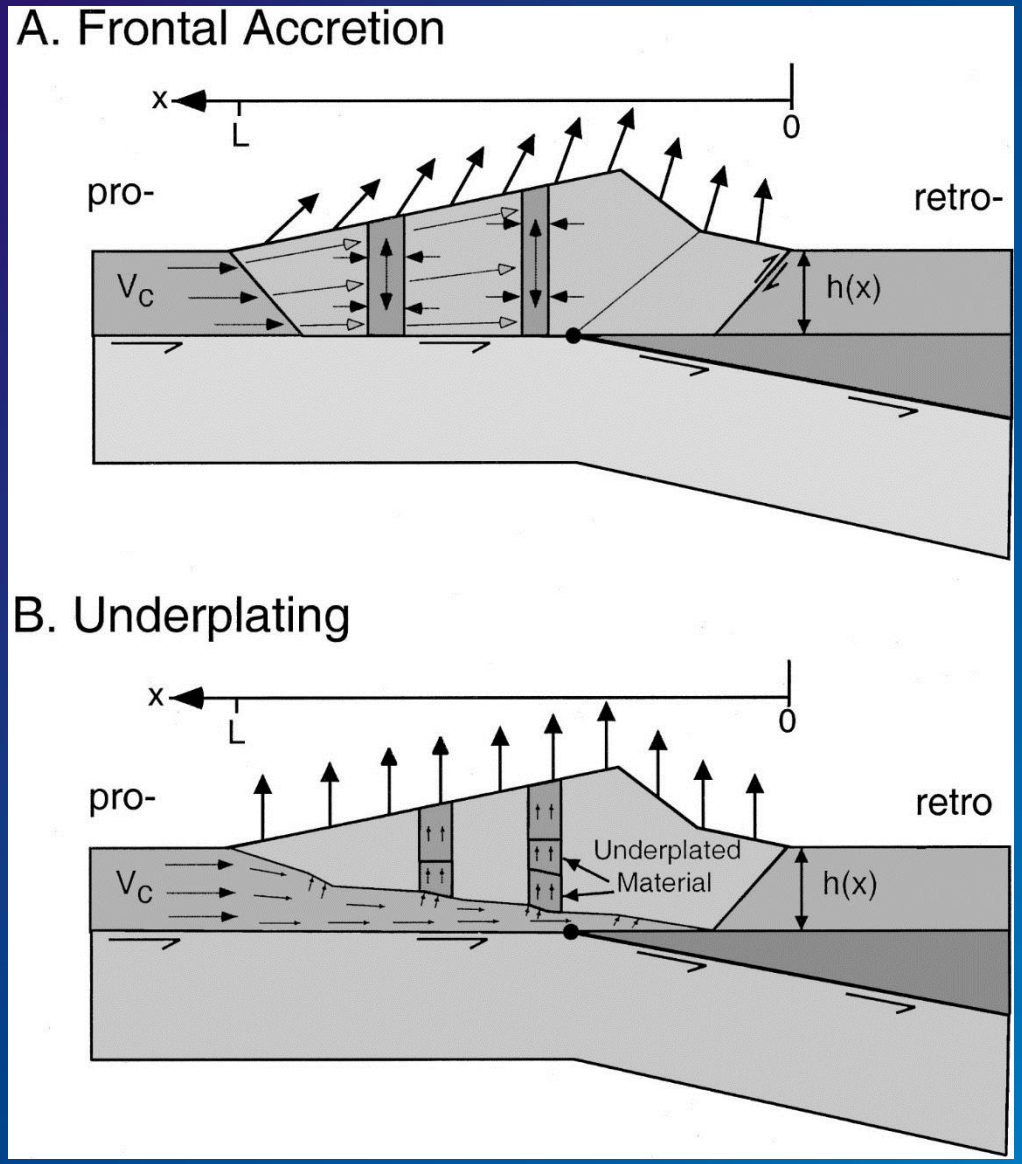

Willett et al., 2001

Davis et al. (1983) model however fundamentally meets several main restrictions.

A first one is related to the assumed homogeneous nature of the material of the wedge, so that widespread reactivation of preexisting faults in the cover is not generally considered.

A second one lies in the assumed rigid and undeformable behaviour of the substratum below the basal décollement, leading generally to implicitely favor thin-skin tectonics styles, so that basement-involved shortening is not accounted for.

Reactivation/inversion of basement faults widespreadly occurs during orogenic evolution of collided passive margins and this process is known to exert a strong control on the evolution of orogen

Number of regional studies have demonstrated the compressional reactivation of preexisting extensional structures within the cover and the basement of foreland thrust belts (e.g., Alps, Urals, Andes, Zagros, Rockies, Taiwan, …).

Signature of basement-involved shortening in foreland thrust belts ?

Basement fault reactivation may induce :

-localization of thrusts and folds in the developing shallow thrust wedge;
-inversion of extensional faults and development of crystalline thrust sheets;
- out-of-sequence thrusting and refolding of shallow nappes;
- development of accommodation structures such as lateral ramps;
- development of basement uplifts.

In foreland thrust belts of young but no longer active orogens (e.g., Pyrenees-Provence), these signatures can therefore be identified in some places by careful structural investigations of the relationships between cover and basement.

In more recent orogens (e.g., western Alps), active basement uplifts recognized by geodesy or gravimetric investigations may complement structural analyses in demonstrating deep basement thrusting.

In still active orogens (e.g., Taiwan, Zagros), seismicity combined with structural analyses provides first-order constraints on deep crustal deformation.

In all cases, the study of inversion of preexisting basement (normal) faults is generally much easier in forelands than in inner parts of orogens where the initial relationships between the basement and its sedimentary cover have generally not been preserved and the initial attitude of the faults has been strongly modified or erased by later evolution.

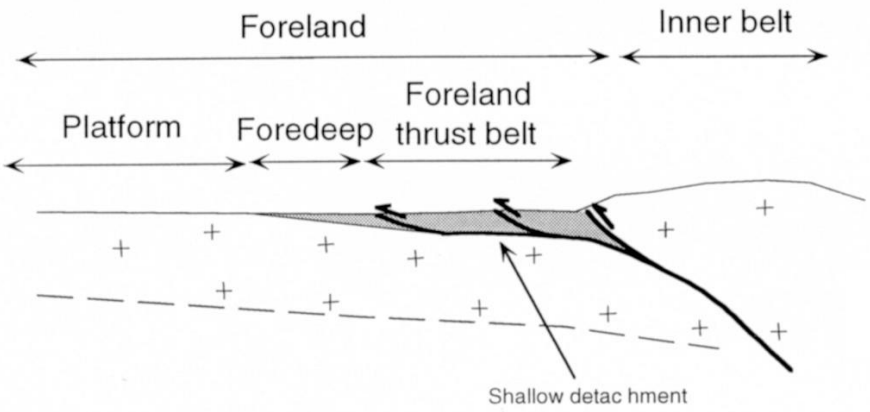

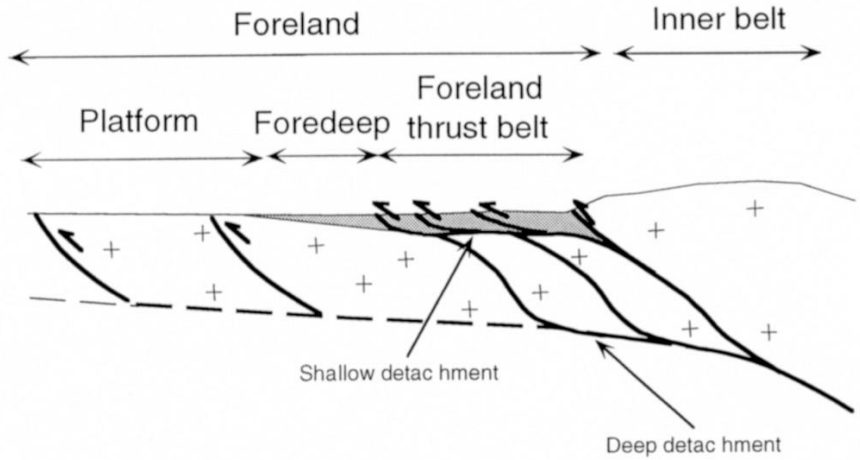

(Lacombe and Mouthereau, 2002)

simple-shear style "subduction"

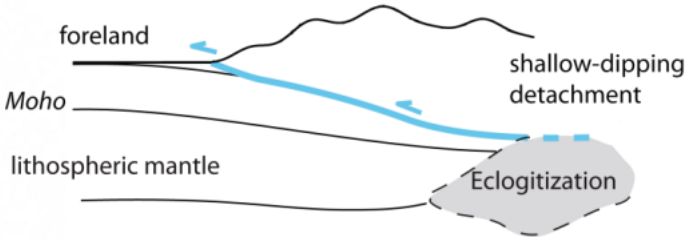

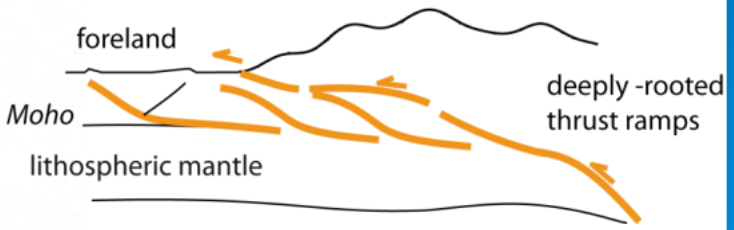

pure-shear style "inversion"

Mouthereau et al,, 2013)

Basement control on the late evolution of fold-and-thrust belts : the Jura case

CARTE GÉOLOGIQUE DE LA FRANCE

à l'échelle du millionième

6e édition

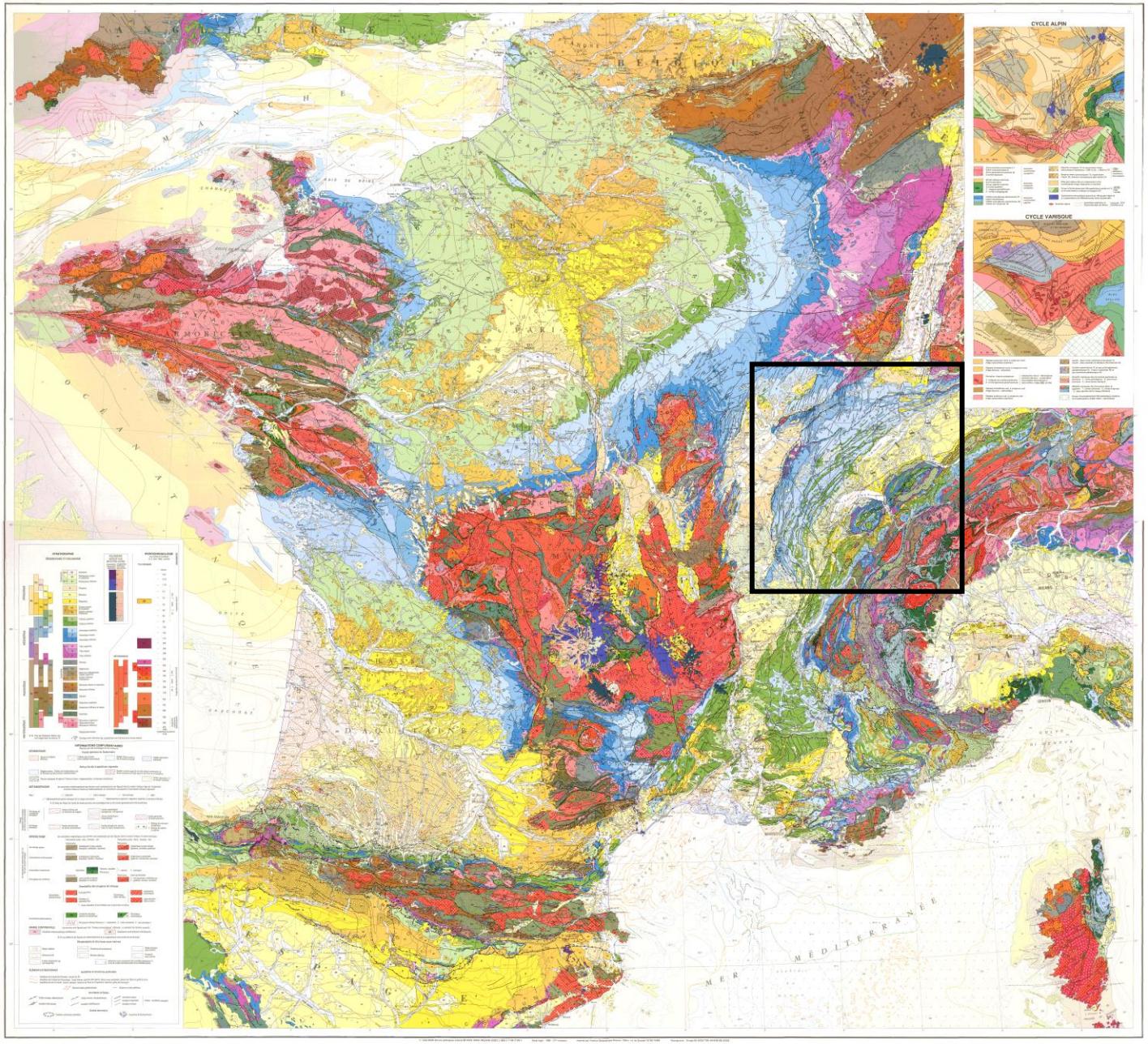

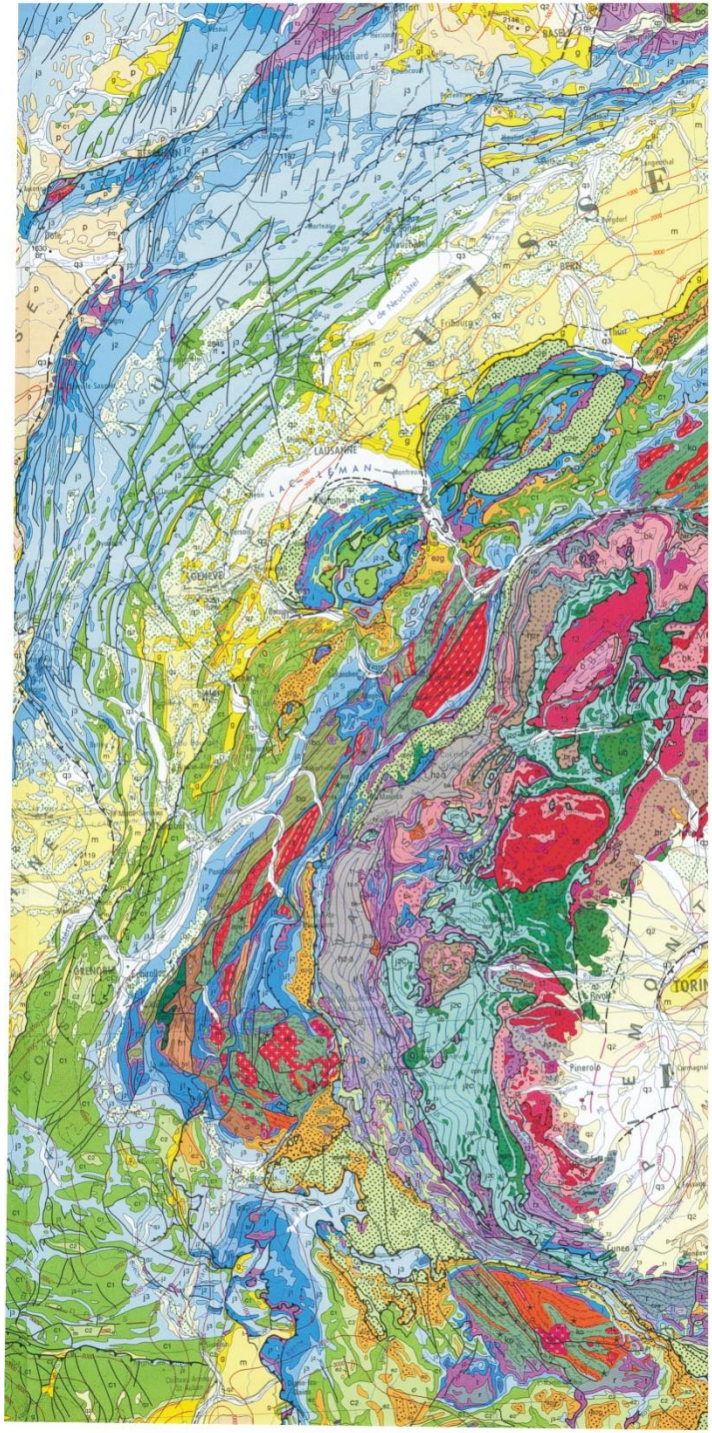
BASEL
BERN
LAUSANNE
GENEVE
LAC LEMAN
SUISSE
TORINO

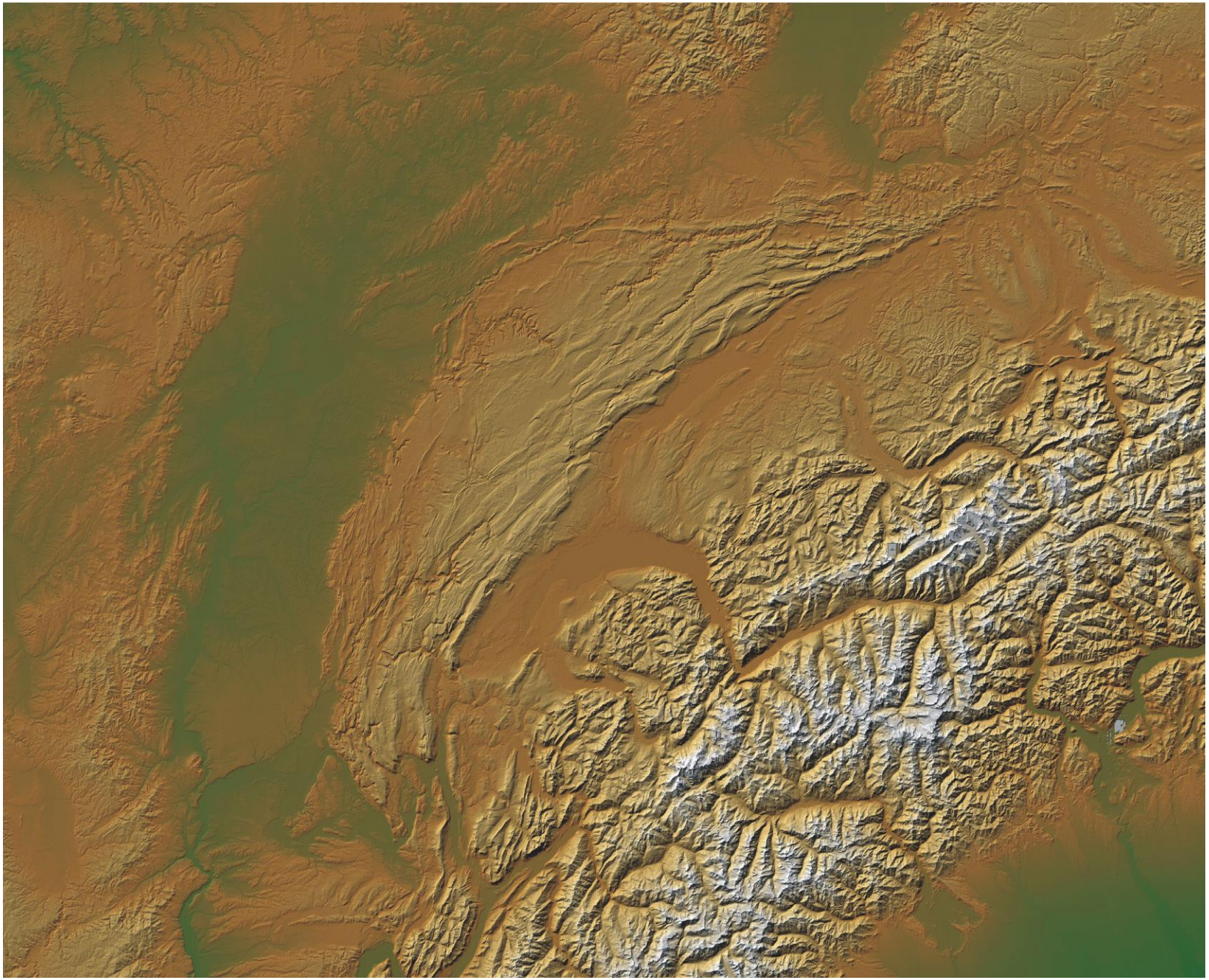

MULHOUSE
BASEL
Montbéliard
Vesoul
Porrentruy
Doubs
Loue
Auxonne
Dole
Biel
Burgdorf
BERN
L. de Neuchâtel
Fribourg
Thun
LAUSANNE
LAC LÉMAN
Montreux
Thonon-les-B.
Sion
GENÈVE
Louhans

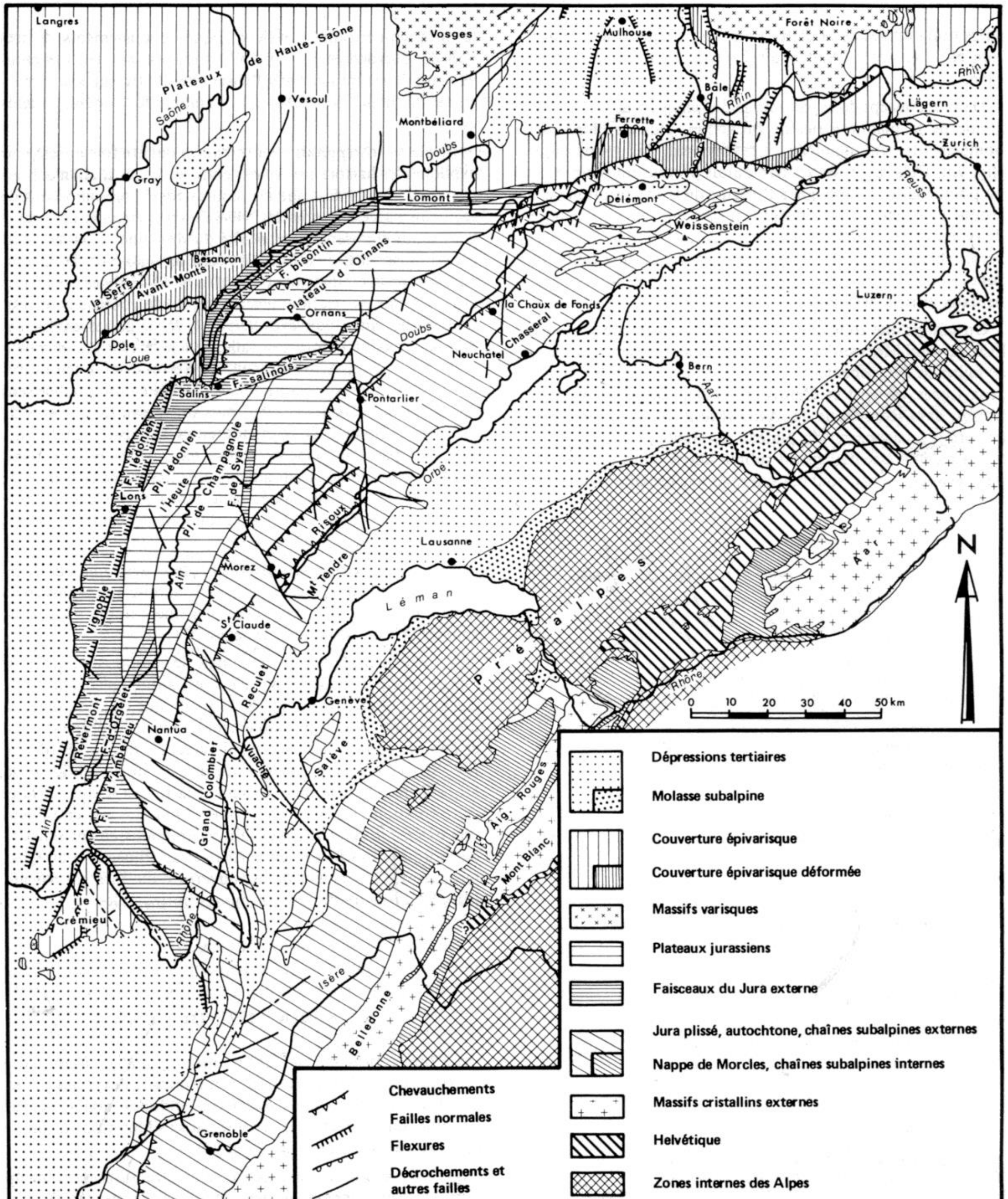

Langres
Plateaux de Haute-Saône
Vosges
Mulhouse
Forêt Noire
Vesoul
Saône
Bâle
Rhin
Montbéliard
Ferrette
Lägern
Zurich
Doubs
Gray
Lomont
Délémont
Weissenstein
Reuss
Besançon
la Serre
Avant-Monts
F. bisontin
Plateau d'Ornans
Ornans
la Chaux de Fonds
Chasseral
Luzern
Dole
Loue
Neuchatel
Bern
Aar
Salins
F. salinois
Pontarlier
F. lédonien
Pl. lédonien
Pl. de Champagnole
F. de Syam
l'Heute
Orbe
Lons
Risoux
Lausanne
Ain
Morez
Mt Tendre
Léman
Préalpes
Aar
St Claude
Vignoble
Recules
Genève
Rhône
Revermont
F. d'Orgelet
Nantua
Grand Colombier
Vuache
Salève
Aig. Rouges
F. d'Ambérieu
Mont Blanc
Ile Crémieu
Isère
Belledonne
Grenoble
0 10 20 30 40 50 km
N
Dépressions tertiaires
Molasse subalpine
Couverture épivarisque
Couverture épivarisque déformée
Massifs varisques
Plateaux jurassiens
Faisceaux du Jura externe
Jura plissé, autochtone, chaînes subalpines externes
Nappe de Morcles, chaînes subalpines internes
Massifs cristallins externes
Helvétique
Zones internes des Alpes
Chevauchements
Failles normales
Flexures
Décrochements et autres failles

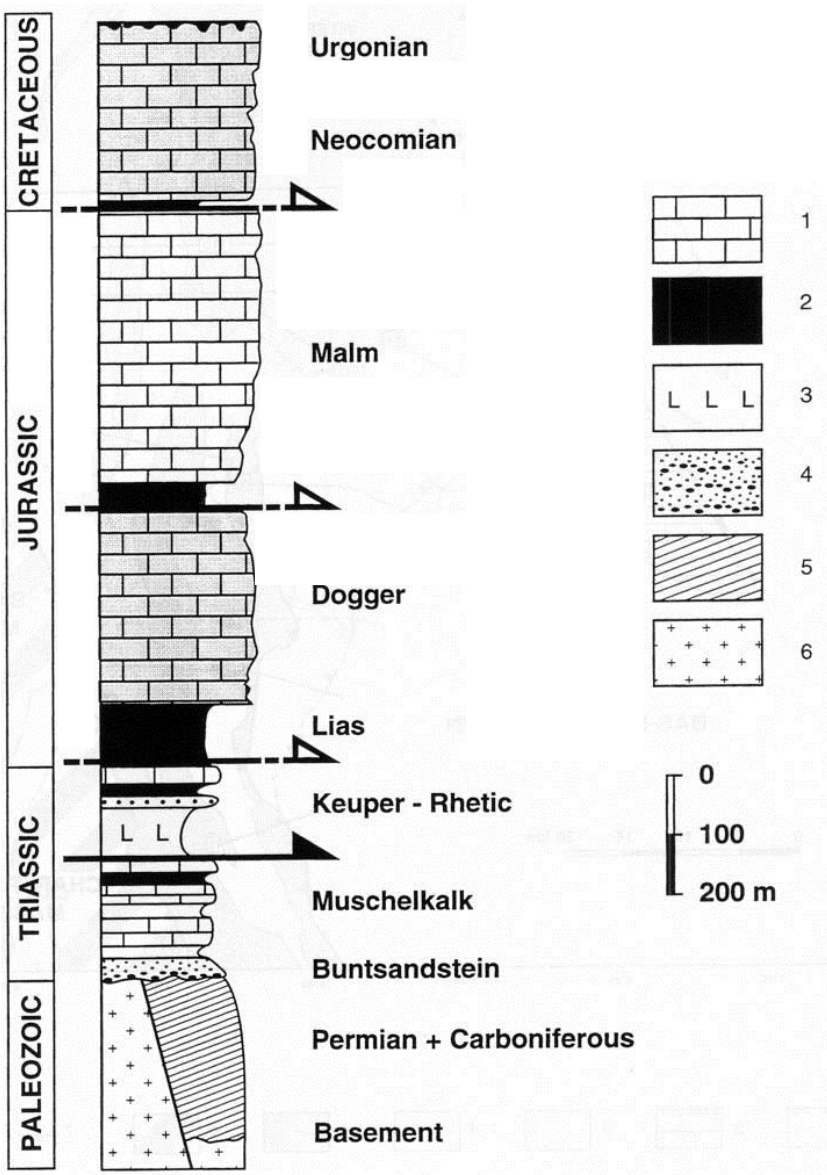
CRETACEOUS
JURASSIC
TRIASSIC
PALEOZOIC
Urgonian
Neocomian
Malm
Dogger
Lias
Keuper - Rhetic
Muschelkalk
Buntsandstein
Permian + Carboniferous
Basement
1
2
3
4
5
6
0
100
200 m

Distribution of Triassic evaporites below the Jura

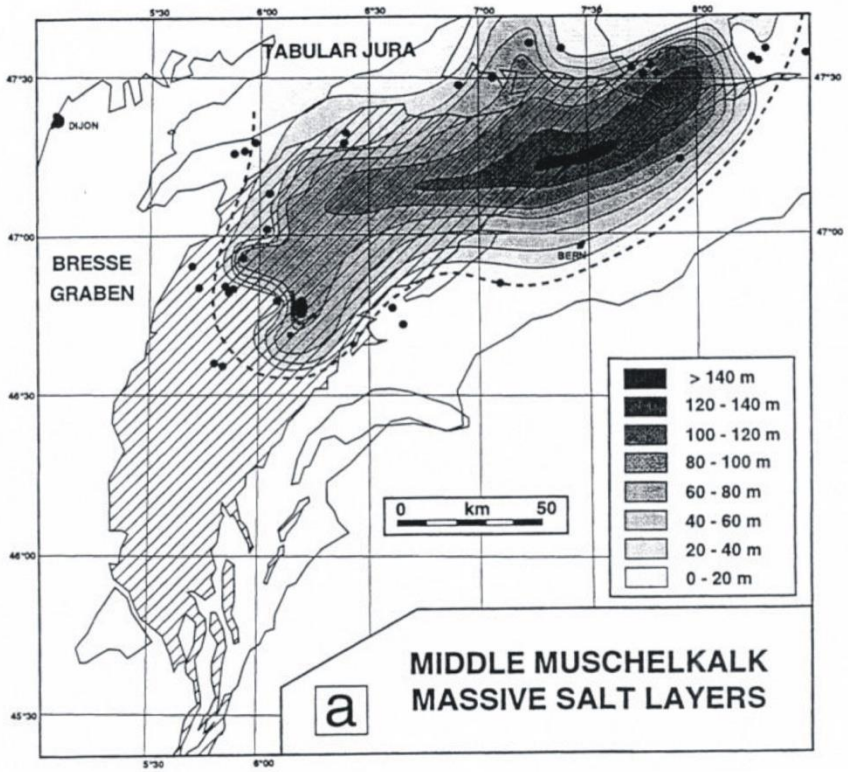

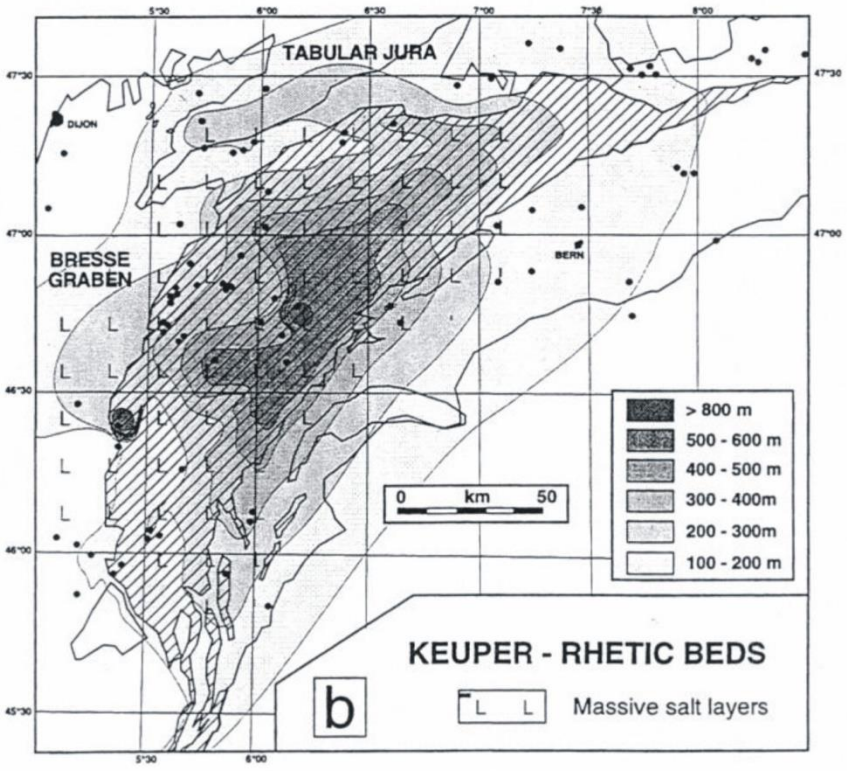

(Lienhard, 1984)

(Philippe, 1995)

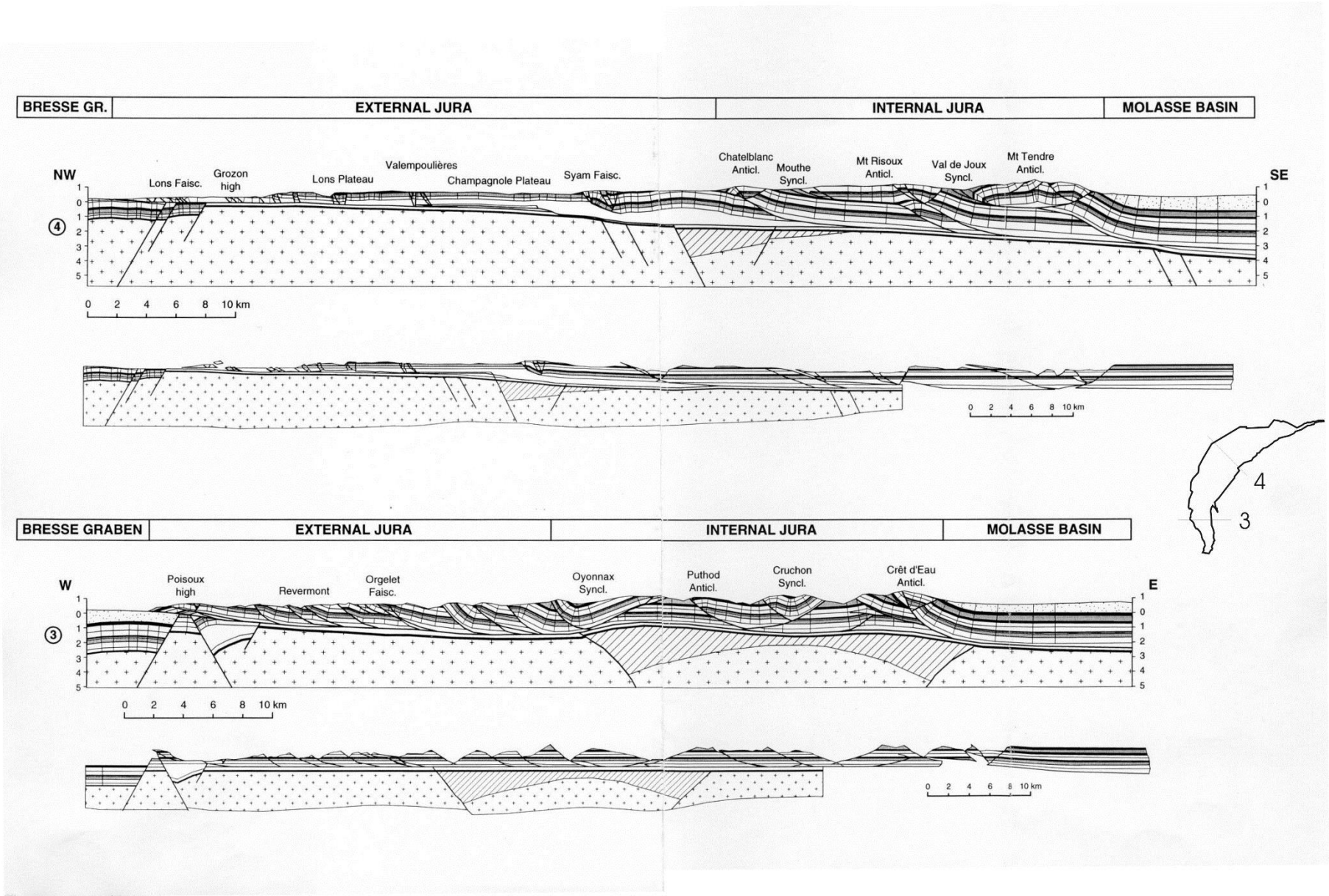

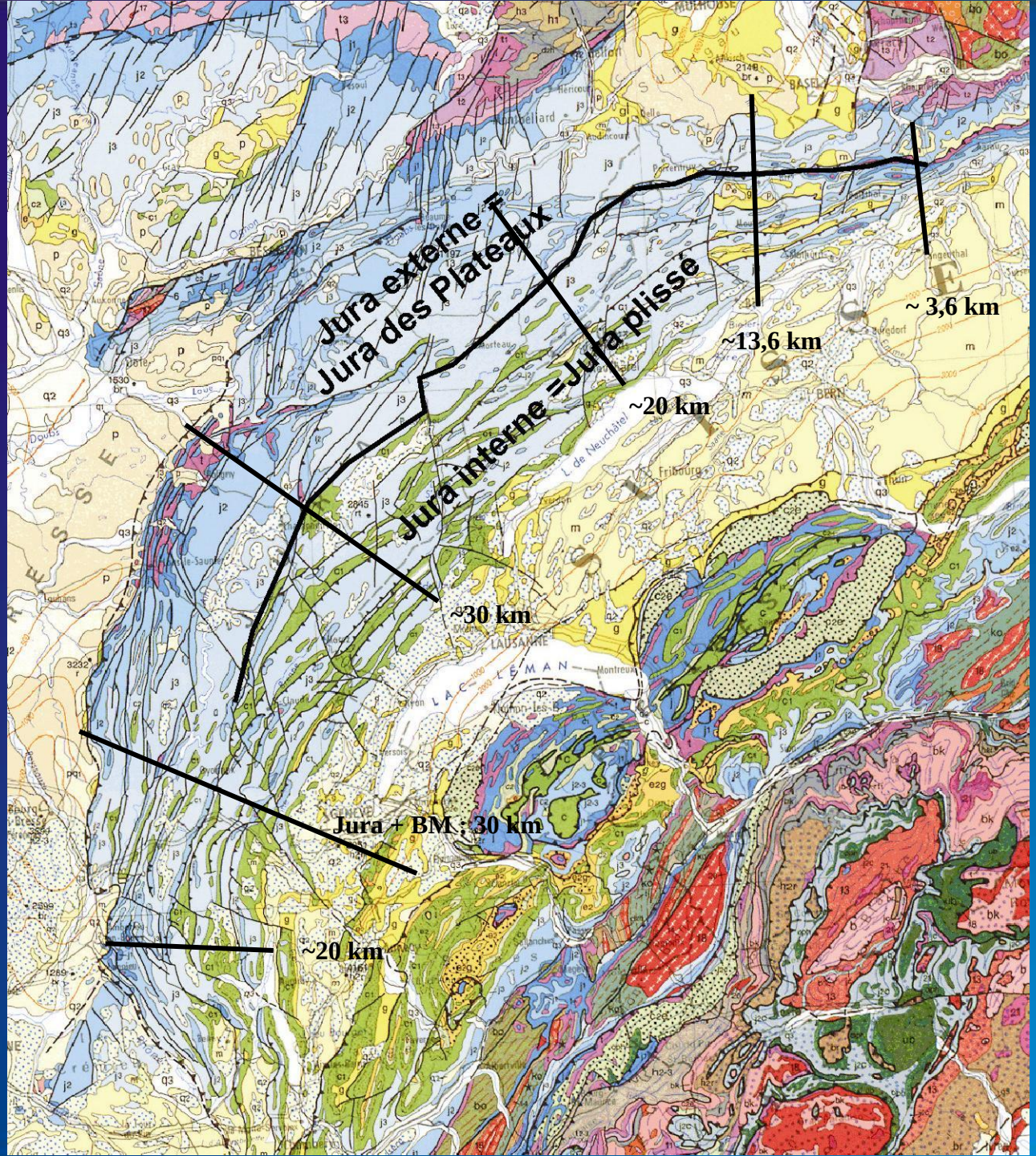
Jura externe =
Jura des Plateaux
Jura interne =Jura plisse
~ 3,6 km
~13,6 km
~20 km
~30 km
Jura + BM : 30 km
~20 km

Most authors consider the formation of the thin-skinned Jura fold-and-thrust belt as a rather short-lived event.

Near its northern rim a maximum age for the onset of thin-skinned deformation is inferred from the Bois de Raube formation, which reveals a biostratigraphic age between 13.8 and 10.5 Ma years and whose sedimentation predates thin-skinned Jura folding in that area.
A maximum age of 9 Ma can be inferred from the western front of the Jura where this fold-and-thrust belt thrusted the Bresse Graben.

Termination of thin-skinned Jura folding is less well constrained. Undeformed karst sediments have been detected in a fold limb located in the central part of the fold-and-thrust belt; their biostratigraphic age implies that folding terminated before some 4.2–3.2 Ma ago in this area. In the case that propagation of the fold-and-thrust belt toward the foreland was in sequence, thin-skinned deformation may have operated longer in the more external parts of the fold-and-thrust belt.

Evidence for ongoing deformation from the northern and northwestern front of the fold-and-thrust-belt is indeed provided by studies in tectonic geomorphology

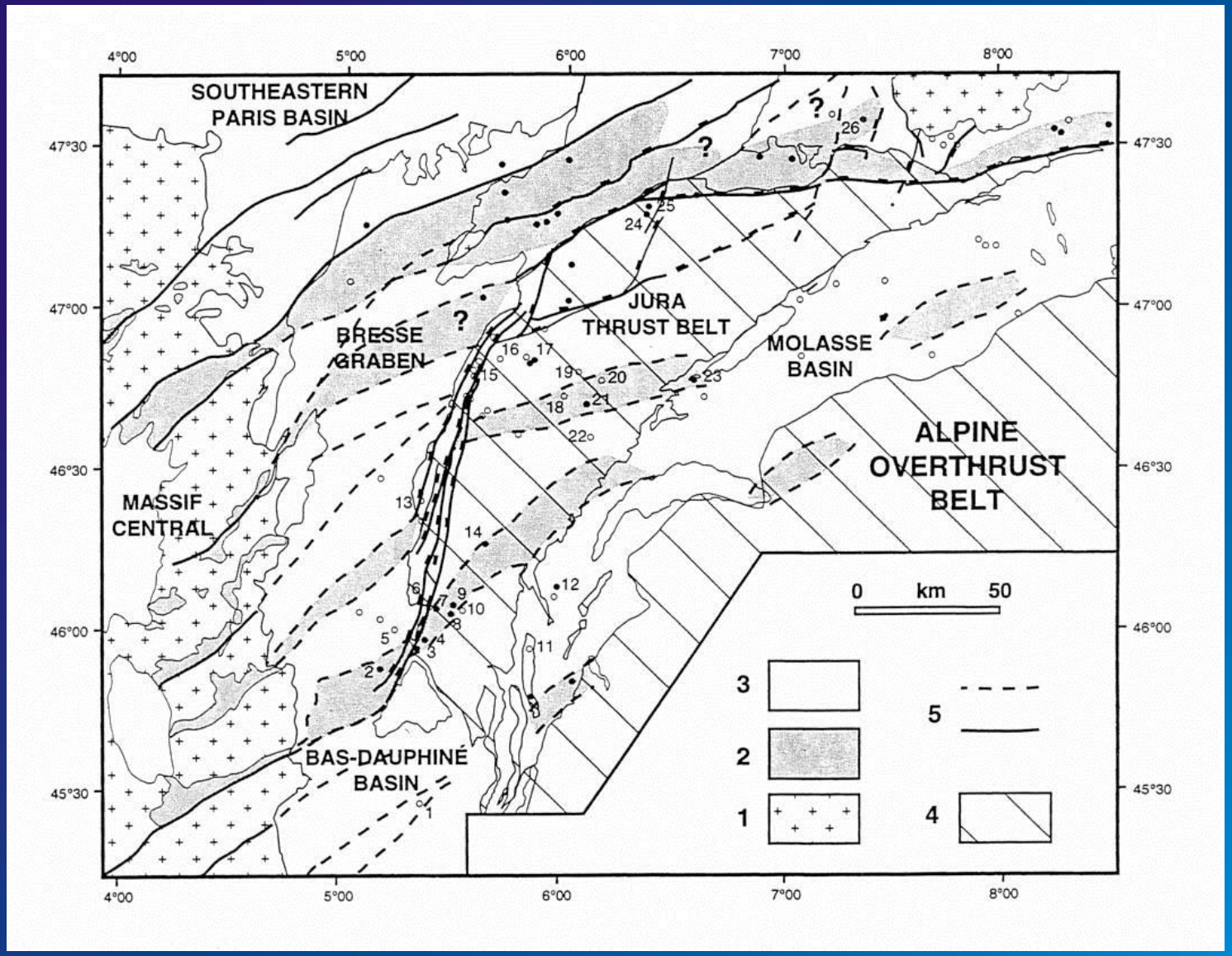

(BRGM, 1980; Truffert et al., 1990)

(Philippe, 1995)

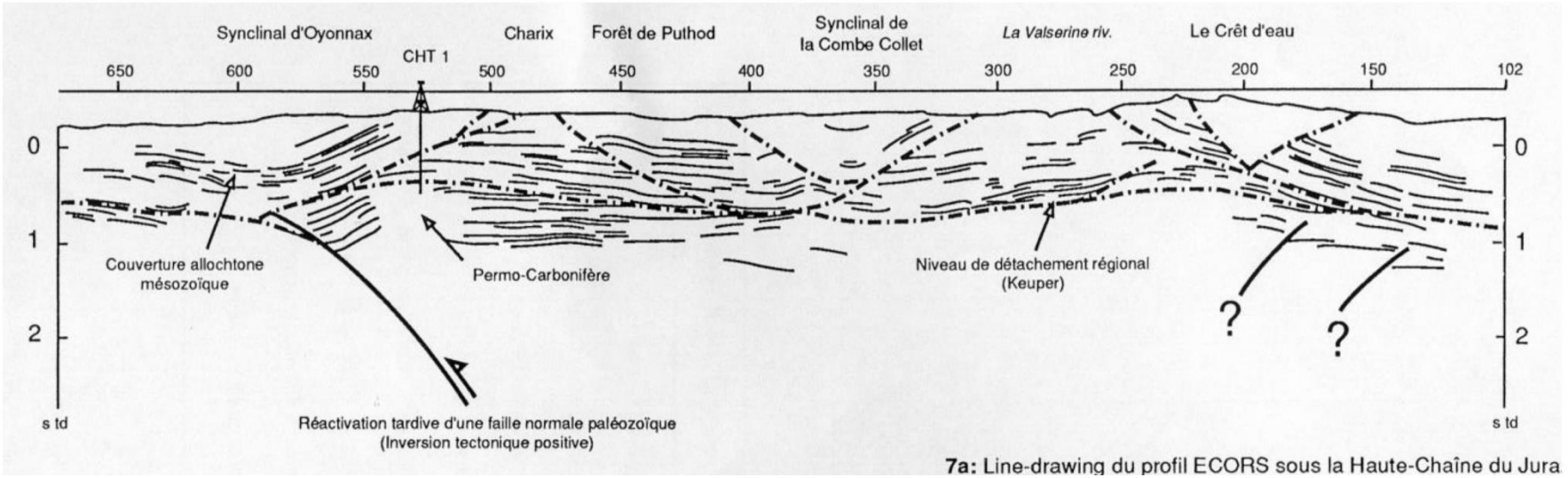

7a: Line-drawing du profil ECORS sous la Haute-Chaîne du Jura

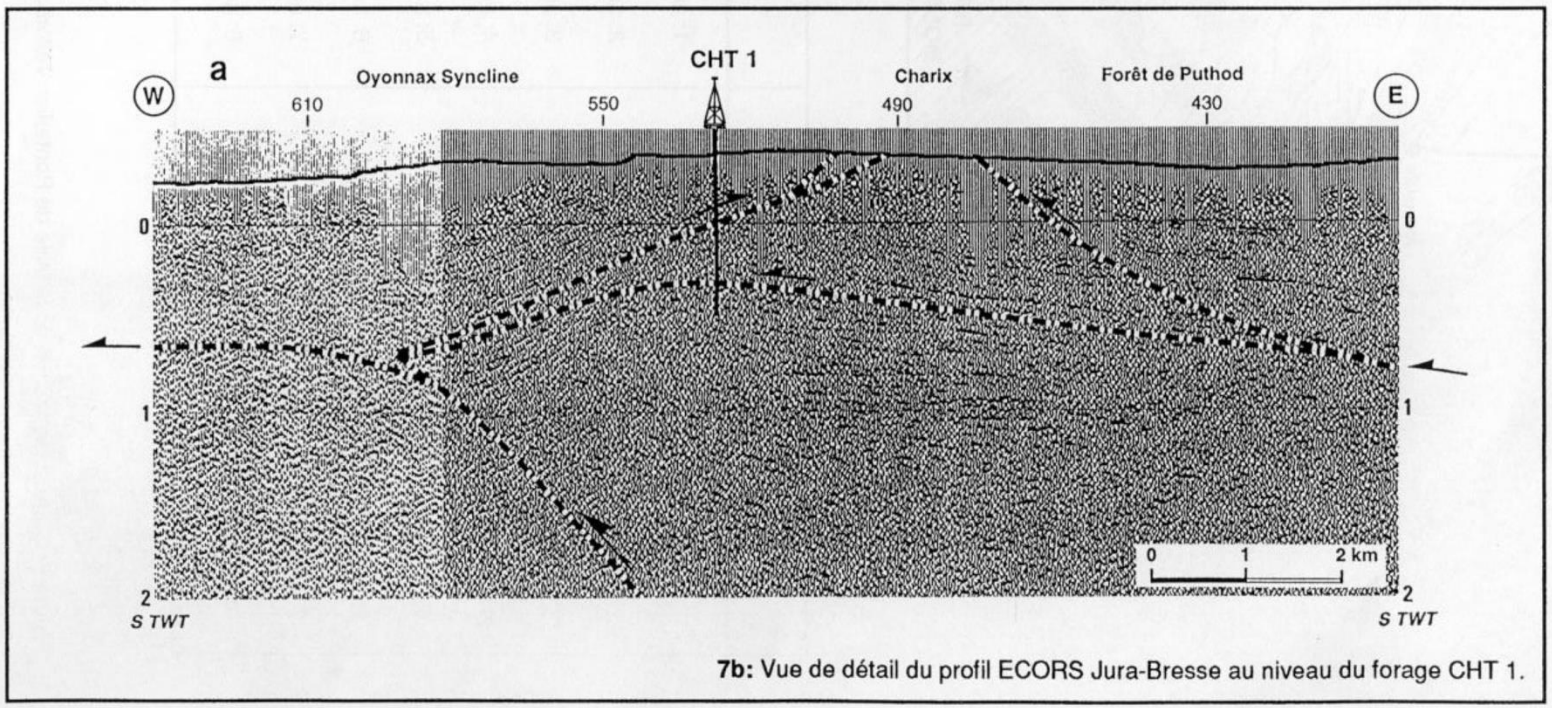

7b: Vue de détail du profil ECORS Jura-Bresse au niveau du forage CHT 1.

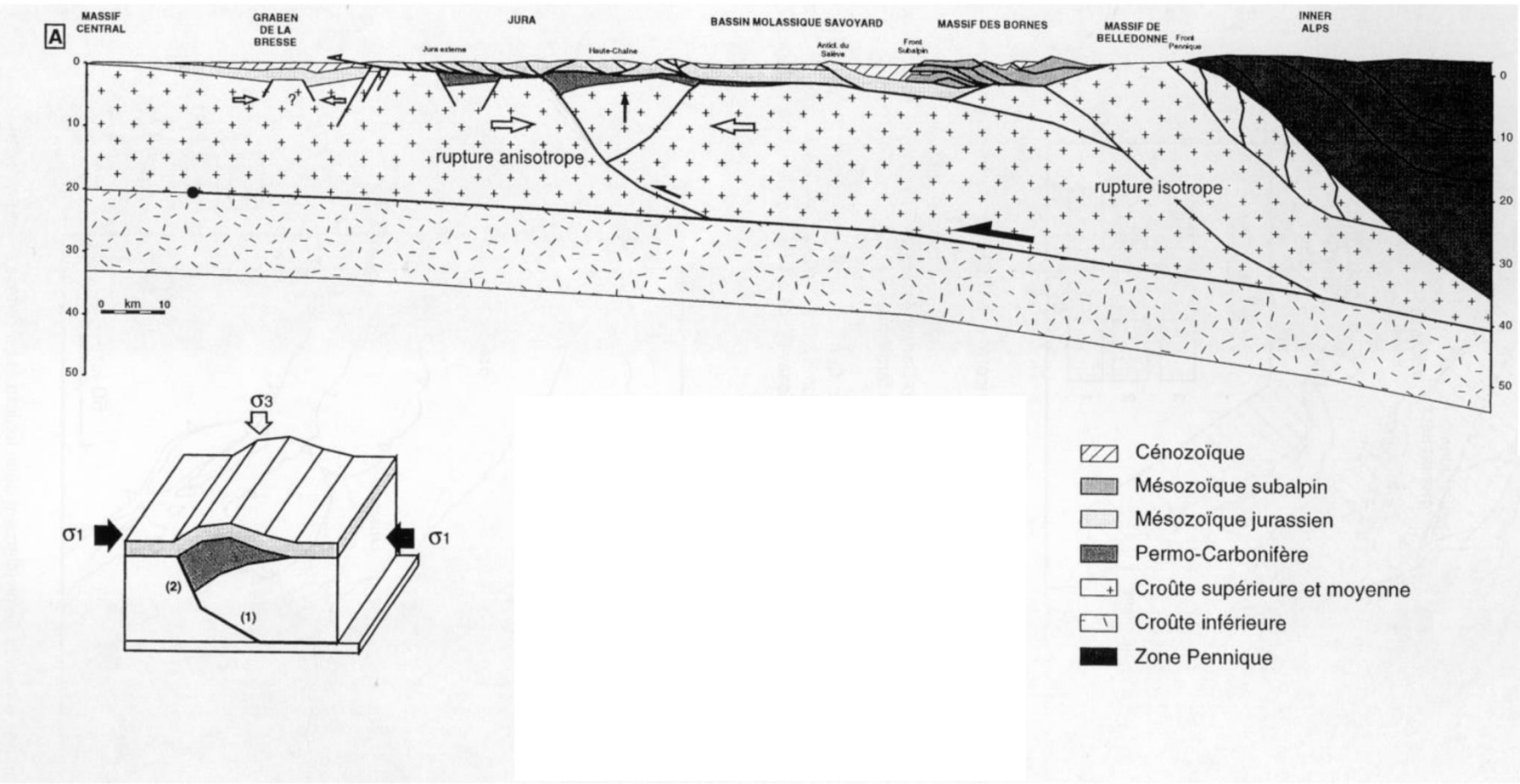

(Philippe, 1995)

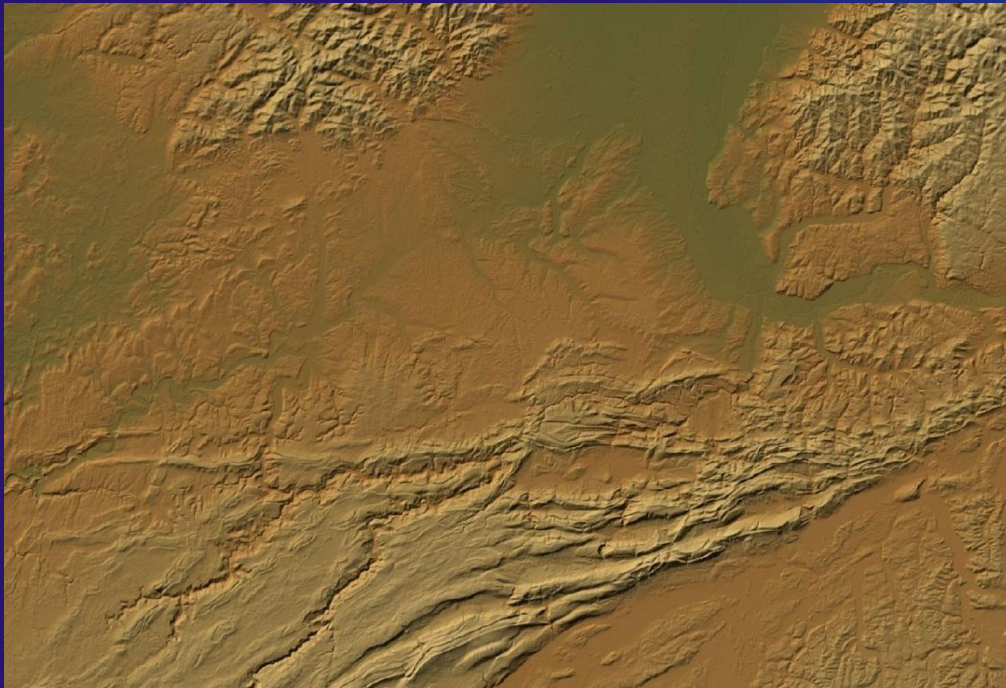

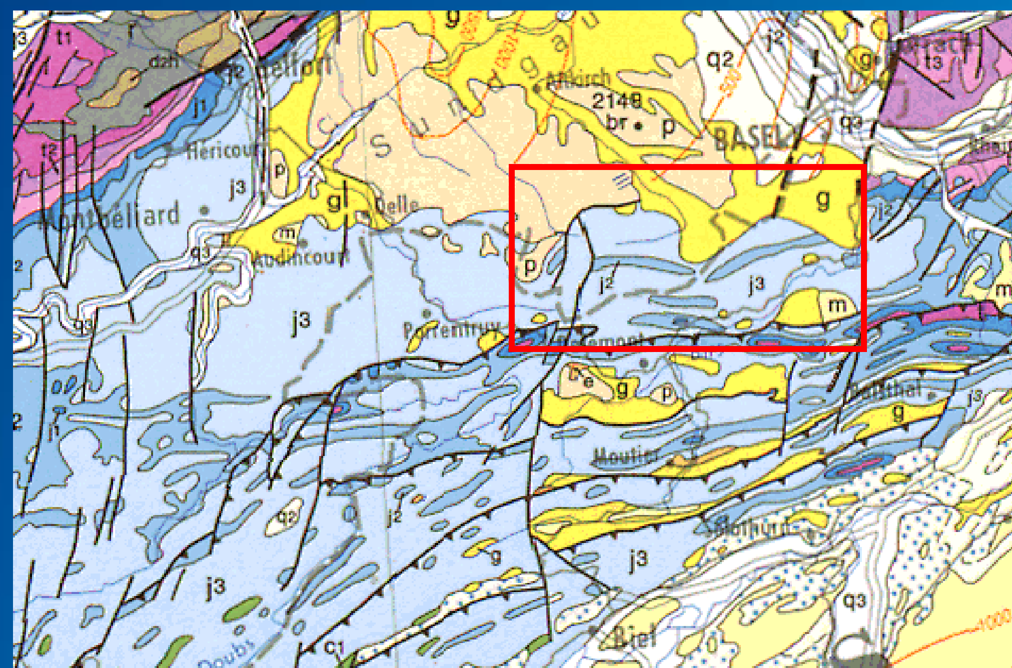

Hericourt
Montbéliard
Delle
Audincourt
Porrentruy
BASEL
Moutier
Biel
Doubs

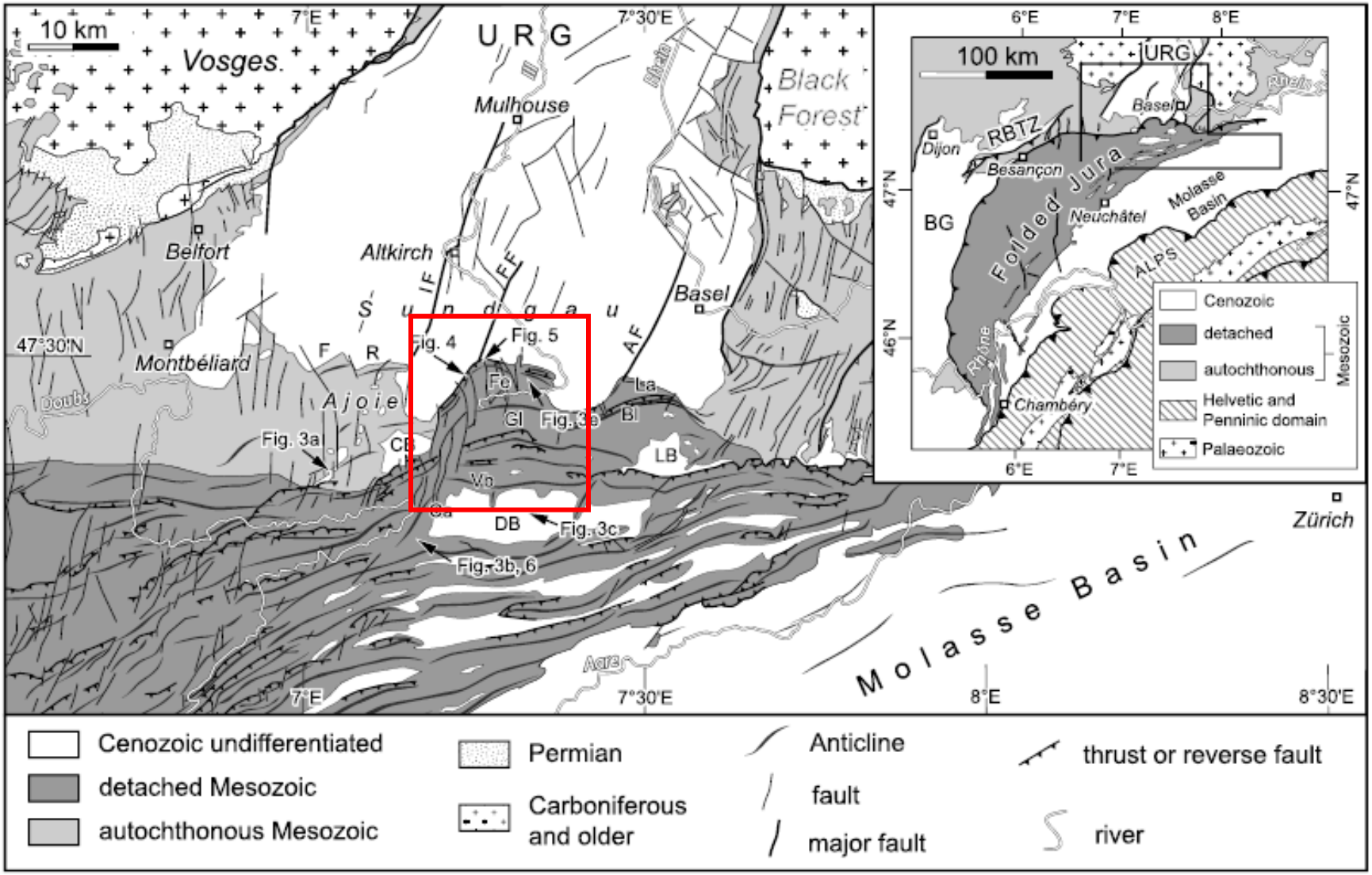

(Ustaszewski and Schmid, 2006)

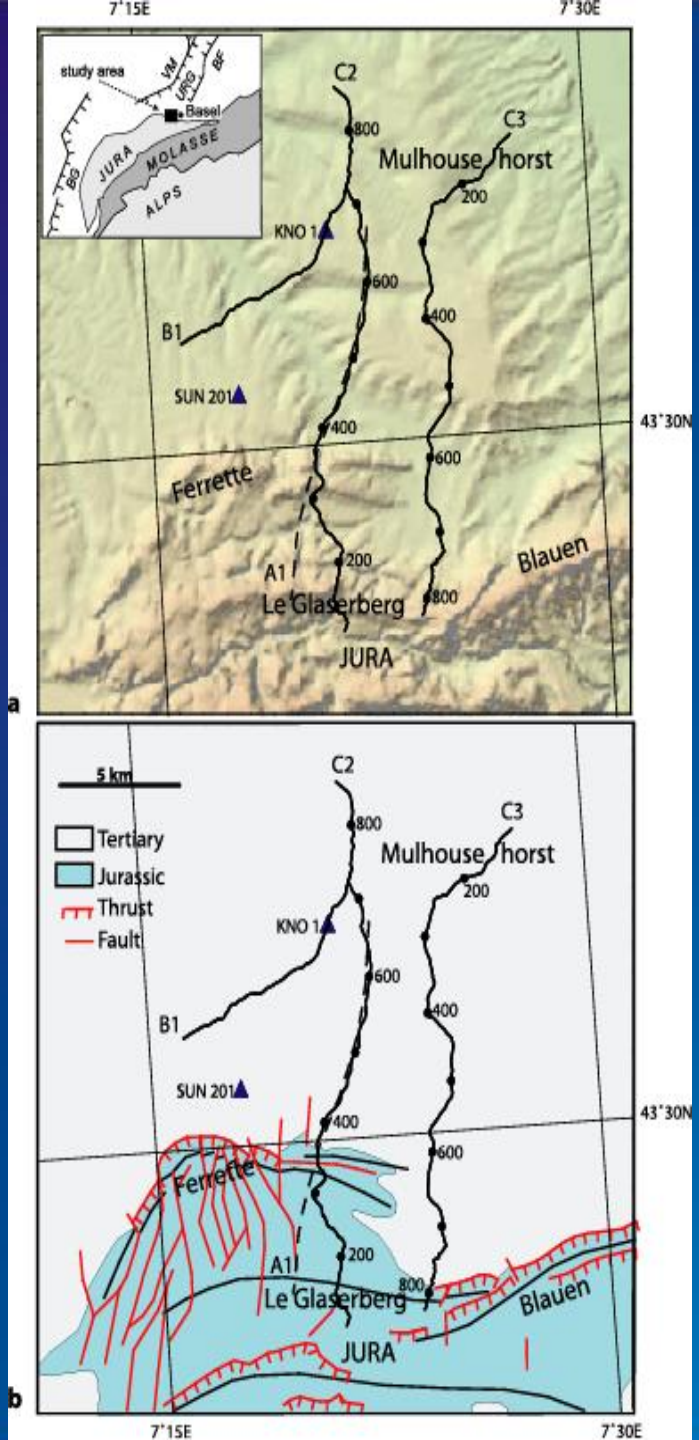

(Rotstein and Schaming, 2004)

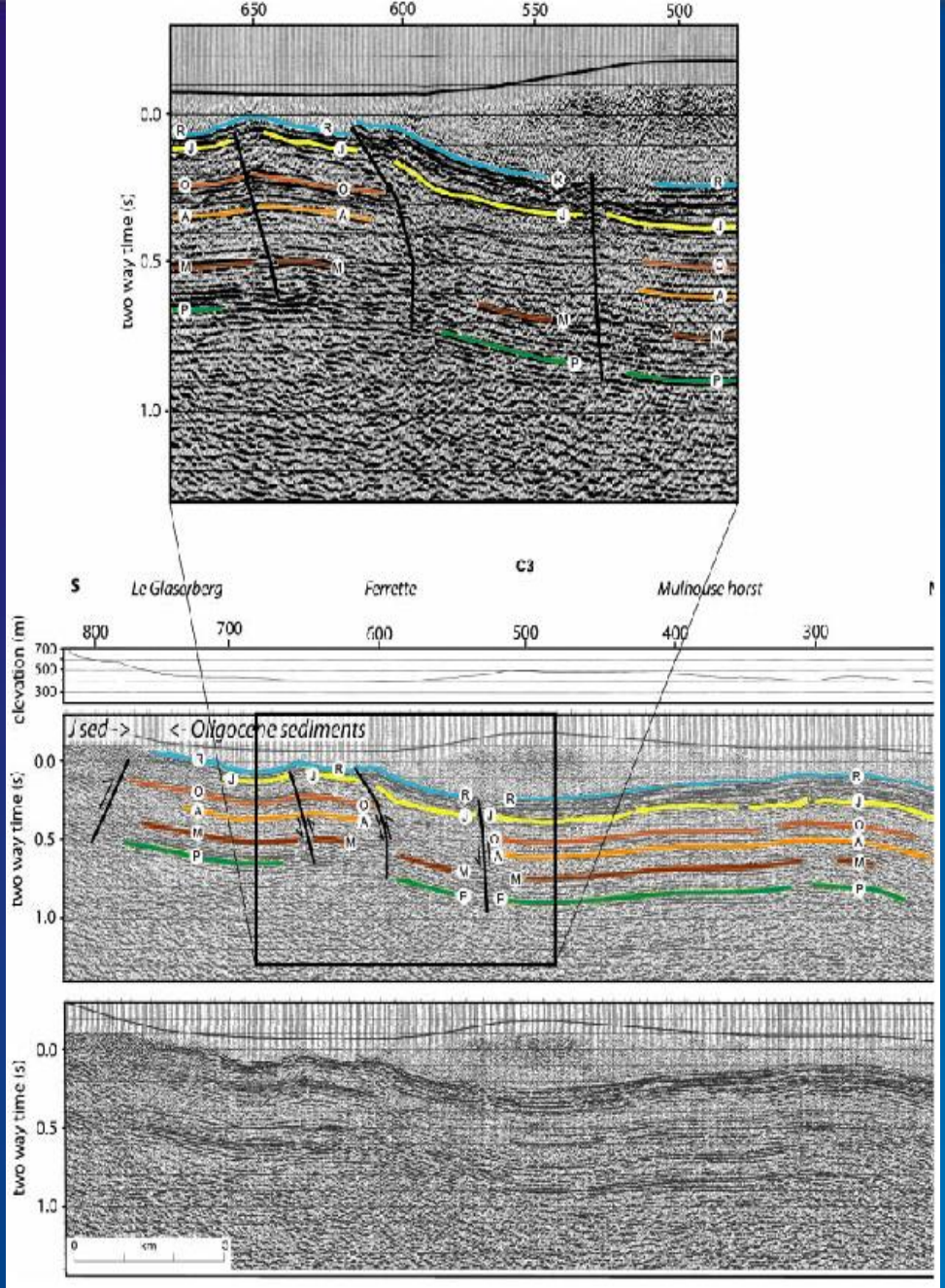

Fig. 3 Uninterpreted and interpreted part of migrated section C3. P, Top Permian; M, Muschelkalk (Triassic); A, Top Aalenian (Jurassic); O, Grande Oolithe (Jurassic); J, Top Jurassic; R, Rupelian. Zero reference is at 350 m above sea-level. Also shown are (1) the ages of the near-surface sediments that suggest thrusting, (2) the surface elevations, (3) the locations of the Ferrette and Le Glaserberg Jura anticlines, and (4) an enlargement of the main faulted area. For location, see Fig. 1.

(Rotstein and Schaming, 2004)

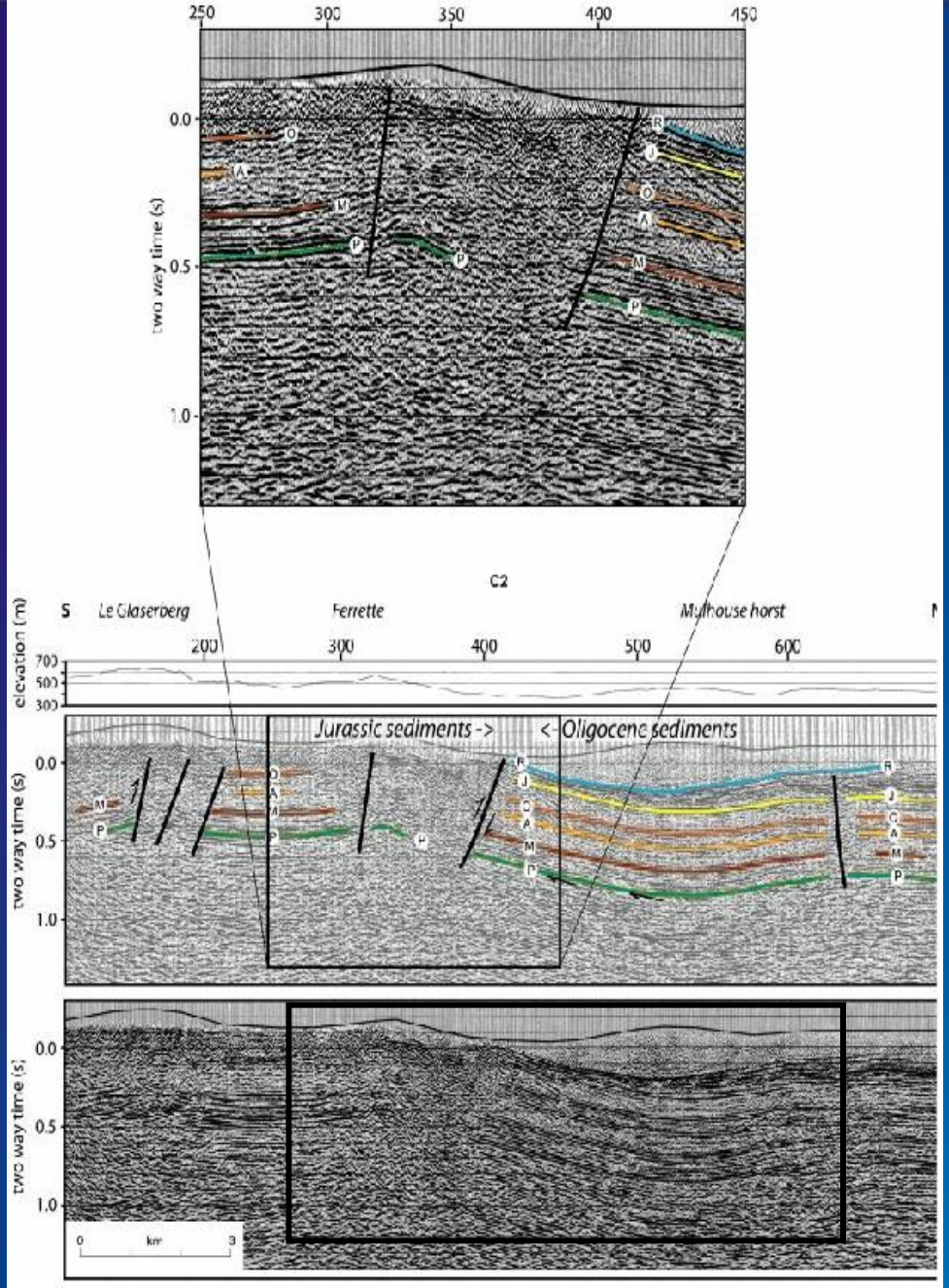

Fig. 2 Uninterpreted and interpreted part of migrated seismic section C2. P, Top Permian; M, Muschelkalk (Triassic); A, Top Aalenian (Jurassic); O, Grande Oolithe (Jurassic); J, Top Jurassic; R, Rupelian. Zero reference is at 350 m above sea-level. Also shown are (1) the ages of the near-surface sediments that suggest thrusting, (2) the surface elevations, (3) the locations of the Ferrette and Le Glaserberg Jura anticlines, and (4) an enlargement of the main faulted area. For location, see Fig. 1.

(Rotstein and Schaming, 2004)

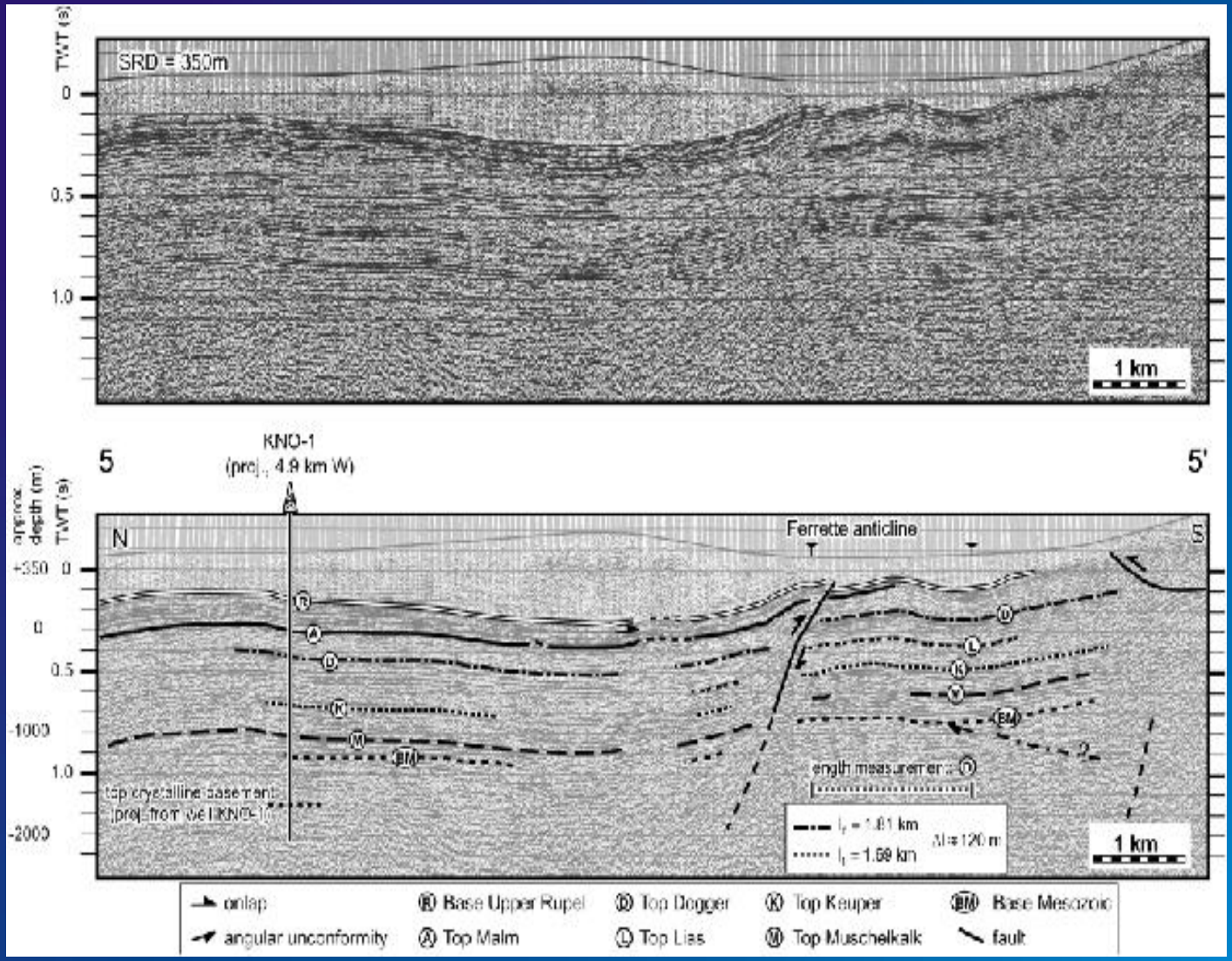

(Ustaszewski and Schmid, 2006)

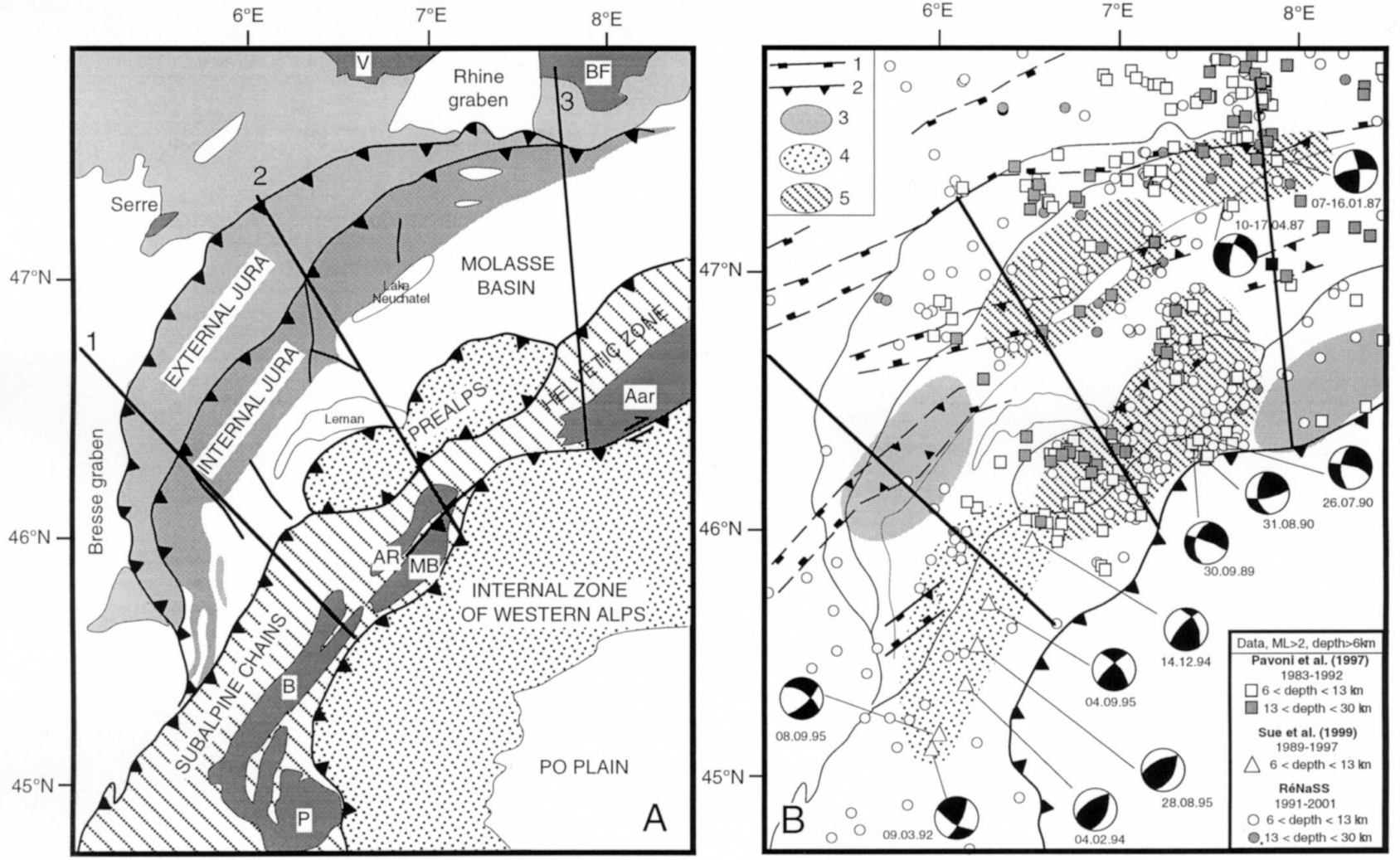

(Lacombe and Mouthereau, 2002)

3, areas of present-day basement-involved shortening inferred from high present-day uplift rates 4, areas of present-day basement-involved shortening inferred from both high present-day uplift rates and seismicity; 5, areas of present-day basement-involved shortening inferred from seismicity.

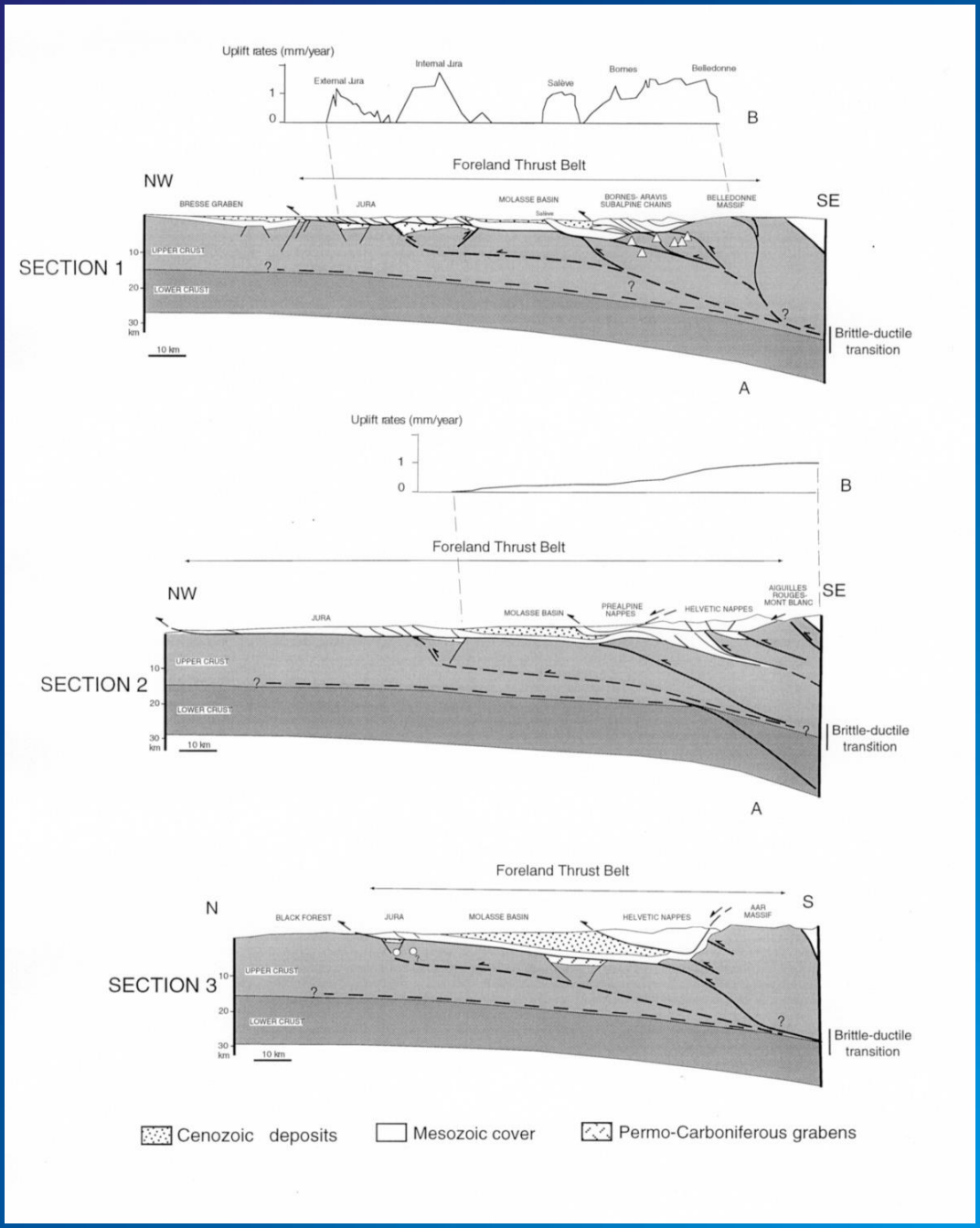

(Lacombe and Mouthereau, 2002)

(Meyer et al., 1994)

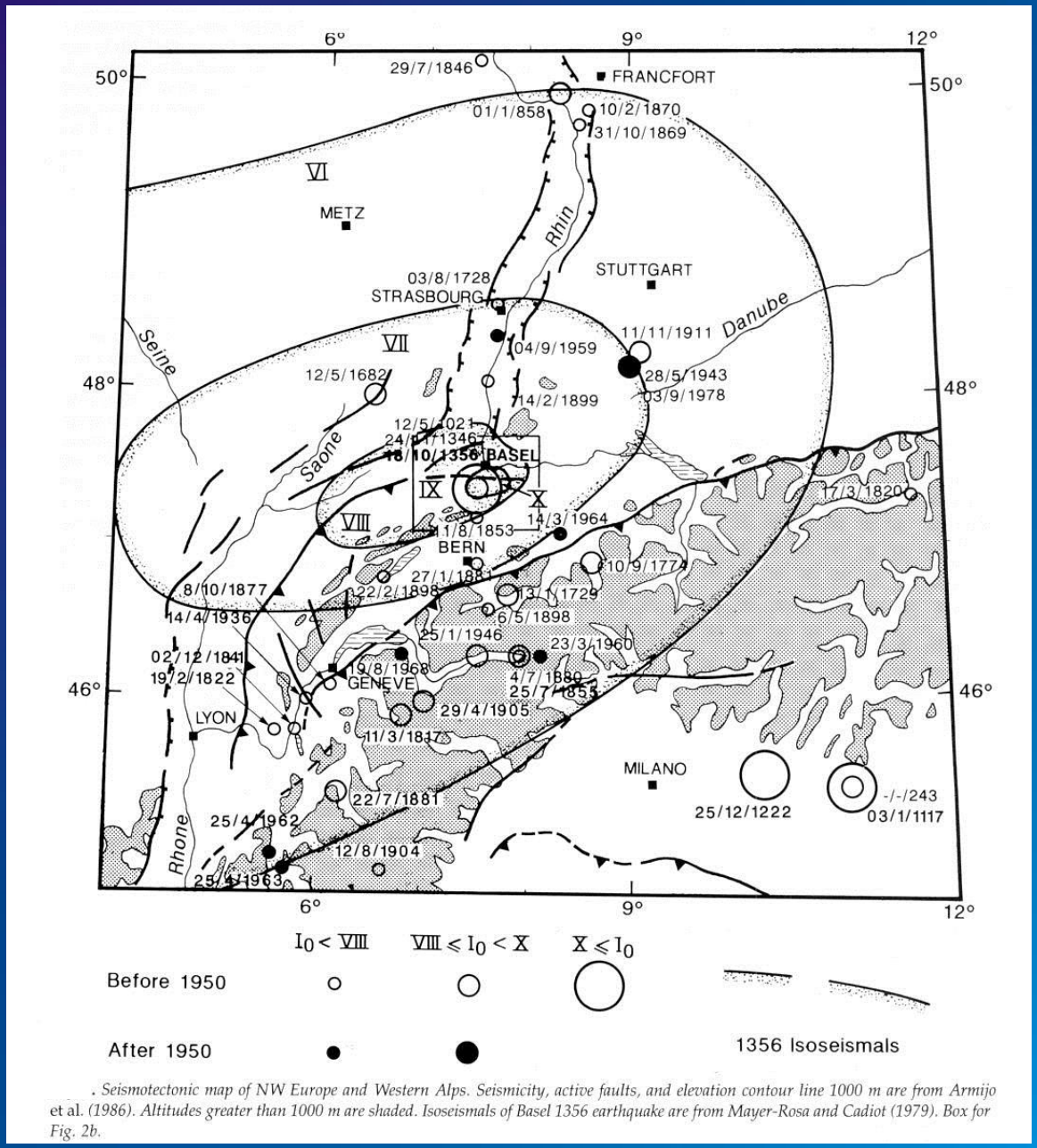

. Seismotectonic map of NW Europe and Western Alps. Seismicity, active faults, and elevation contour line 1000 m are from Armijo et al. (1986). Altitudes greater than 1000 m are shaded. Isoseismals of Basel 1356 earthquake are from Mayer-Rosa and Cadiot (1979). Box for Fig. 2b.

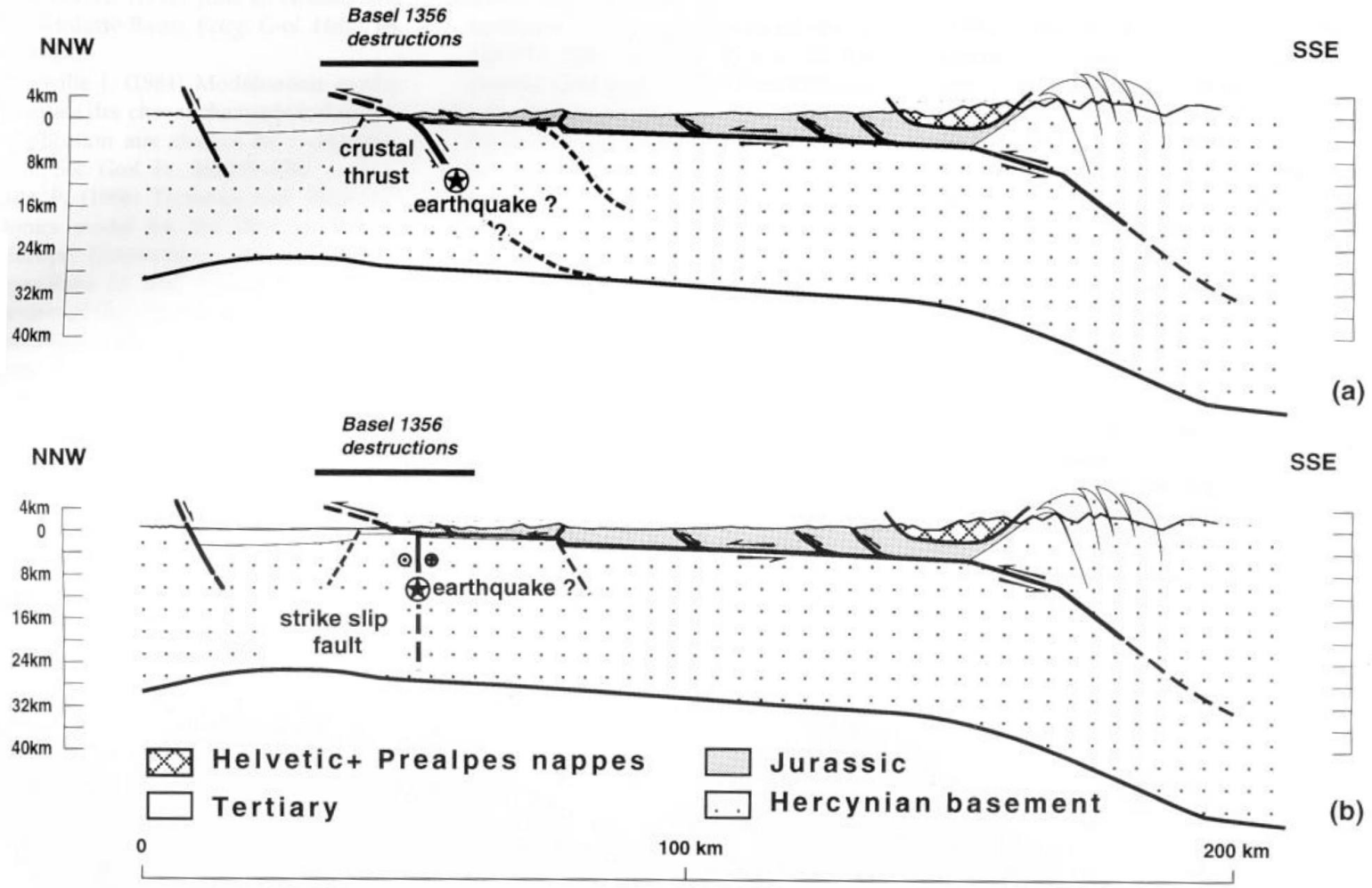

Plausible fault plane geometries for the Basel 1356 earthquake. (a) reactivation of a basement thrust fault beneath the detachment; (b) reactivation of a basement strike-slip fault beneath the detachment.

(Meyer et al., 1994)

Basement control on the kinematics of fold-and-thrust belts : the Laramide belt case

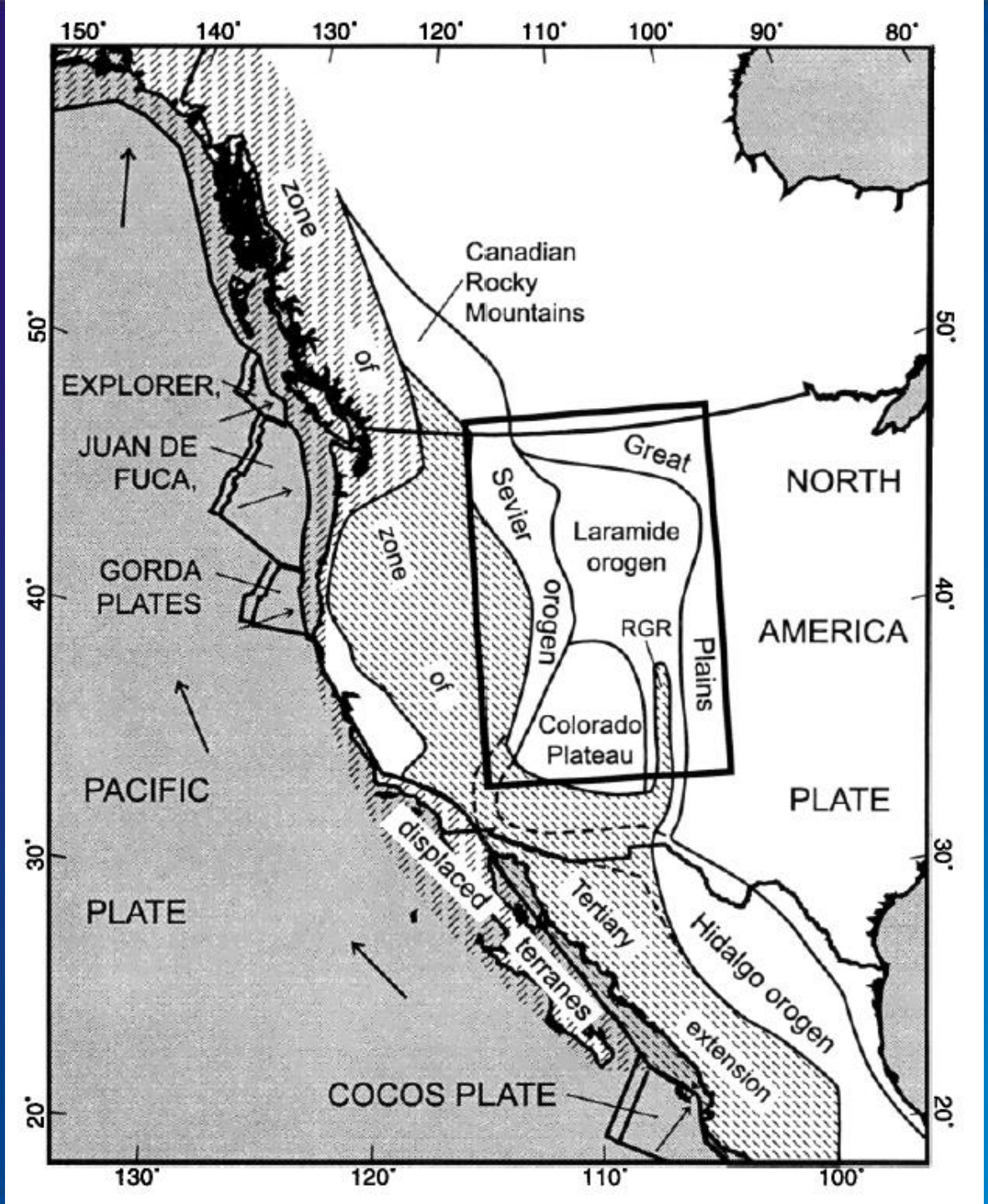
150°
140°
130°
120°
110°
100°
90°
80°
50°
40°
30°
20°
zone
of
Canadian
Rocky
Mountains
EXPLORER,
JUAN DE
FUCA,
GORDA
PLATES
PACIFIC
PLATE
Great
Sevier
orogen
Laramide
orogen
RGR
Plains
Colorado
Plateau
NORTH
AMERICA
PLATE
displaced
terranes
Tertiary
Hidalgo orogen
extension
COCOS PLATE
130°
120°
110°
100°

The Sevier belt

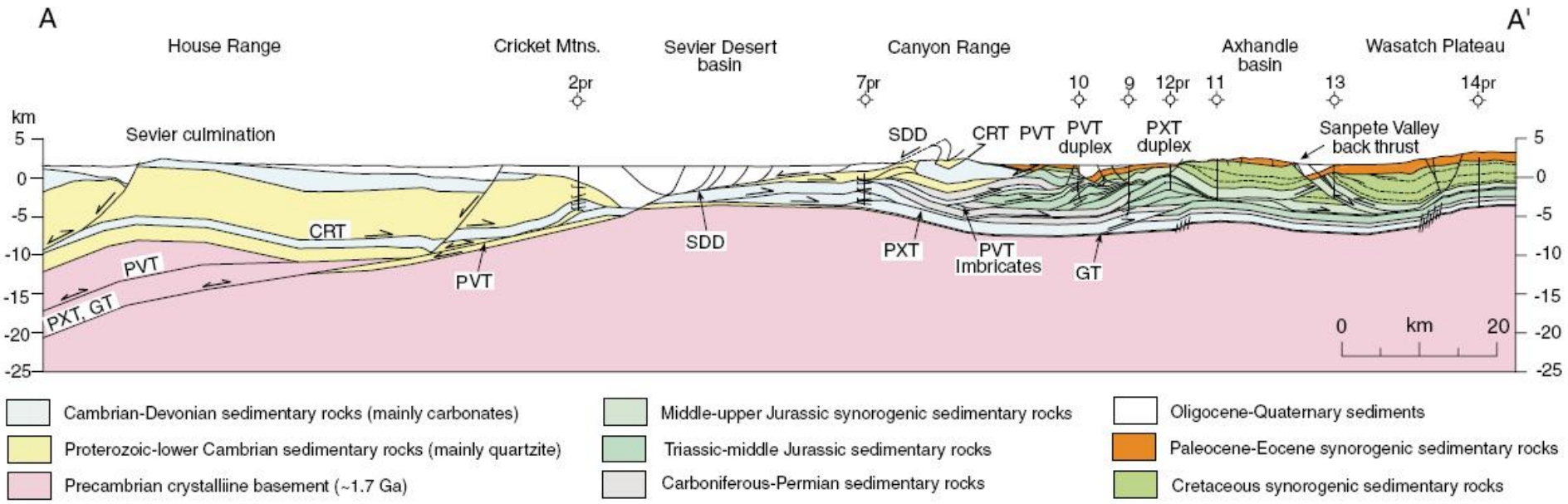

Regional balanced cross-section A–A′ of the Sevier fold-and-thrust belt in central Utah, based in part on Coogan et al. (1995), Royse (1993), Standlee (1984), and Consortium for Continental Reflection Profiling (COCORP) deep seismic-reflection profile (Allmendinger et al., 1983, 1986). Numerals indicate industry wells that were used to constrain the section. Letters (pr) after well numbers indicate where data were projected more than a few kilometers into the plane of the cross section. See Figure 2 for location of cross section and legend of industry wells. CRT—Canyon Range thrust; PVT—Pavant thrust; PXT—Paxton thrust; GT—Gunnison thrust; SDD—Sevier Desert detachment.

De Celles and Coogan (2004)

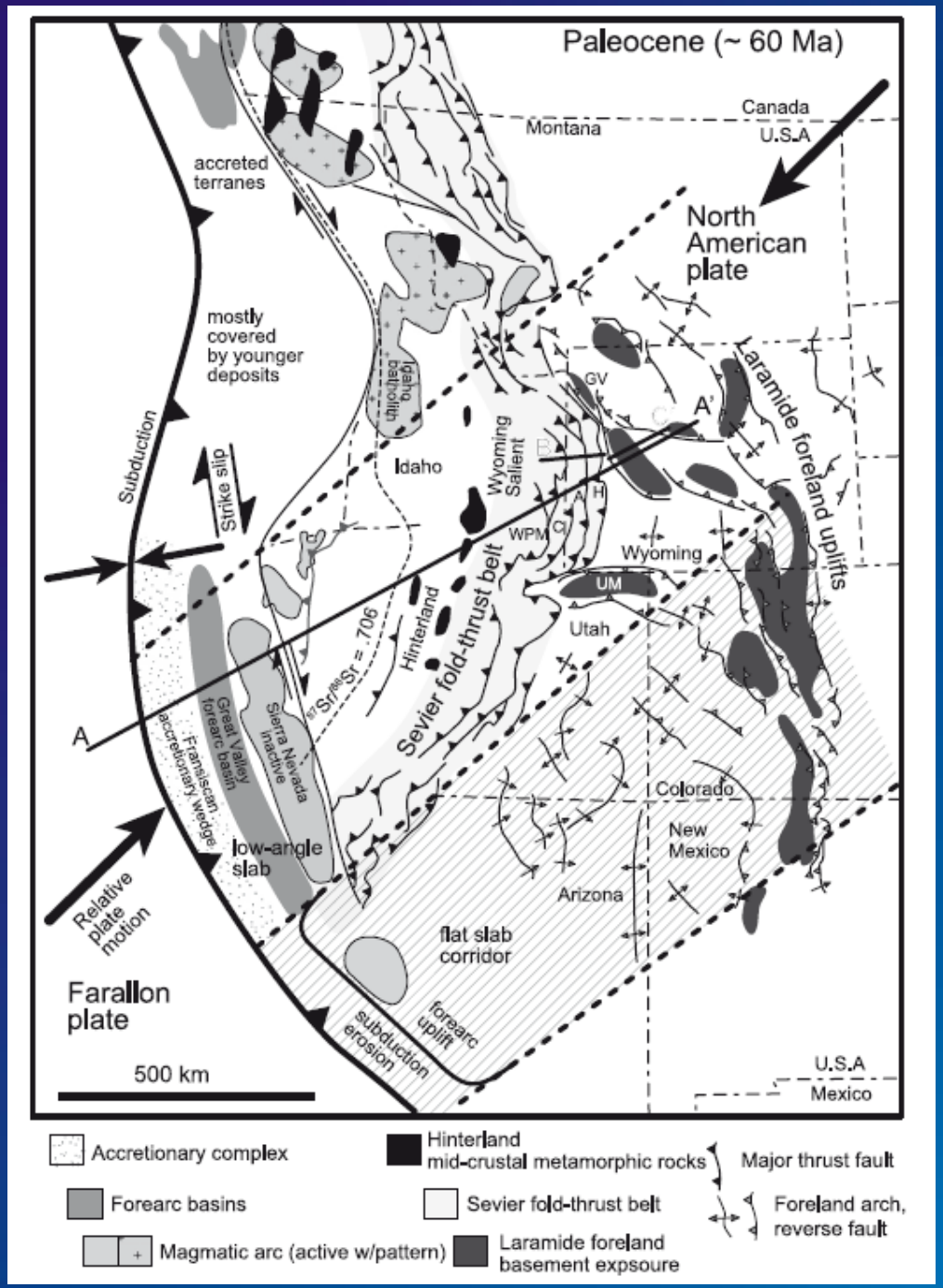

(Weil and Yonkee, 2012)

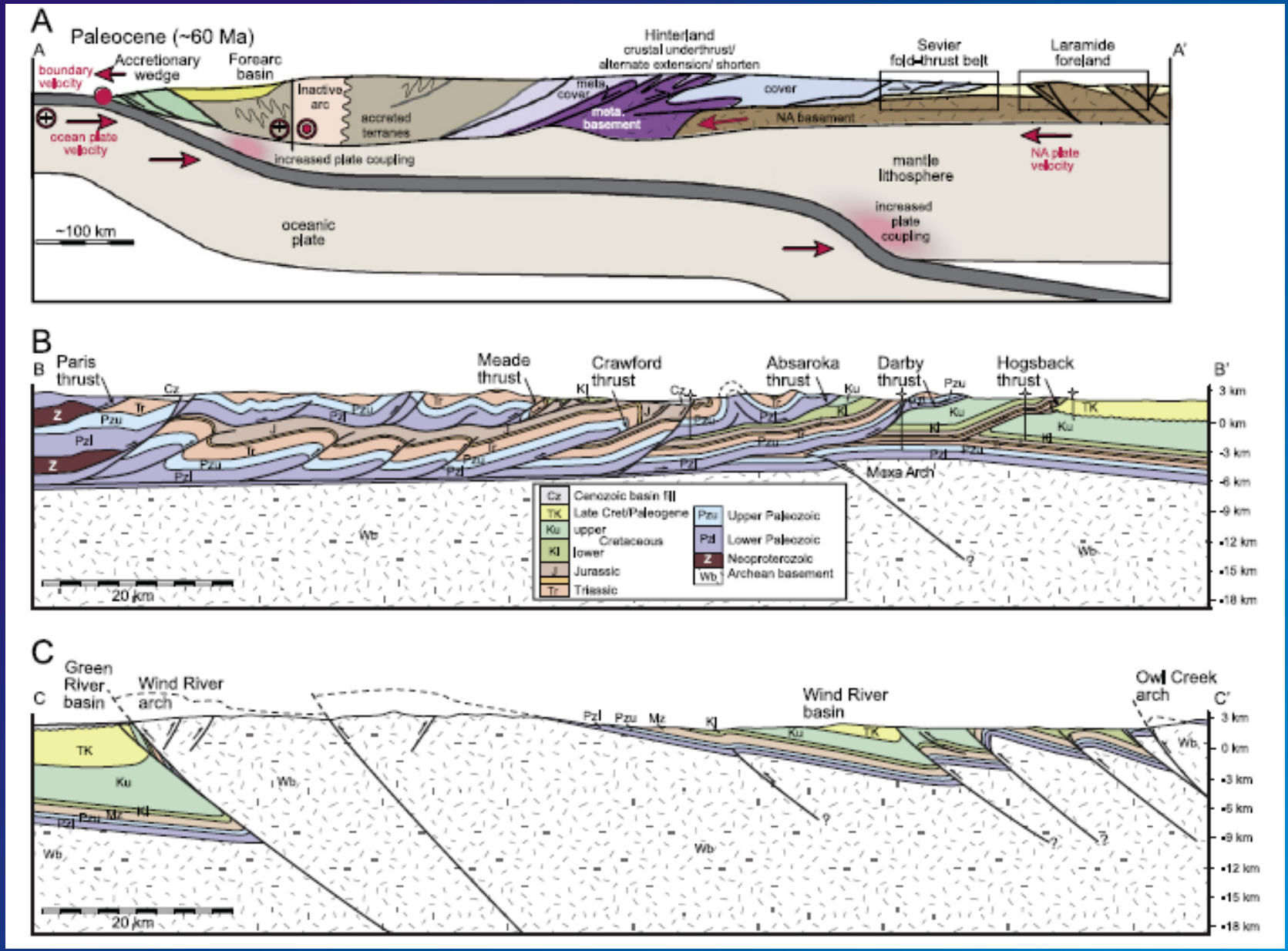

(Weil and Yonkee, 2012)

Bird (2002)

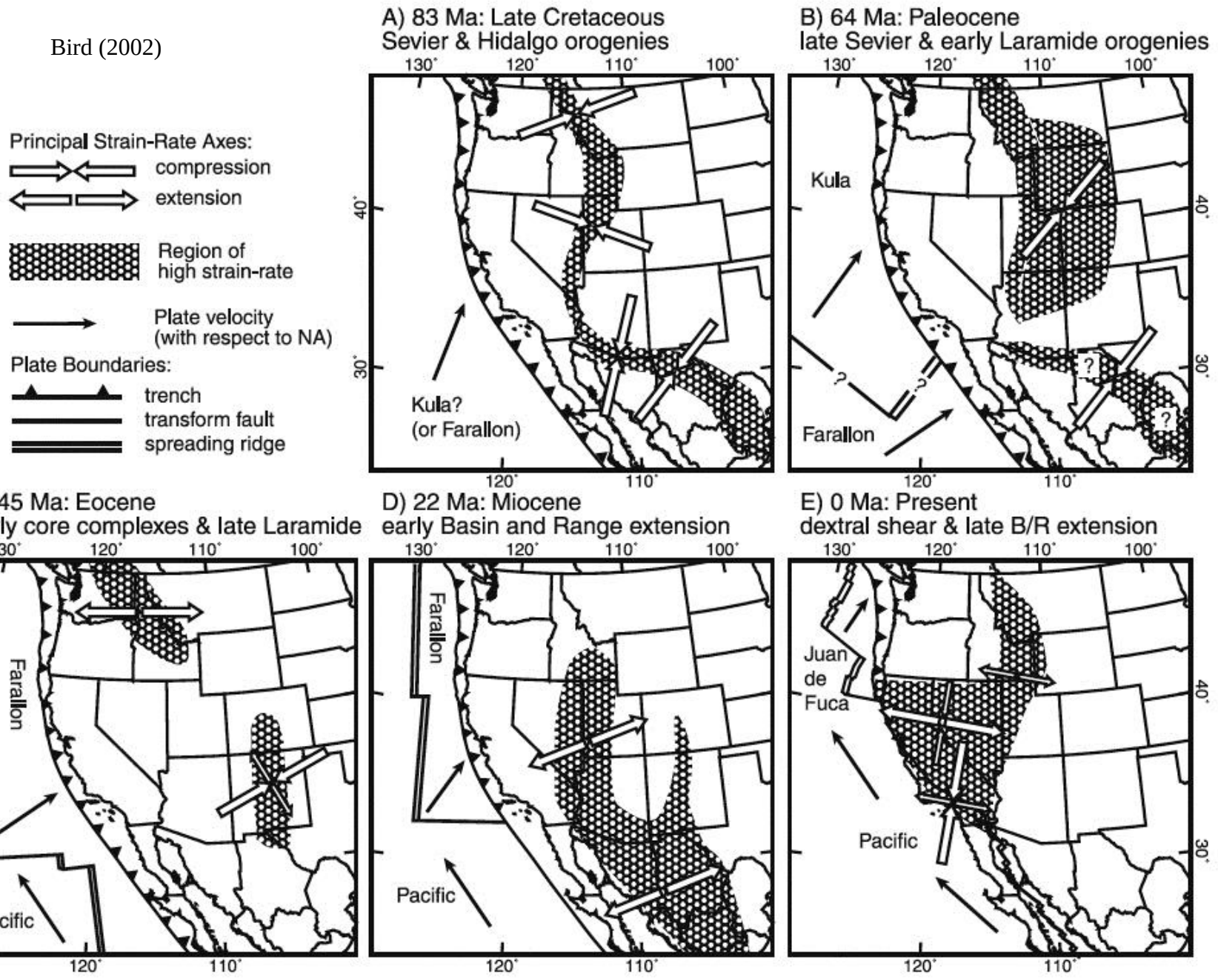
Principal Strain-Rate Axes:
compression
extension
Region of high strain-rate
Plate velocity (with respect to NA)
Plate Boundaries:
trench
transform fault
spreading ridge
A) 83 Ma: Late Cretaceous
Sevier & Hidalgo orogenies
Kula?
(or Farallon)
B) 64 Ma: Paleocene
late Sevier & early Laramide orogenies
Kula
Farallon
C) 45 Ma: Eocene
early core complexes & late Laramide
Farallon
Pacific
D) 22 Ma: Miocene
early Basin and Range extension
Farallon
Pacific
E) 0 Ma: Present
dextral shear & late B/R extension
Juan de Fuca
Pacific
130°
120°
110°
100°
40°
30°

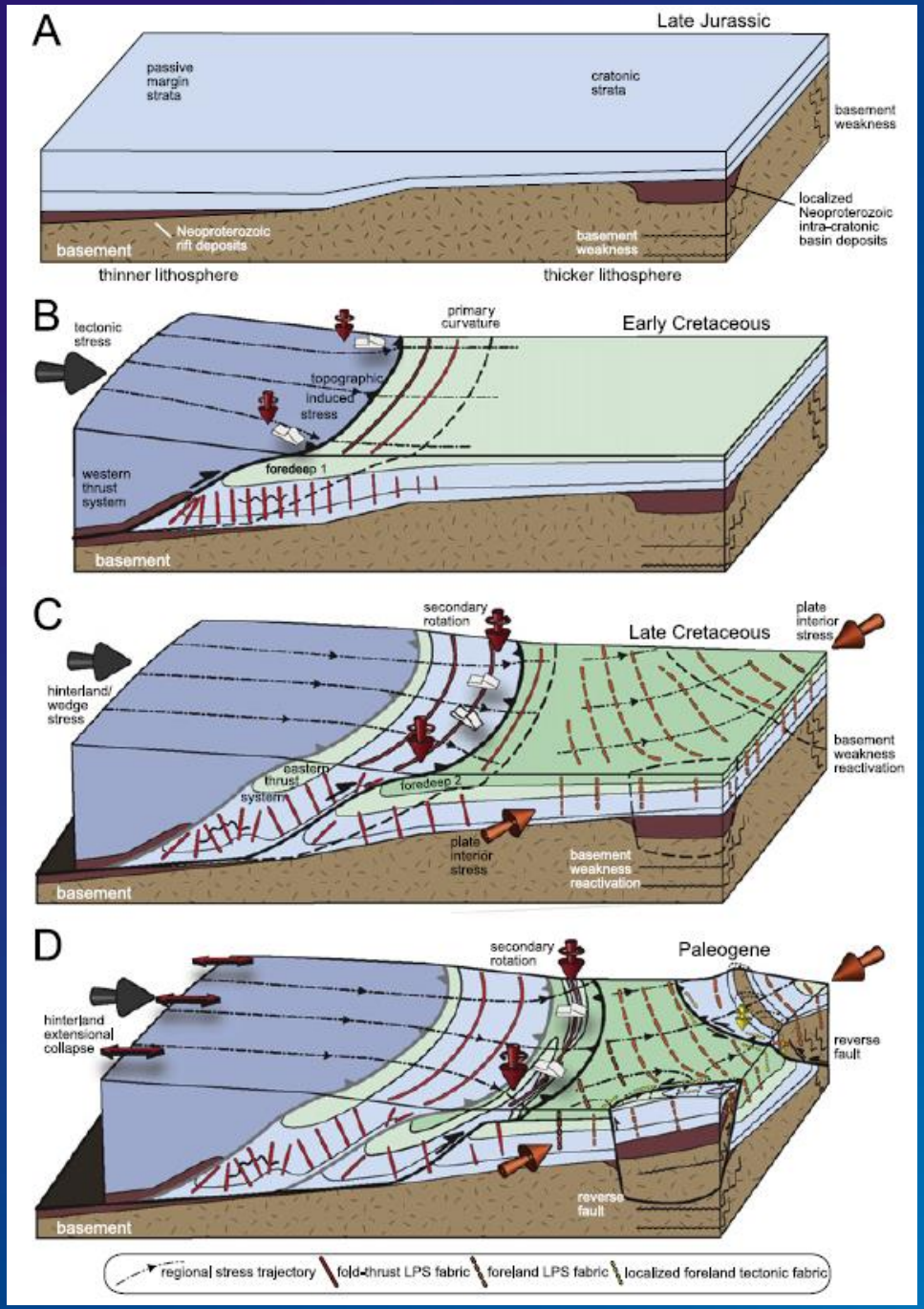

(Weil and Yonkee, 2012)

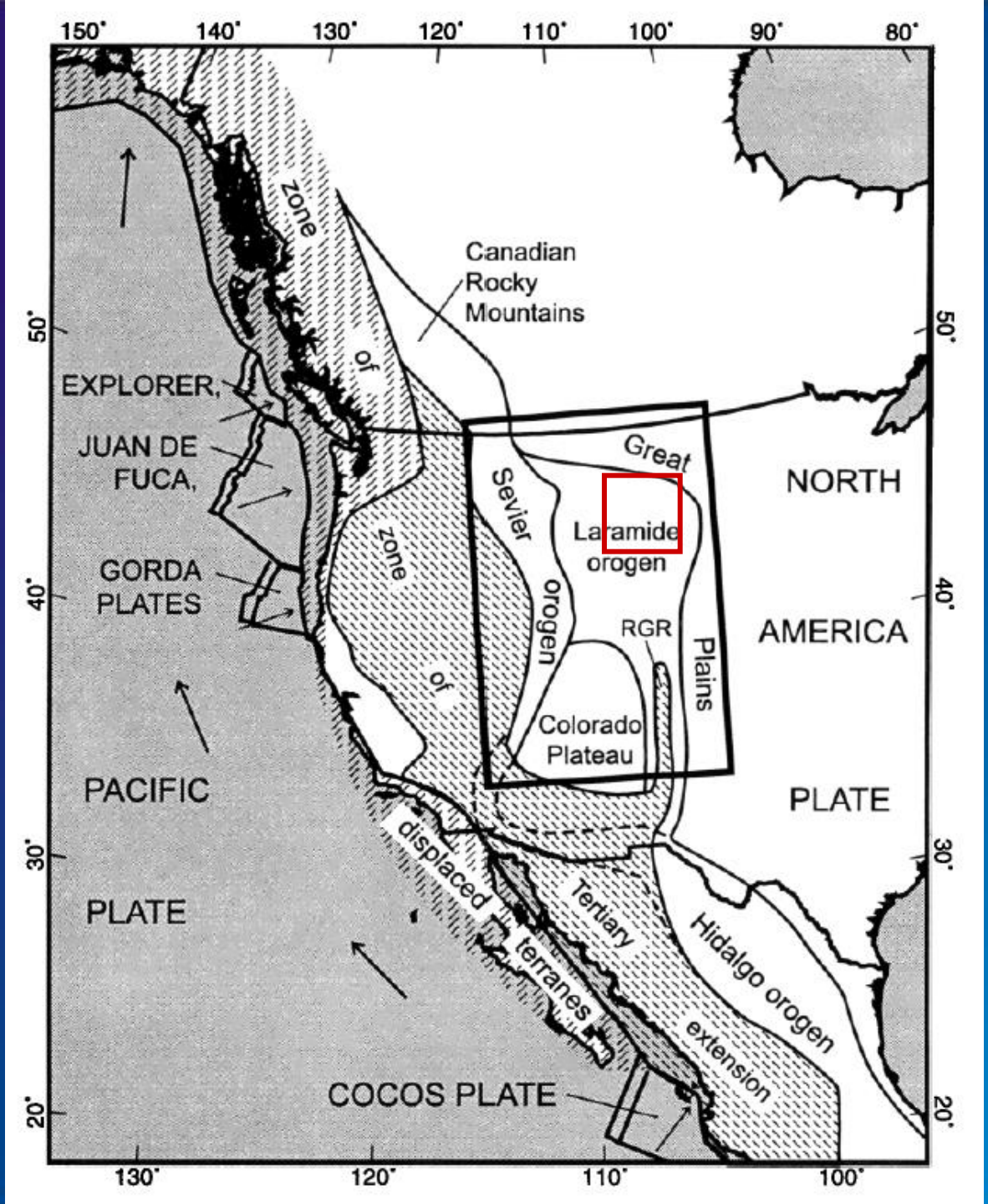
150°
140°
130°
120°
110°
100°
90°
80°
50°
40°
30°
20°
Canadian
Rocky
Mountains
EXPLORER,
JUAN DE
FUCA,
GORDA
PLATES
PACIFIC
PLATE
zone
of
Great
Sevier
orogen
Laramide
orogen
RGR
Plains
Colorado
Plateau
NORTH
AMERICA
PLATE
displaced
terranes
Tertiary
Hidalgo orogen
extension
COCOS PLATE

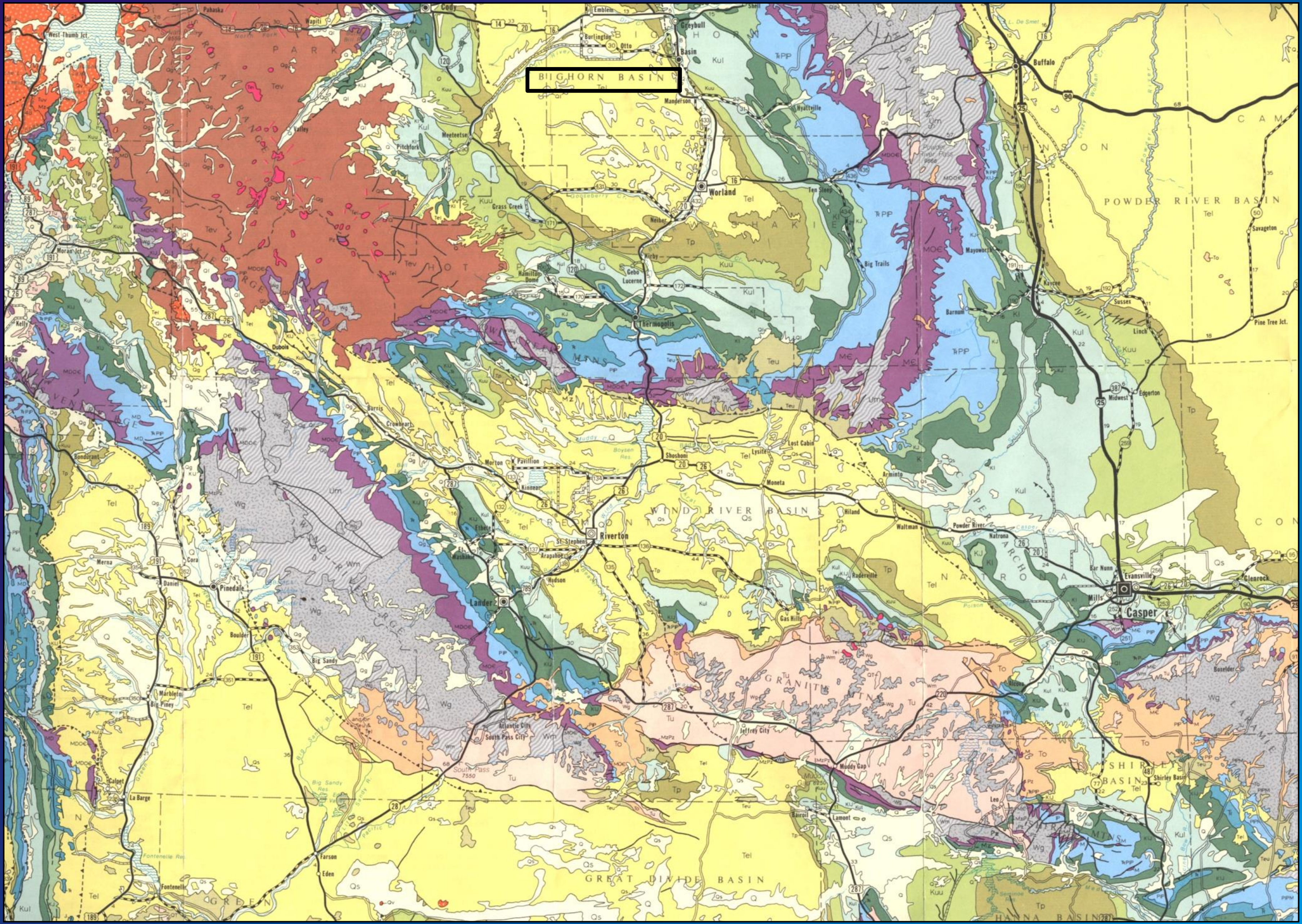
BIGHORN BASIN

Jurassic – Cretaceous: The Western Interior Basin

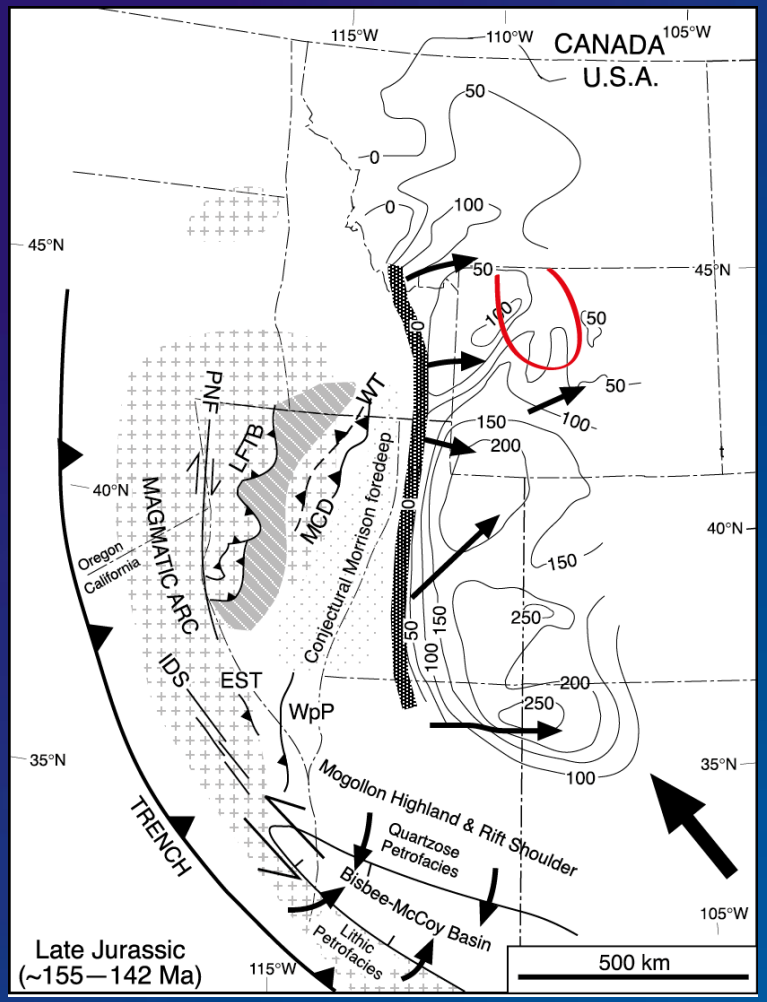

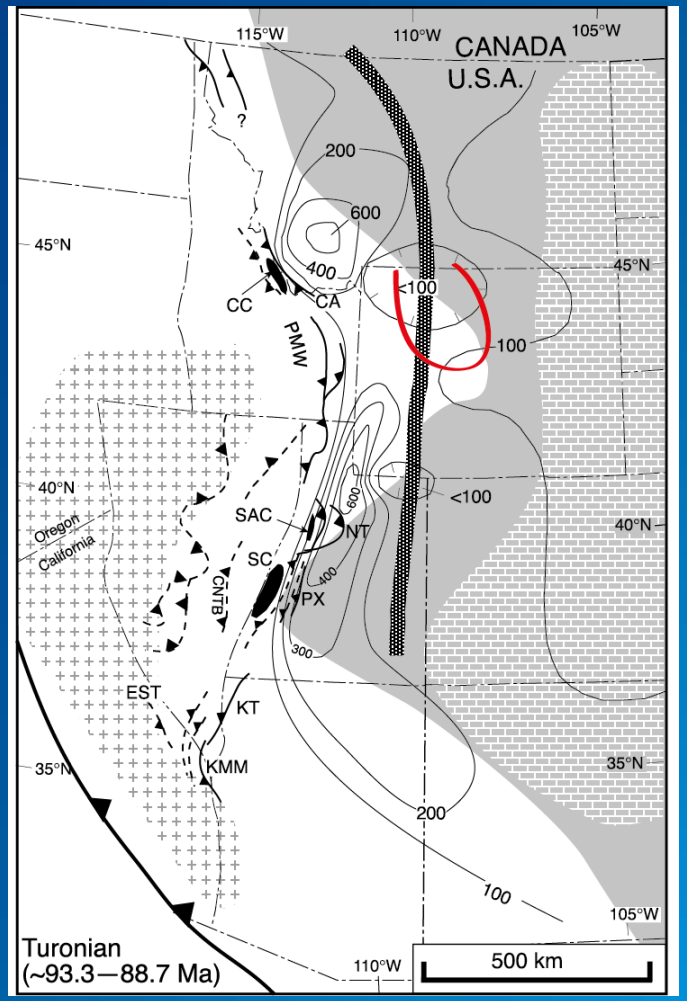

DeCelles, 2004

Late Cretaceous – Paleocene: The Bighorn Basin

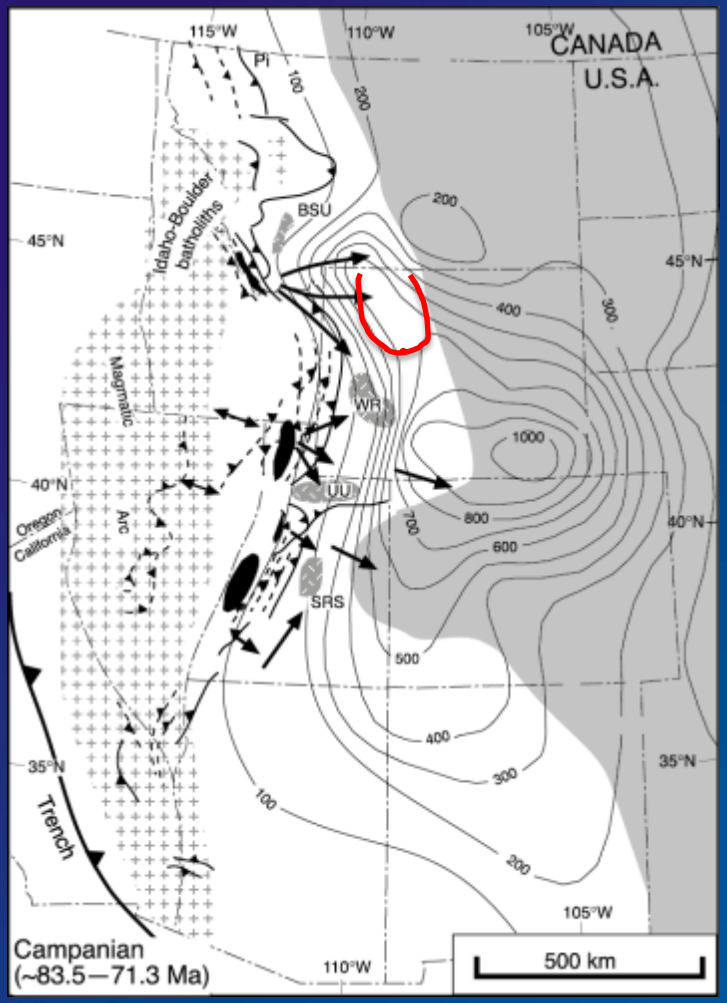

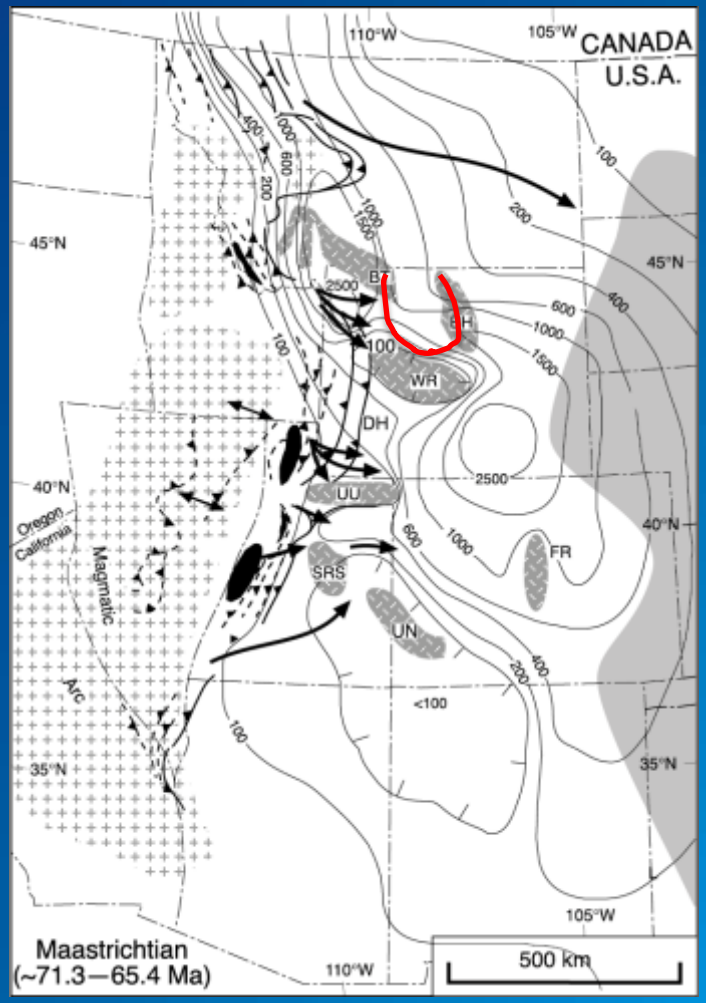

DeCelles, 2004

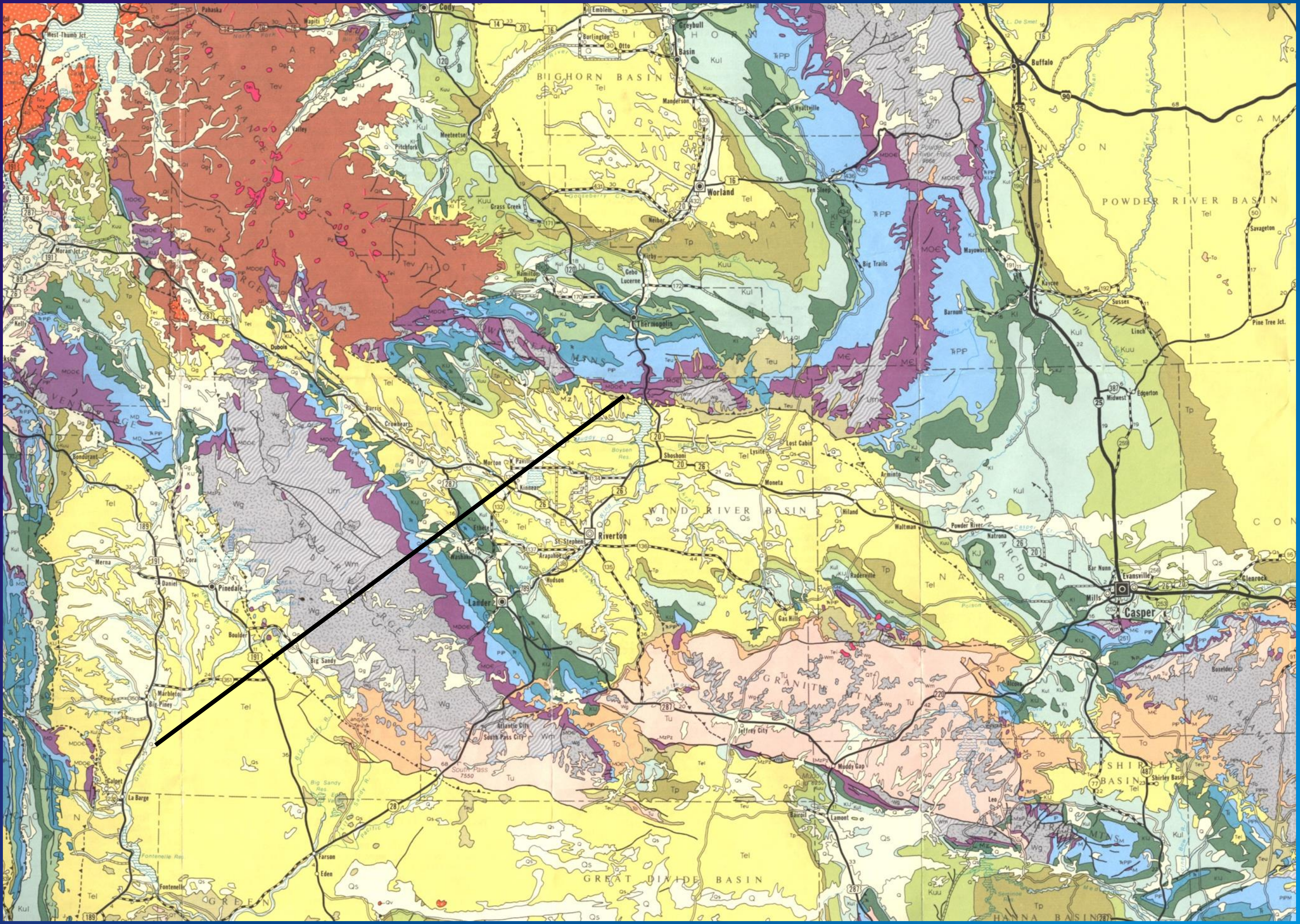

Cody
Greybull
Basin
Buffalo
BIGHORN BASIN
Worland
Ten Sleep
POWDER RIVER BASIN
Thermopolis
Shoshoni
Riverton
Lander
Pinedale
Boulder
Big Sandy
WIND RIVER BASIN
Casper
Evansville
Mills
GRANITE MTNS
South Pass
Atlantic City
South Pass City
Jeffrey City
Muddy Gap
Shirley Basin
Farson
Eden
GREAT DIVIDE BASIN
HANNA BASIN
La Barge
Big Piney
Marbleton
Daniel
Dubois
Kinnear
Hudson
Moneta
Lysite
Lost Cabin
Midwest
Edgerton
Kaycee
Mayoworth
Big Trails
Hyattville
Manderson
Meeteetse
Grass Creek
Fontenelle
Pine Tree Jct.
Savageton

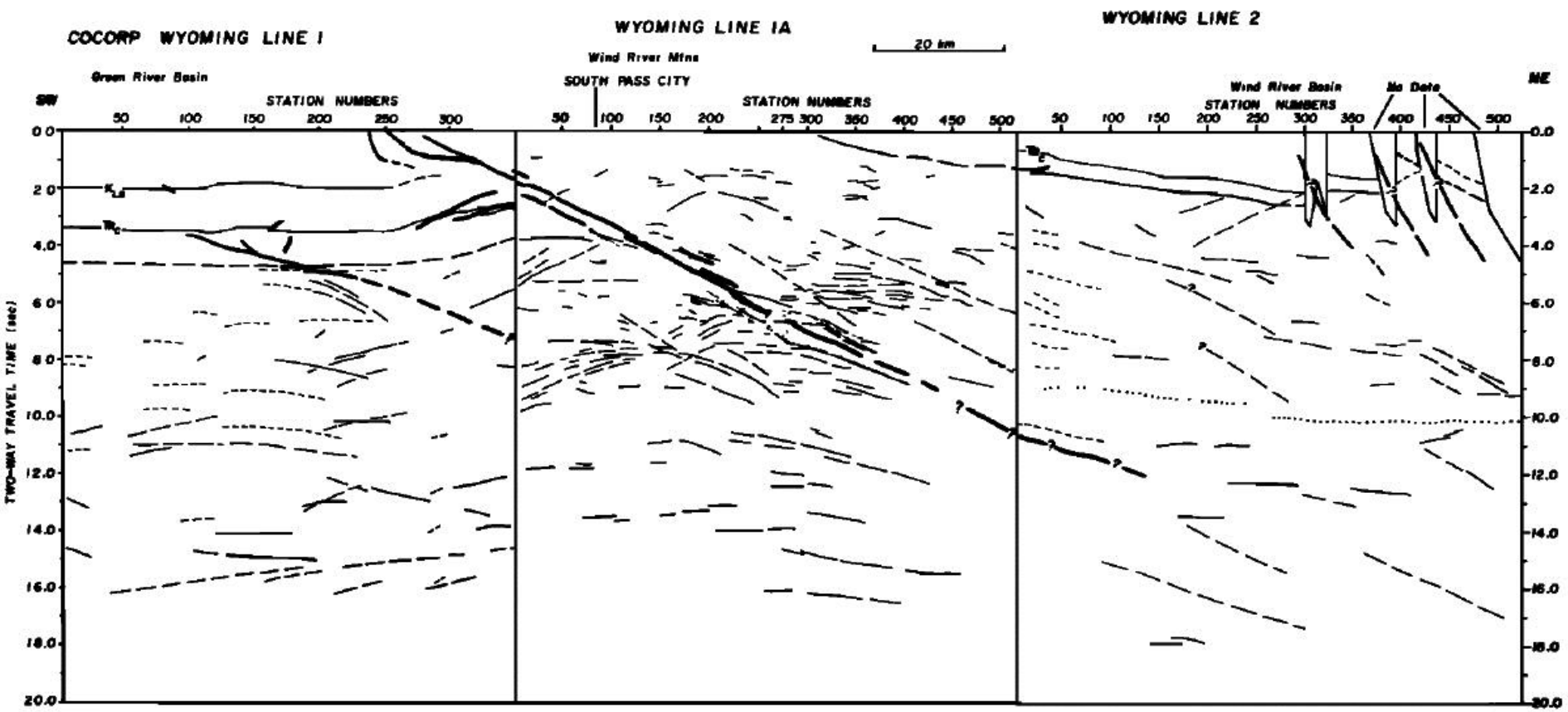

Smithson et al. (1979)

Beaudoin, PhD thesis, 2012

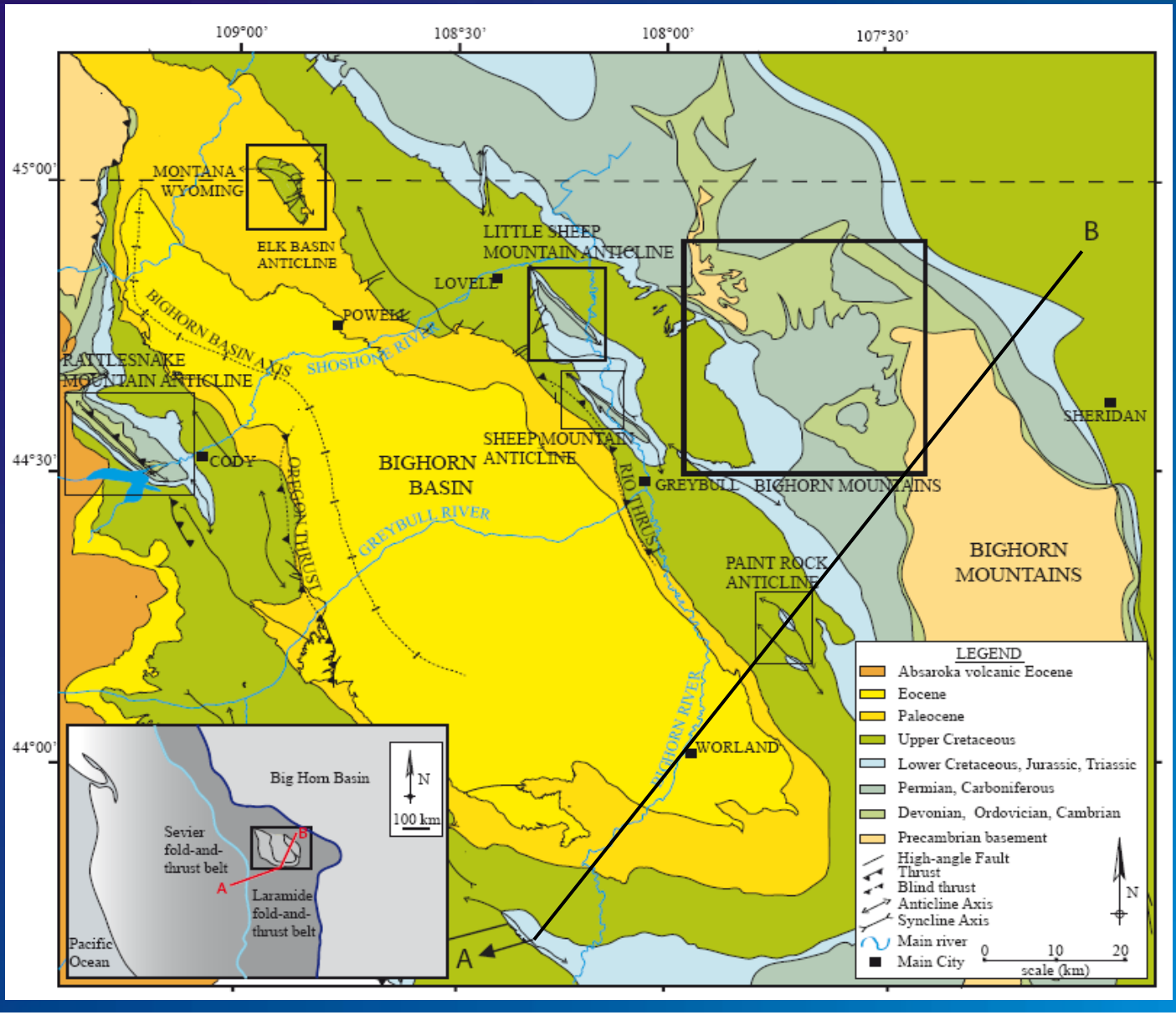

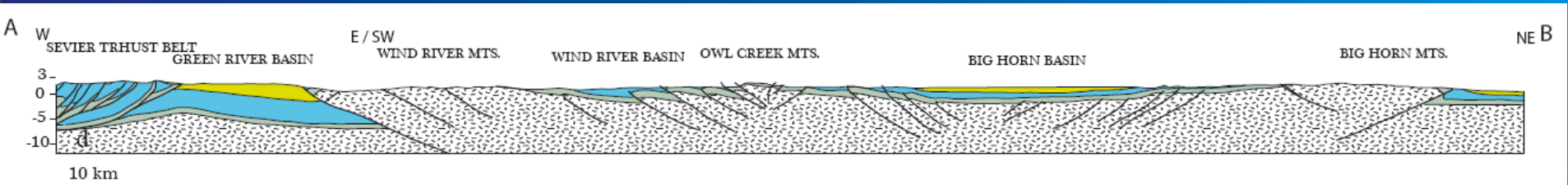

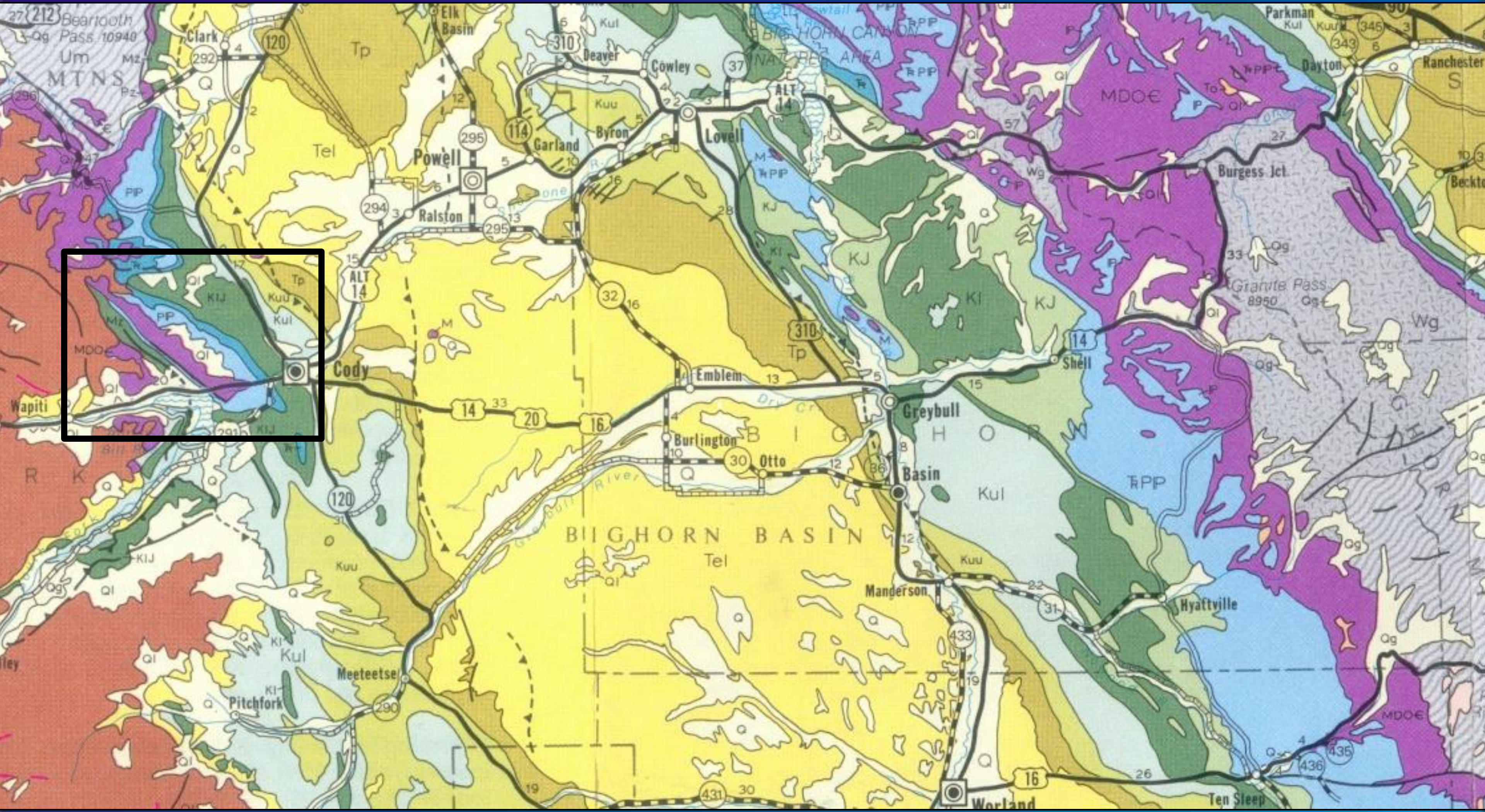

Beartooth Pass 10940
MTNS
Clark
Elk Basin
Deaver
Cowley
BIG HORN CANYON NAT. REC. AREA
Parkman
Dayton
Ranchester
Powell
Garland
Byron
Lovell
Ralston
Burgess Jct
Granite Pass 8950
Cody
Wapiti
Emblem
Greybull
Shell
Burlington
Otto
Basin
BIGHORN BASIN
Manderson
Hyattville
Meeteetse
Pitchfork
Worland
Ten Sleep

10 km

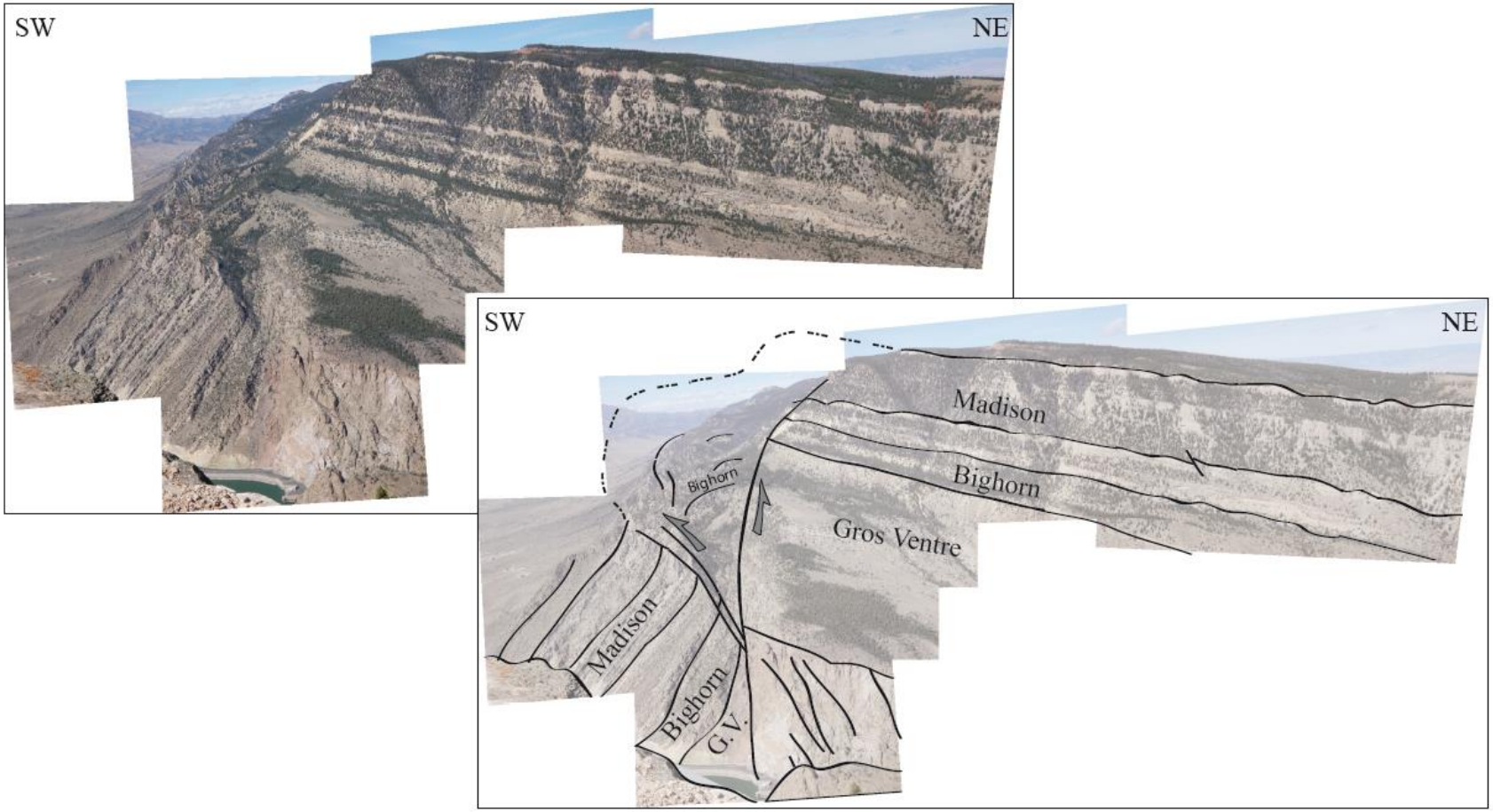

Beaudoin et al., 2012

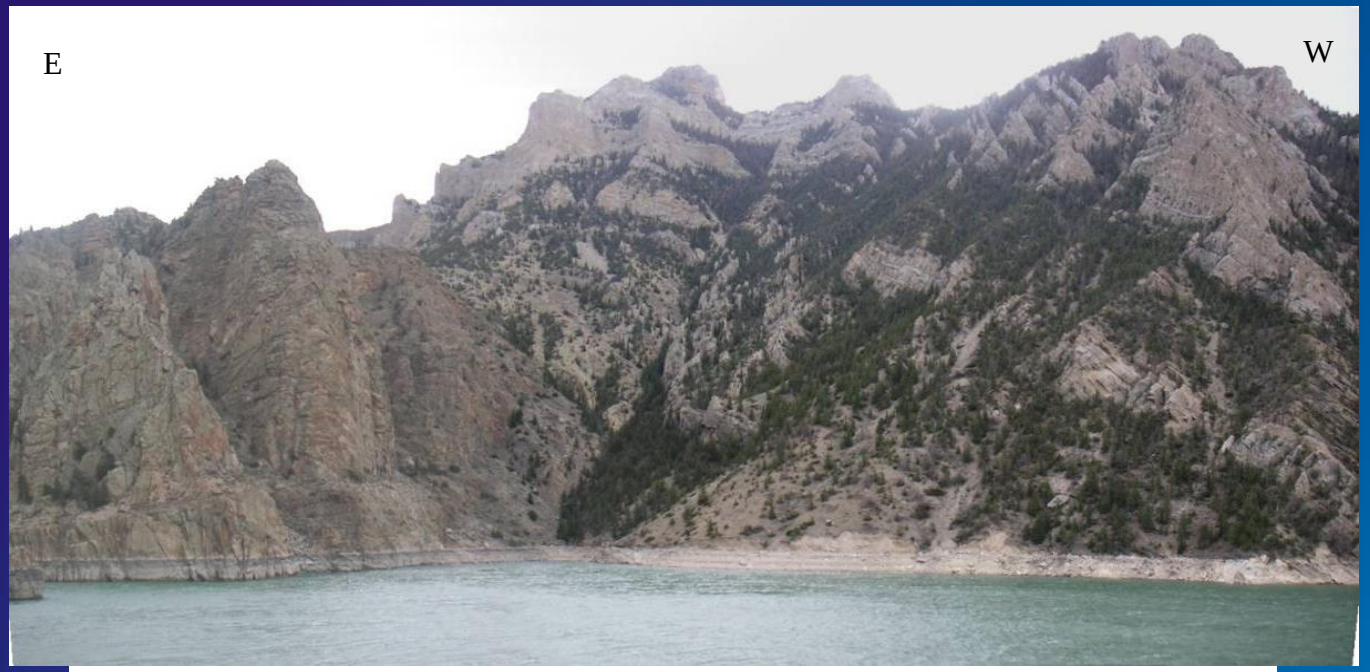
E
W

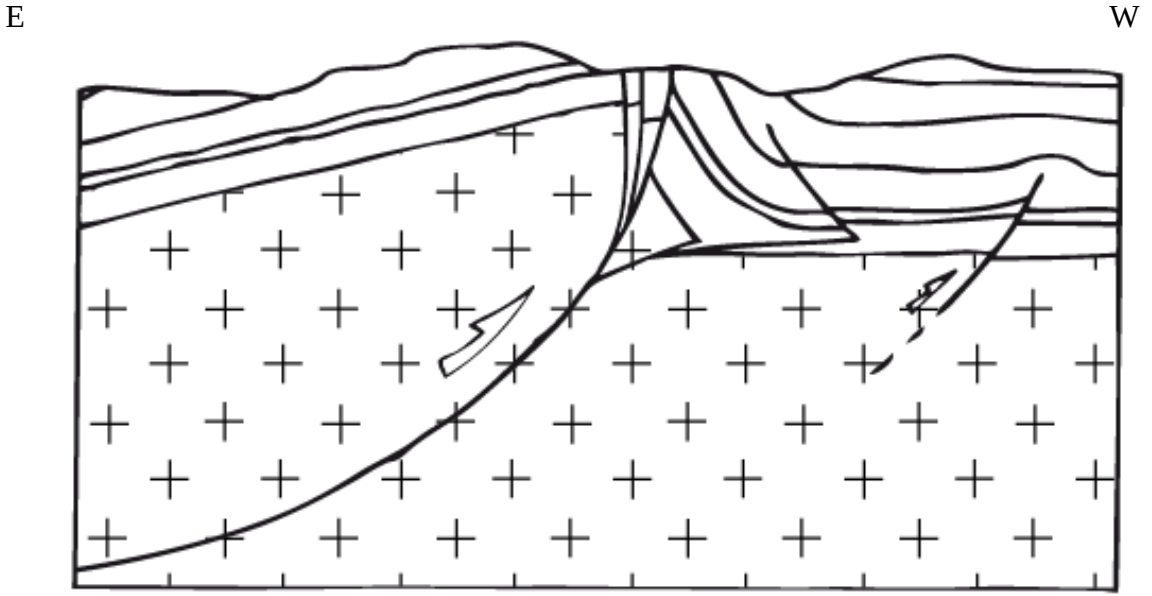
E
W

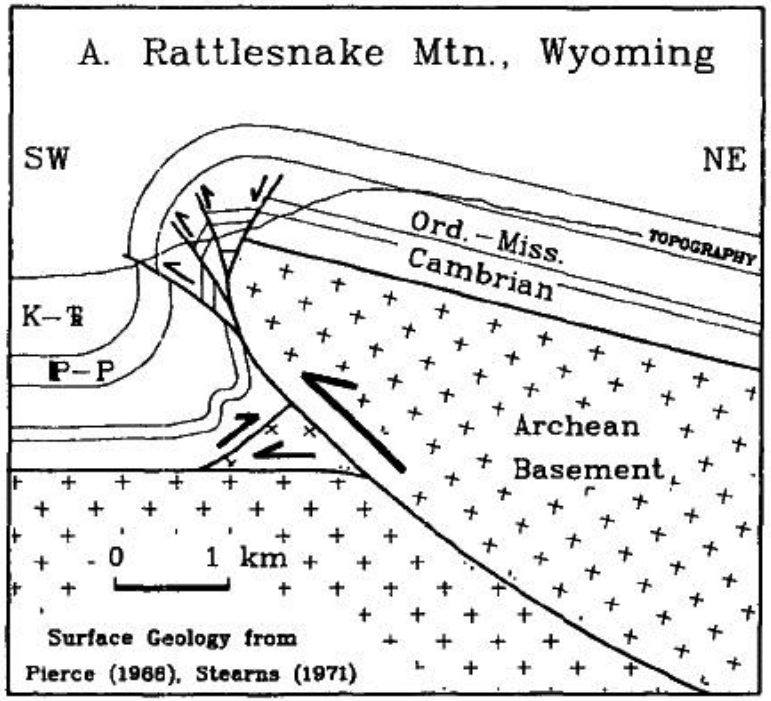
A. Rattlesnake Mtn., Wyoming
SW
NE
Ord.–Miss.
Cambrian
TOPOGRAPHY
K–T
P–P
Archean
Basement
0
1 km
Surface Geology from
Pierce (1966), Stearns (1971)

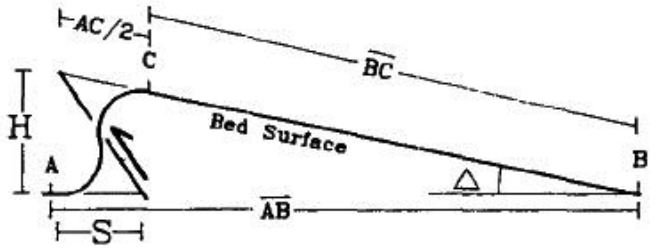
B. Fault Dip Calculation
AC/2
C
BC
H
A
Bed Surface
B
AB
S
△ = Hanging Wall Dip – Footwall Dip
AC and AB Are Bed Lengths
H = (BC + AC/2) sin △
S = Total Shortening – Tilt Shortening
S = AB – AB – (BC + AC/2) (1 – cos△)
Fault Dip Relative to Footwall = arctan (H/S)

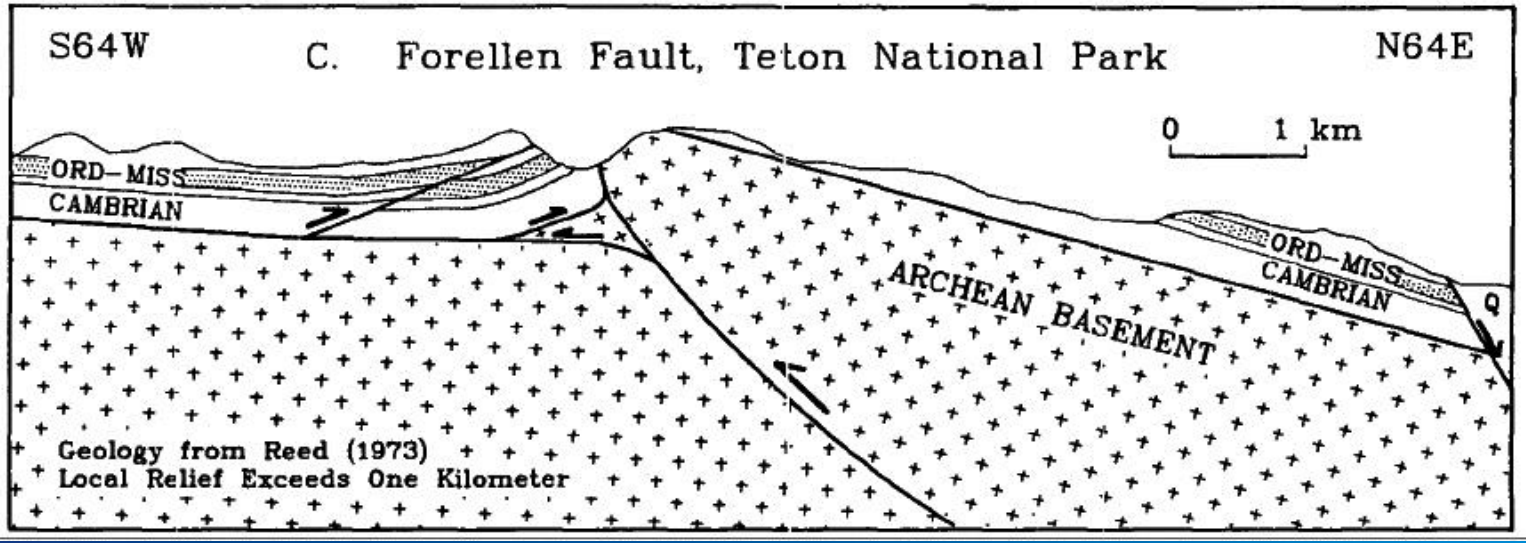
S64W
C. Forellen Fault, Teton National Park
N64E
0
1 km
ORD–MISS
CAMBRIAN
ARCHEAN BASEMENT
ORD–MISS
CAMBRIAN
Q
Geology from Reed (1973)
Local Relief Exceeds One Kilometer

Erslev (1986)

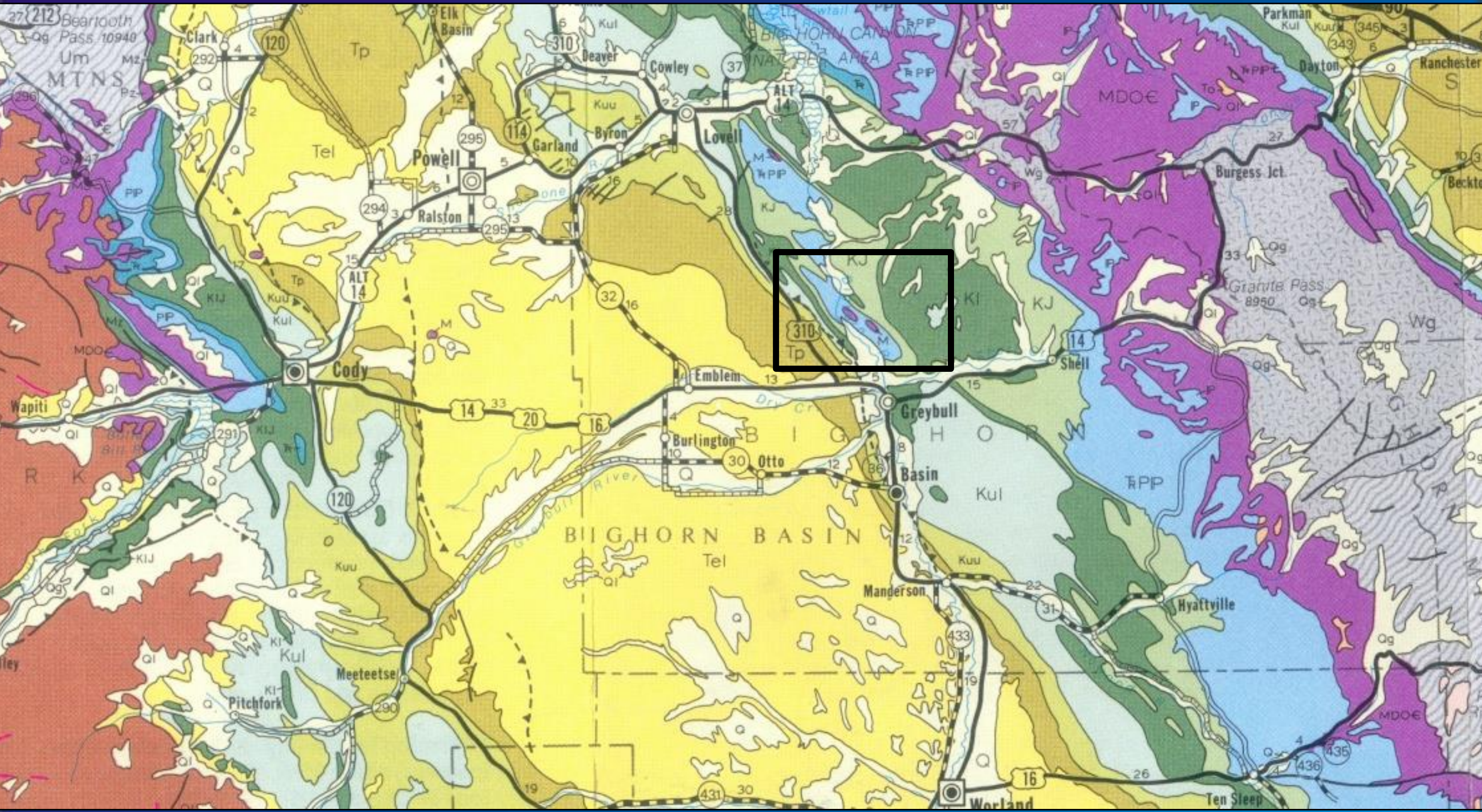
Beartooth Pass 10940
MTNS
Clark
Elk Basin
Deaver
Cowley
BIG HORN CANYON NAT. REC. AREA
Parkman
Dayton
Ranchester
Powell
Garland
Byron
Lovell
Ralston
Burgess Jct
Granite Pass 8950
Cody
Emblem
Shell
Wapiti
Greybull
Burlington
Otto
Basin
BIGHORN BASIN
Manderson
Hyattville
Meeteetse
Pitchfork
Worland
Ten Sleep

10 km

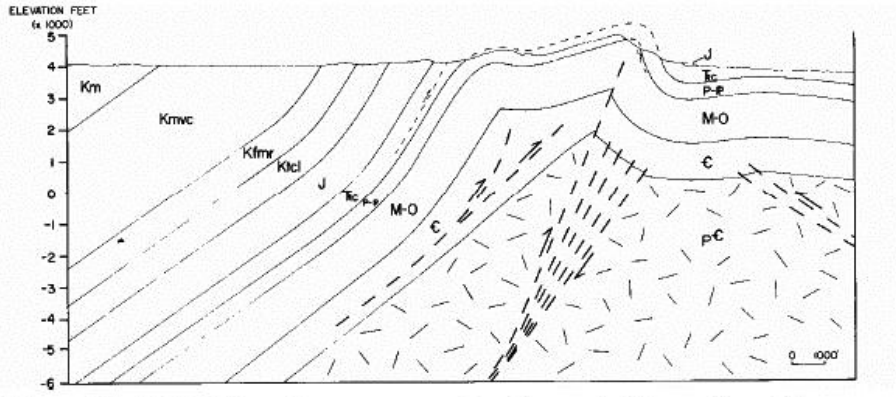

SW–NE trending cross section through Sheep Mountain anticline from Hennier and Spang, 1983. Bedding dips and Formation contacts are constrained by surface mapping and geologic markers from exploration wells. Hennier and Spang postulate a relatively undeformed basement with multiple thrust planes in an overall wedge shaped geometry to generate folding in the overlying sediments.

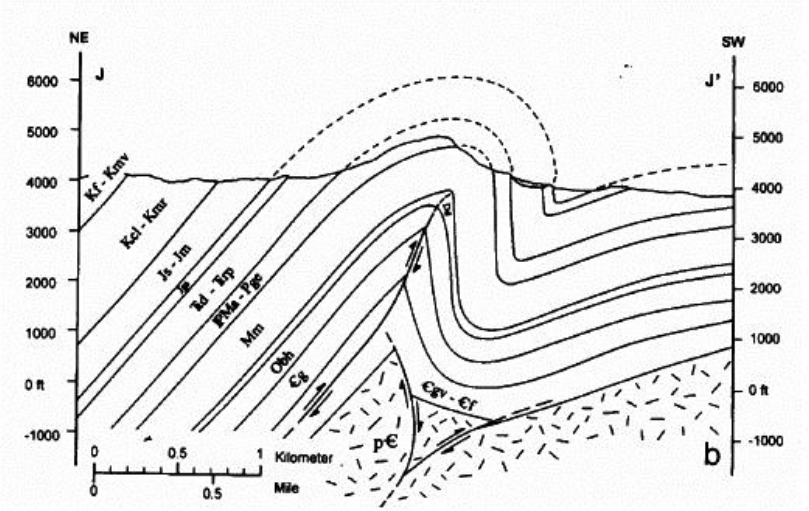

SW-NE trending cross-section through Sheep Mountain anticline from Forster et al., 1996. Bedding dips and Formation are constrained by surface mapping and geologic markers from exploration wells. A wedge shaped fault zone is hypothesized as the mechanism by which overlying strata fold.

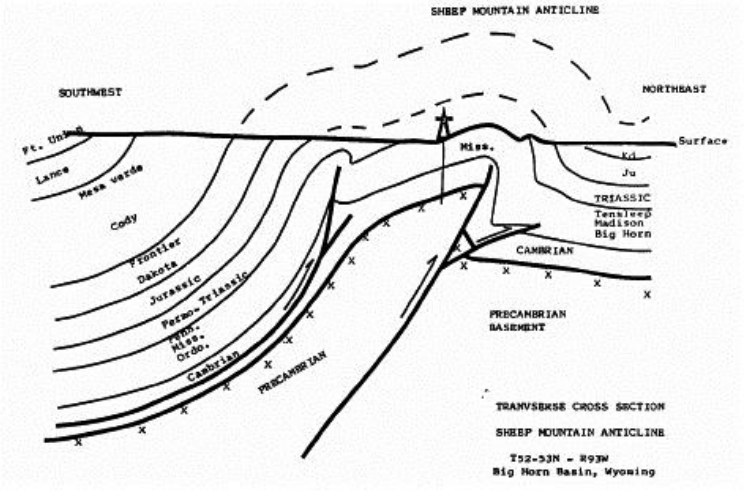

SW-NE trending cross-section through Sheep Mountain anticline from Brown, 1984. Geological constraints are not given, but are most likely surface dips and formation markers from wells. Brown proposes substantial basement folding and a wedge shaped fault zone beneath the forelimb of Sheep Mountain.

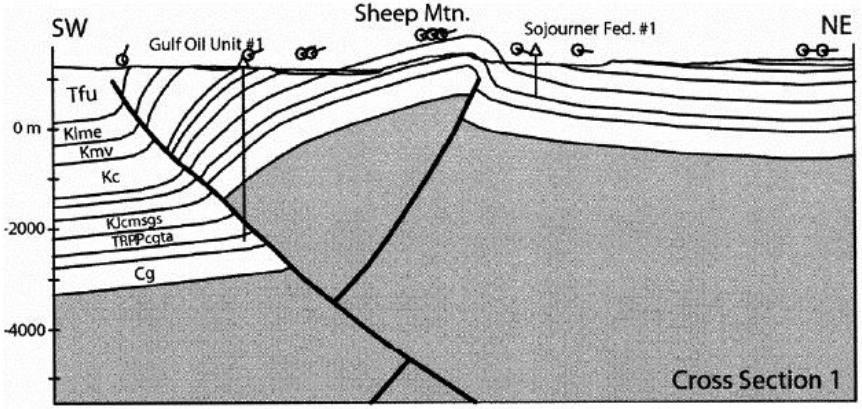

SW-NE trending cross-section through Sheep Mountain anticline from Stanton and Erslev, 2002. Geological constraints are surface dips, formation markers from wells, and three 2D seismic profiles. Stanton and Erslev propose a moderately folded basement. Their kinematic modeling suggests that the Rio thrust fault slipped after slip along the fault beneath Sheep Mountain Anticline had already uplifted the fold.

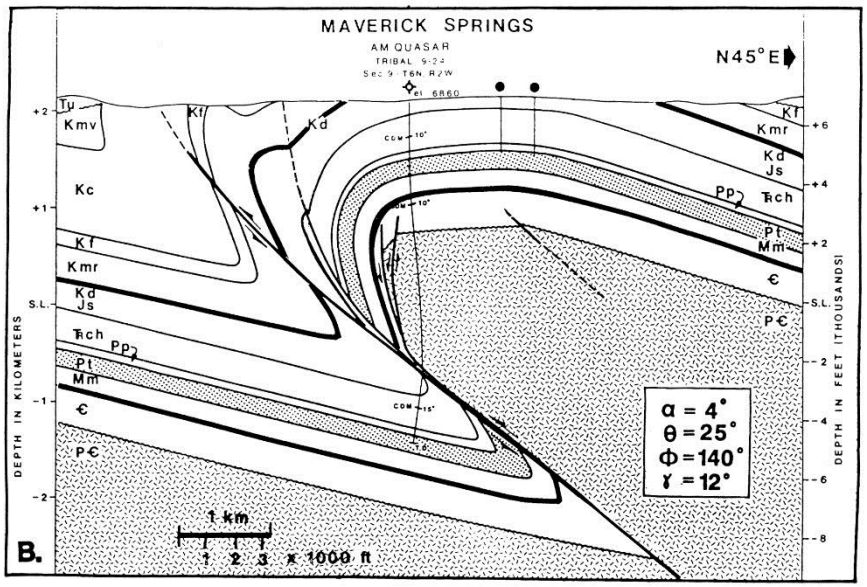

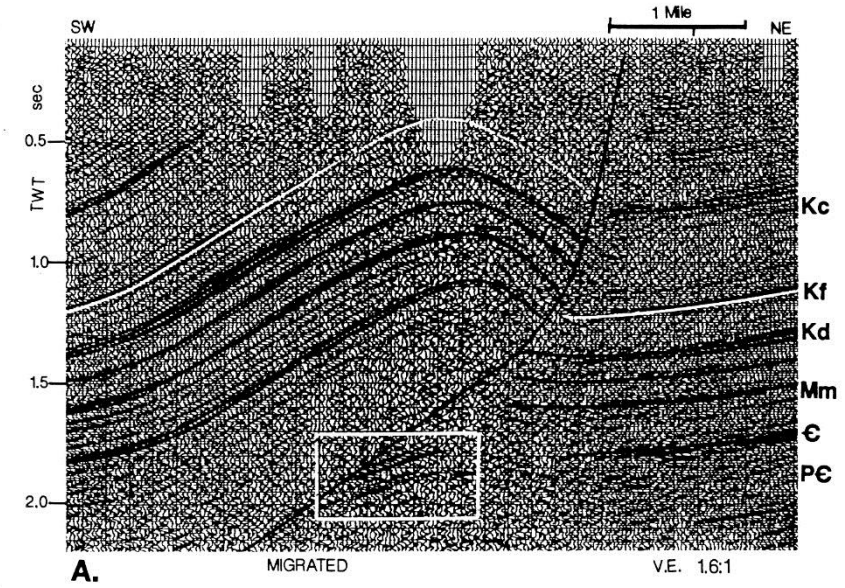

Stone (1993)

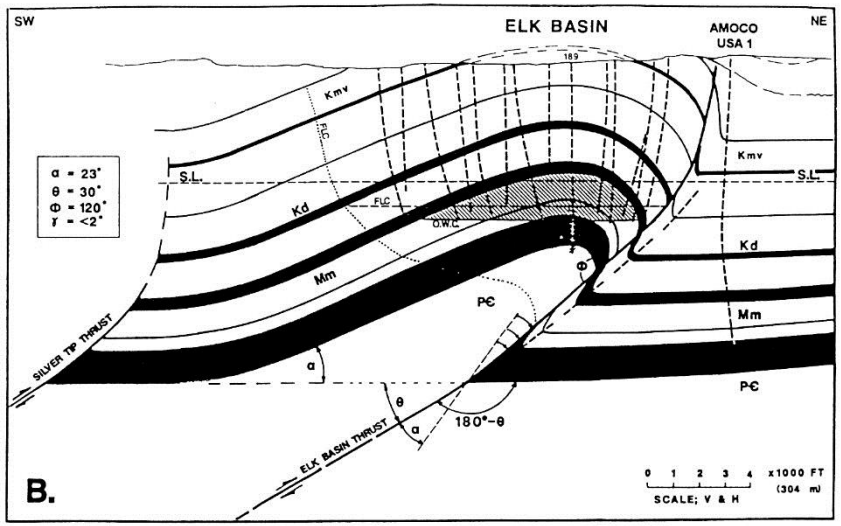

Elk Basin anticline, a mature thrust fold. A: Time-migrated, interpreted seismic profile (600% dynamite, 1969; modified from Weitzel, 1985). TWT is two-way traveltime. B: Structural cross section (see Fig. 15 C) showing well control, common Paleozoic oil pool (diagonally lined with oil-water contact (O.W.C.), a fault-limited chord (FLC) at the base of the Dakota (Kd) horizon, and values for the various angles (modified from Stone, 1983a). S.L. is sea level.

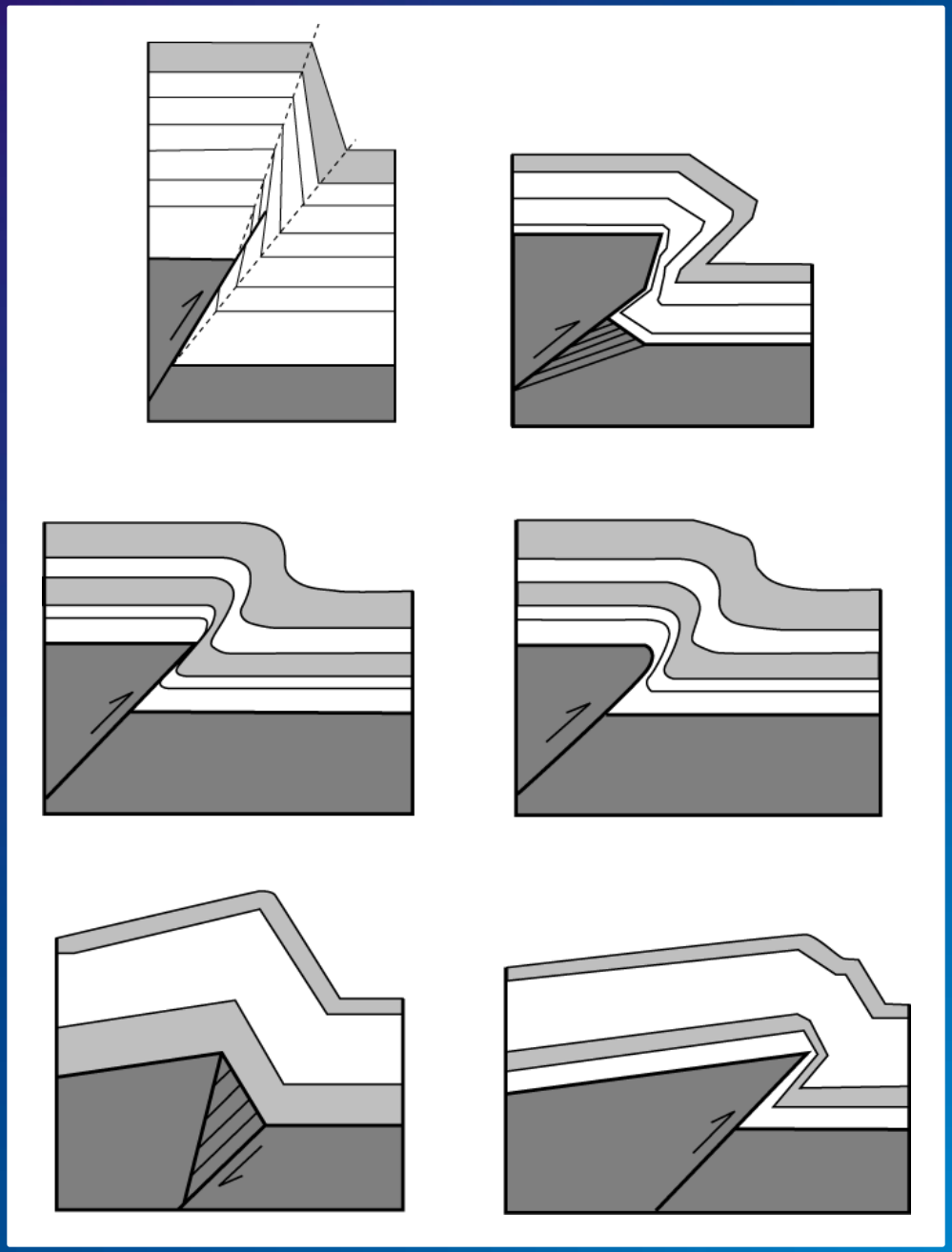

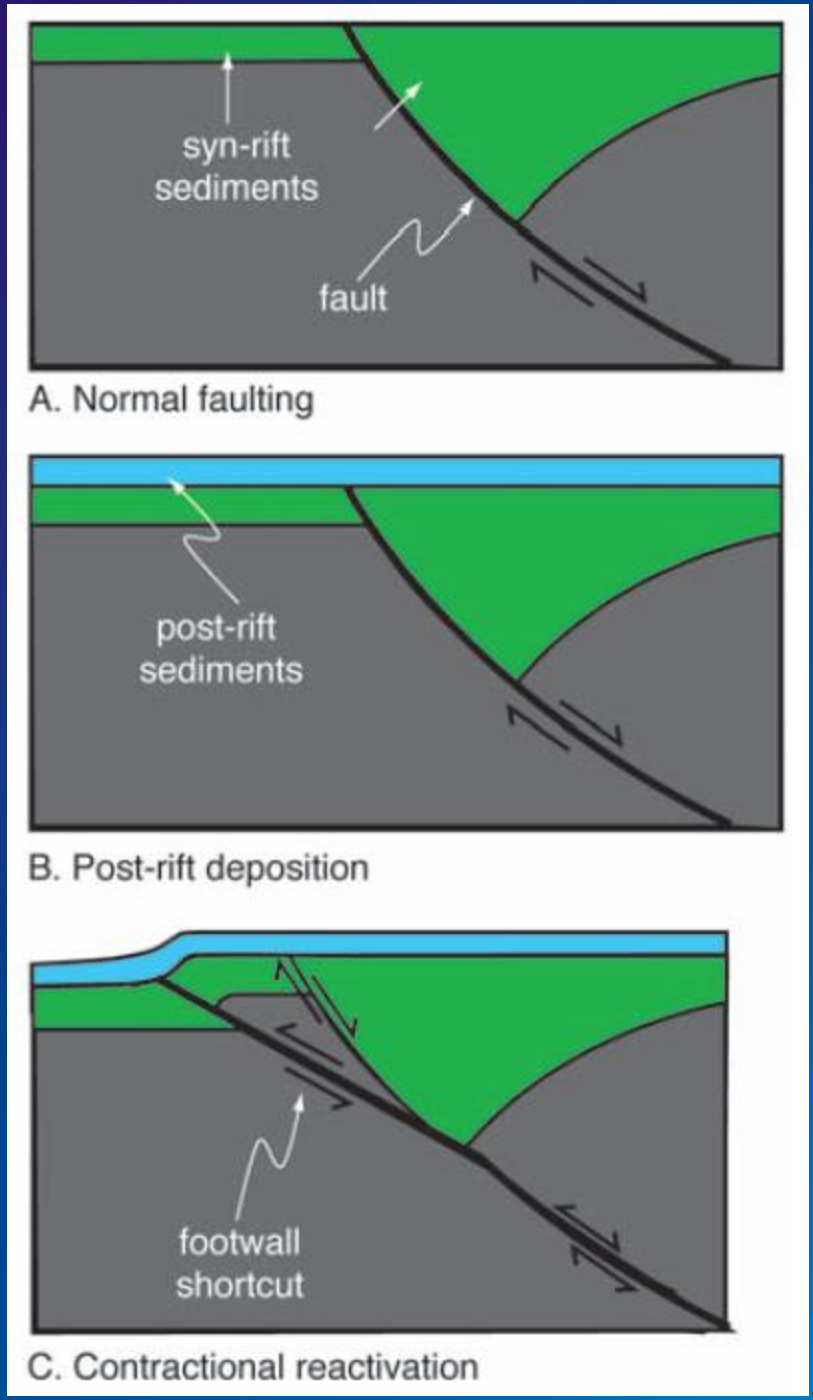
syn-rift
sediments
fault
A. Normal faulting
post-rift
sediments
B. Post-rift deposition
footwall
shortcut
C. Contractional reactivation

Bump (2004)

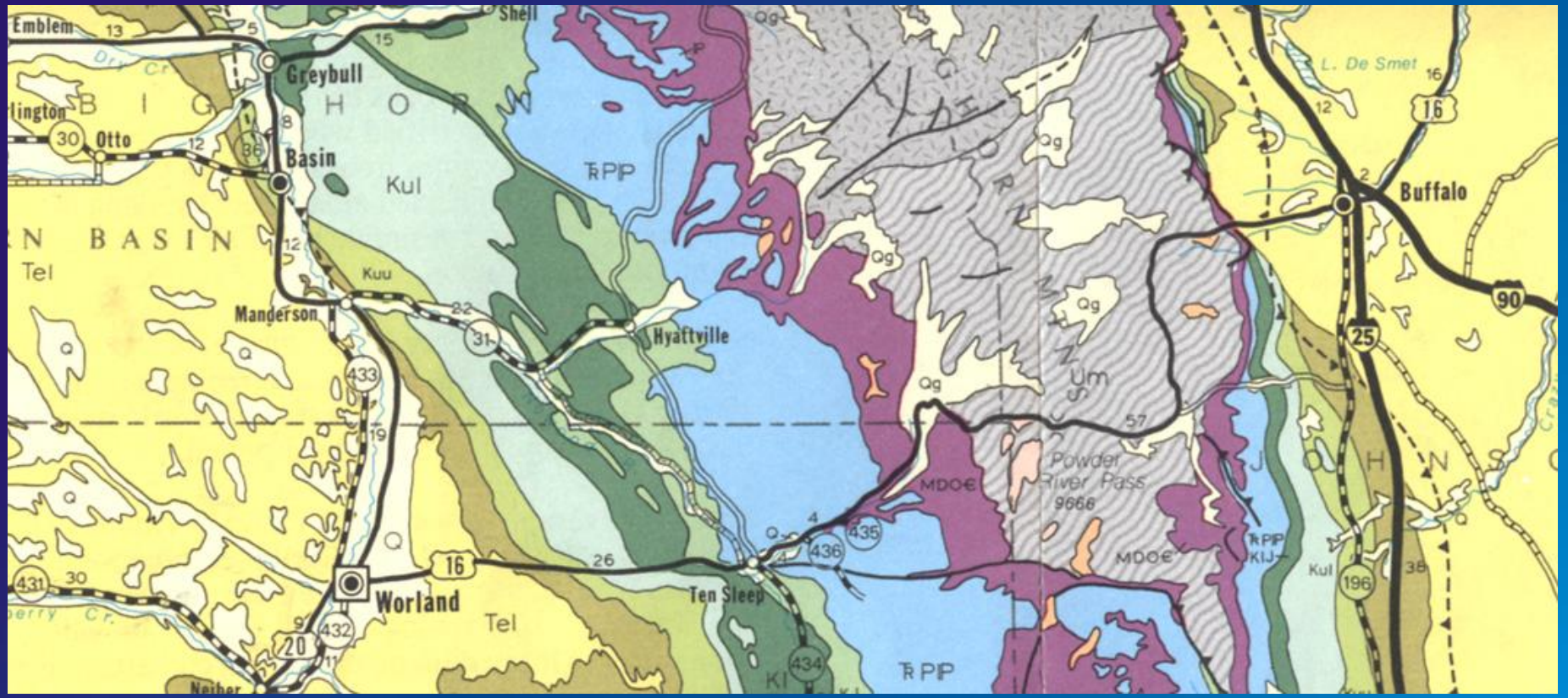
Emblem
Shell
Greybull
Otto
Basin
Kul
TrPP
Tel
Kuu
Manderson
Hyattville
Qg
Um
Powder River Pass
9666
MDOe
Ten Sleep
Worland
Buffalo
L. De Smet
16
90
25
433
435
436
431
432
434
196
20
31

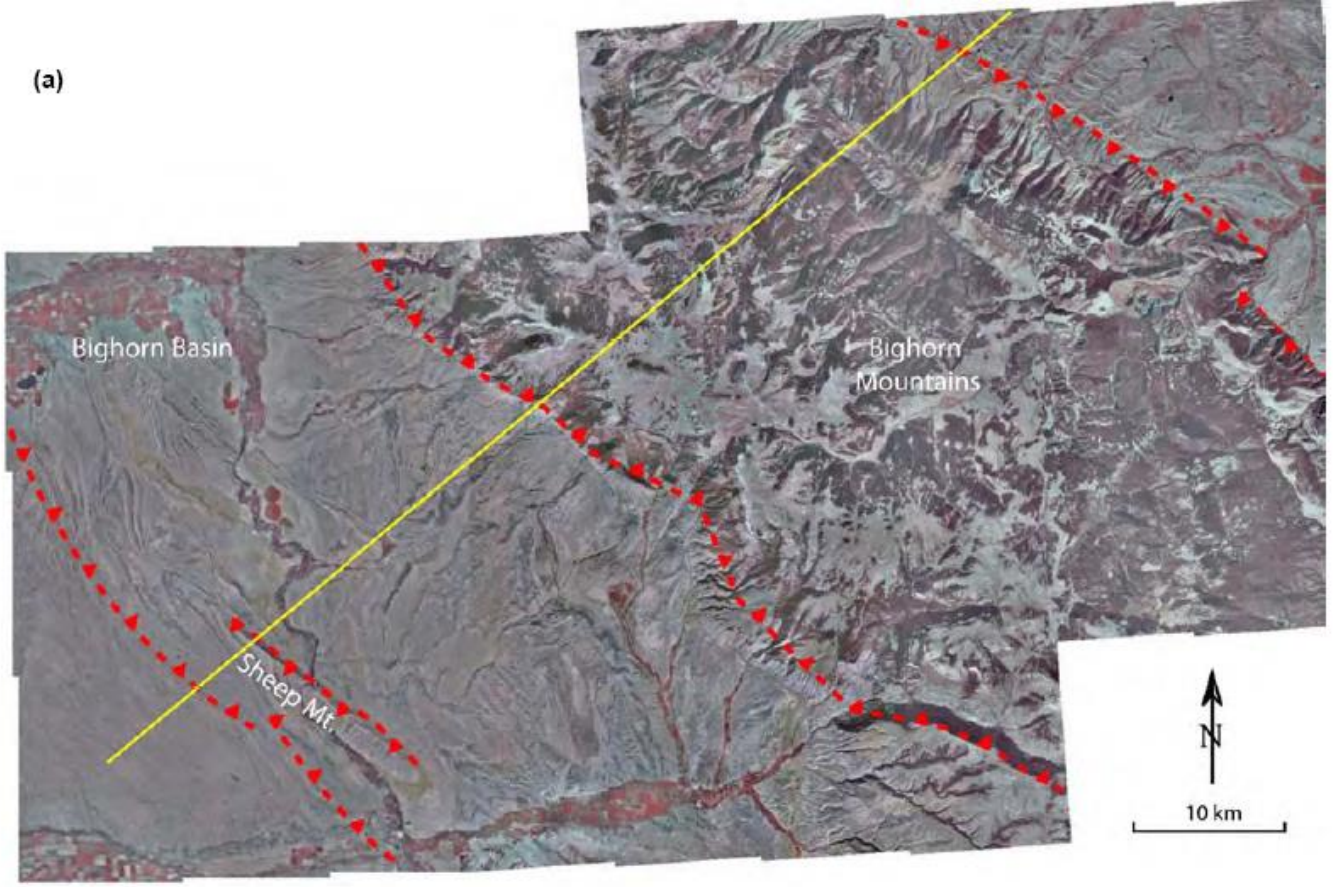
(a)
Bighorn Basin
Bighorn
Mountains
Sheep Mt.
N
10 km

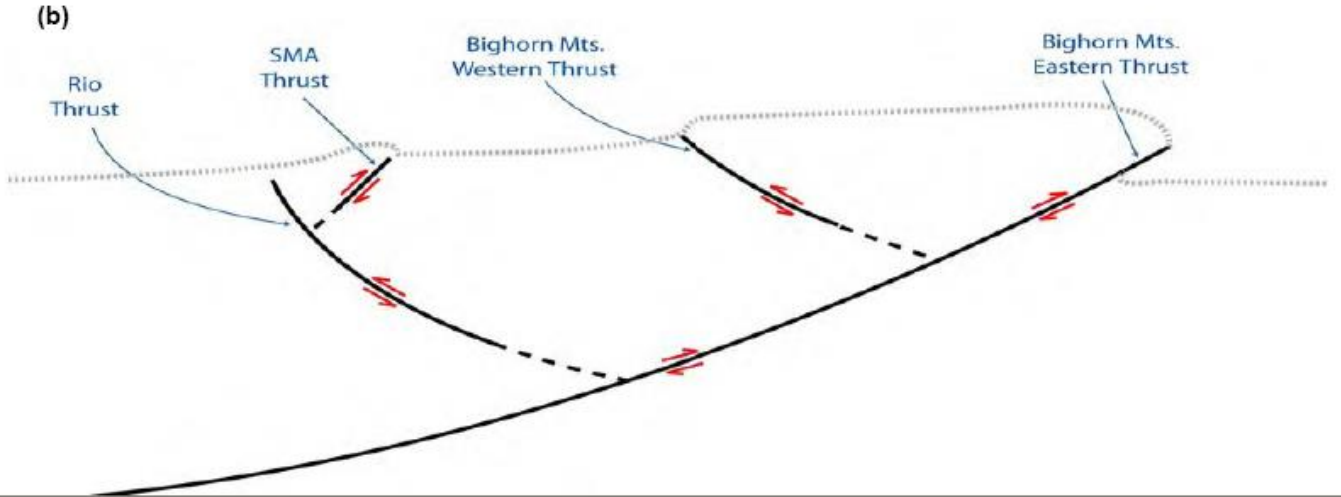
(b)
Rio
Thrust
SMA
Thrust
Bighorn Mts.
Western Thrust
Bighorn Mts.
Eastern Thrust

Basement-Involved, Second-Order Anticlinal Structures

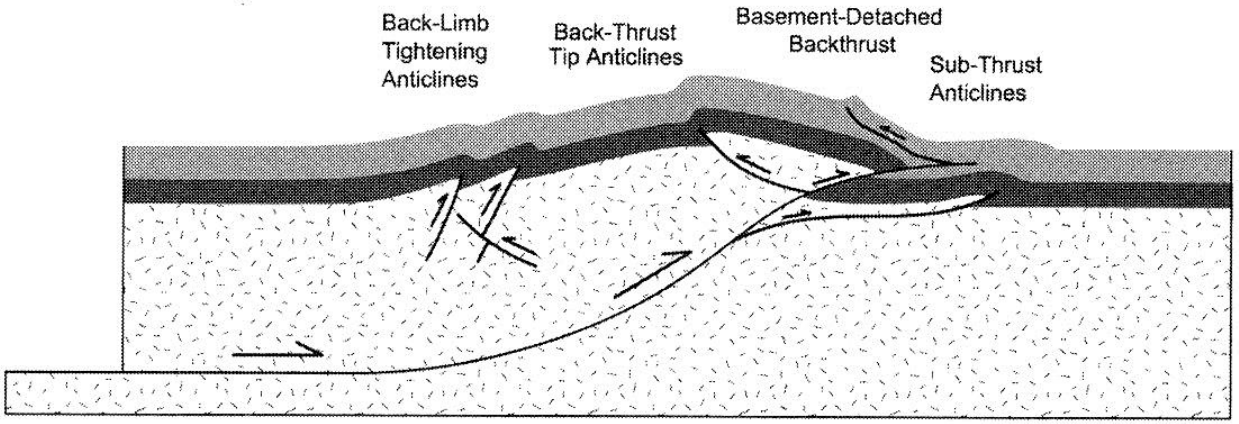

Restored Section

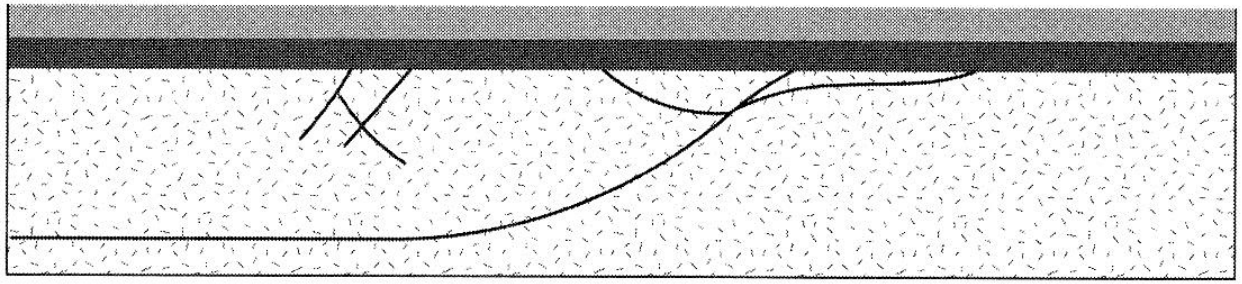

Erslev (2005)

Marshak et al. (2000)

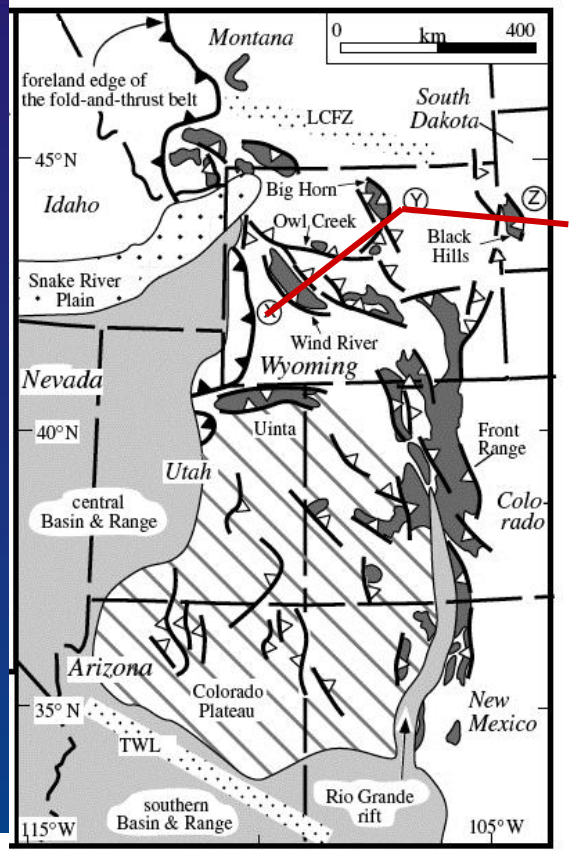

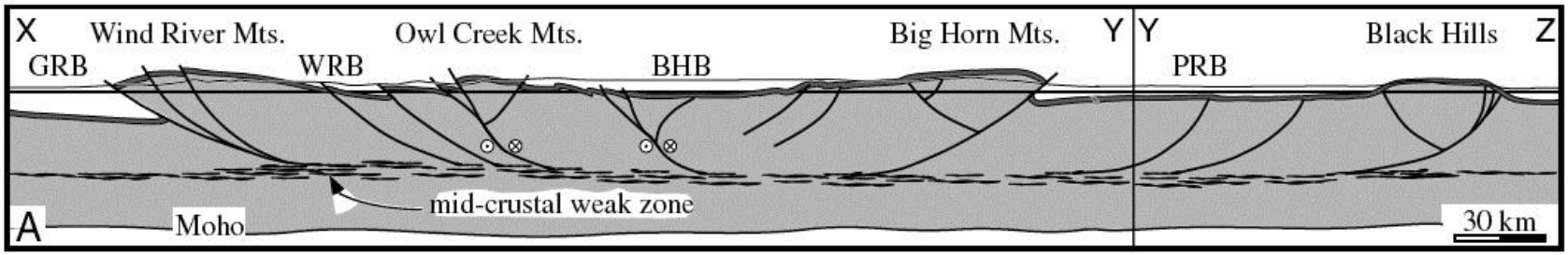

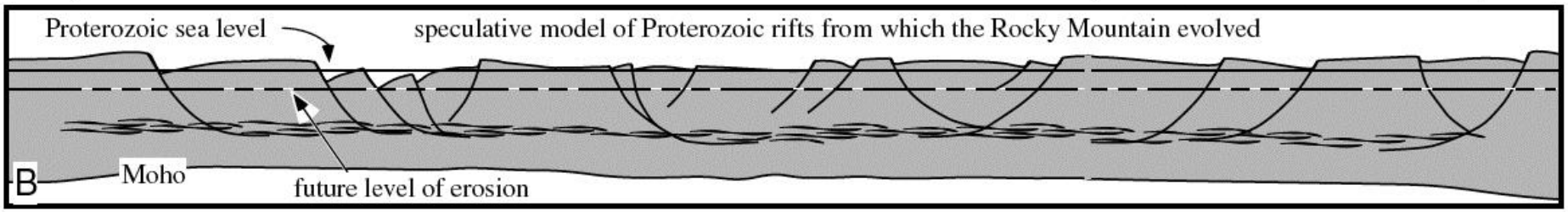

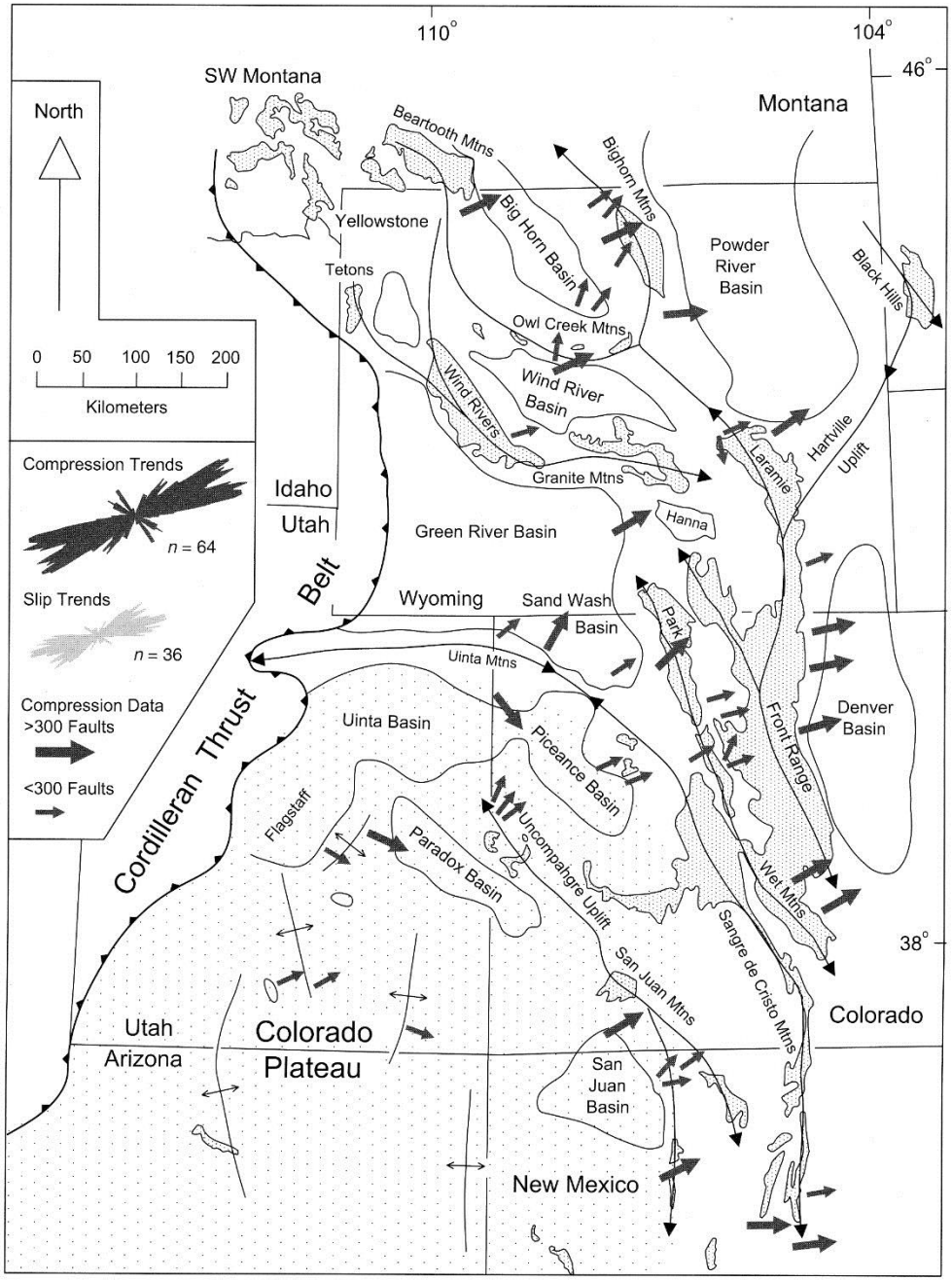

Figure 1. Tectonic map of the Rocky Mountain region showing the major Laramide arches, which are commonly cored by Precambrian crystalline basement exposures (fine stipple), as well as the adjoining Colorado Plateau (coarse stipple) and Cordilleran thrust belt. Average compression directions from minor faults are shown as arrows; smoothed (10°) rose diagrams show all compression and slip directions from Table 2.

Erslev (2009)

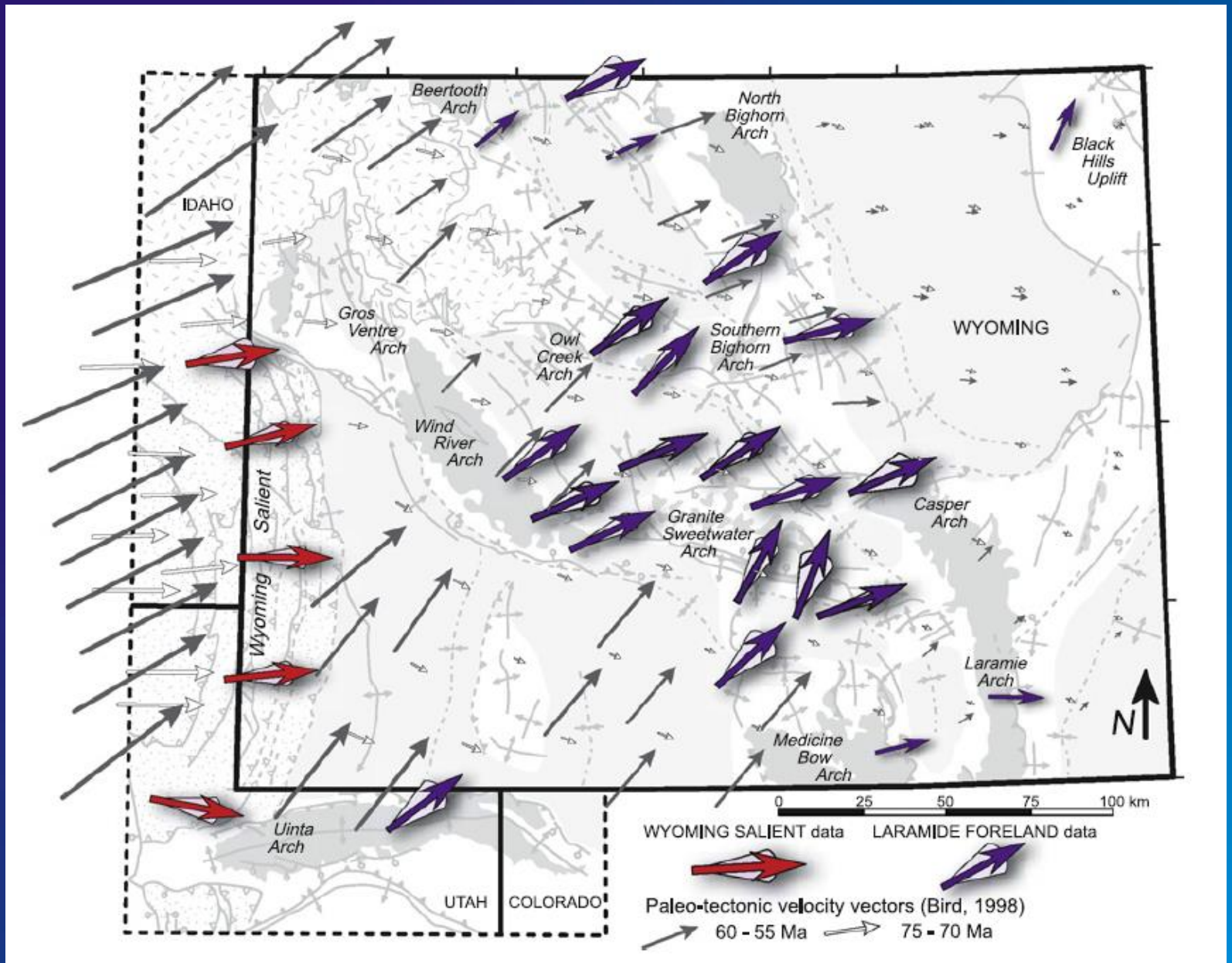

(Weil and Yonkee, 2012)

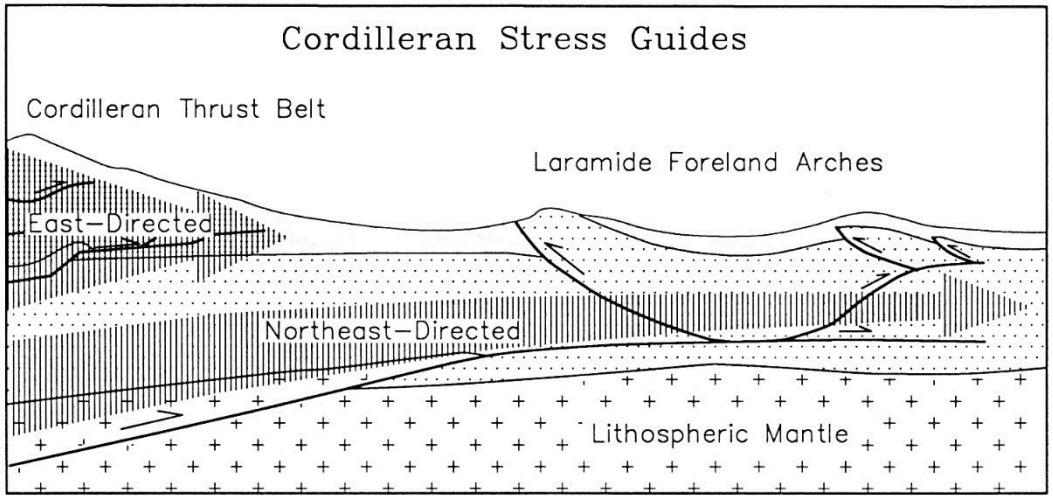

Schematic cartoon showing multiple stress guides and multilevel detachment during Cordilleran-Laramide lateral compression.

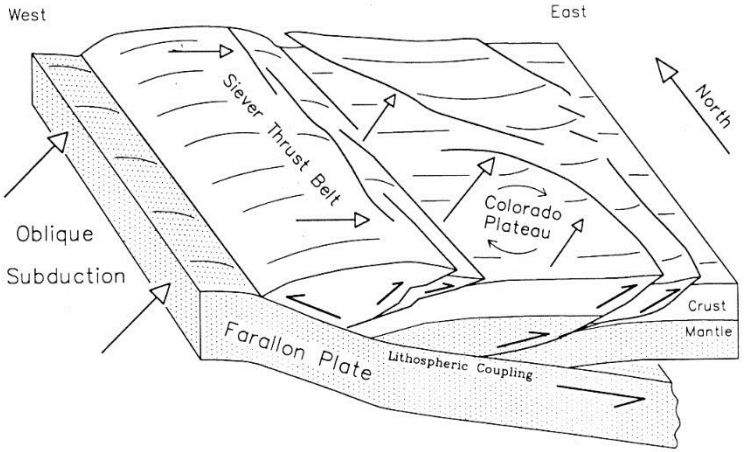

Schematic block diagram showing the development of Laramide structures by crustal detachment during lithospheric coupling in a low-angle subduction west of the Rockies. Note that variable slip on the detachment could explain the rotation of the Colorado Plateau.

Erslev (1993)

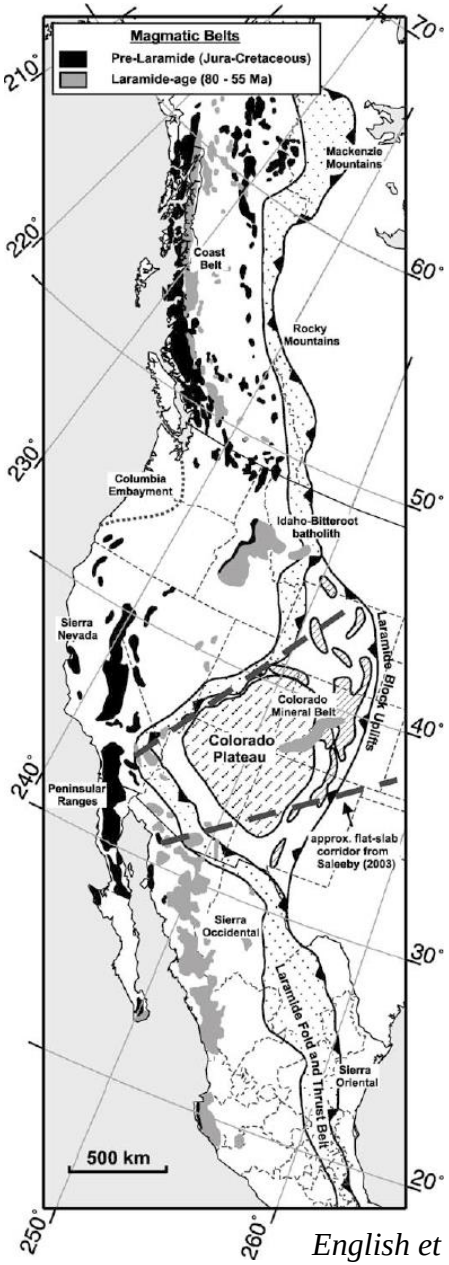

English et al., 1993

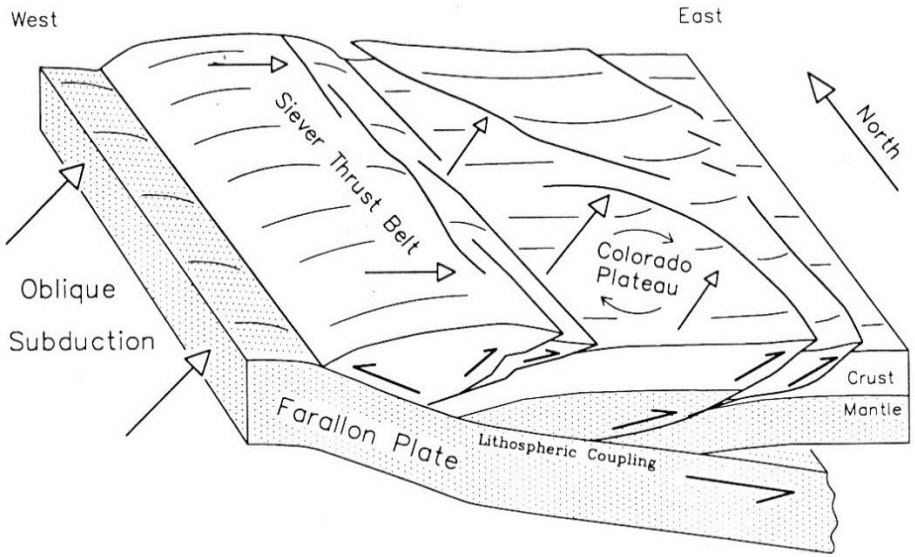

Erslev, 1993

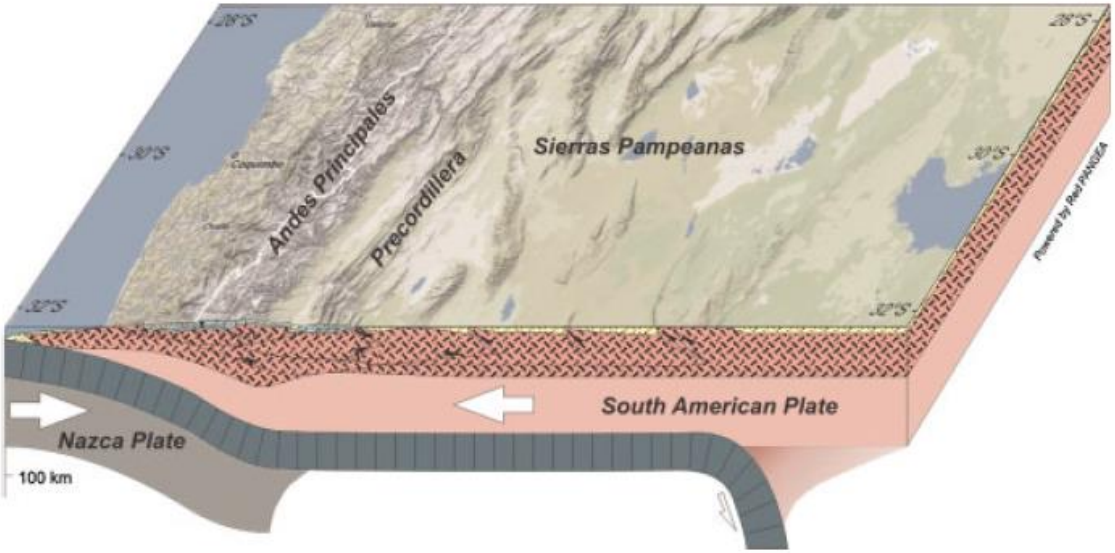

Ramos, 2010

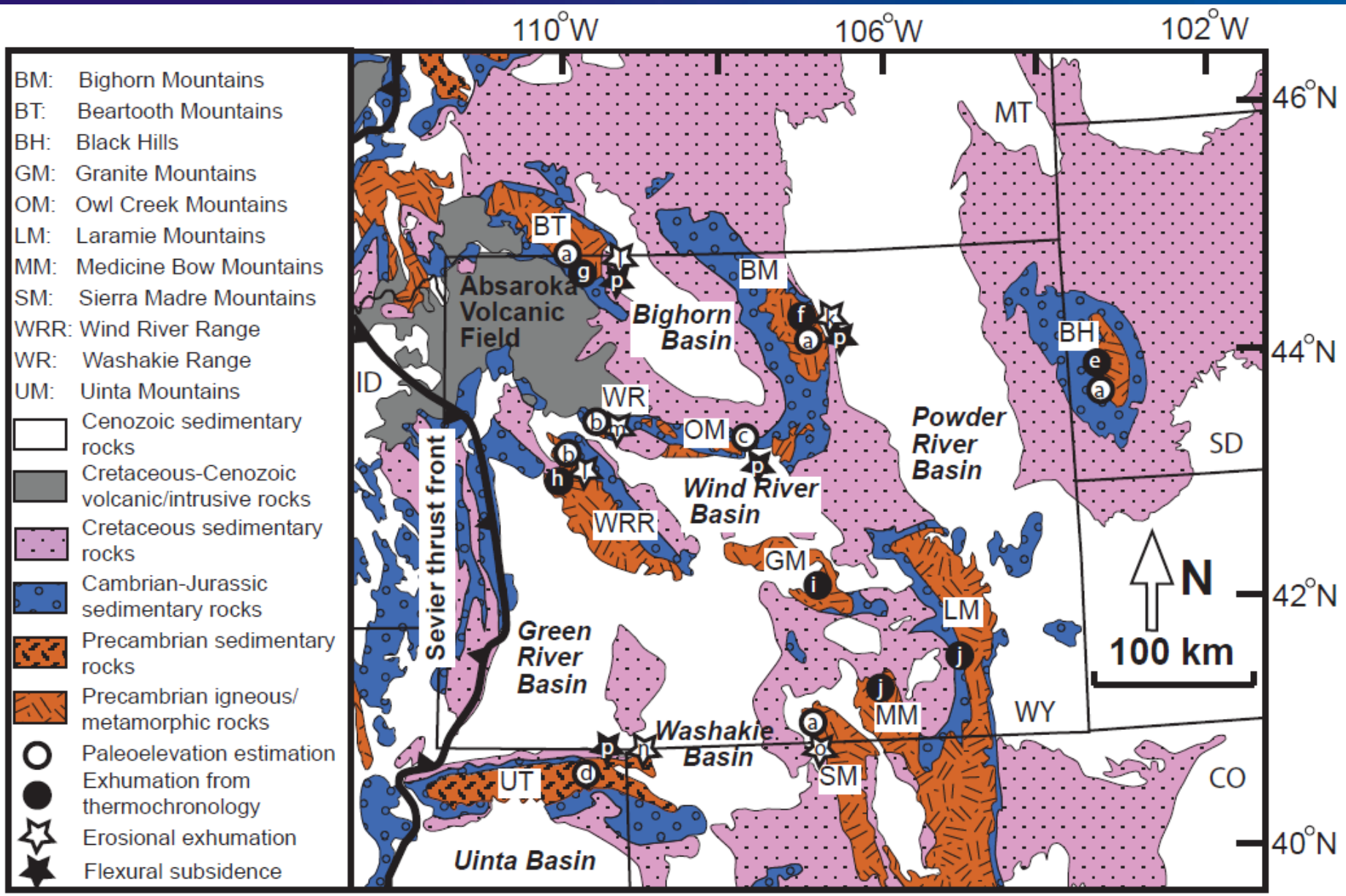
110°W
106°W
102°W
46°N
44°N
42°N
40°N
BM: Bighorn Mountains
BT: Beartooth Mountains
BH: Black Hills
GM: Granite Mountains
OM: Owl Creek Mountains
LM: Laramie Mountains
MM: Medicine Bow Mountains
SM: Sierra Madre Mountains
WRR: Wind River Range
WR: Washakie Range
UM: Uinta Mountains
Cenozoic sedimentary rocks
Cretaceous-Cenozoic volcanic/intrusive rocks
Cretaceous sedimentary rocks
Cambrian-Jurassic sedimentary rocks
Precambrian sedimentary rocks
Precambrian igneous/ metamorphic rocks
Paleoelevation estimation
Exhumation from thermochronology
Erosional exhumation
Flexural subsidence
MT
ID
WY
SD
CO
BT
BM
BH
WR
OM
WRR
GM
LM
MM
SM
UT
Absaroka Volcanic Field
Bighorn Basin
Powder River Basin
Wind River Basin
Green River Basin
Washakie Basin
Uinta Basin
Sevier thrust front
N
100 km

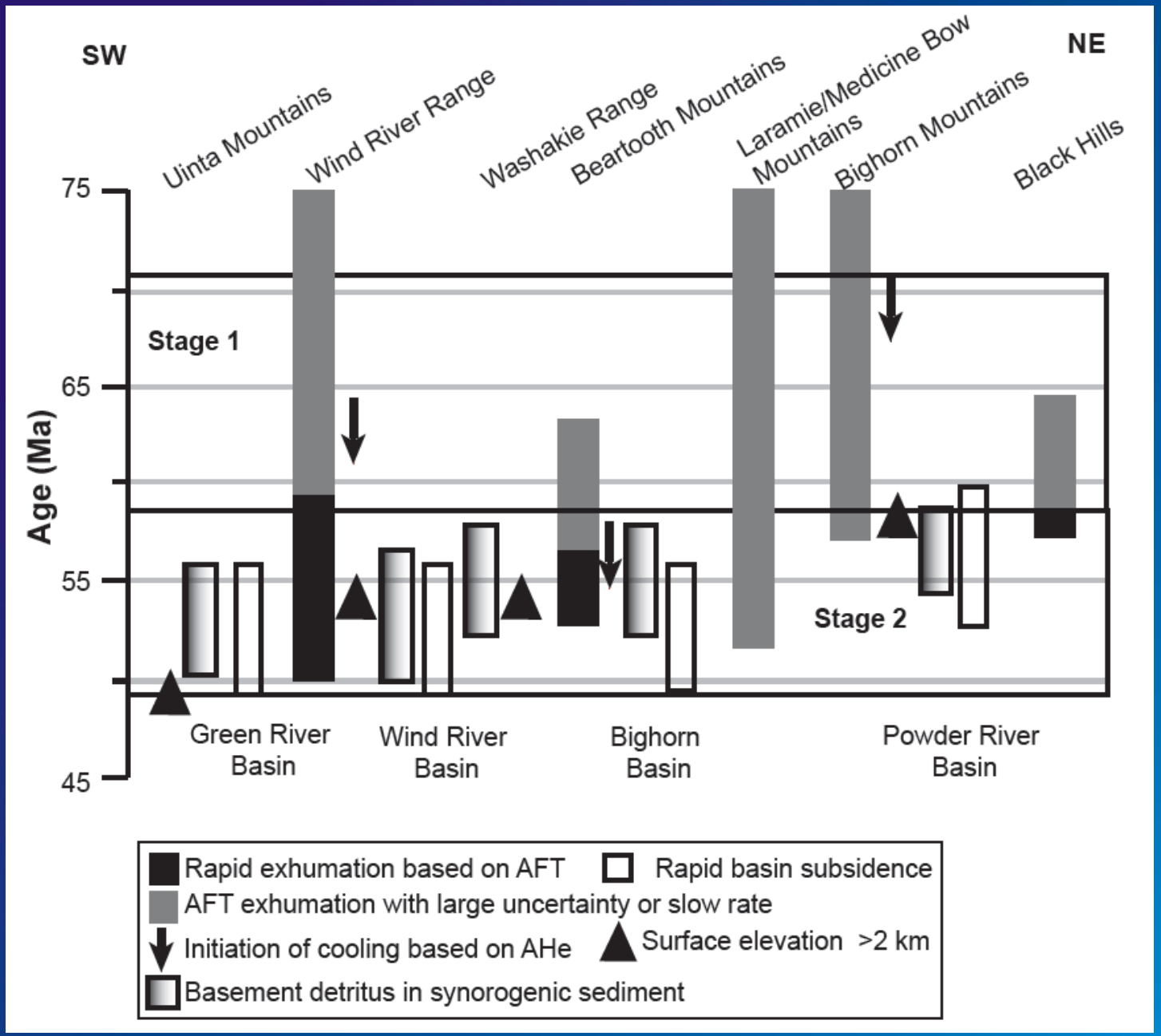

Fan and Carrapa, 2014

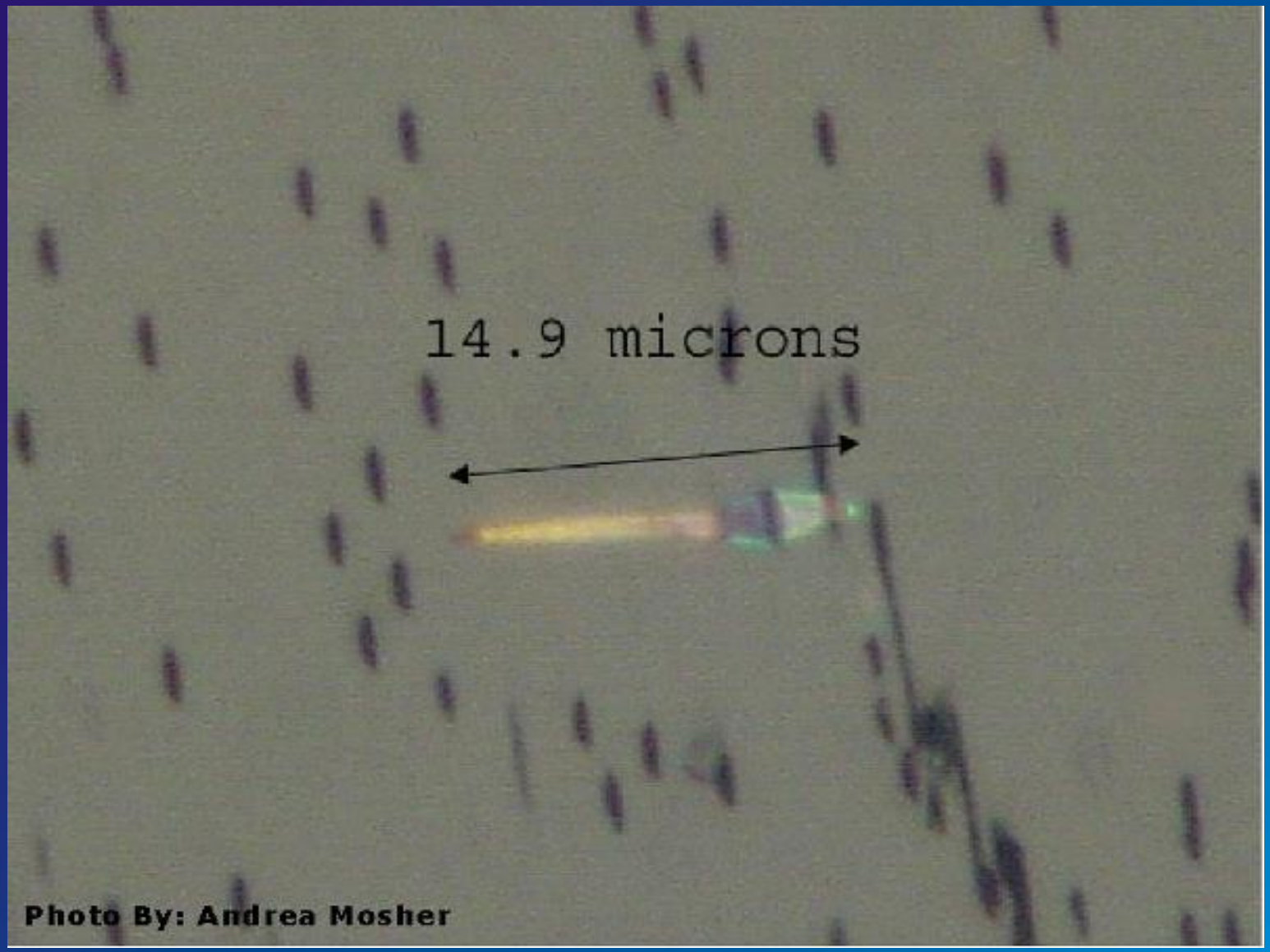
14.9 microns
Photo By: Andrea Mosher

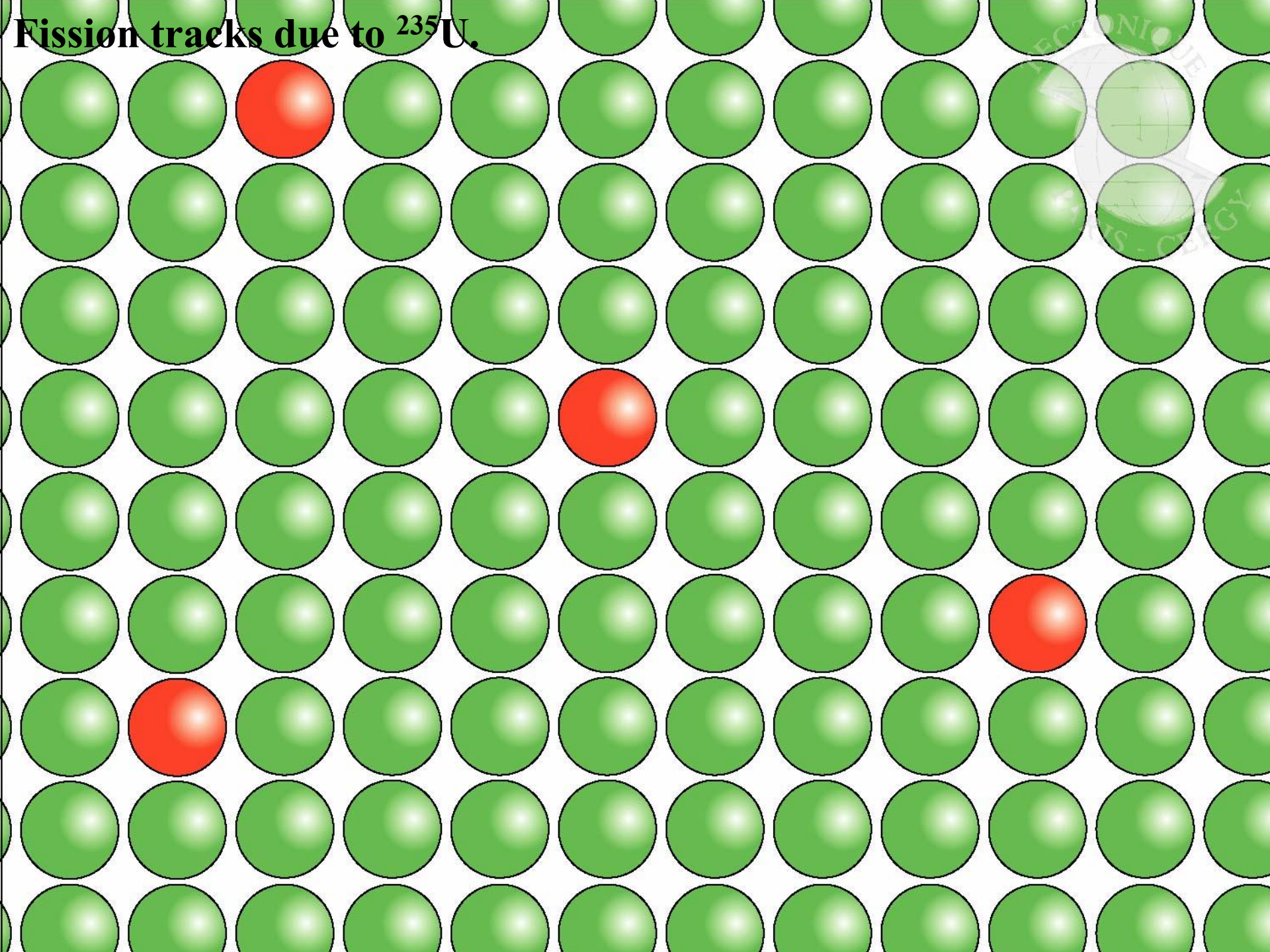
Fission tracks due to ^{235}U.

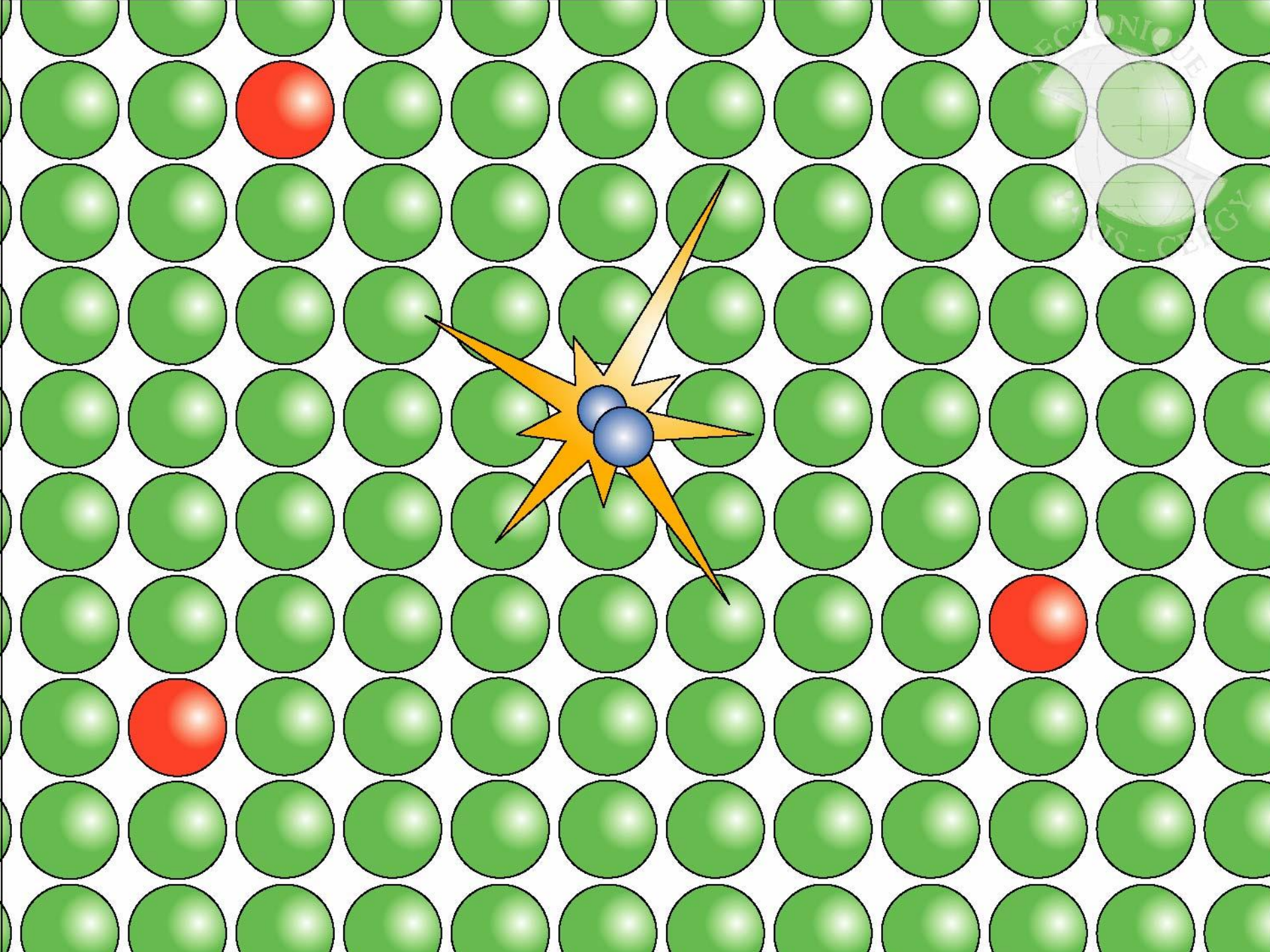

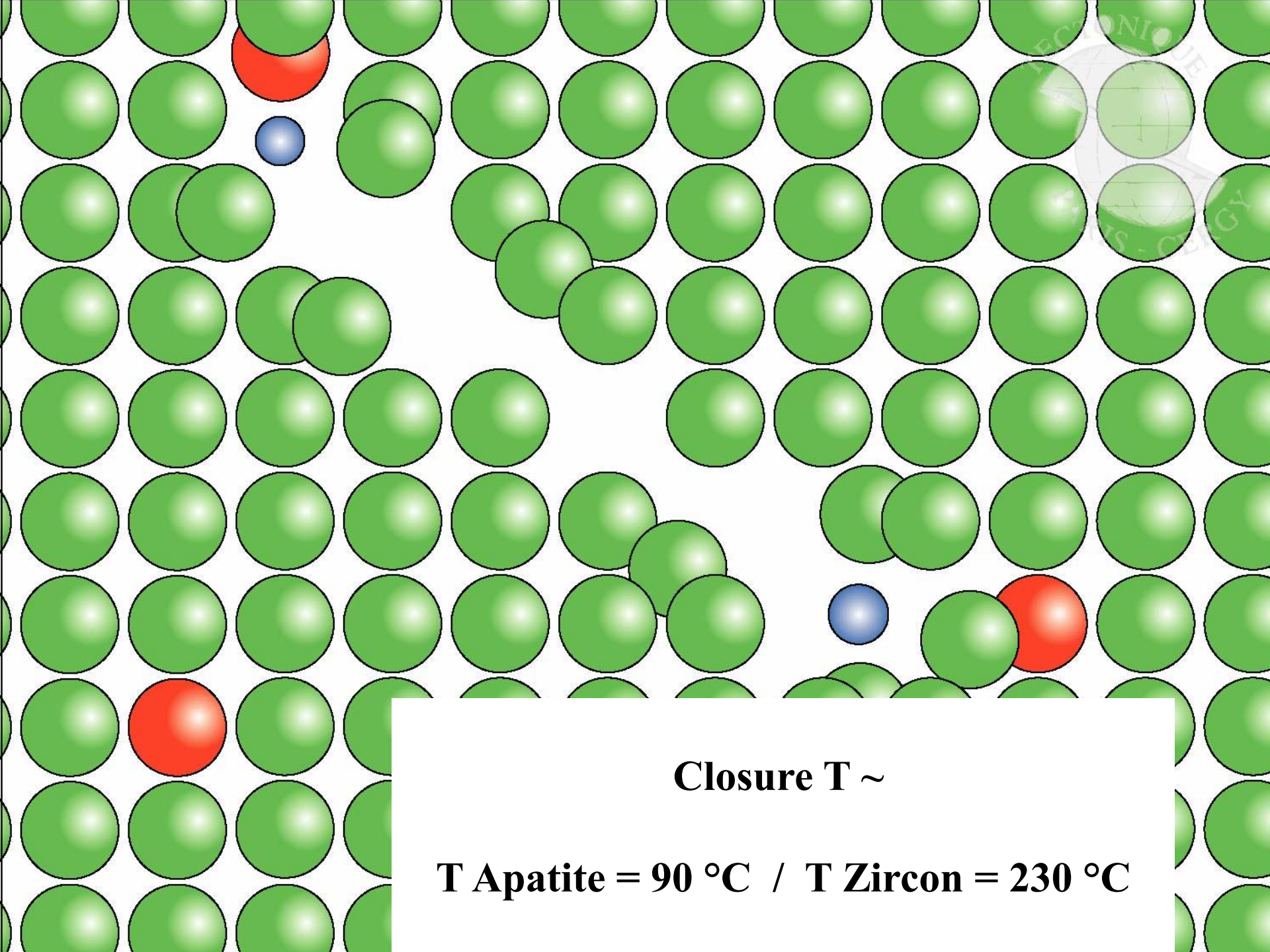

Closure T ~

T Apatite = 90 °C / T Zircon = 230 °C

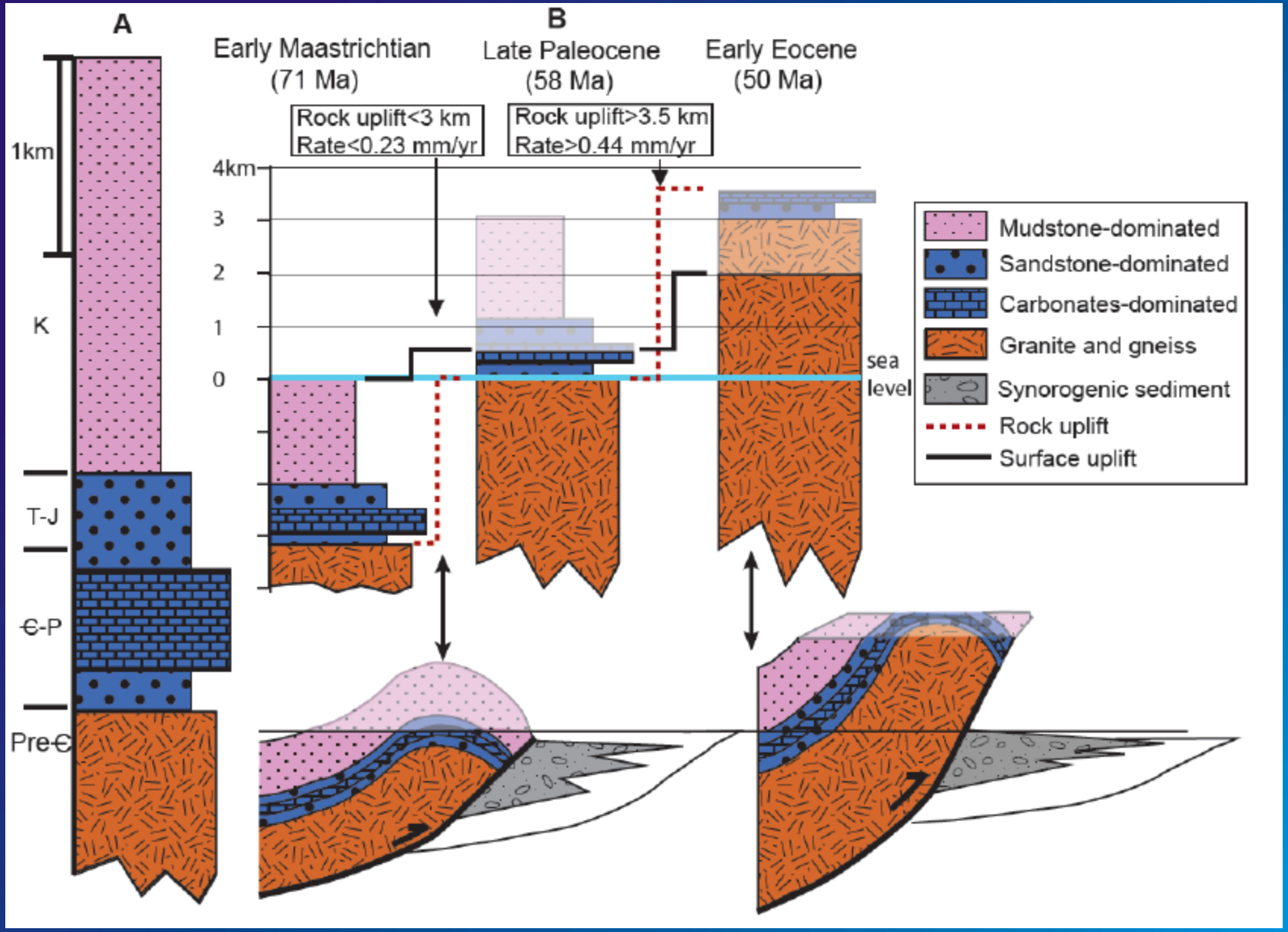

Fan and Carrapa, 2014

Basement control on along-strike variations of fold-and-thrust belts : the Taiwan case

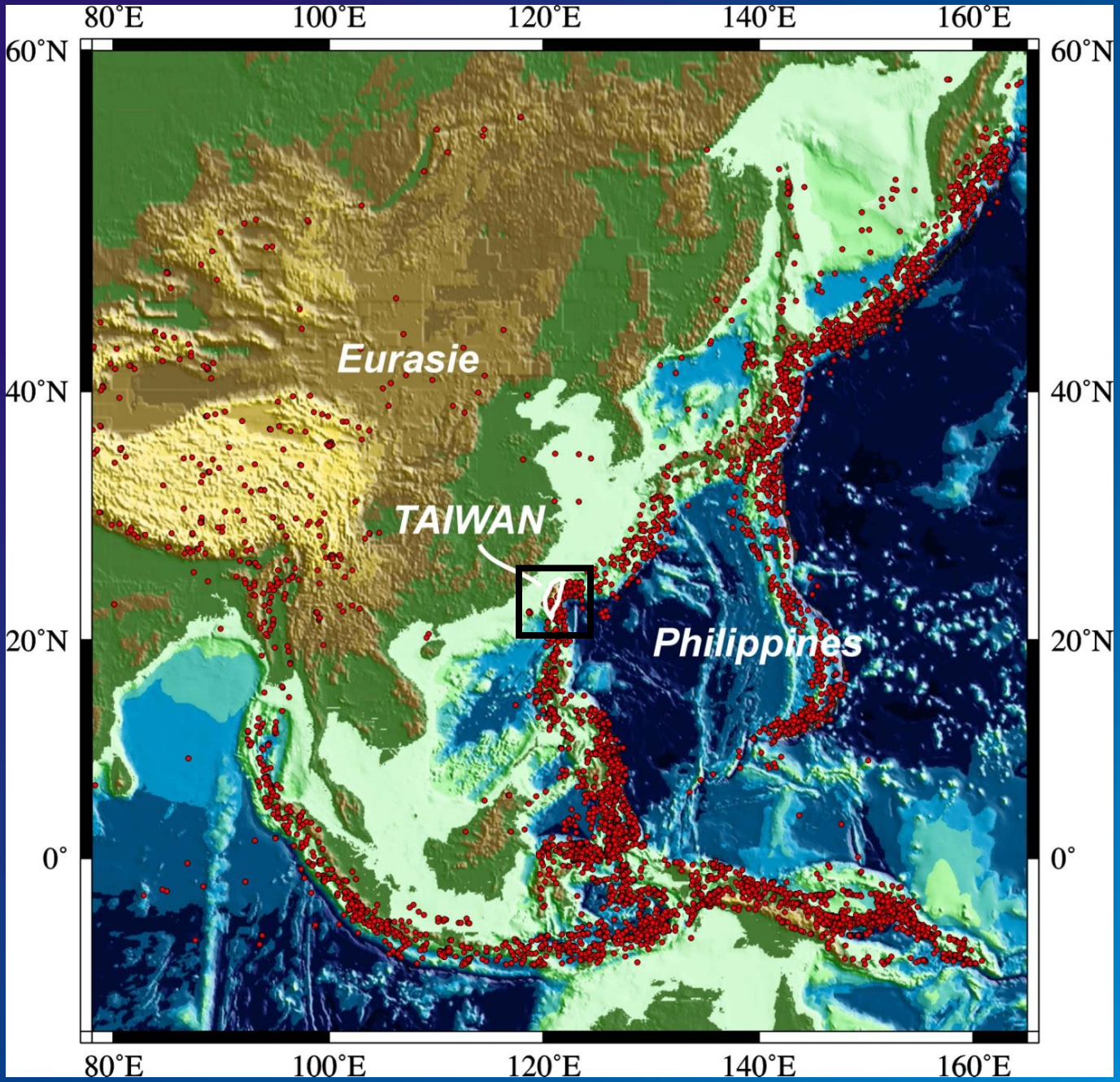
80°E
100°E
120°E
140°E
160°E
60°N
40°N
20°N
0°
Eurasie
TAIWAN
Philippines

A Plio-Pleistocene collision between the N-S Luzon volcanic arc and the ENE Paleogene chinese continental passive margin

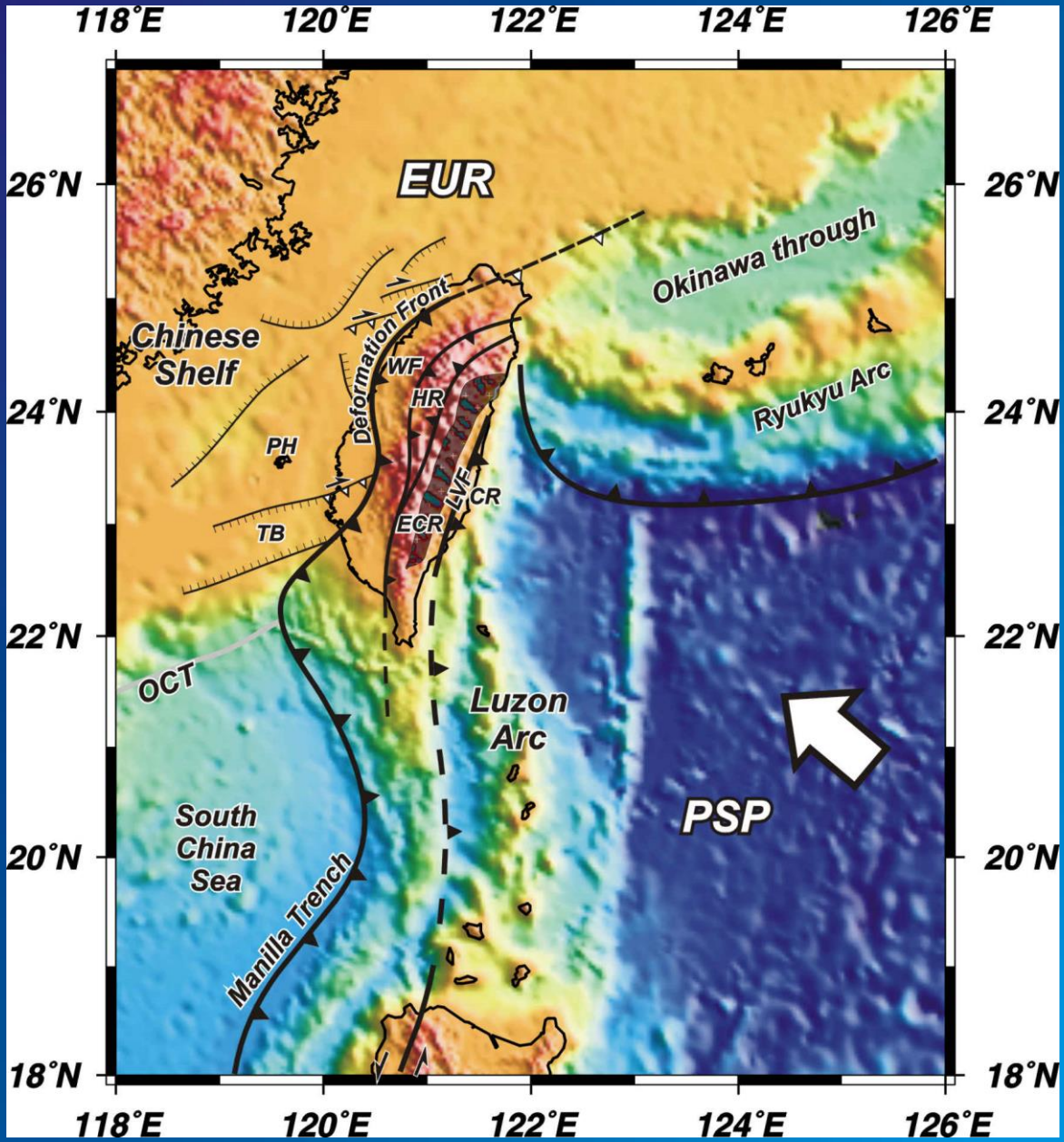

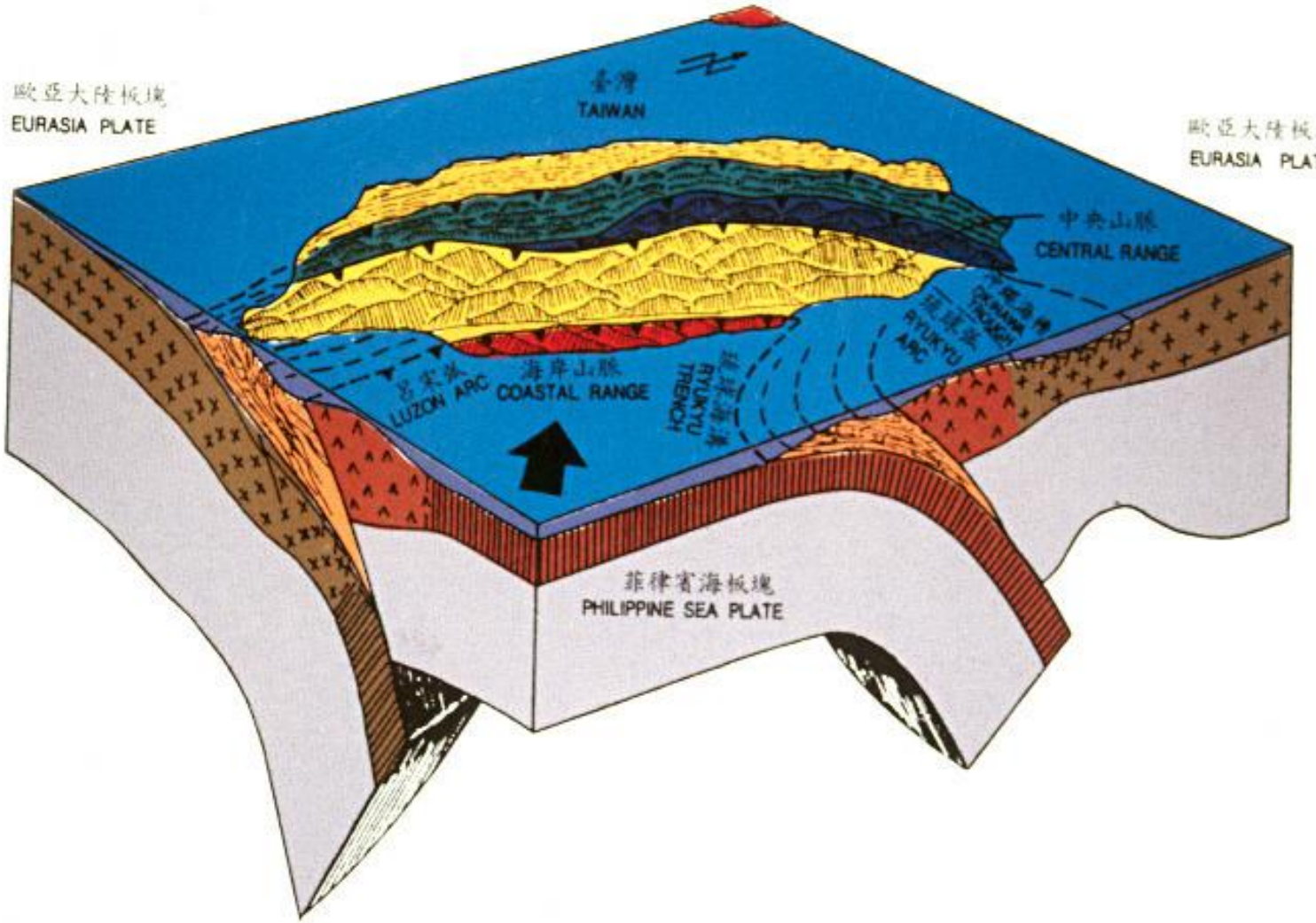

(Angelier, 1986)

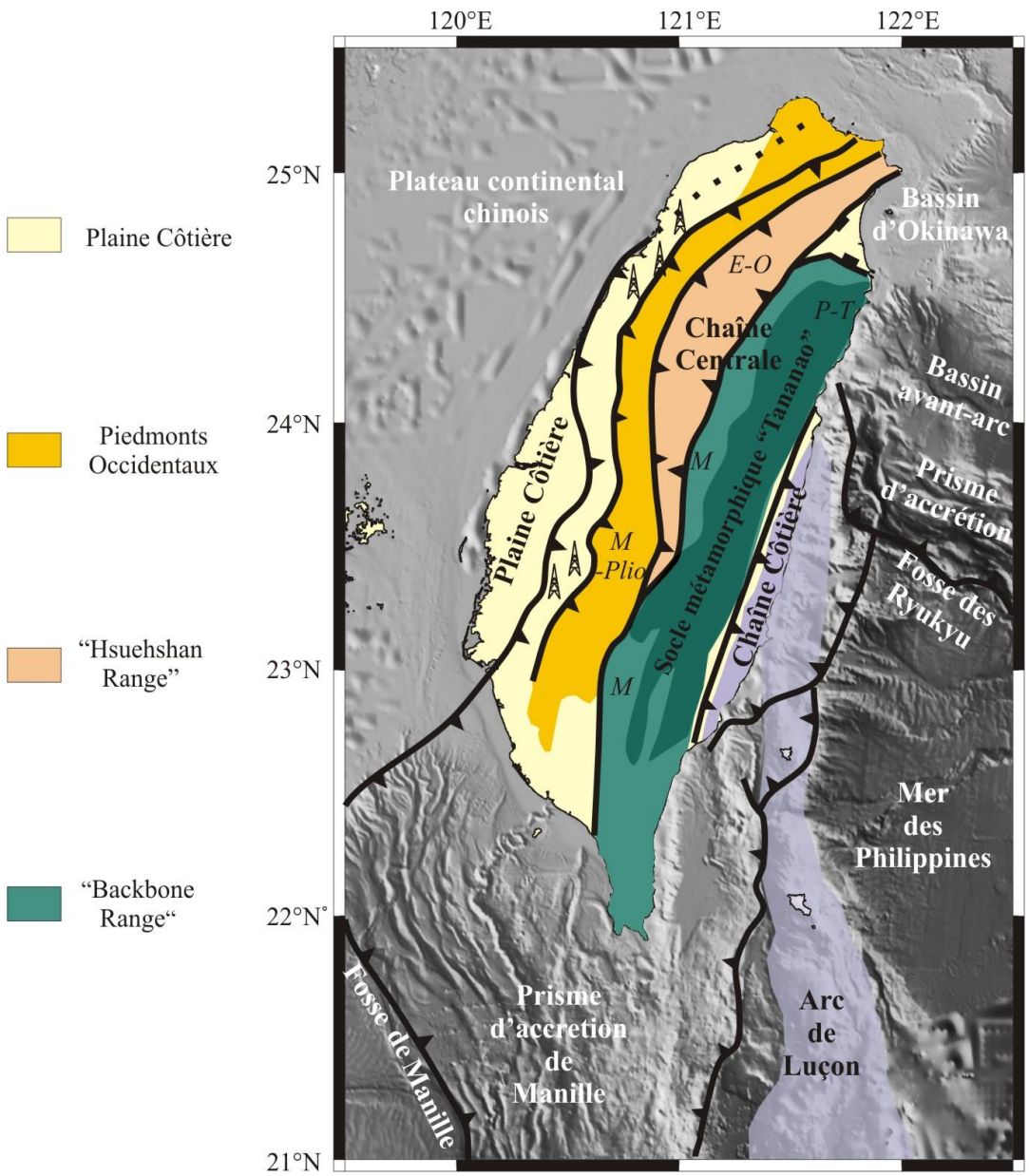
120°E
121°E
122°E
25°N
24°N
23°N
22°N
21°N
Plaine Côtière
Piedmonts Occidentaux
"Hsuehshan Range"
"Backbone Range"
Plateau continental chinois
Bassin d'Okinawa
E-O
P-T
Chaîne Centrale
Bassin avant-arc
Prisme d'accrétion
Fosse des Ryukyu
Plaine Côtière
M
M -Plio
M
Socle métamorphique "Tananao"
Chaîne Côtière
Mer des Philippines
Fosse de Manille
Prisme d'accretion de Manille
Arc de Luçon

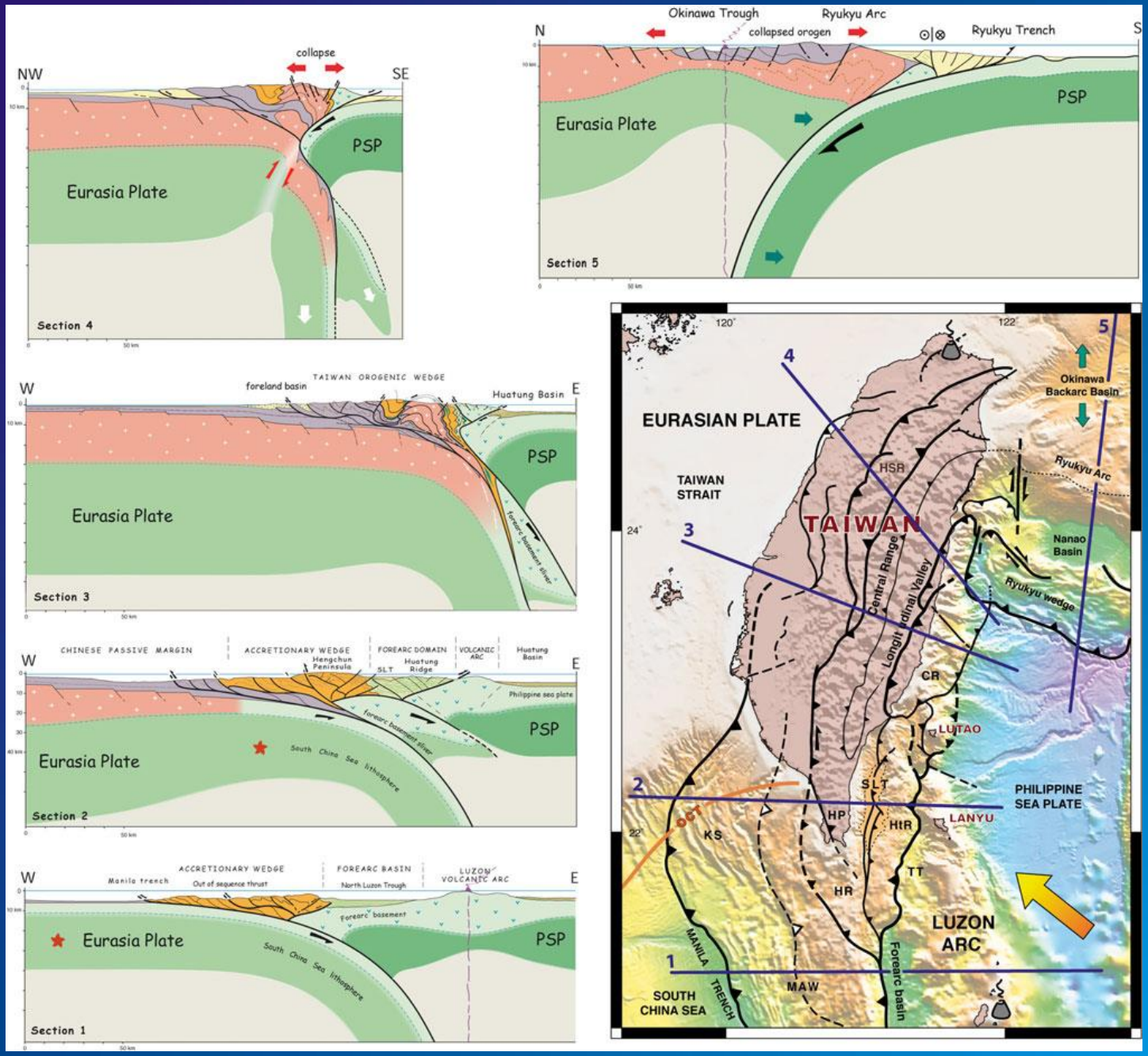

(Molli and Malavieille, 2011)

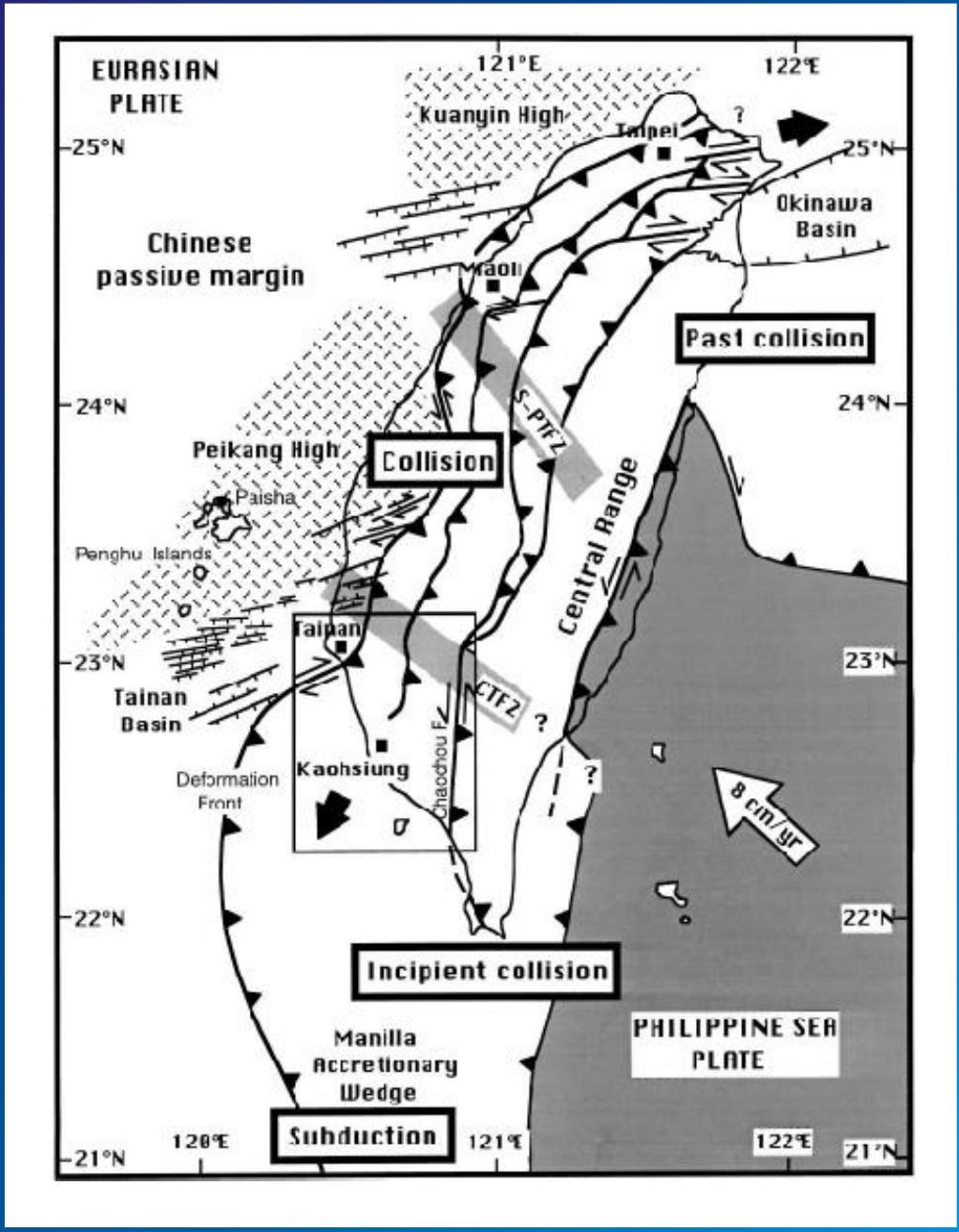

(Lacombe et al., 2001; Modified after Lallemand and Tsien, 1997)

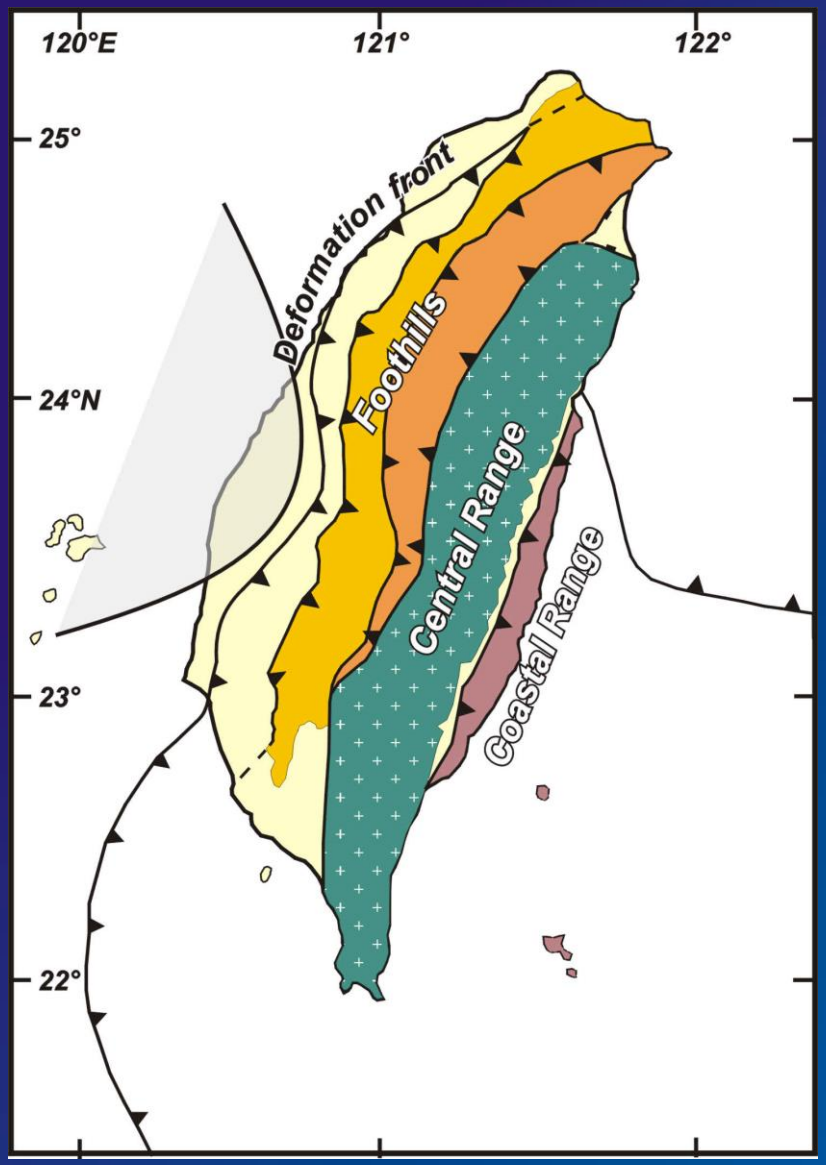
120°E
121°
122°
25°
24°N
23°
22°
Deformation front
Foothills
Central Range
Coastal Range

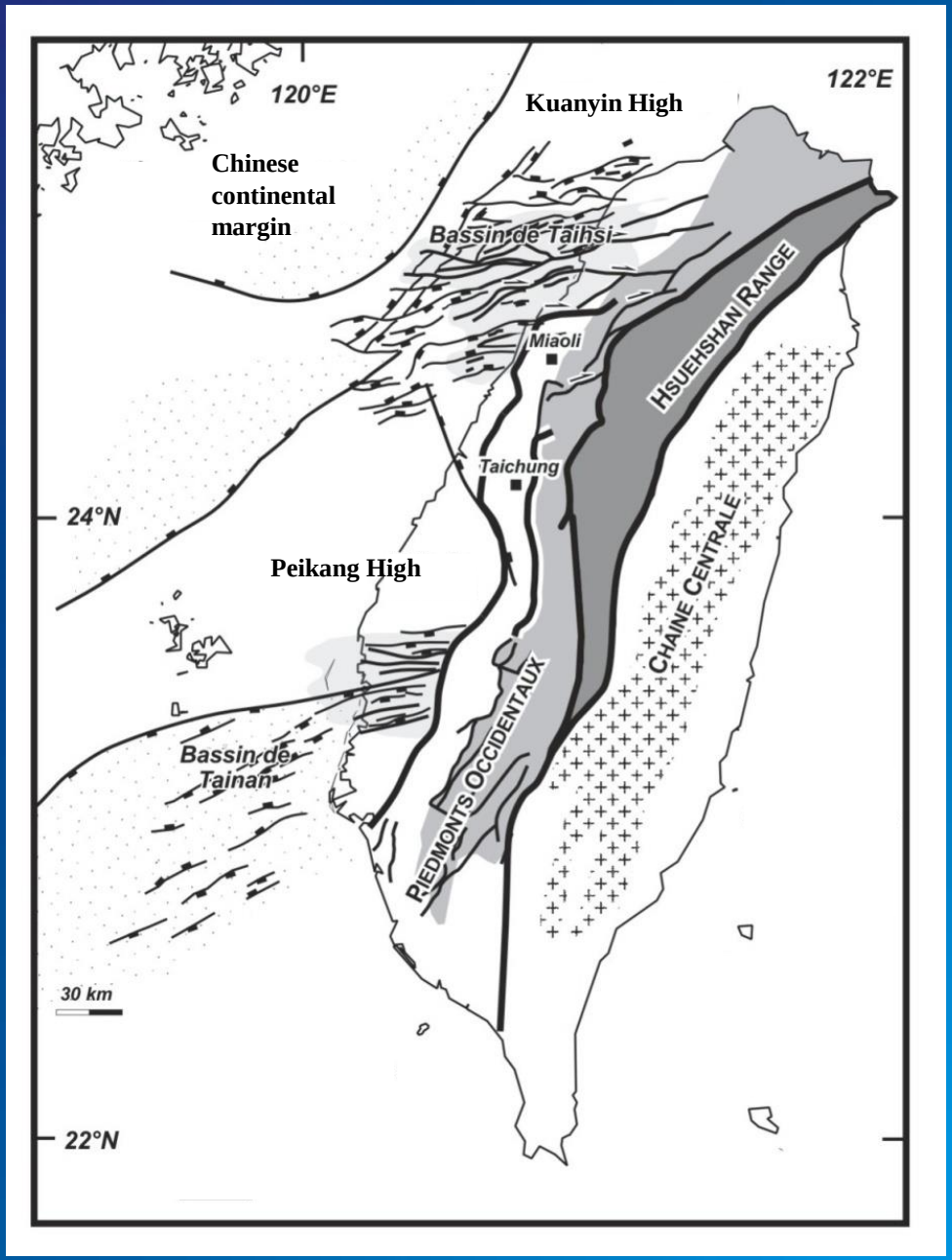
120°E
122°E
Kuanyin High
Chinese continental margin
Bassin de Taihsi
Miaoli
HSUEHSHAN RANGE
Taichung
24°N
Peikang High
CHAINE CENTRALE
PIEDMONTS OCCIDENTAUX
Bassin de Tainan
30 km
22°N

Steady critical wegde model for Taiwan

Critically tapered wegde (with thin-skinned approximation)

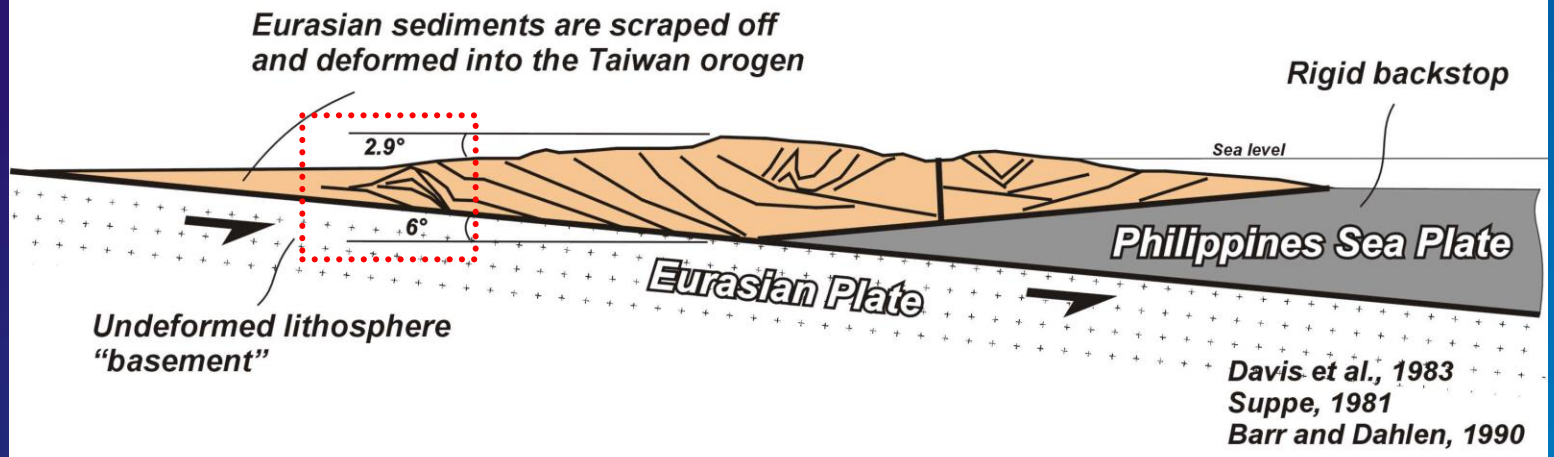

+

Wedge shape (taper) unchanged through time

Steady development

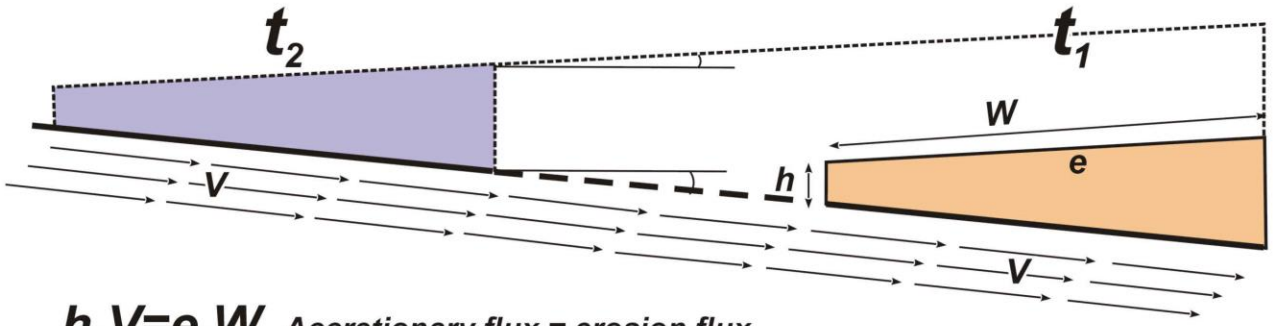

$h.V=e.W$ Accretionary flux = erosion flux

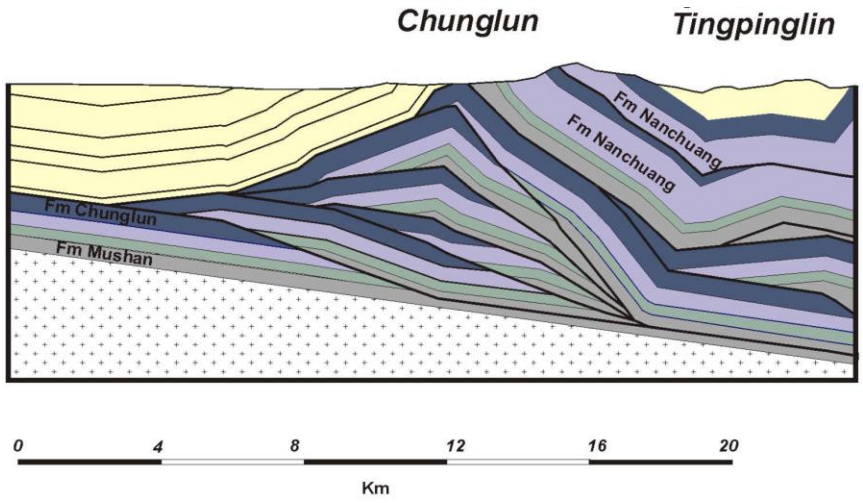

Thin-skinned hypothesis

Large shortening
of the sedimentary cover

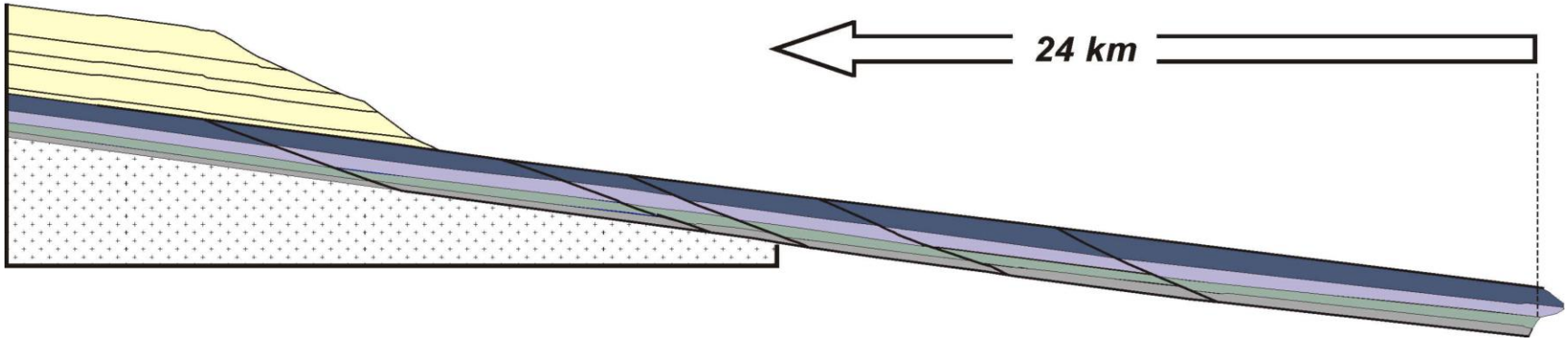

Basement topography

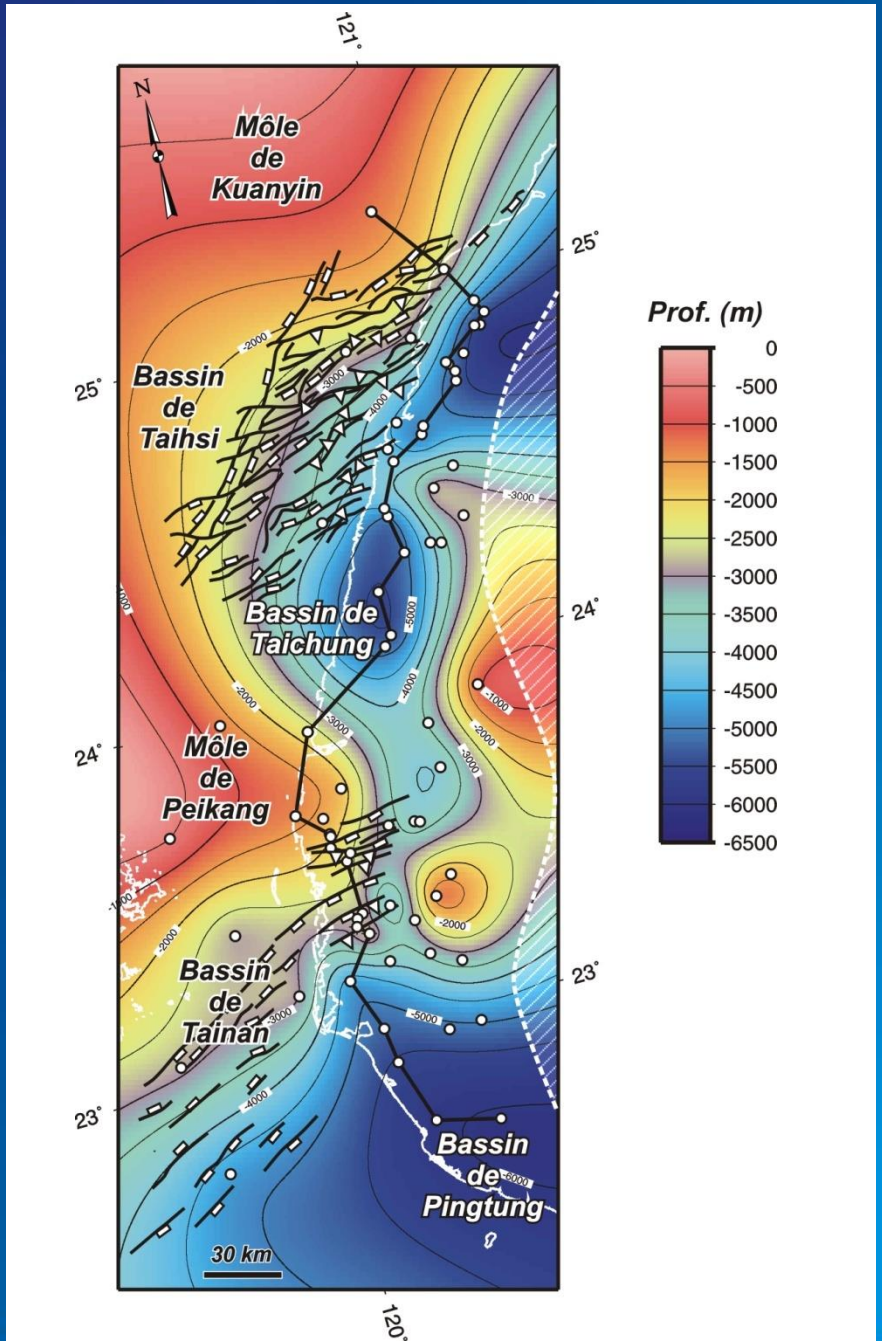

(Mouthereau et al., 2002)

Structural inheritance and inversion south of the basement highs

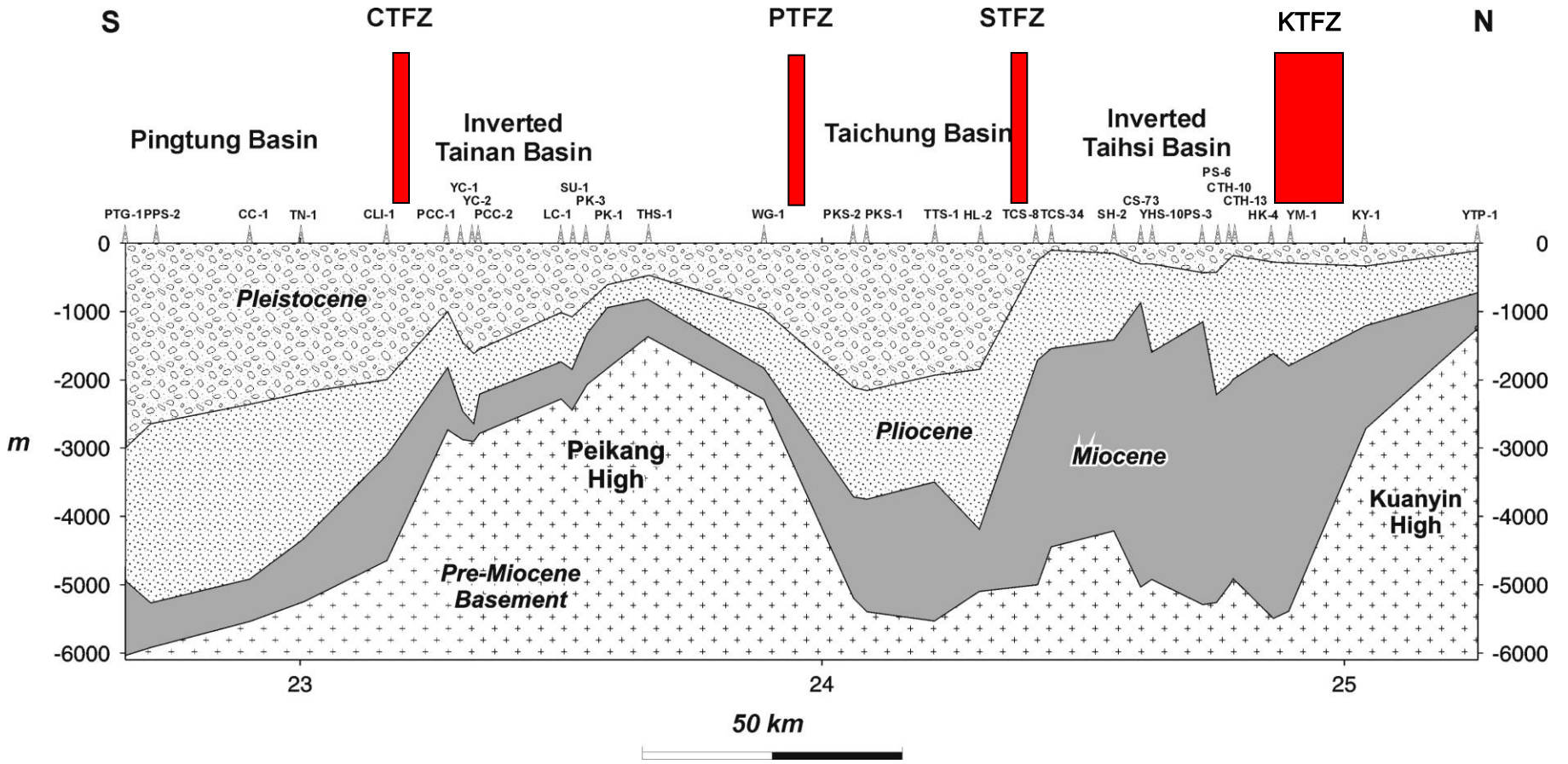

(Mouthereau et al., 2002)

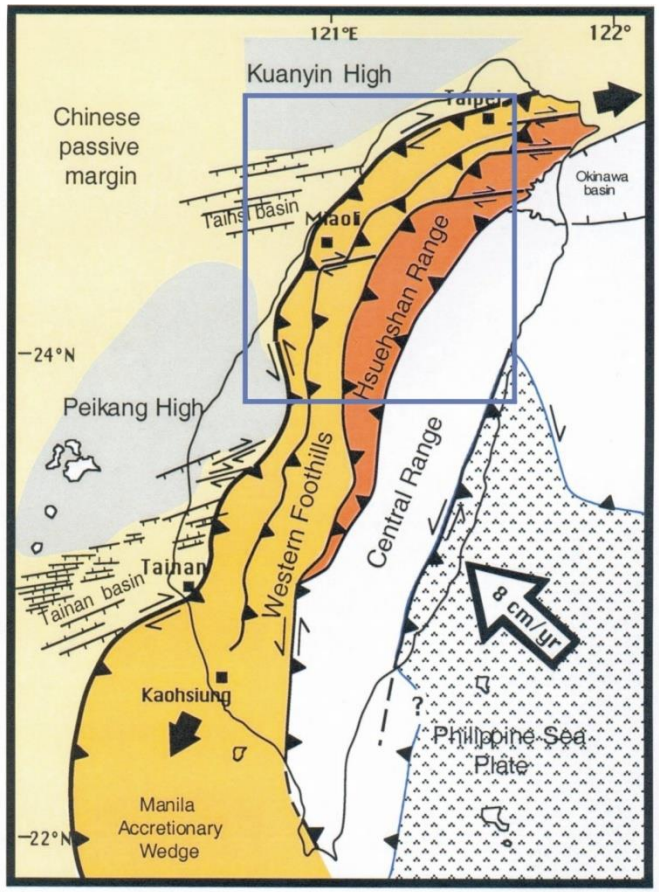

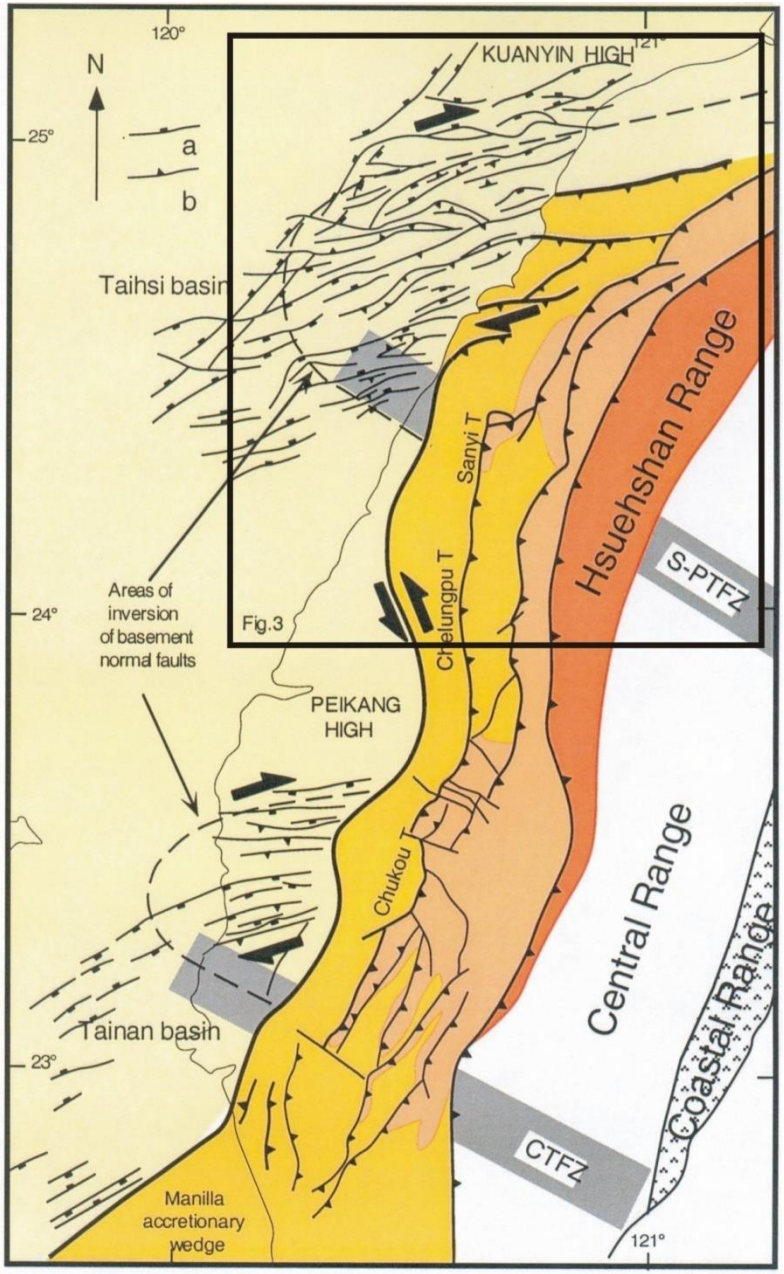

(Lacombe and Mouthereau, 2002)

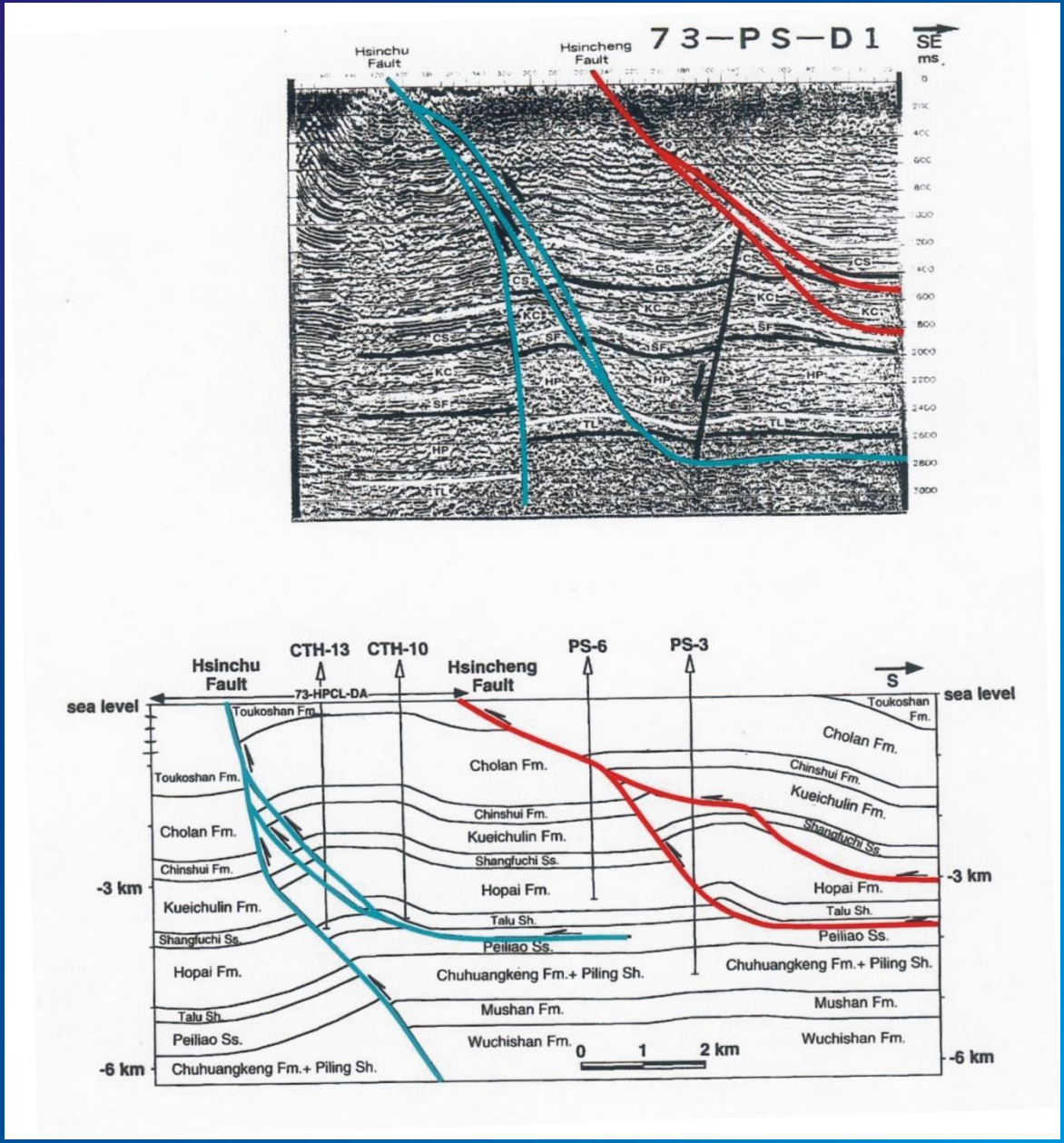

(Yang et al., 1996)

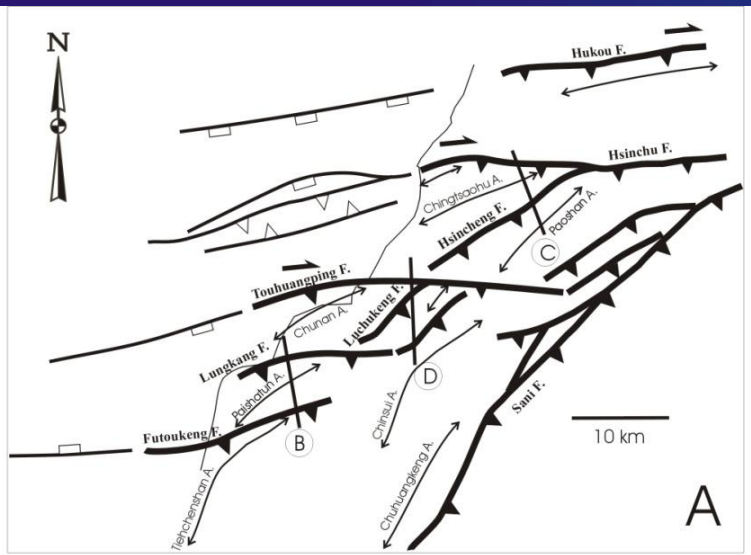

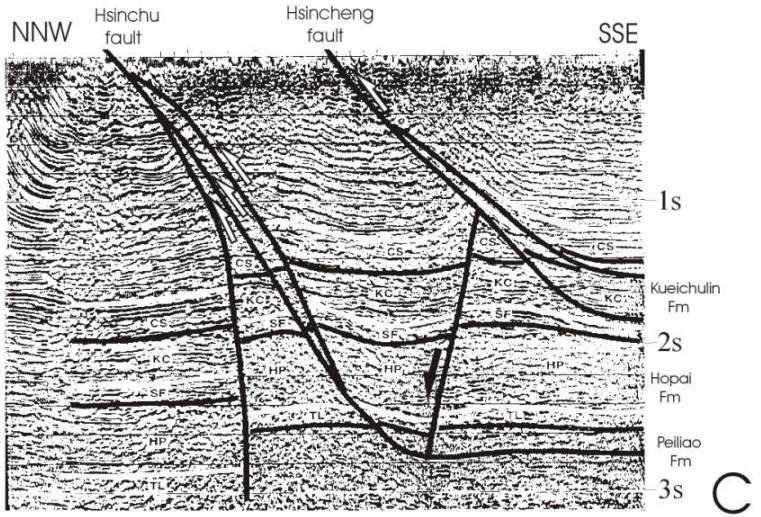

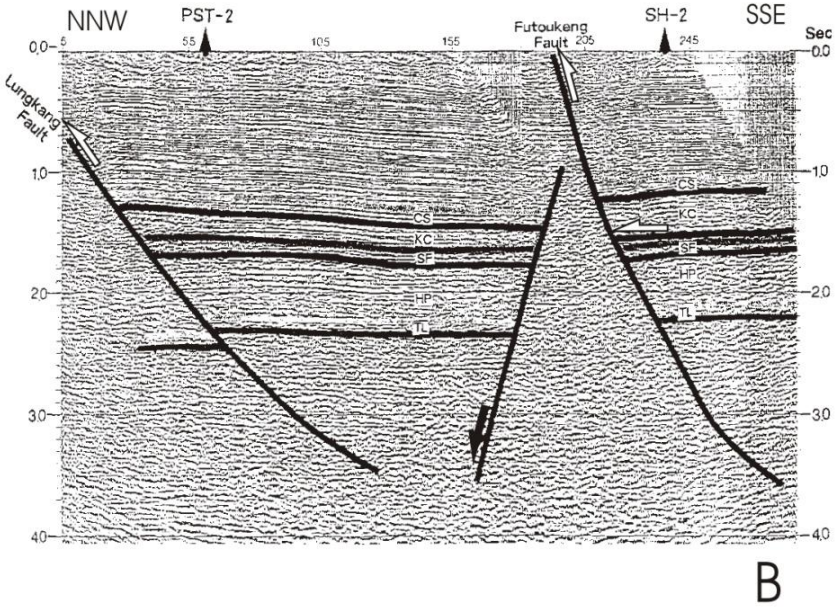

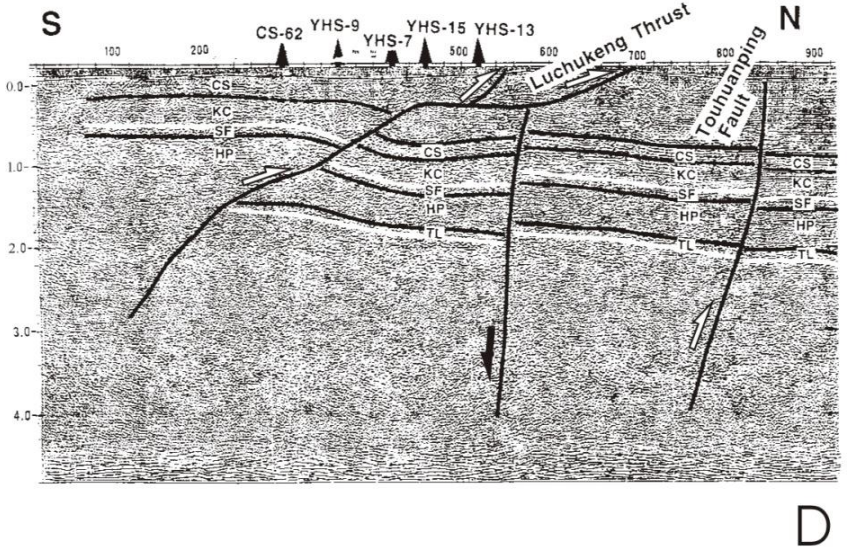

(Lacombe et al., 2003; profiles from Yang et al., 1994, 1996, 1997)

2 very different visions of the structural style in northern Taiwan

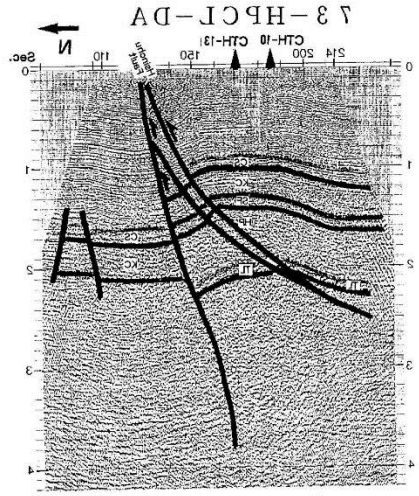

(*Yang et al.*, 1996)

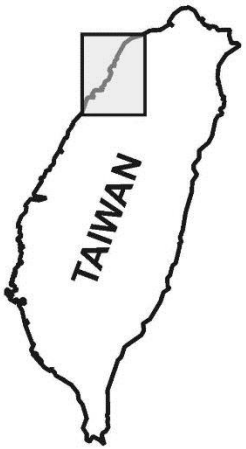

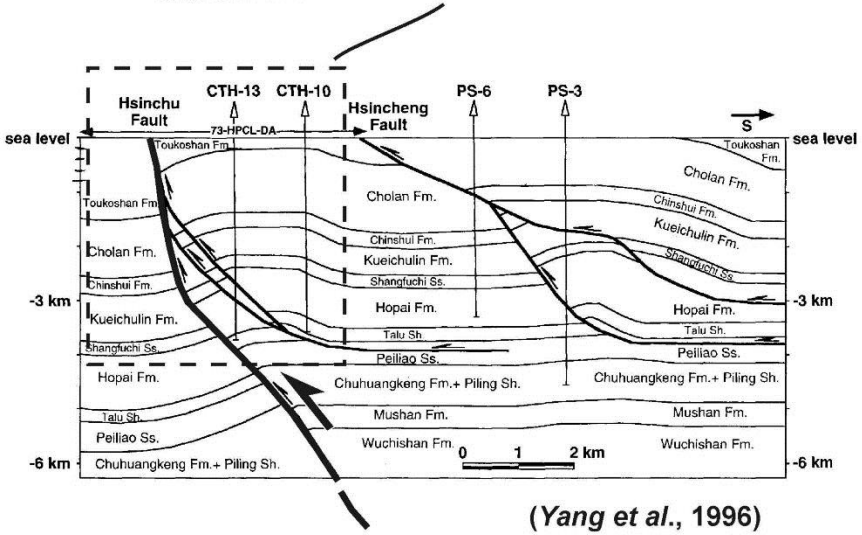

(*Yang et al.*, 1996)

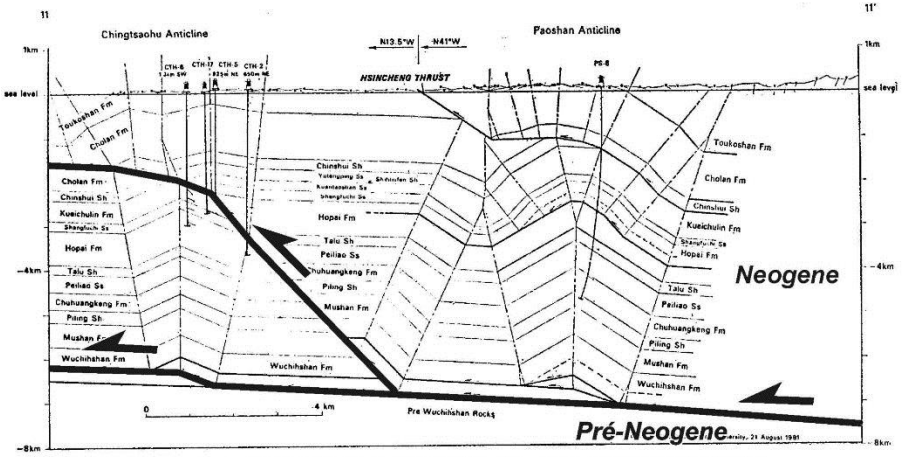

Figure 2. Structural interpretation through section 11-11′ in the northern part of the Miaoli-Hsinchu area.

(*Namson, 1981*)

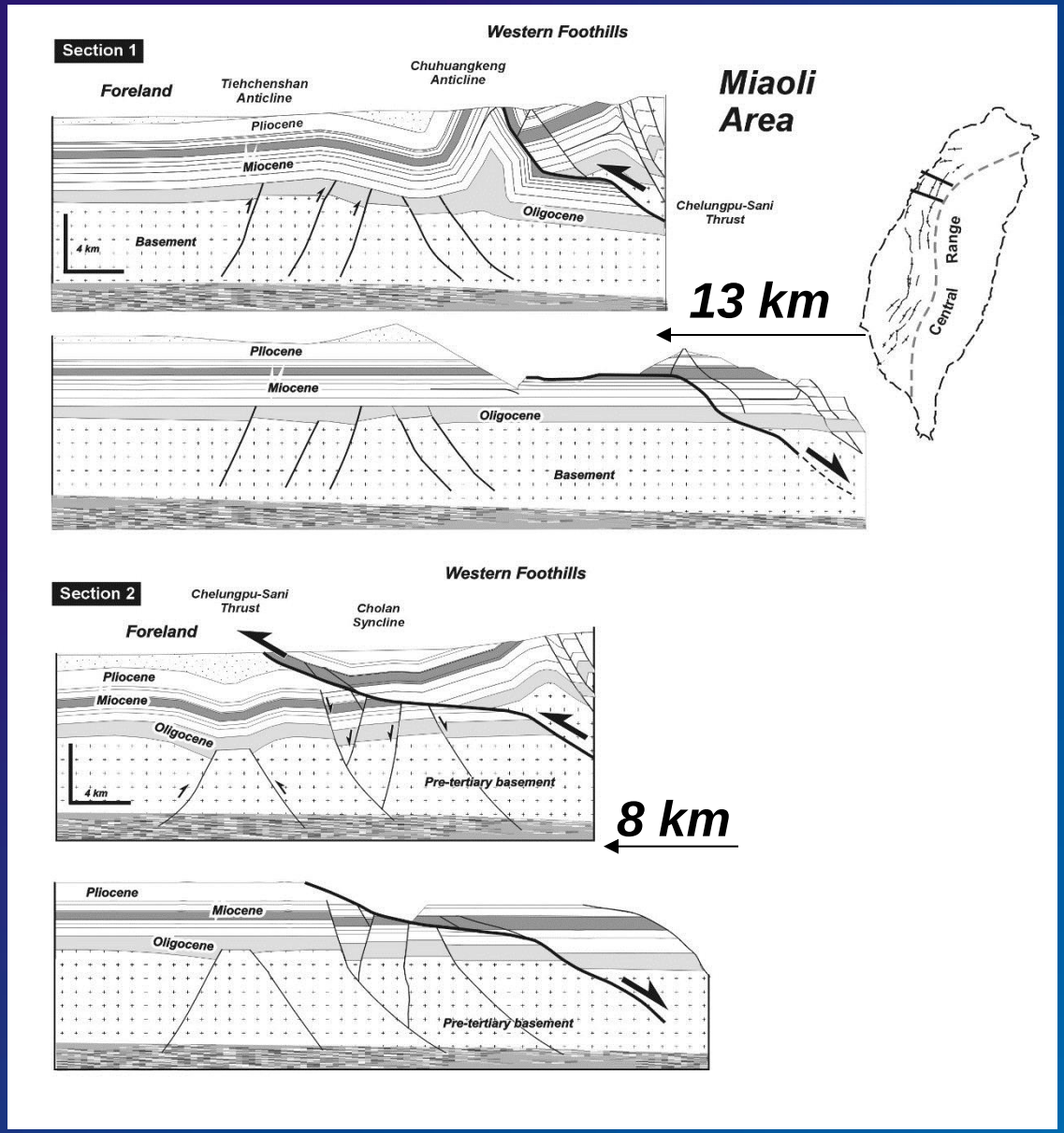

(Mouthereau and Lacombe, 2006)

Superimposed decoupling in the sedimentary cover and basement controlled by structural inheritance

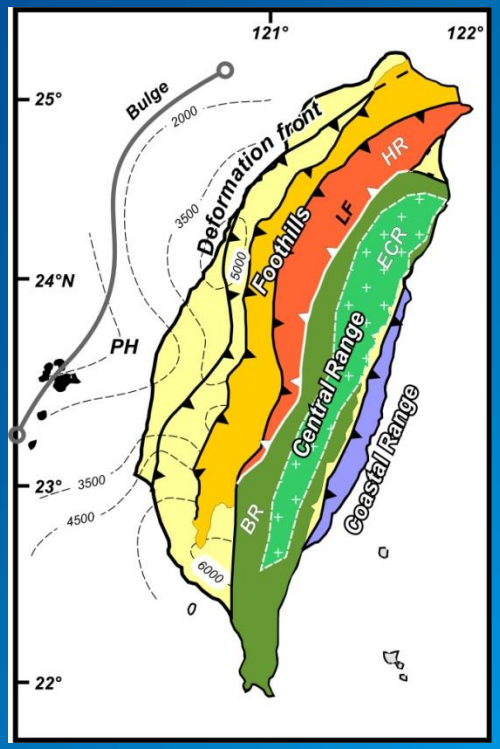

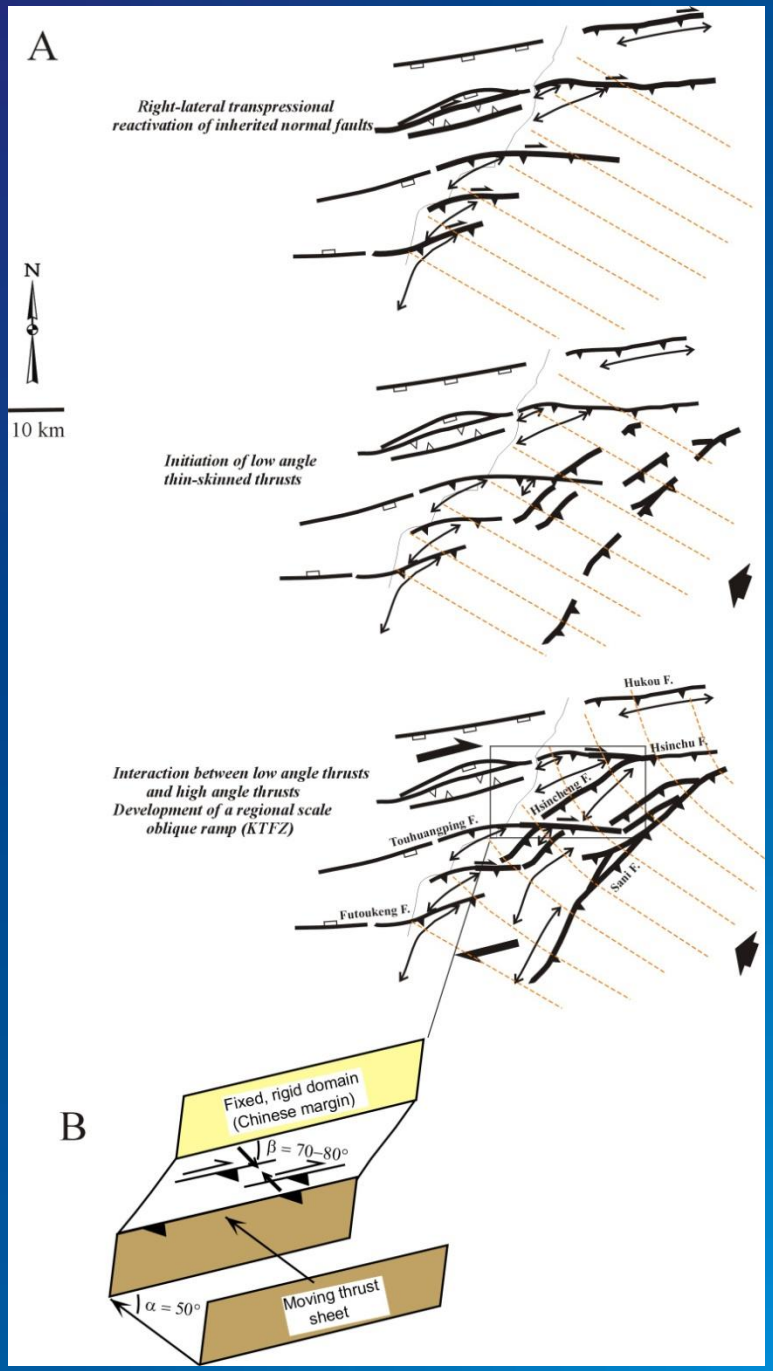

(Lacombe et al., 2003)

(Lacombe et al., 2003)

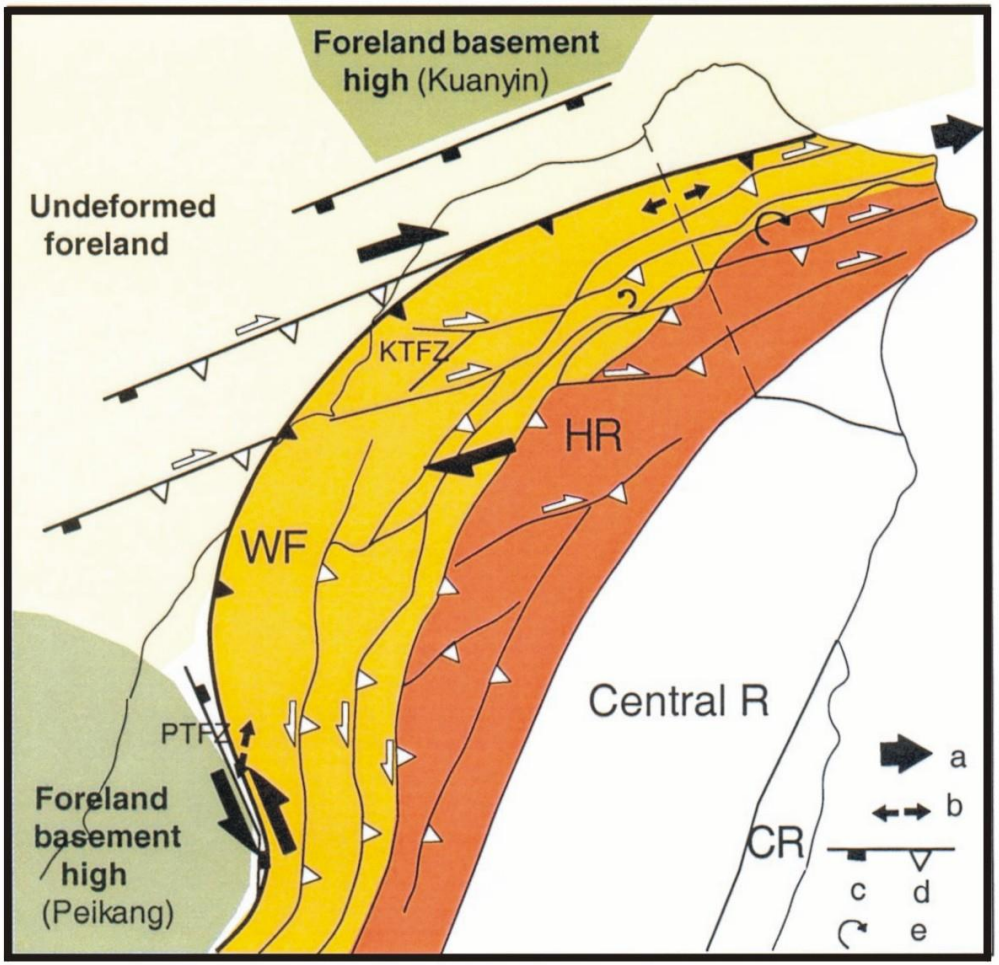

NW Taiwan : the position of the salient's apex coincides with the location of the precollisional depocenter (thickest strata) in the basin from which the salient formed.

The NW Taiwan salient mainly formed in response to the along-strike variation in the pre-orogenic basin thickness, leading to recognize this salient as a basin-controlled salient.

It differs from arcs formed in thin-skinned orogens in that deformation was accommodated by both thin-skinned shallow thrusts and basement faults and therefore that both the cover and the basement are involved in collisional shortening.

→ « Passive » and/or « active » basement control on geometry (segmentation, curvature,) and kinematics of fold-thrust belts

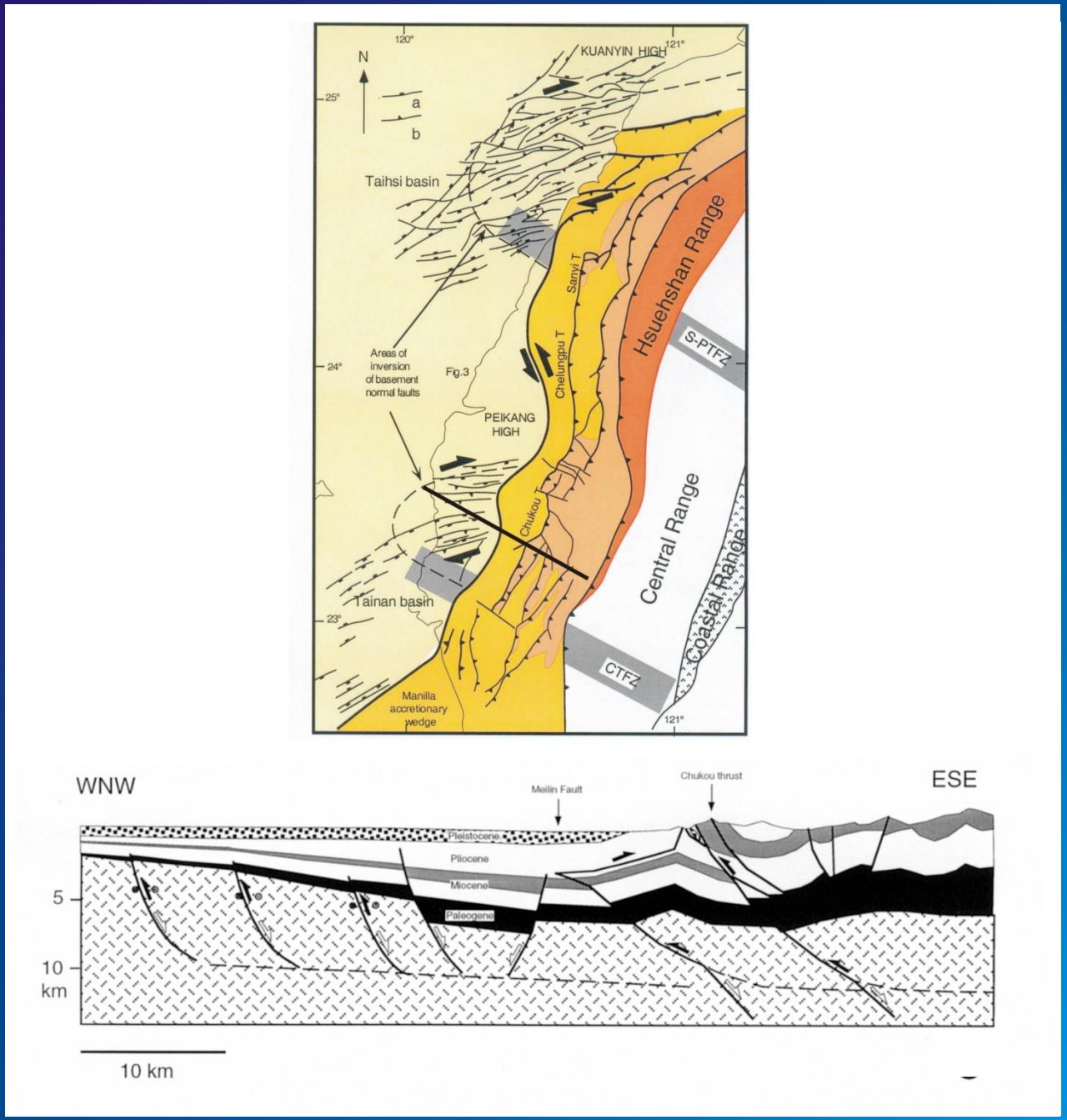

(Lacombe and Mouthereau, 2002)

2 very different visions of the structural style in central Taiwan

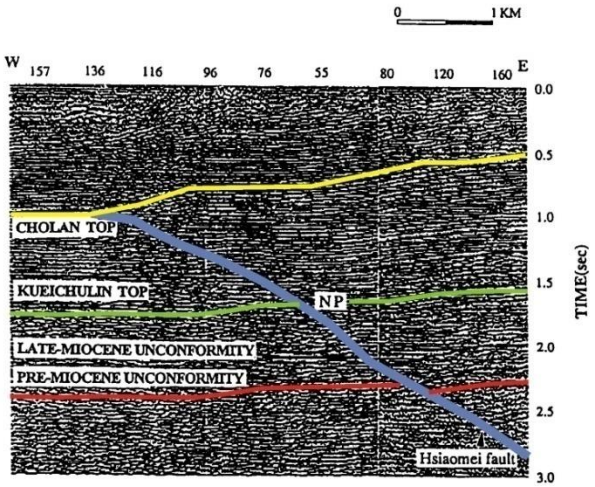

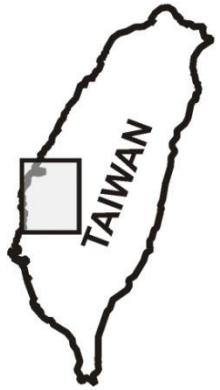

Hung et al., 1999

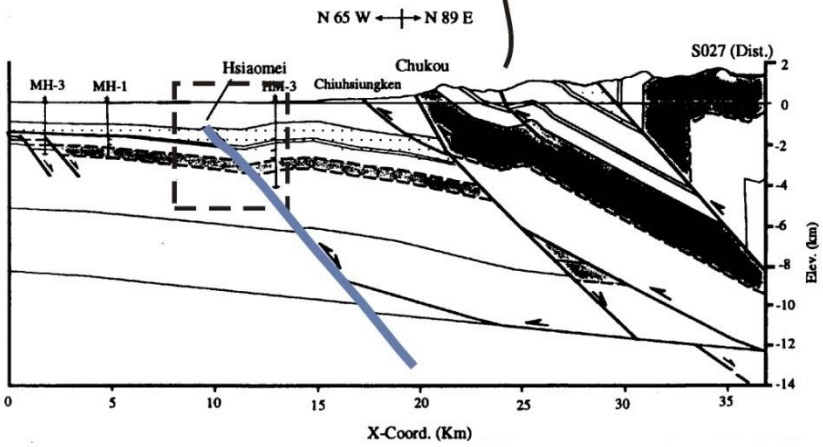

Suppe and Namson, 1979

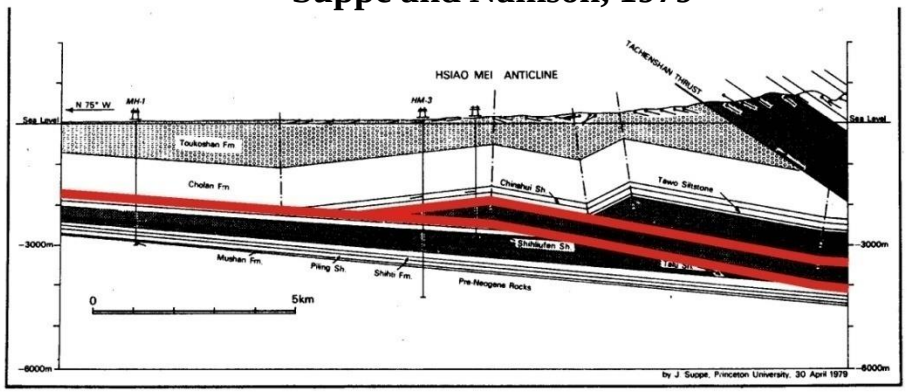

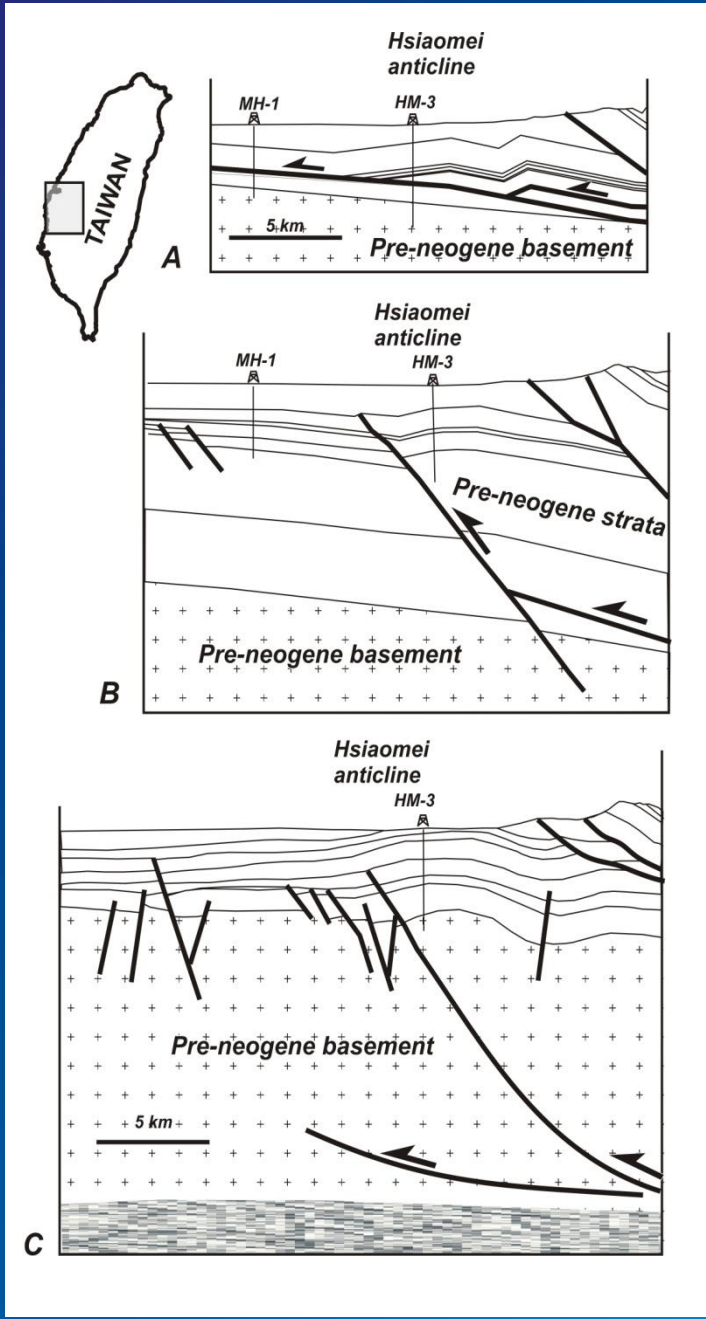

(Mouthereau and Lacombe, 2006)

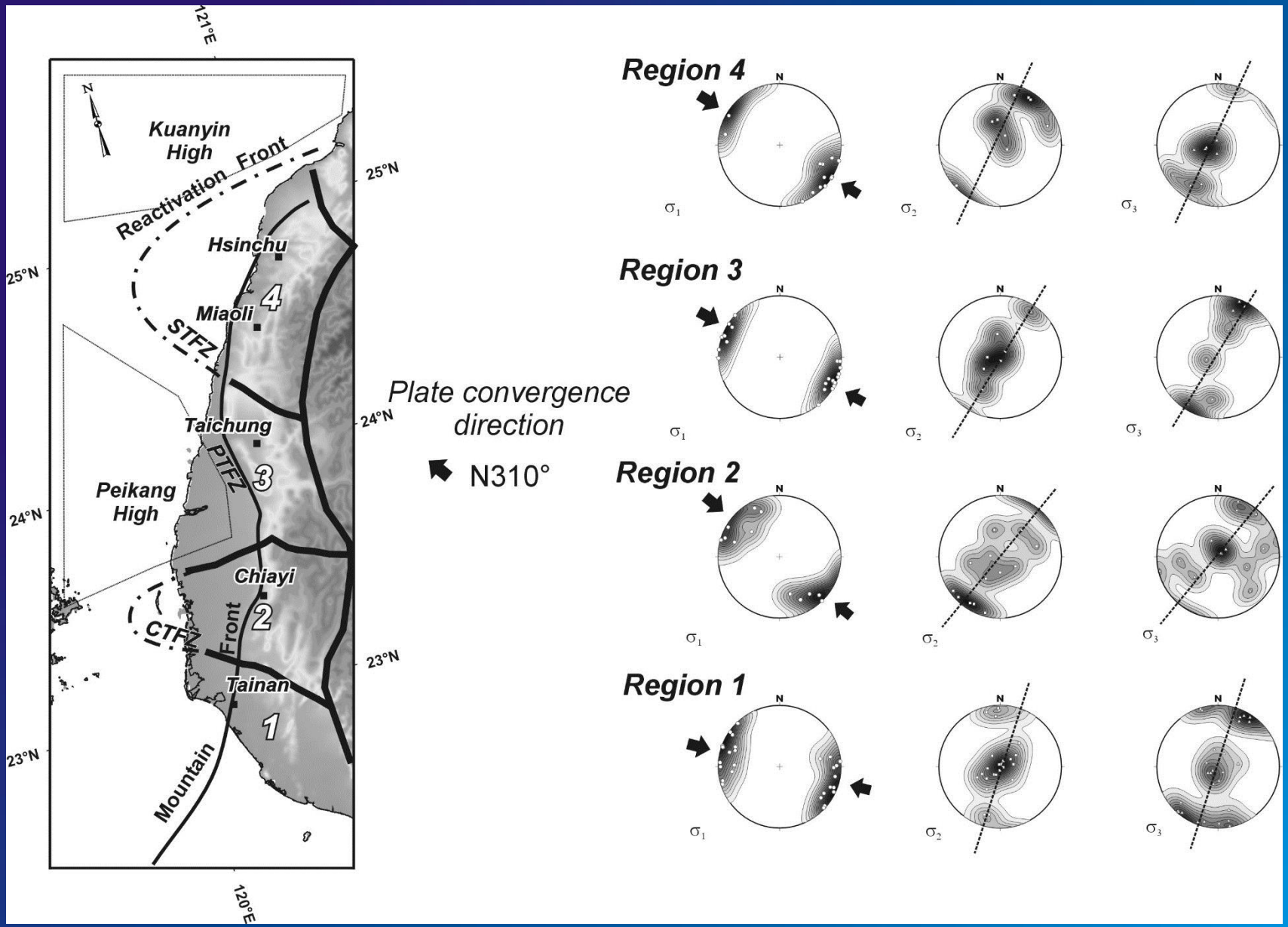

(Mouthereau et al., 2002)

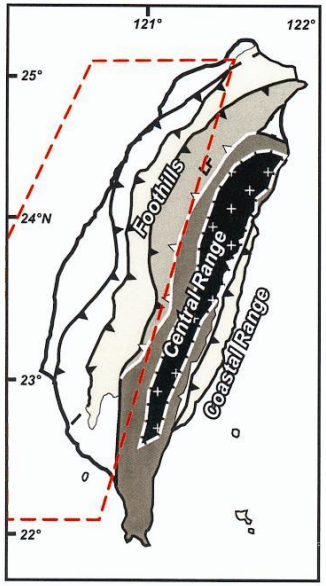

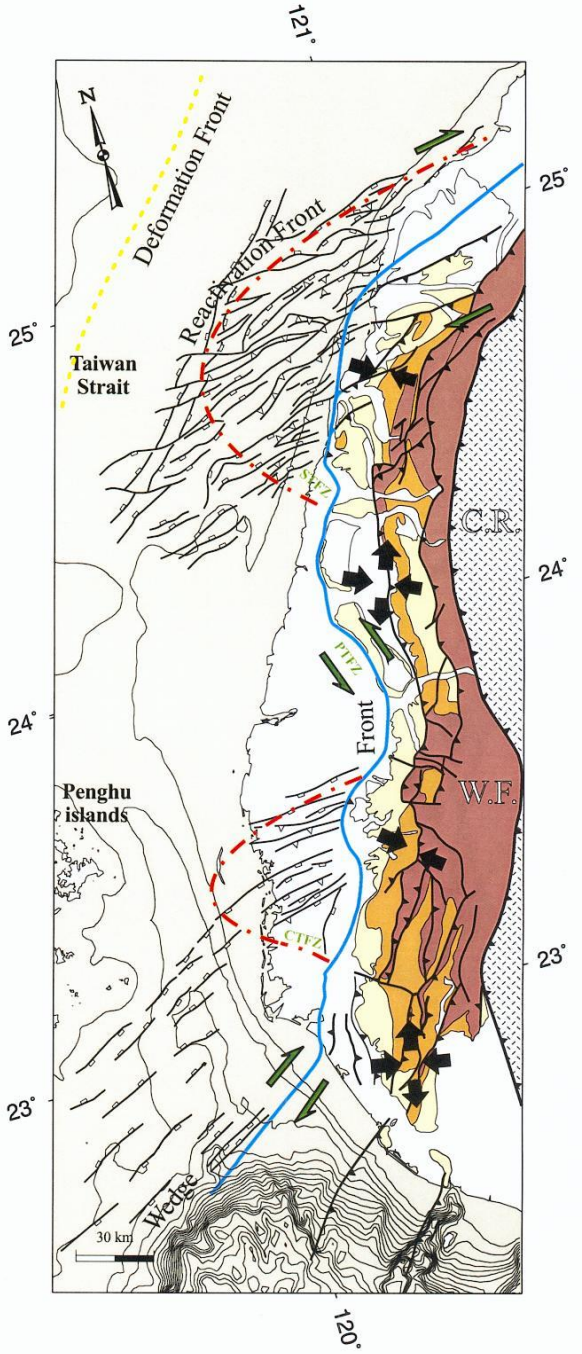

(Mouthereau et al., 2002)

(Lacombe and Mouthereau, 2002)

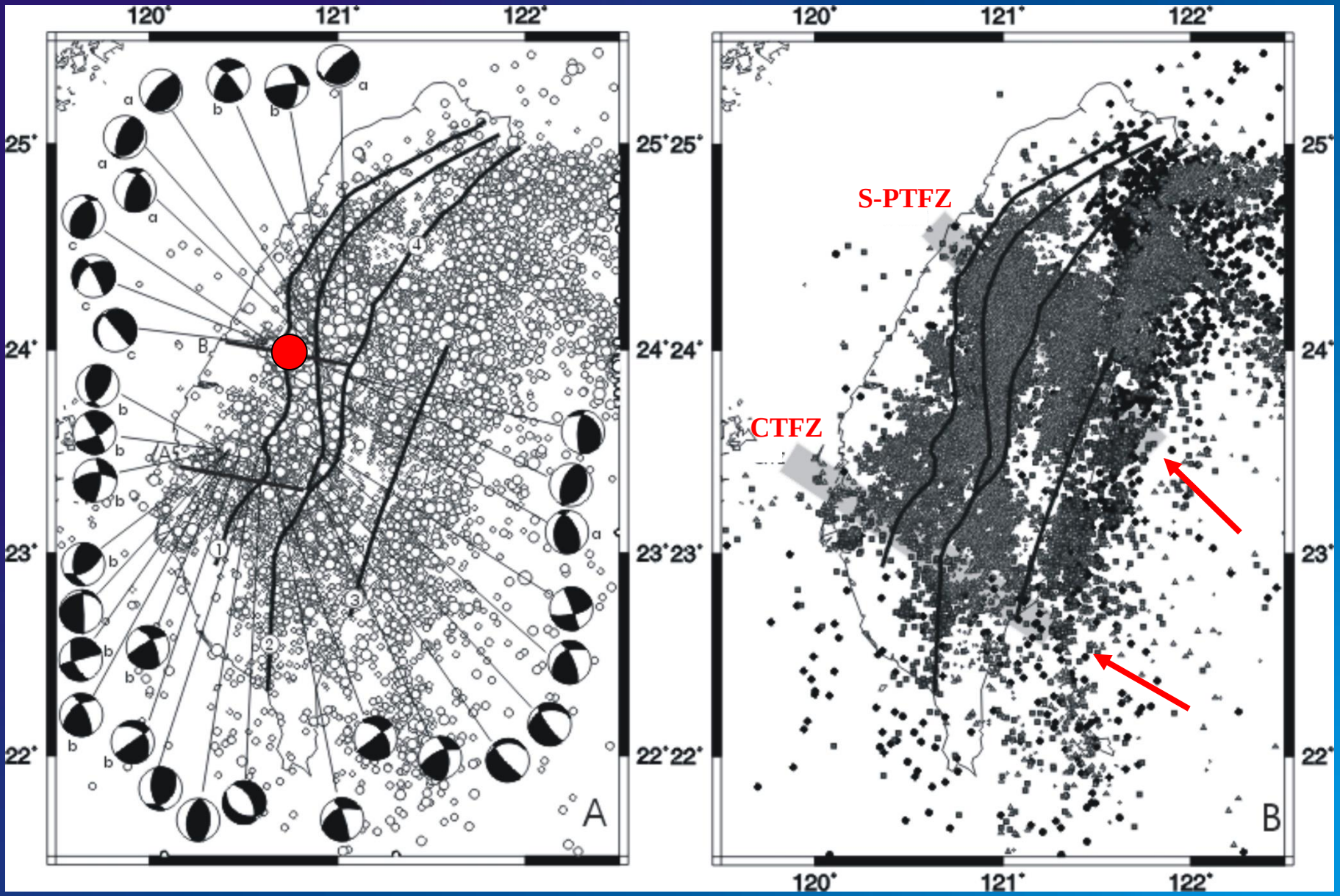

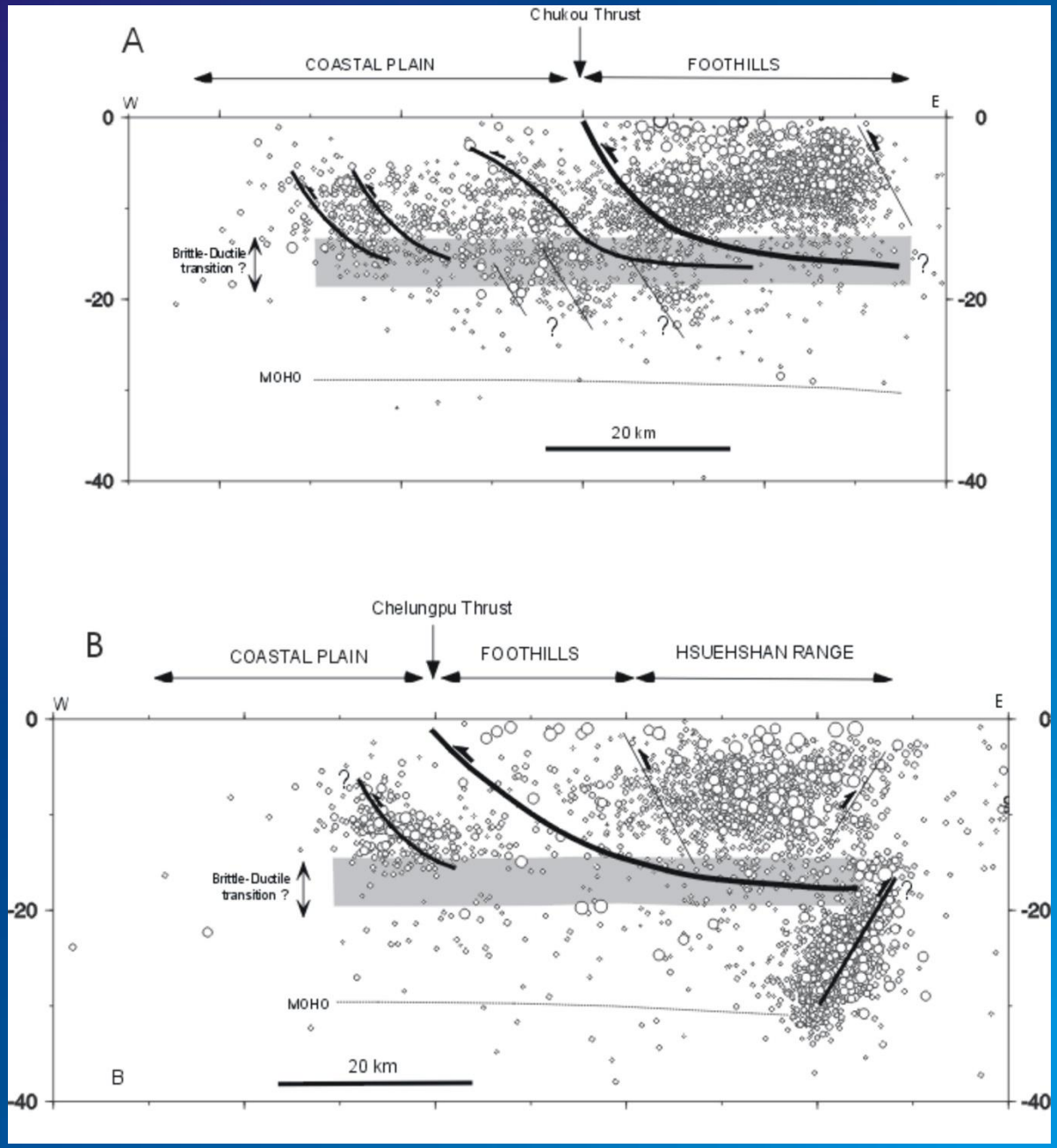

(Lacombe and Mouthereau, 2002)

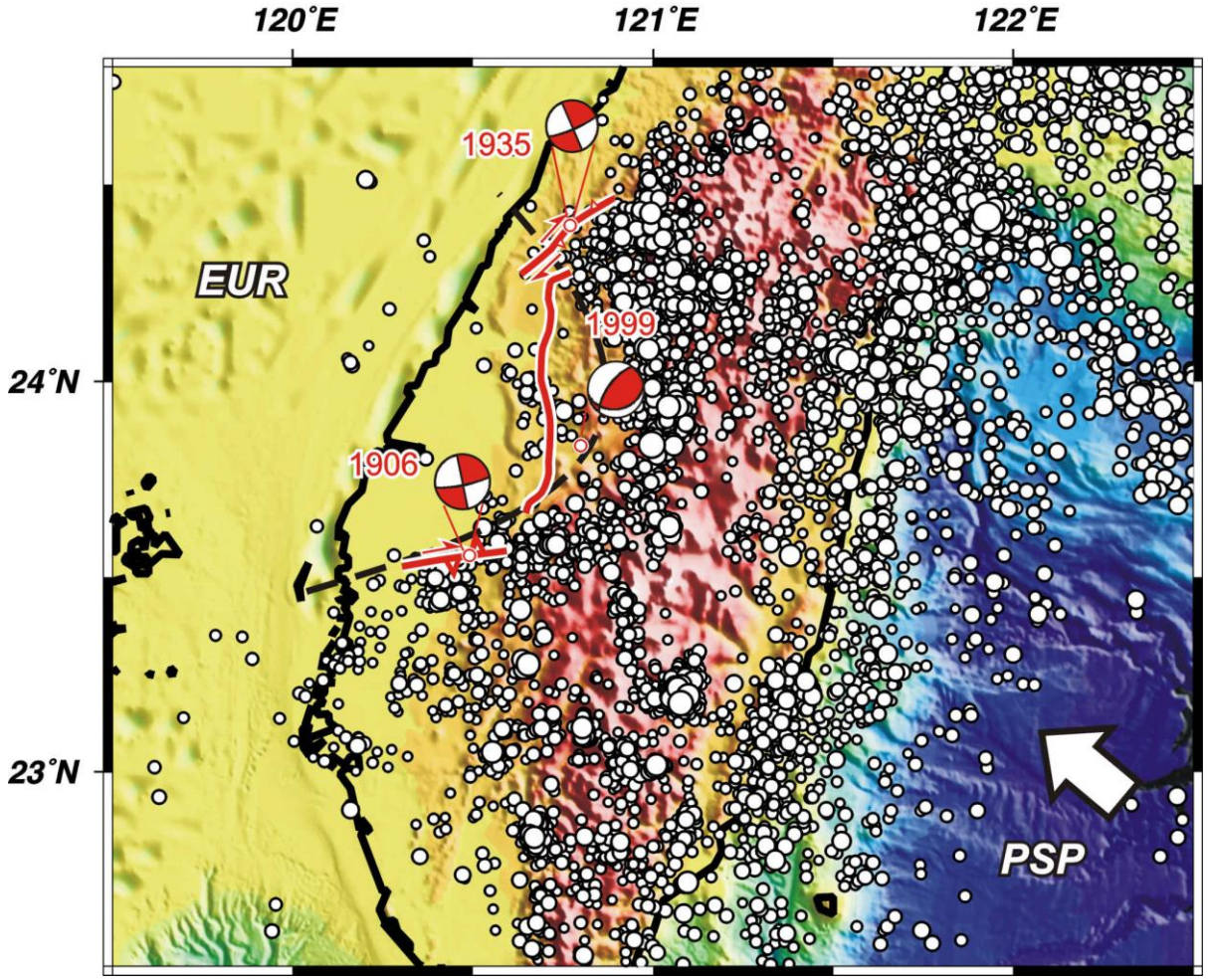
120˚E
121˚E
122˚E
24˚N
23˚N
1935
1999
1906
EUR
PSP

Chichi (Mw=7.9)

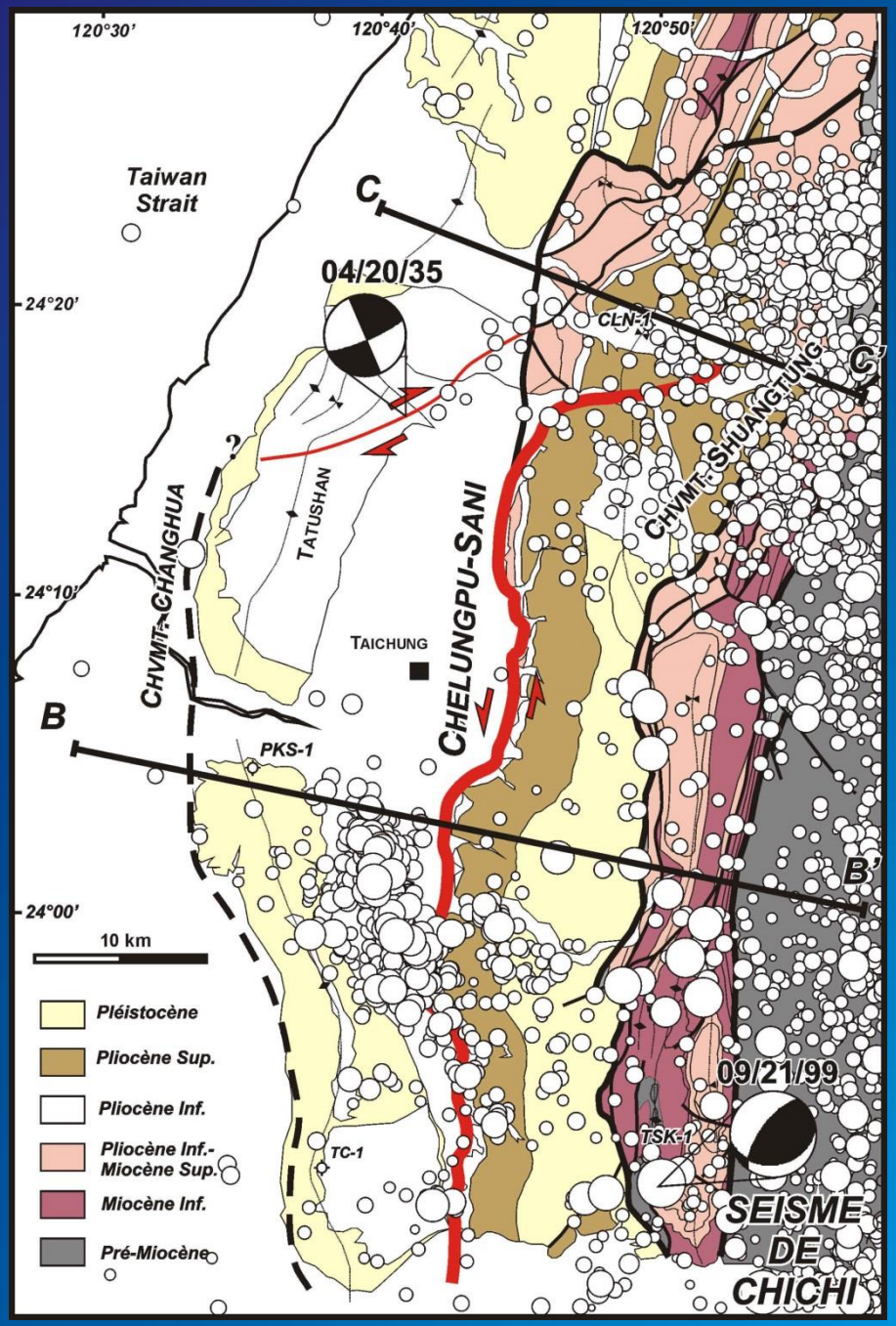
120°30'
120°40'
120°50'
Taiwan Strait
C
C'
04/20/35
24°20'
CLN-1
CHVMT-SHUANGTUNG
?
TATUSHAN
CHVMT-CHANGHUA
CHELUNGPU-SANI
24°10'
TAICHUNG
B
PKS-1
B'
24°00'
10 km
Pléistocène
Pliocène Sup.
Pliocène Inf.
Pliocène Inf.-Miocène Sup.
Miocène Inf.
Pré-Miocène
TC-1
09/21/99
TSK-1
SEISME DE CHICHI

The Chichi earthquake :
initiation of a thrust ramp dipping 30° at 11-12 km which connects to the Chelungpu thrust (an inherited normal fault)

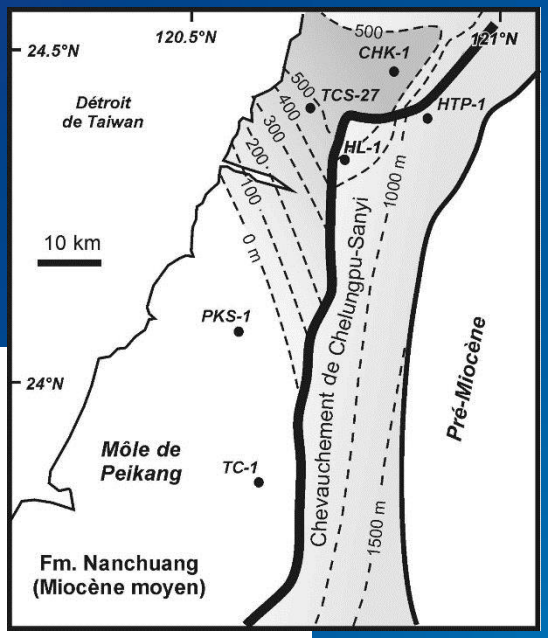

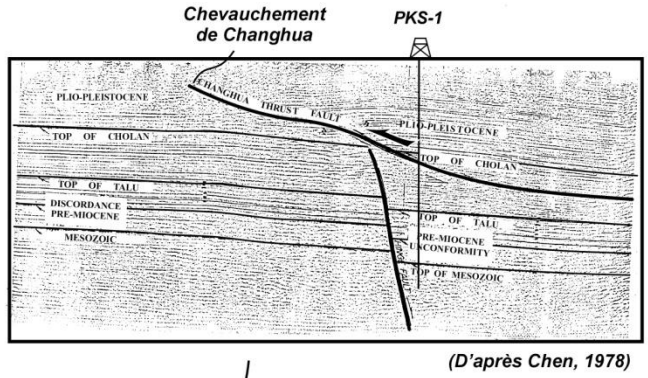

(D'après Chen, 1978)

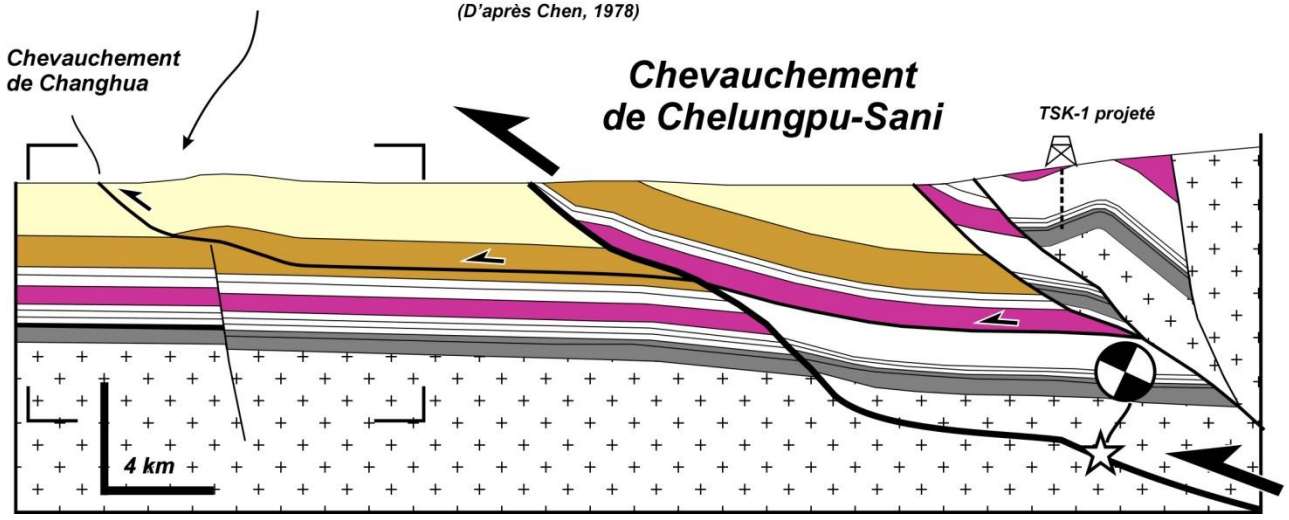

(Mouthereau et al, 2001)

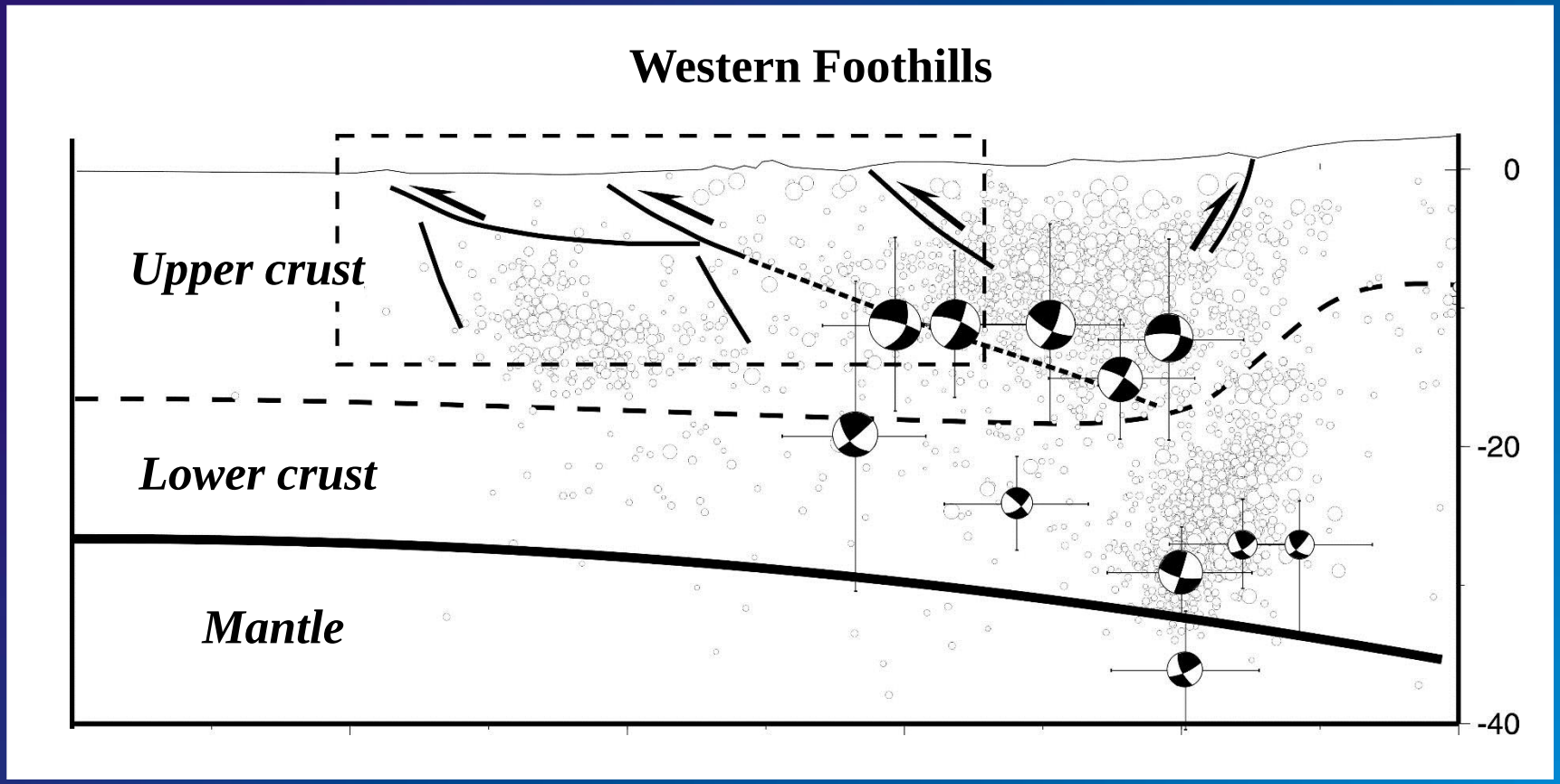

(Kao et al., 2000)

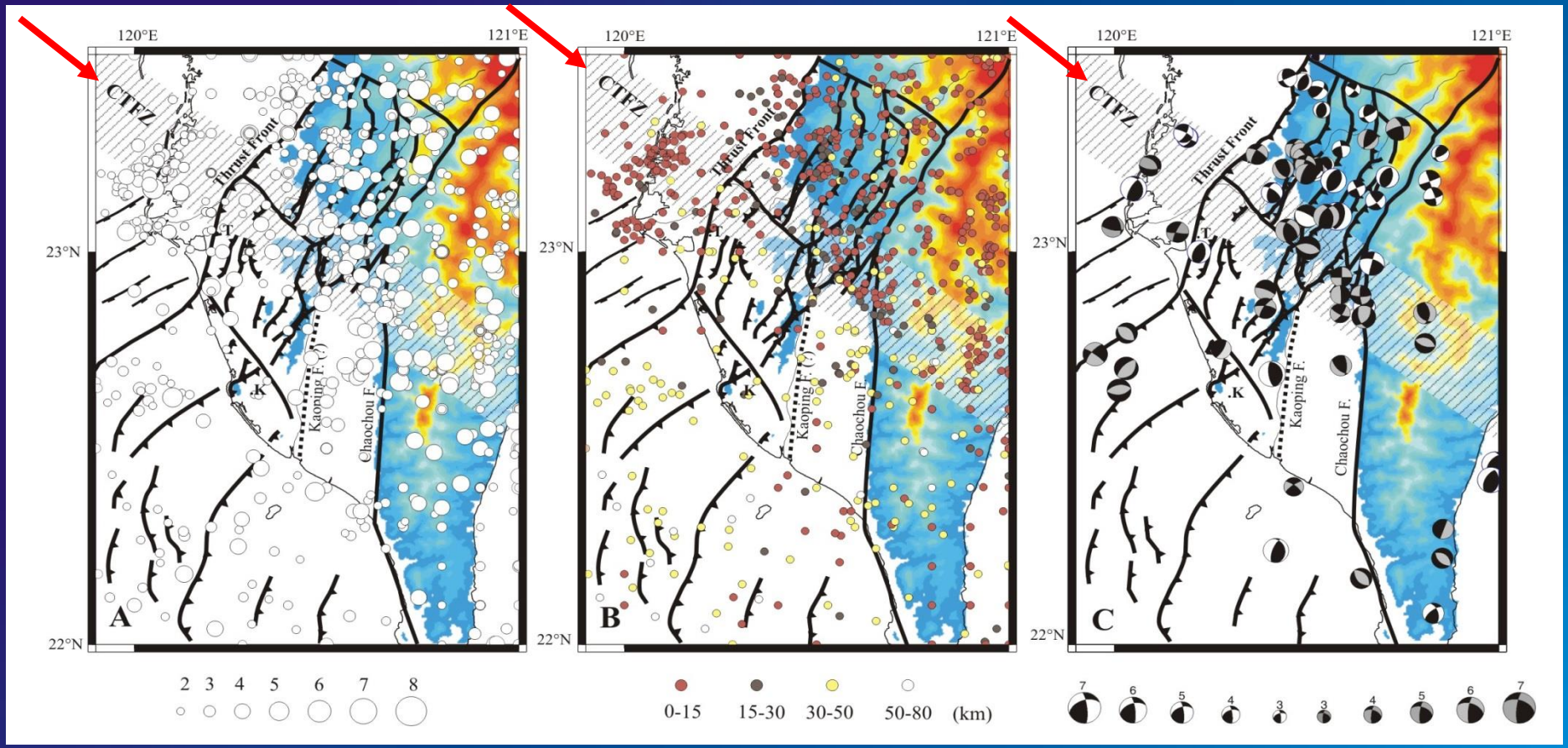

(Lacombe et al., 2001)

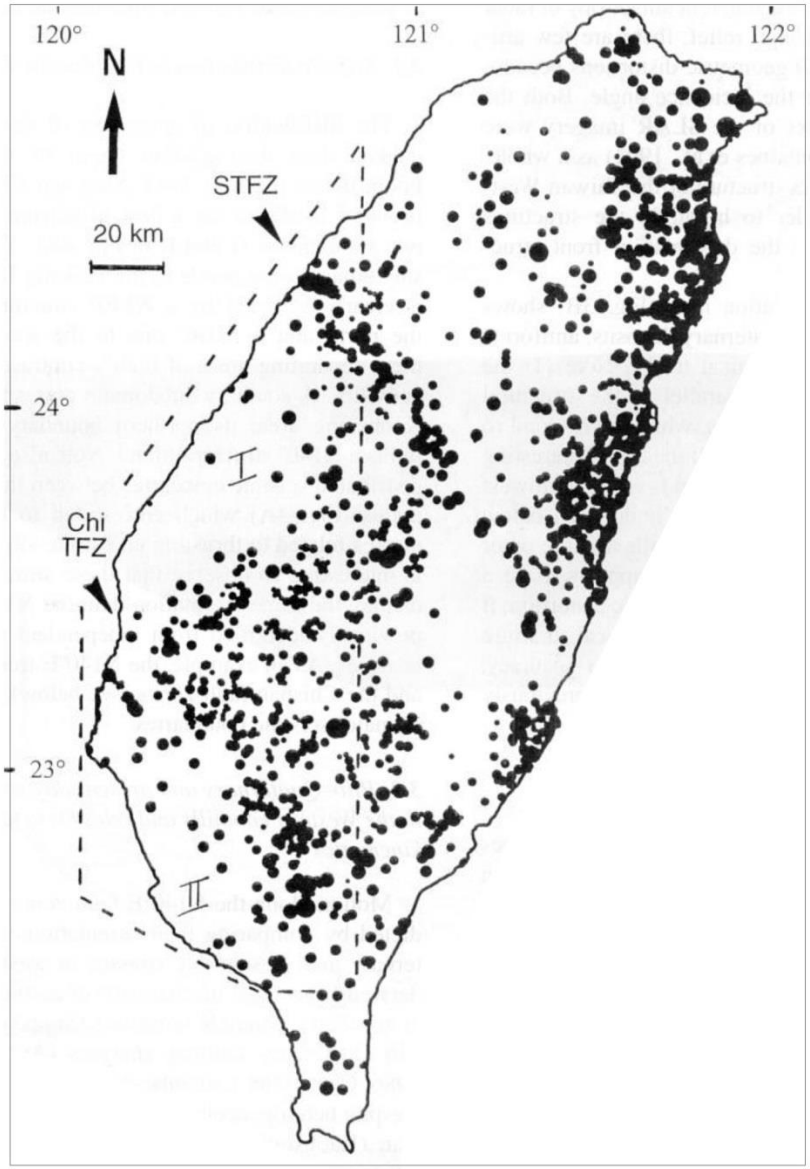

(Deffontaines et al., 1997)

(Rau et al, 2013)

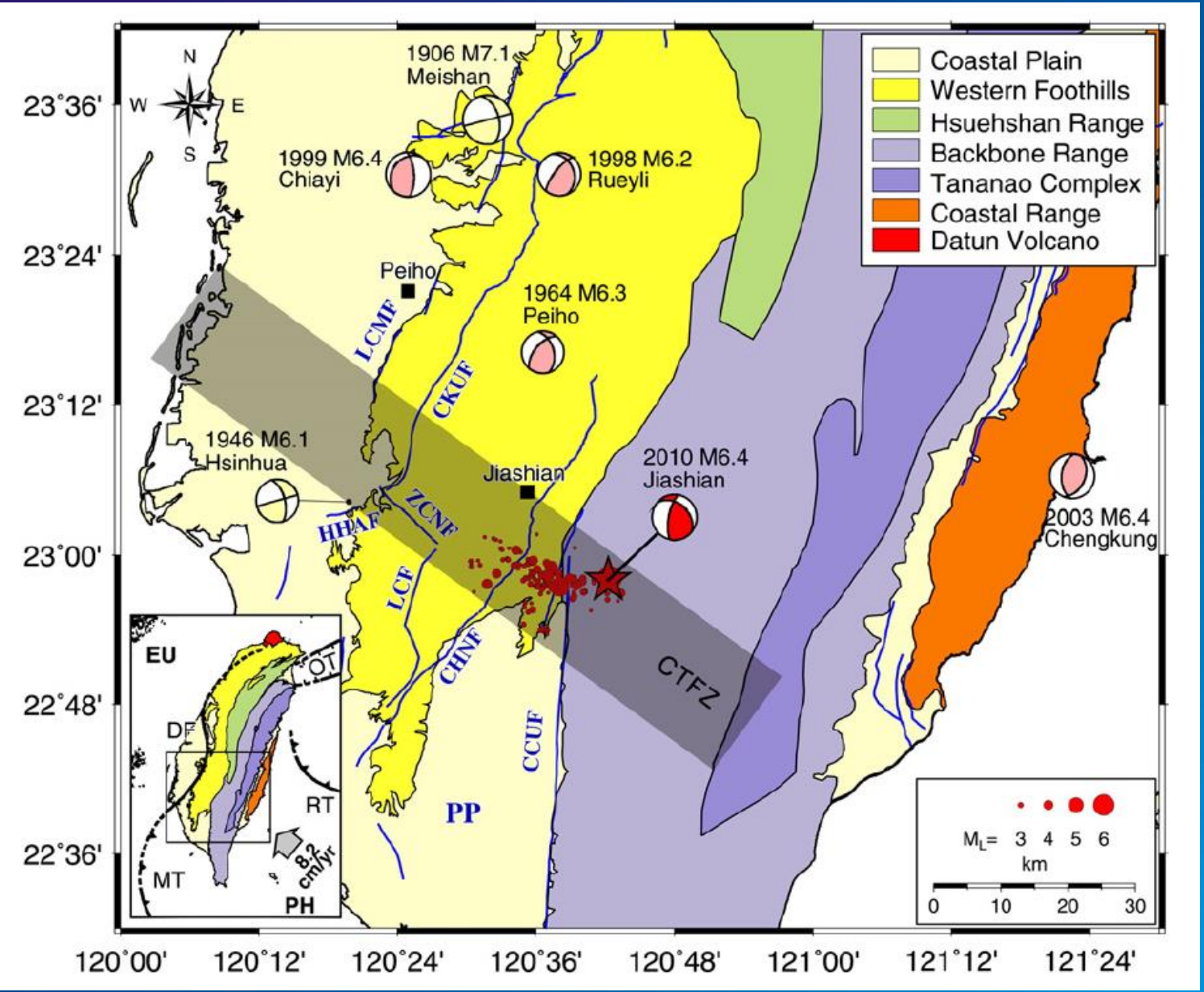

2010 March 4, Mw 6.3 Jia-Shian earthquake

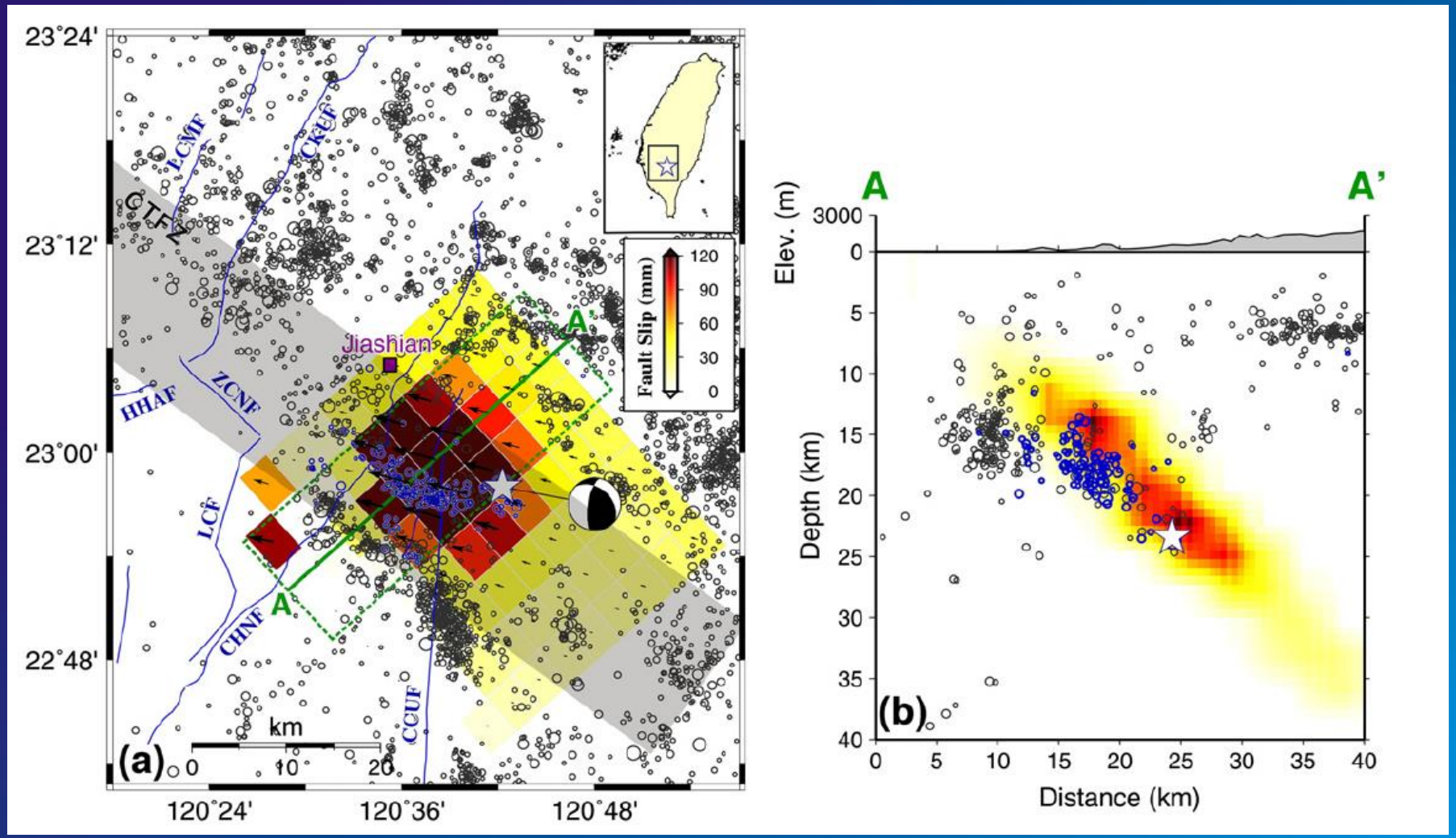

(Rau et al, 2013)

2010 March 4, Mw 6.3 Jia-Shian earthquake

ML 6.2 and ML 6.5 2013 Nantou earthquakes

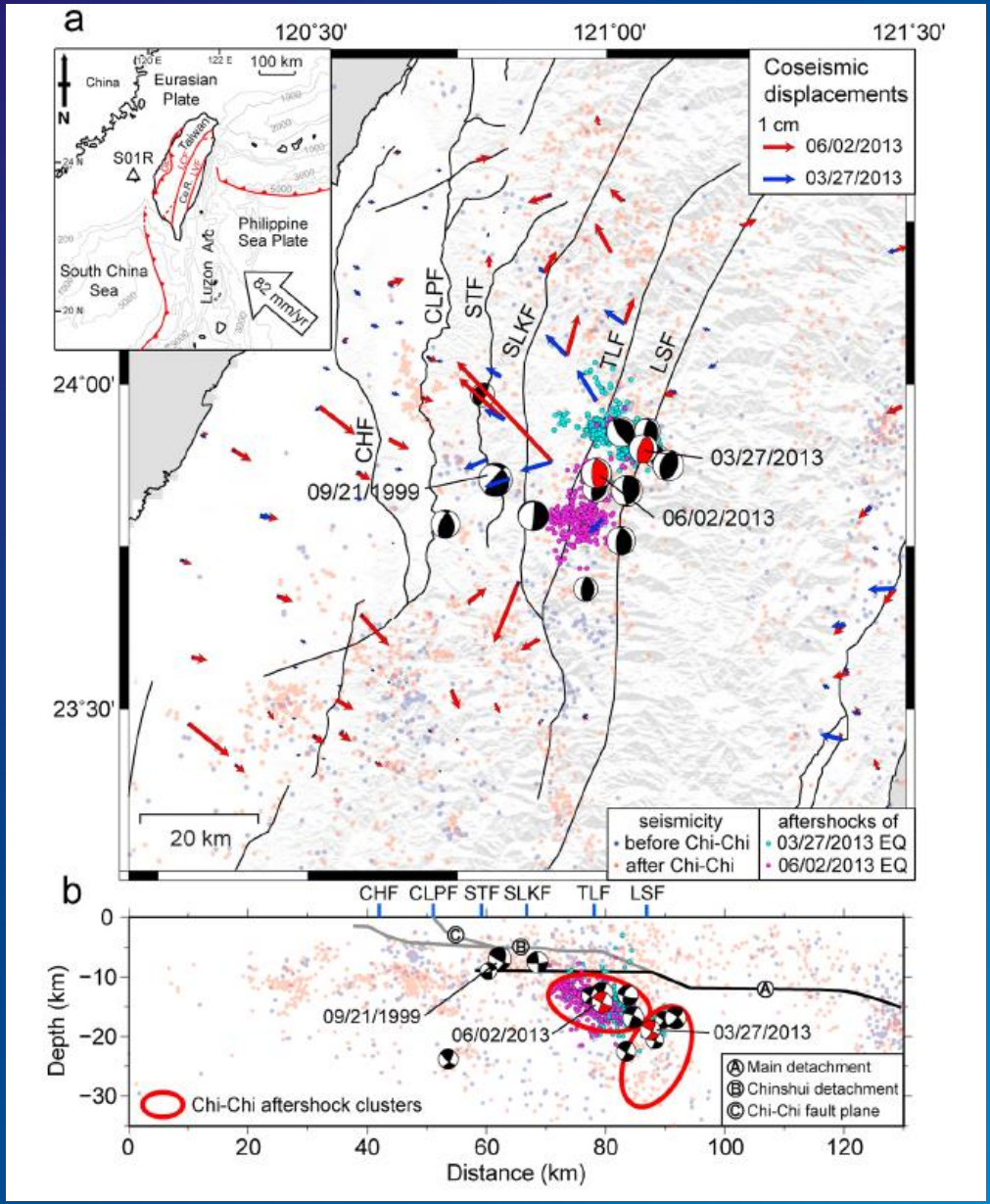

(Chuang et al, 2013)

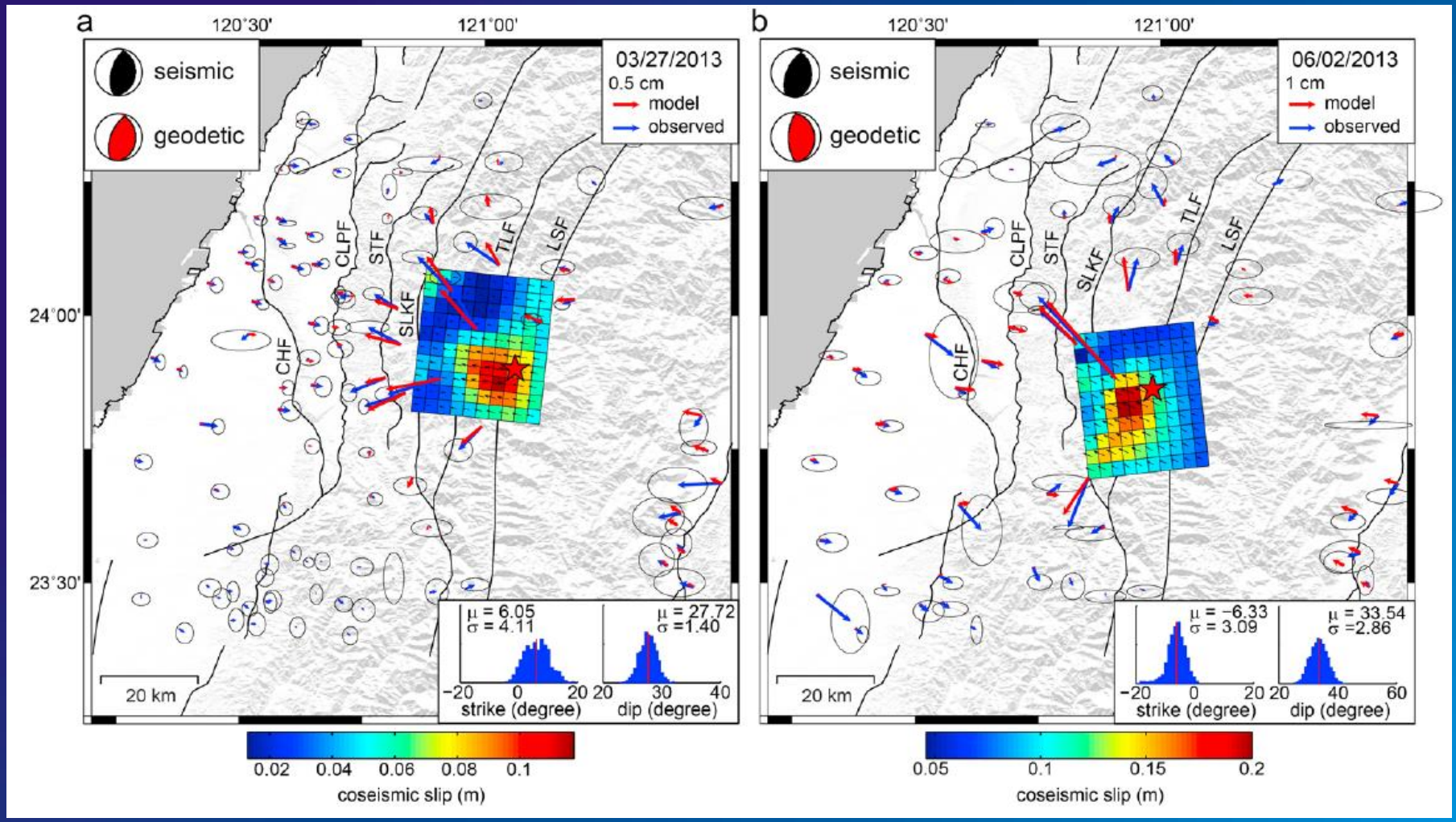

(Chuang et al, 2013)

ML 6.2 and ML 6.5 2013 Nantou earthquakes

ML 6.2 and ML 6.5 2013 Nantou earthquakes

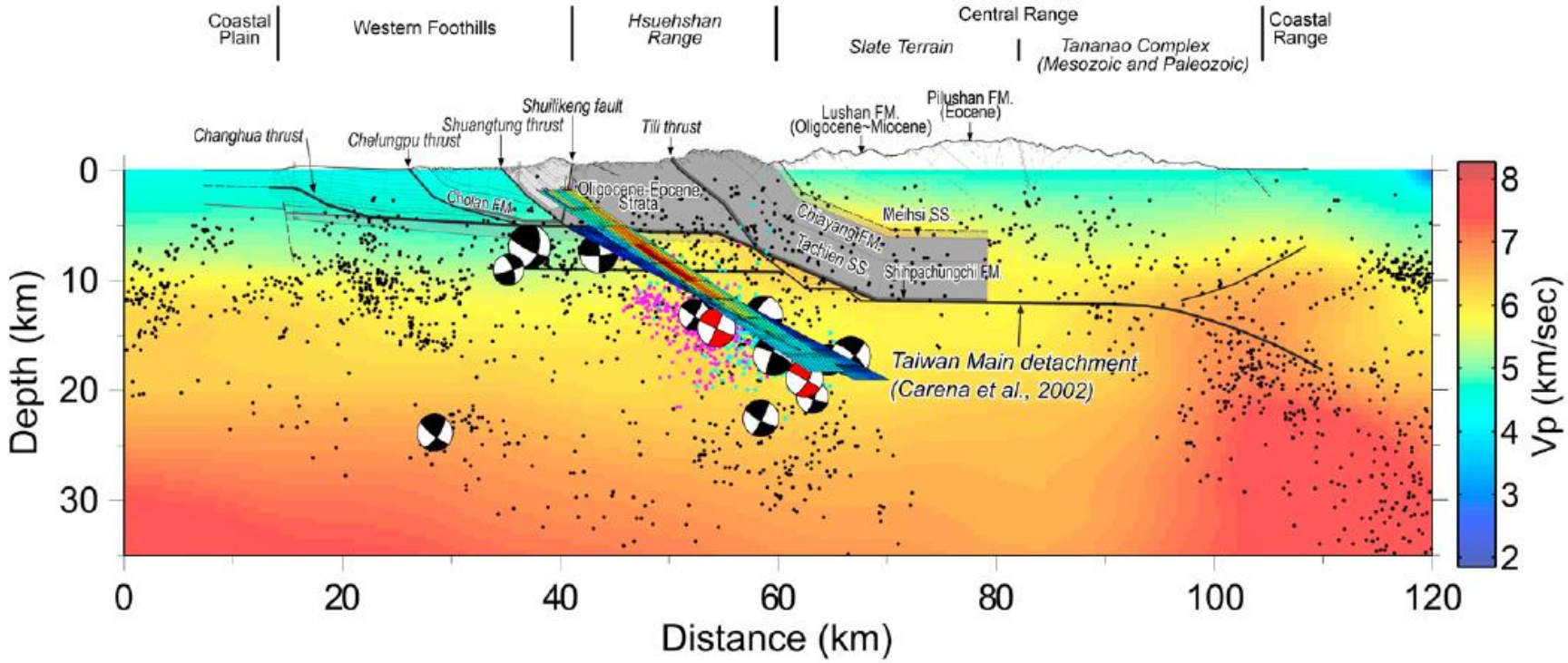

(Chuang et al, 2013)

The earthquakes occur on essentially the same 30° dipping fault plane ramping up from ~20 km depth near a cluster of 1999 Chi-Chi earthquake aftershocks to the shallow detachment and the Chi-Chi fault plane.

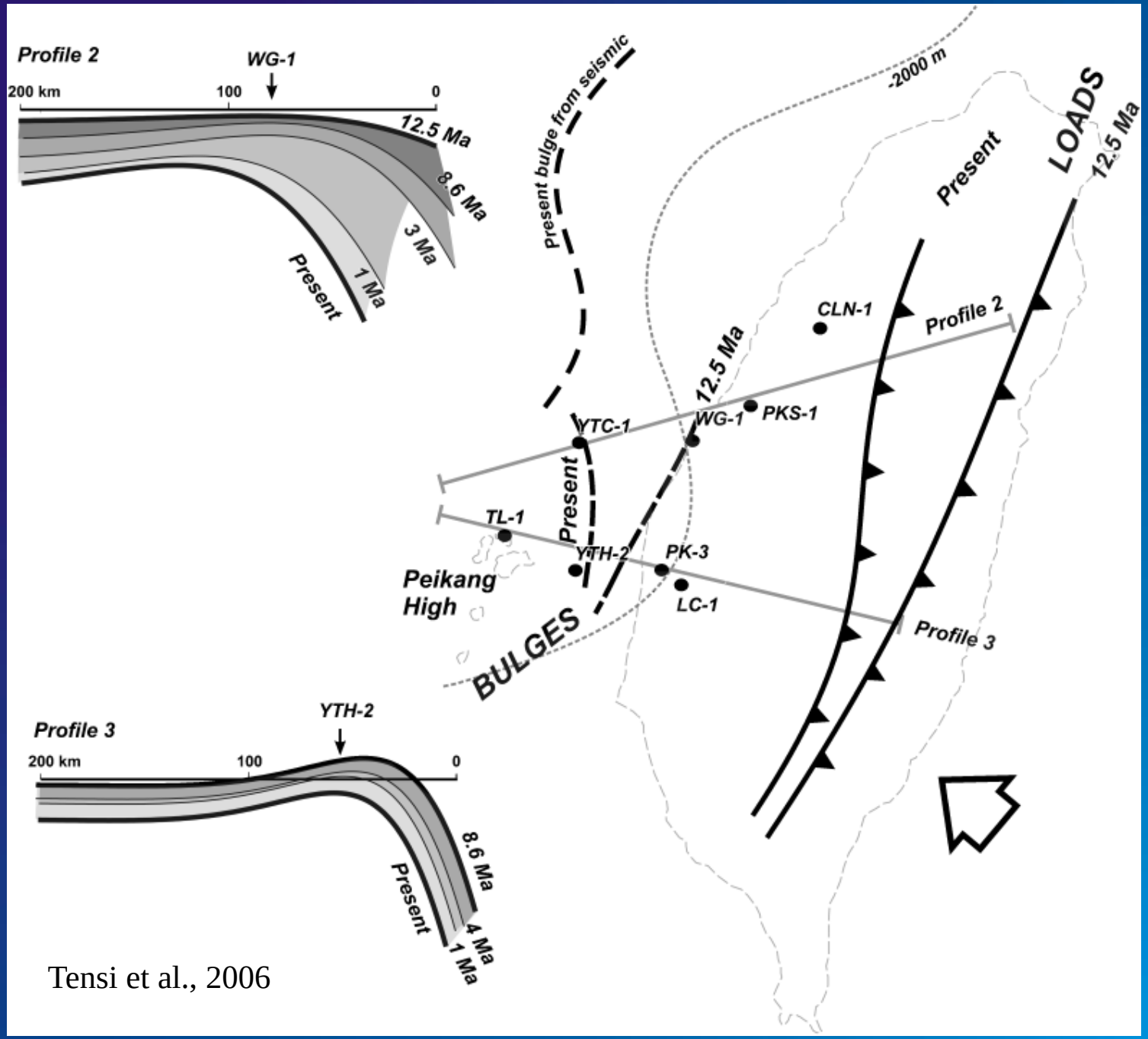

Tensi et al., 2006

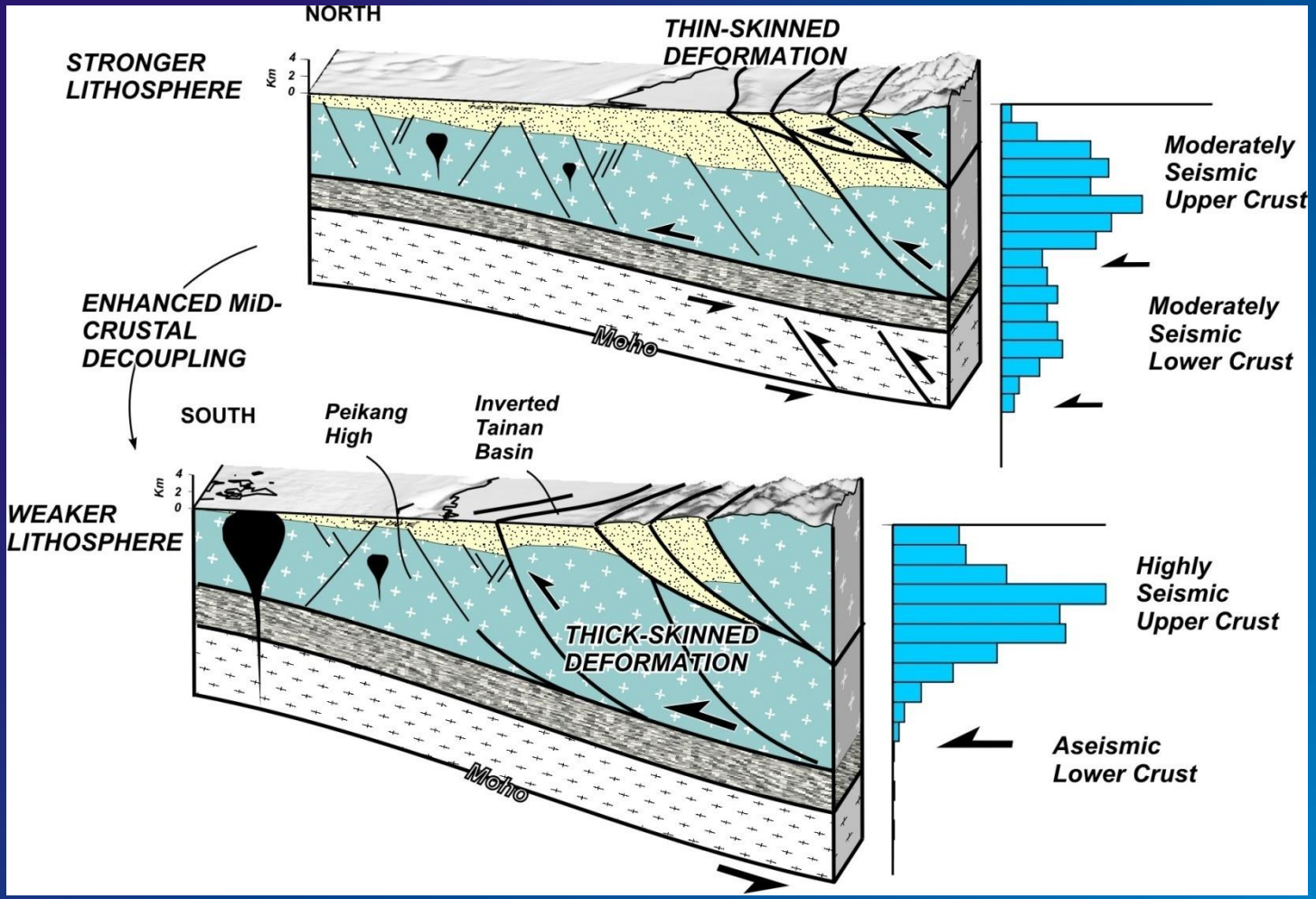

The degree of basement involvement *vs* thin-skinned deformation increases as the lithosphere weakens (rheology of the lower crust)

(Mouthereau and Petit, 2003)

Taiwan : no longer an example of thin-skinned accretionary wedge ?

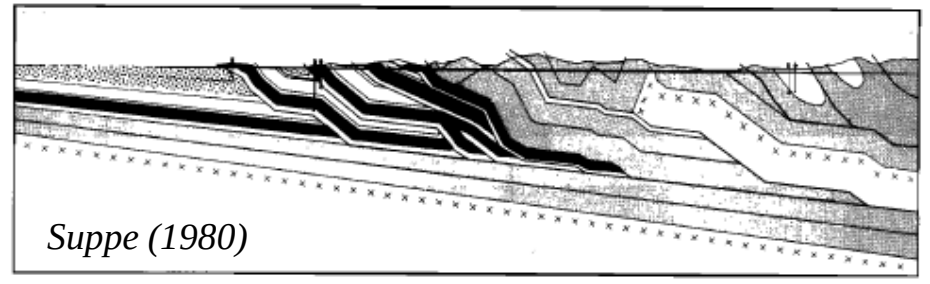

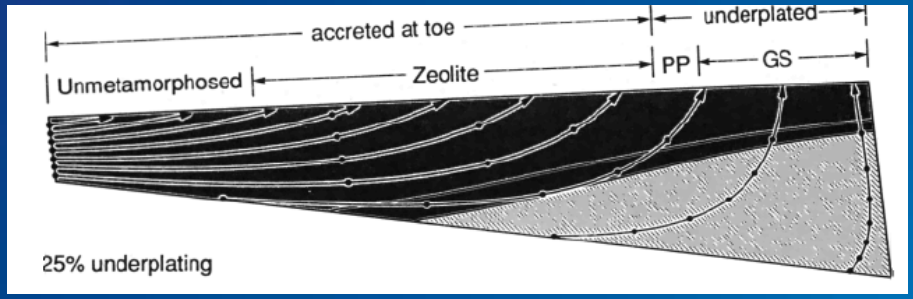

25% underplating (*Barr et al., 1991*)

50% underplating (*Fuller et al., 2006*)

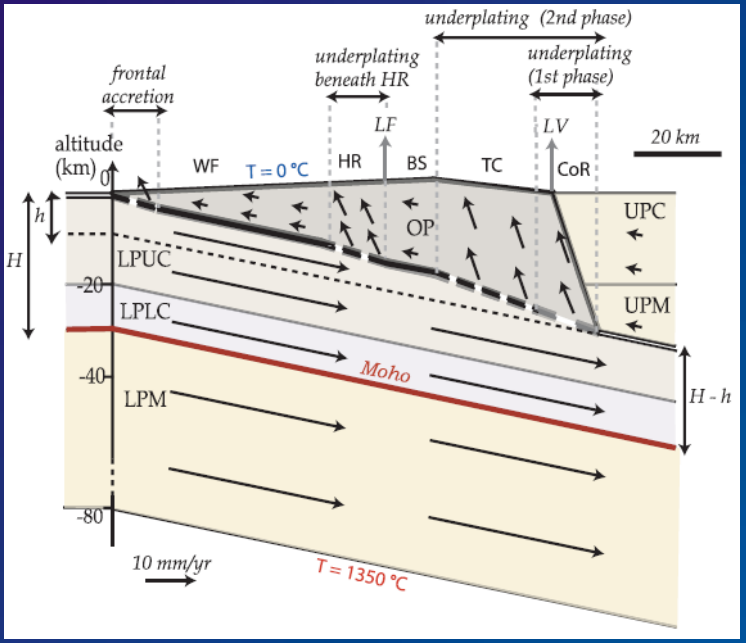

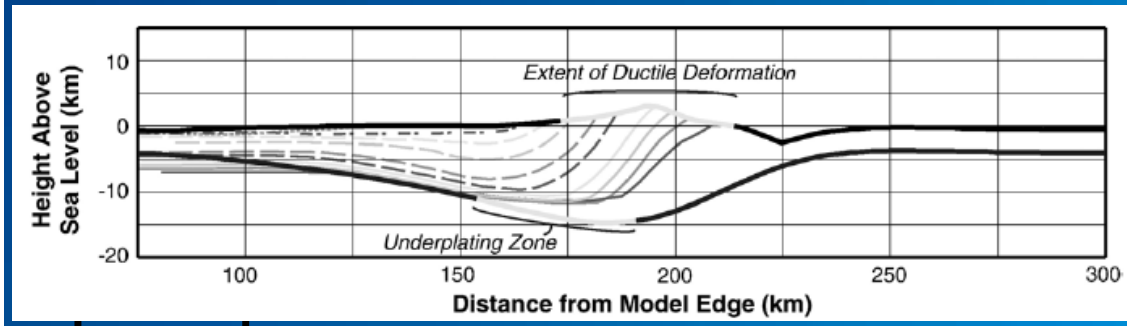

90% underplating since 1.5 Ma
(*Simoes et al., 2007*)

Two end-member models explain exhumation in the Taiwan Central Range

1. **Subduction of EUR crust**

Burial of Eurasian rocks followed by underplating/exhumation below a shallow continental wedge

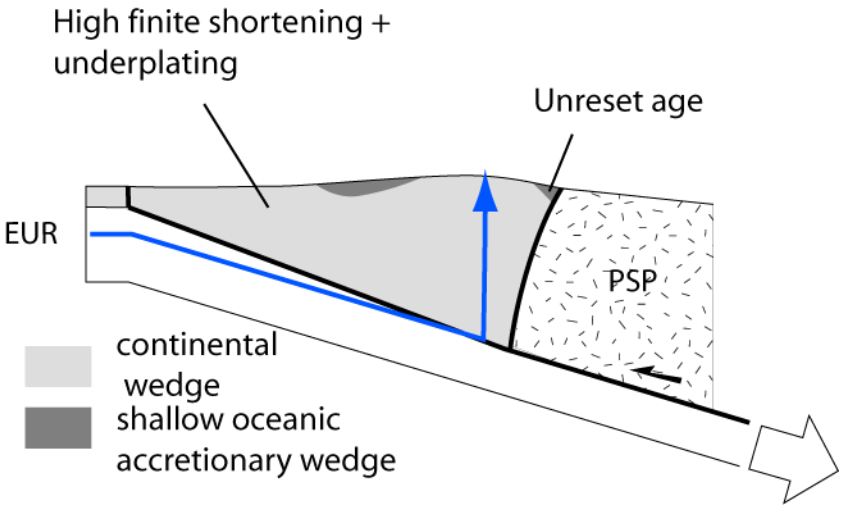

2. **Collision of EUR crust**

Little burial of Eurasian rocks
in a thick collision wedge that exhumes deep structural levels in a dome-like manner

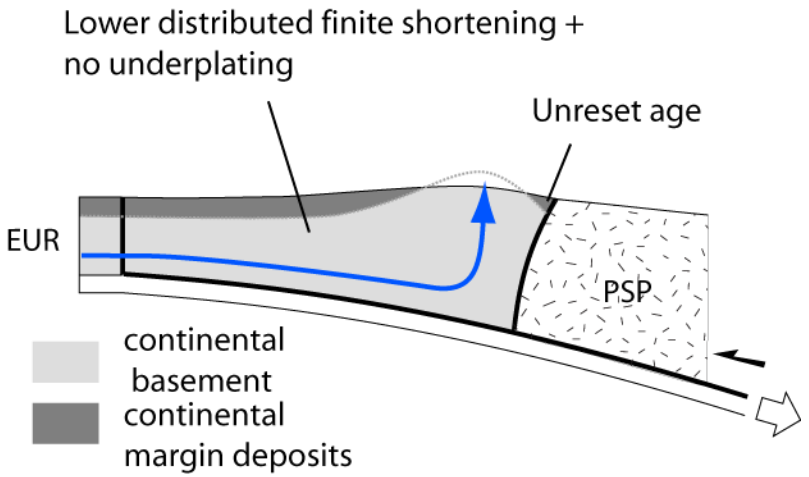

Taiwan : inverted Tertiary rifted margin
Shortening : ~35 %

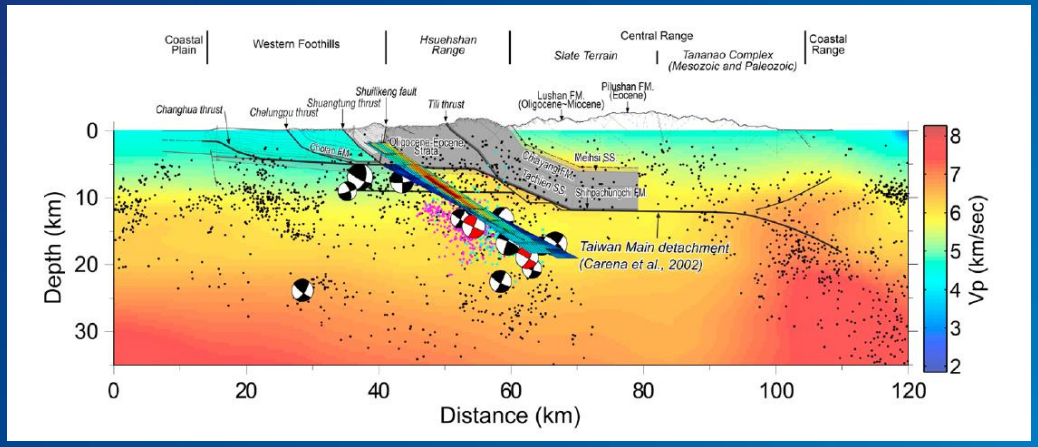

Convergence 80 km/Ma
Erosion rate 6-8 km/Ma

Thick-skinned tectonic style
"pure-shear"

Decoupling within middle-lower crust
h ~ 20 km

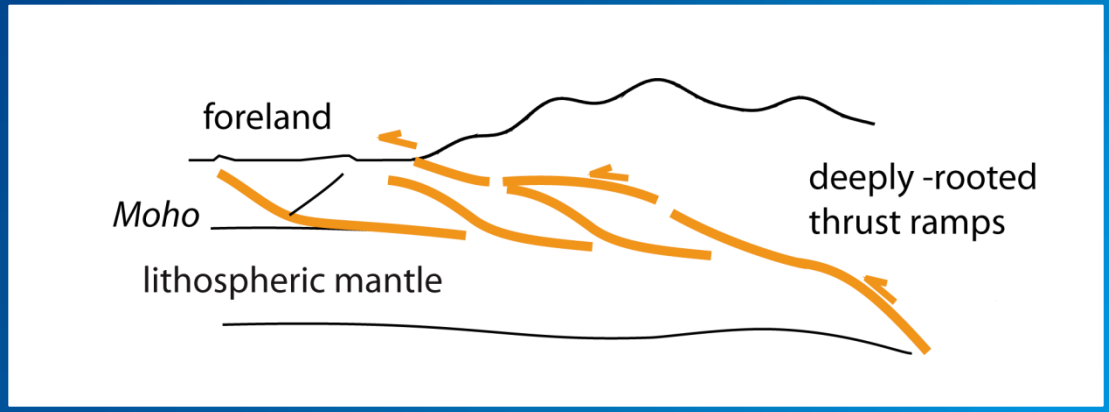

Some first-order controlling factors of the structure of fold-and-thrust belts

Deformation in orogens

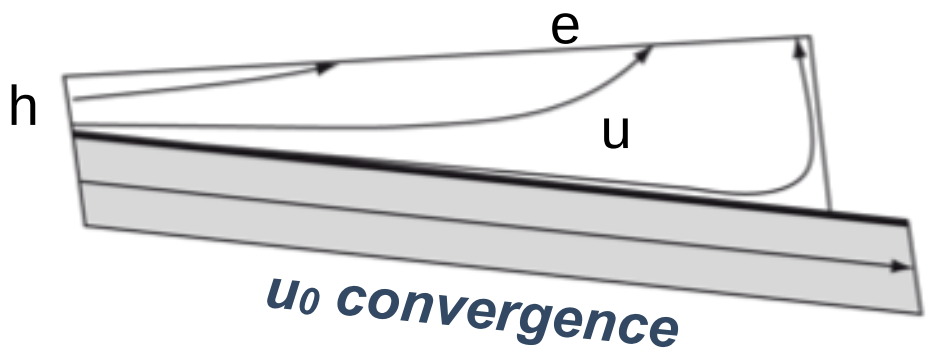

Displacement

Erosion

$$u(x,z) = \frac{1}{h(x)} \int_0^x \varepsilon(x)\,dx$$

Accreted thickness

h(x) ⇨ inheritance

Shortening (%)

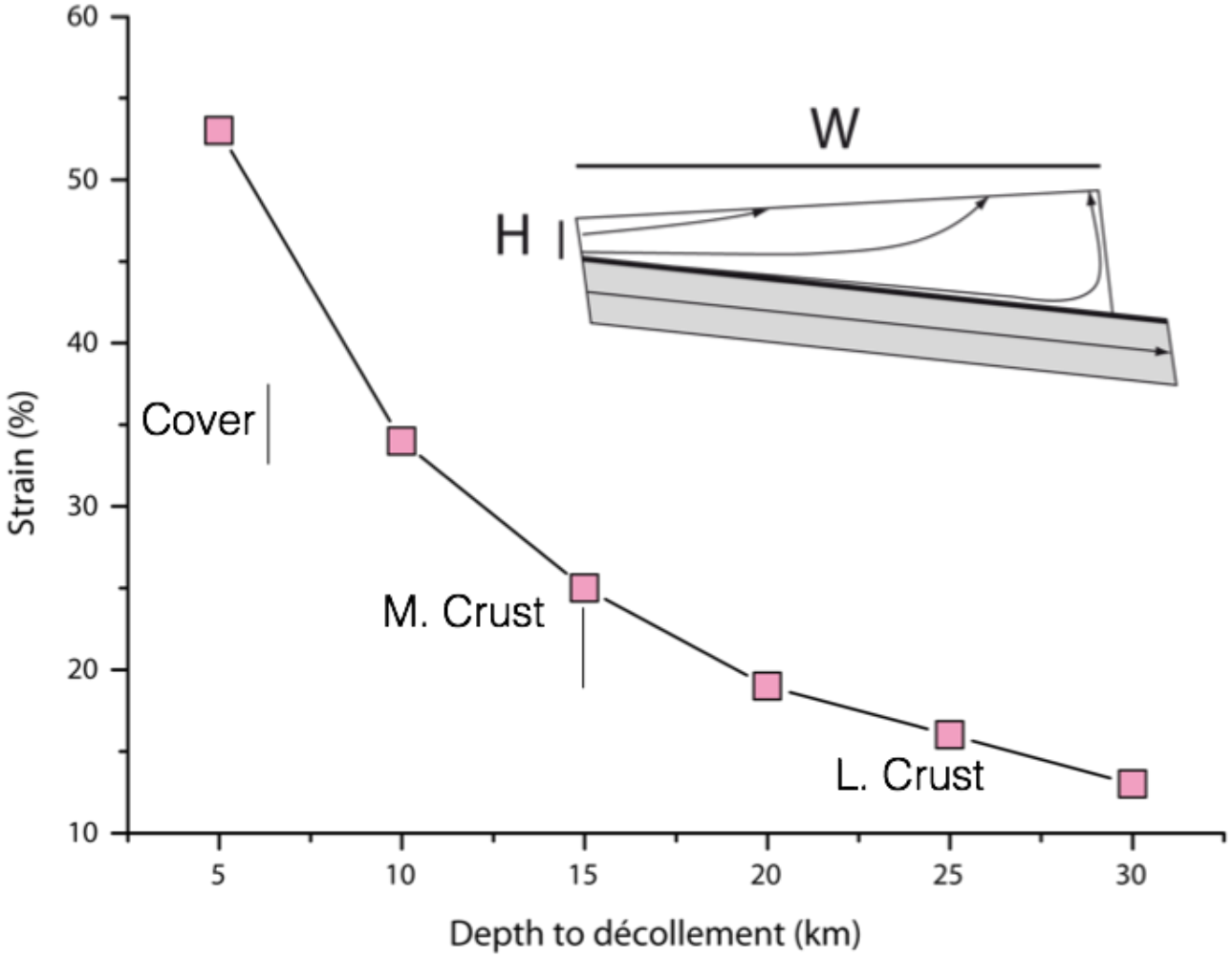

Shortening
→ DL/L (%)

Linear erosion
0 →5.5 km/Myr

Convergence =
4.6 km/Myr

Décollement → 3°

Taiwan : inverted Tertiary rifted margin

Shortening : ~35 %

Convergence 80 km/Ma
Erosion rate 6-8 km/Ma

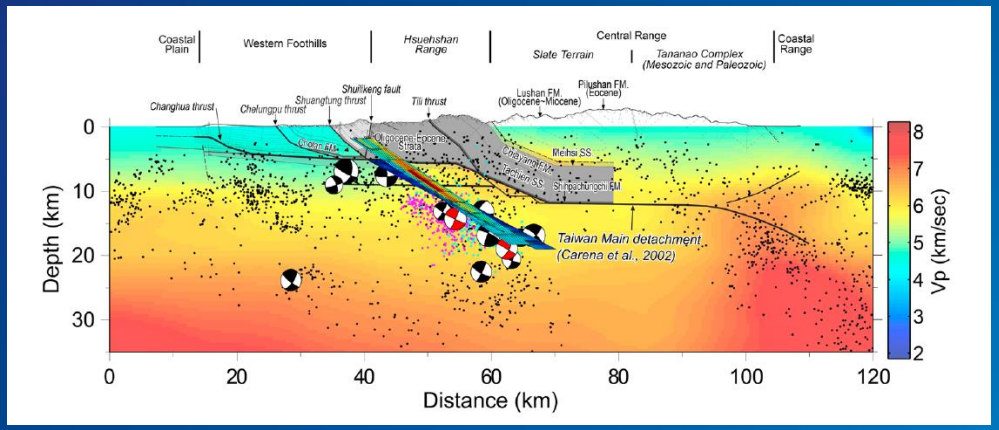

Chuang et al. (2013)

thick-skinned tectonics style
"pure-shear"

Decoupling within middle-lower crust
h ~ 20 km

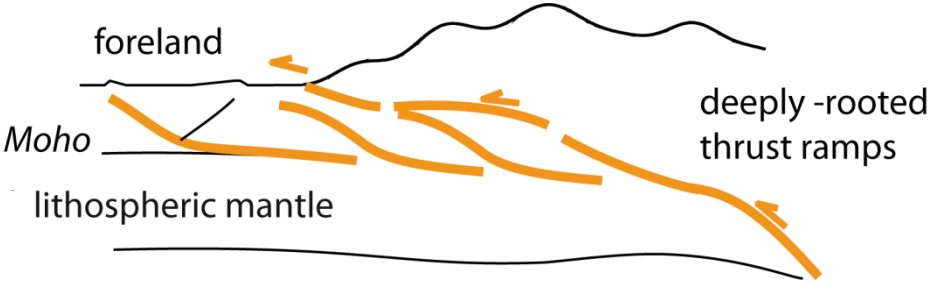

Zagros : inverted Mesozoic rifted margin

Shortening : ~37 %

Convergence 7km/Ma
Erosion rate <2 km/Ma

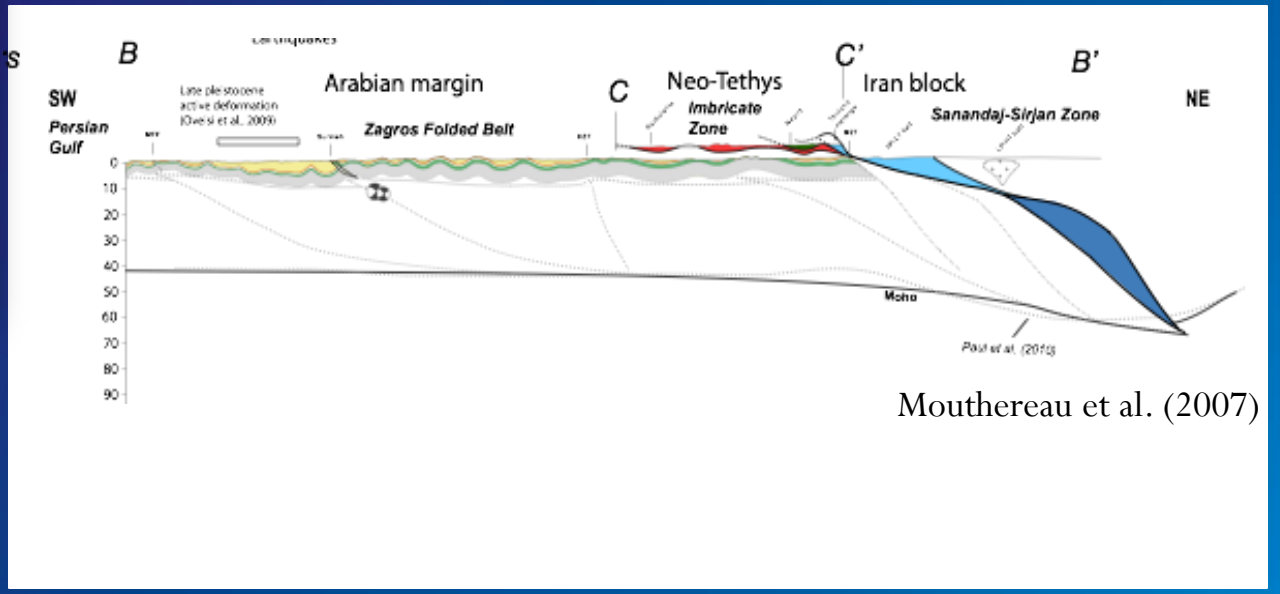

Mouthereau et al. (2007)

Thick-skinned tectonic style
"pure-shear"

Decoupling within middle-lower crust
h ~ 15-20 km

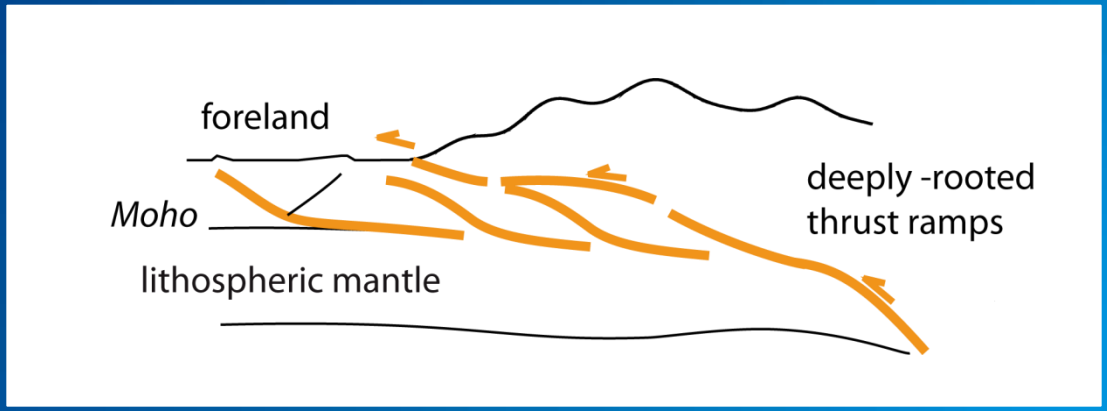

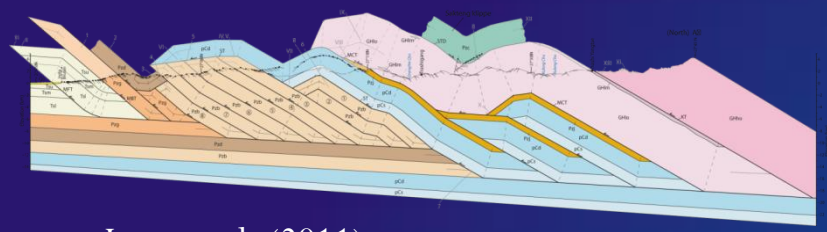

Long et al. (2011)

Himalaya : « underthrusting of a paleo-proterozoic craton

Shortening : ~ 70 %

Convergence 50 km/Ma
Erosion rate3-5 km/Ma

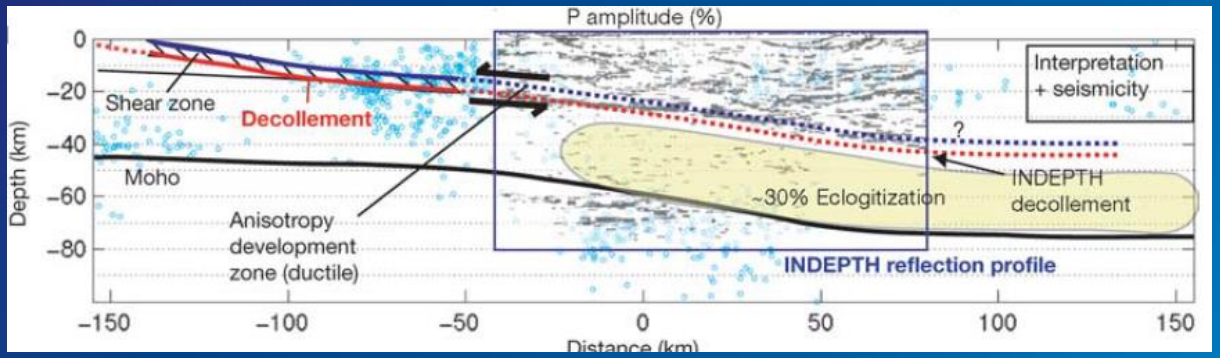

Schulte-Pelkum et al. (2005)

Thin-skinned tectonics style
"simple shear"

Décollement
h <10 km

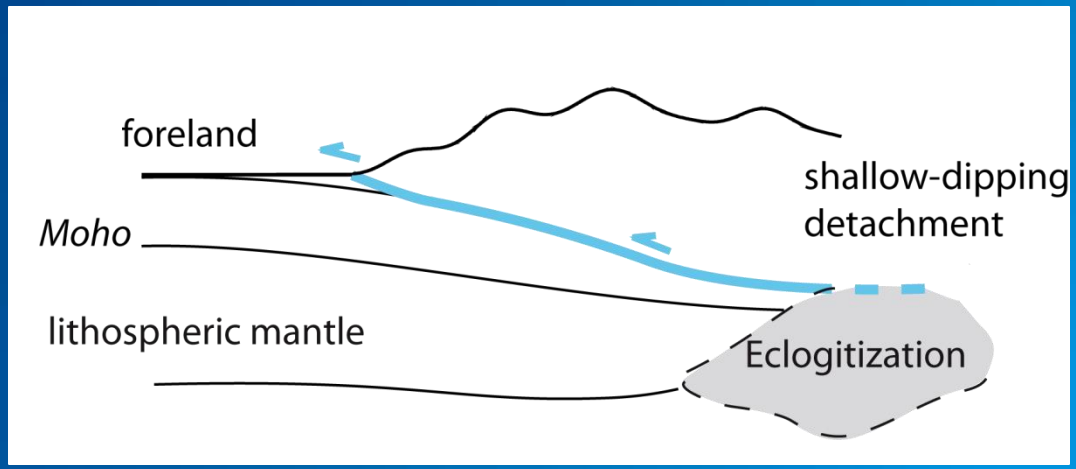

Two main modes of accretion - why?

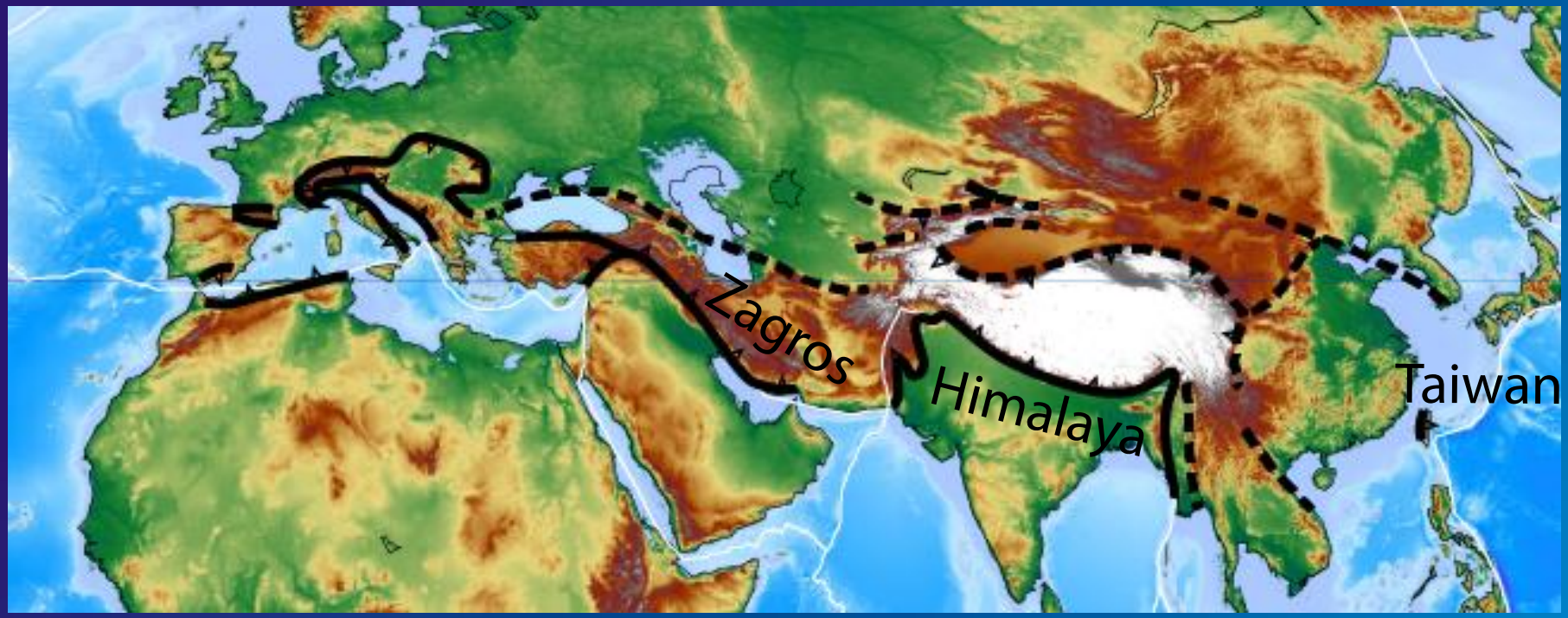

h < 10 km

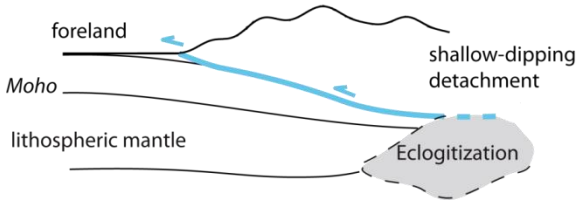

h > 15-20 km

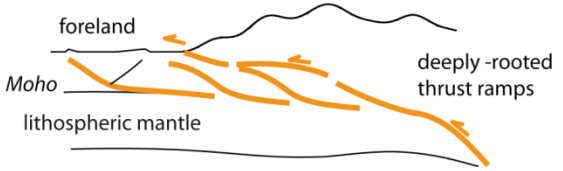

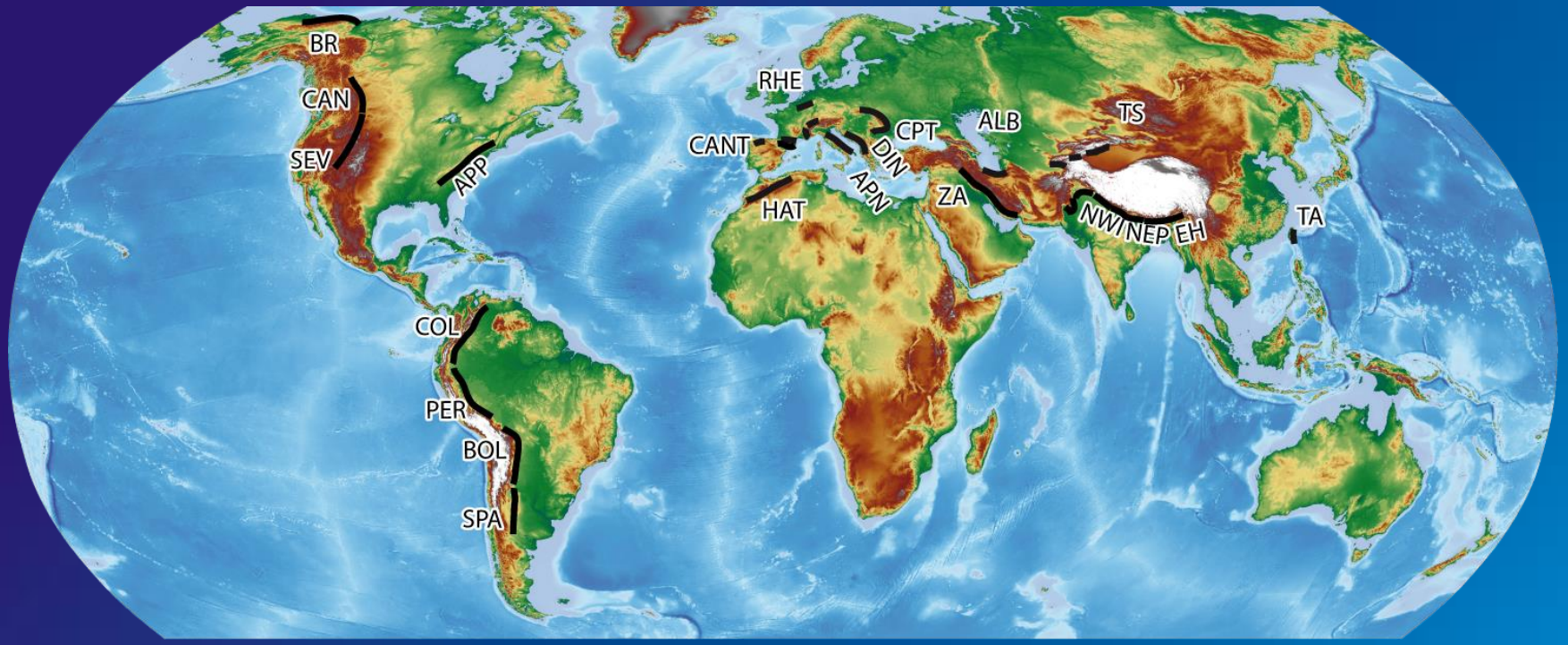

Estimates of shortening in 30 fold-and-thrust belts worldwide

Courtesy of F. Mouthereau

Shortening /structure

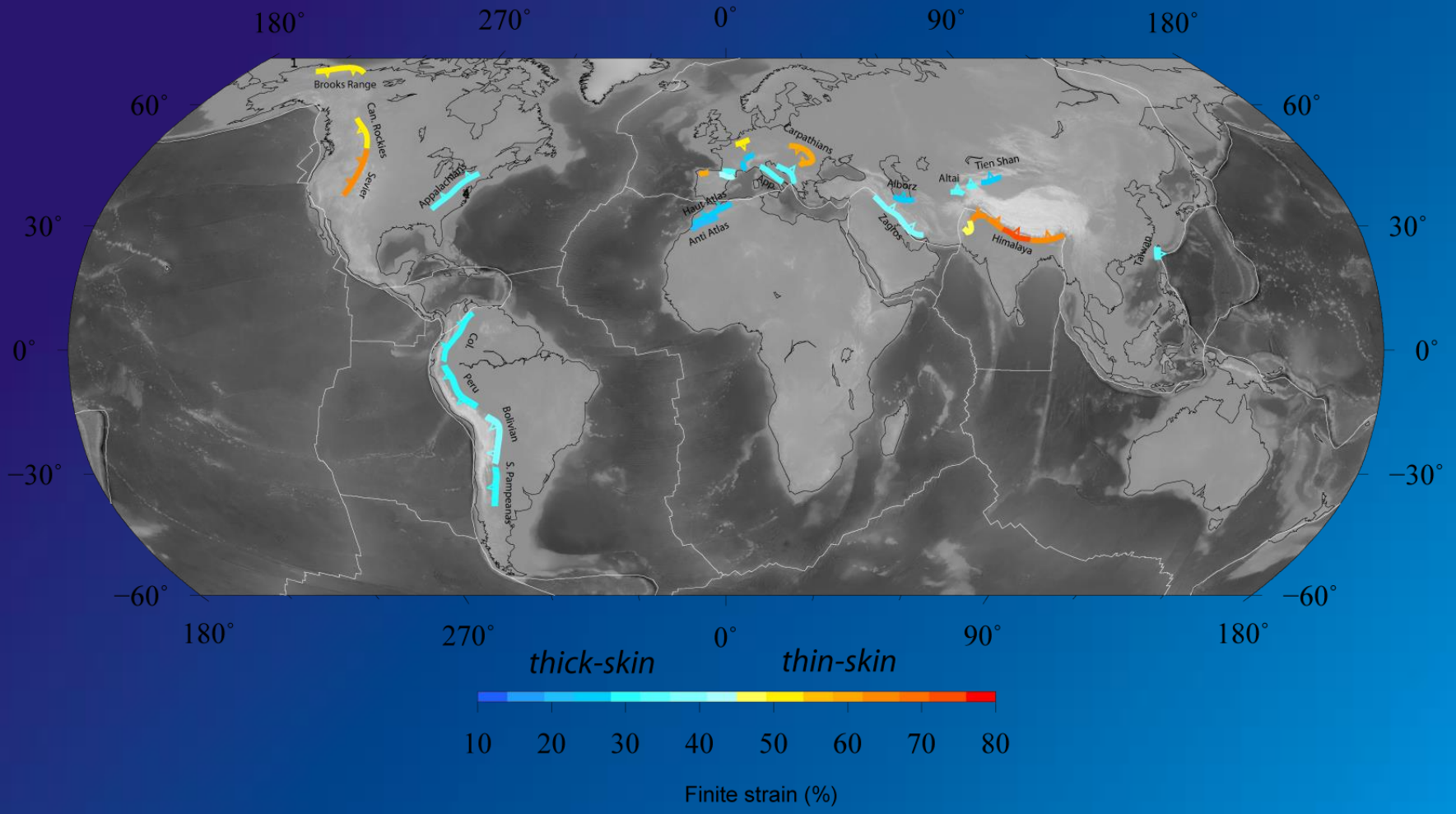

Thin-skinned ~40-75%
Thick-skinned ~20-40%

Long-term strength of continents

(18,633 Te values)

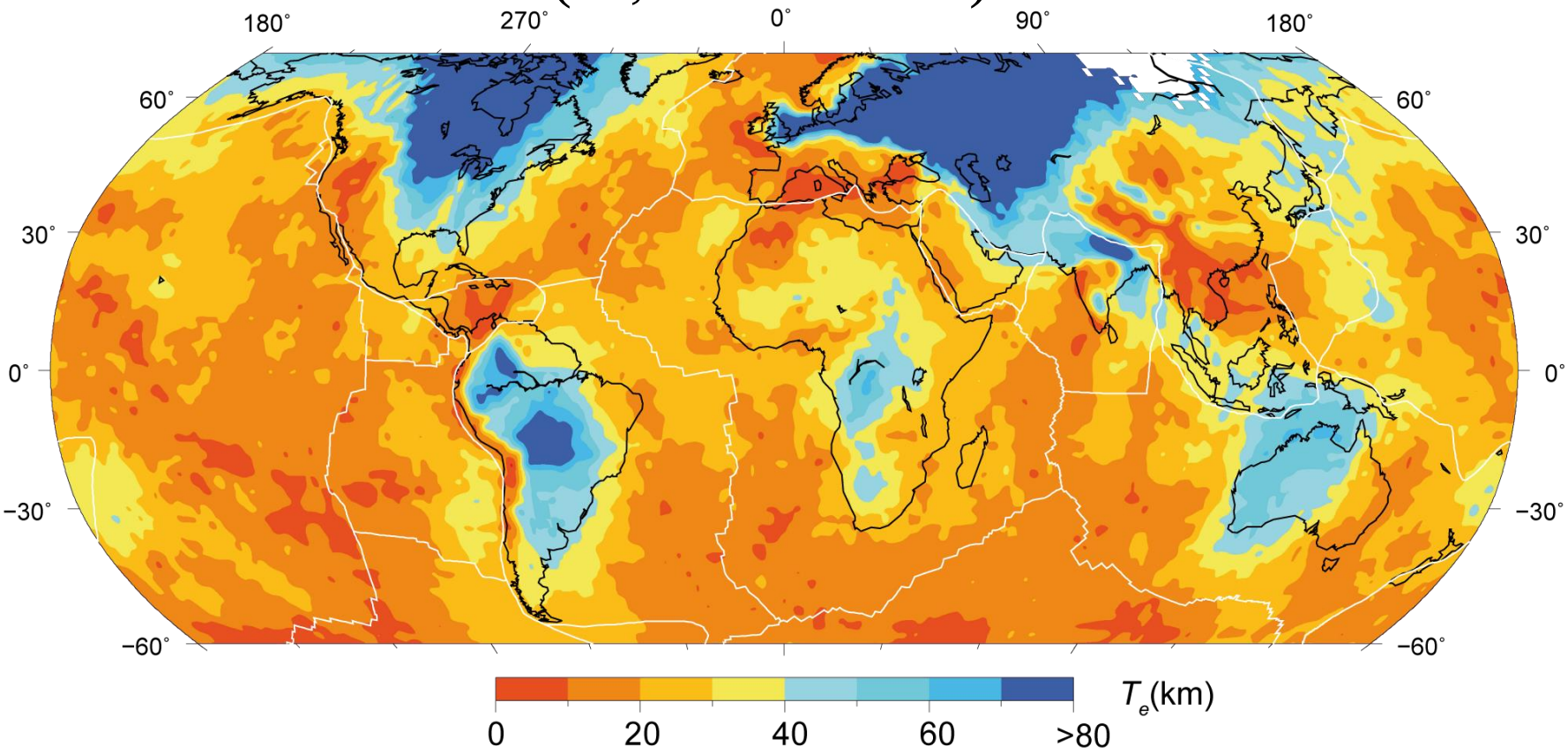

Gravimetry + flexure analysis

Mouthereau et al. (2013)

Thermotectonic age of continents
= age of the last tectono-magmatic event

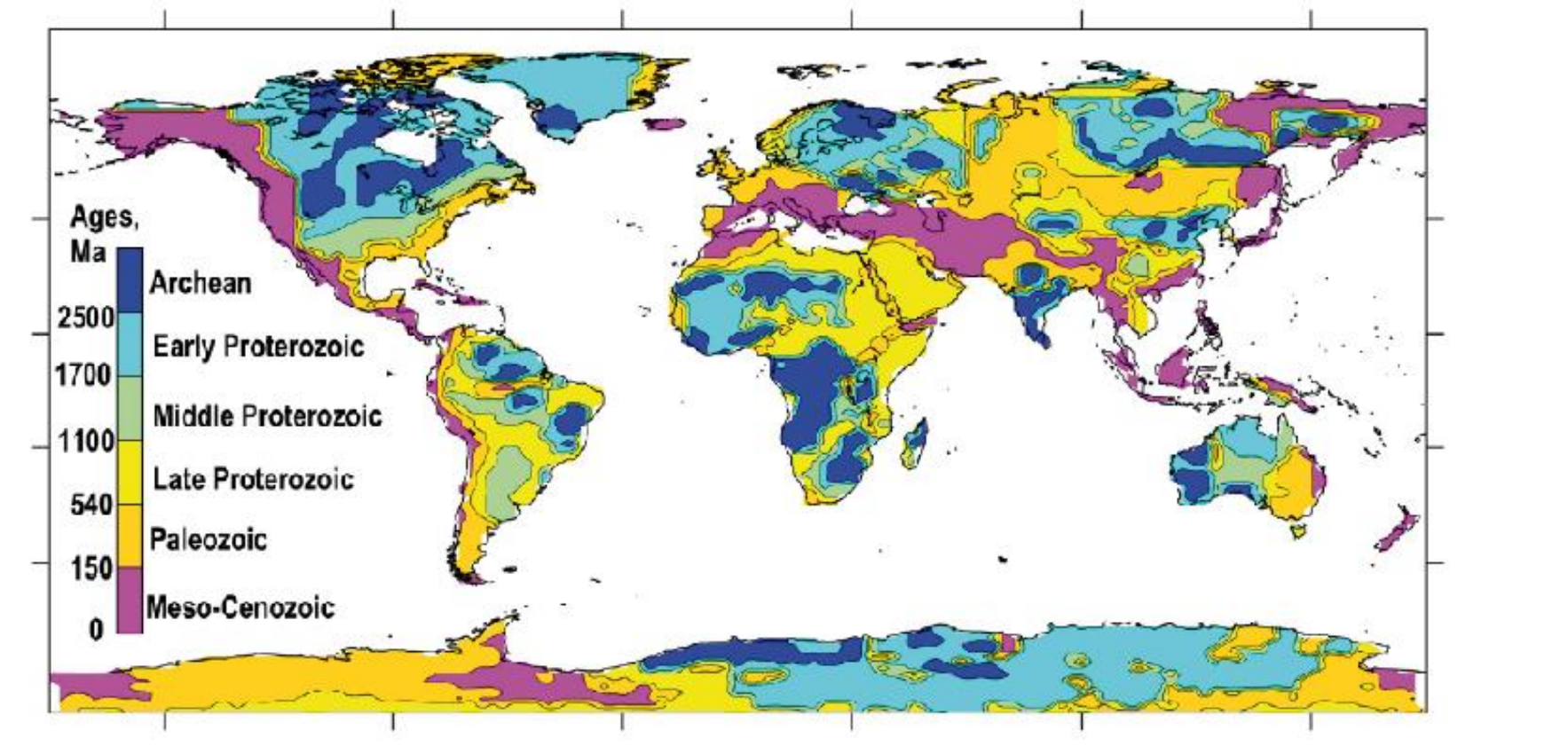

Artemieva (2006)

Mouthereau et al. (2013)

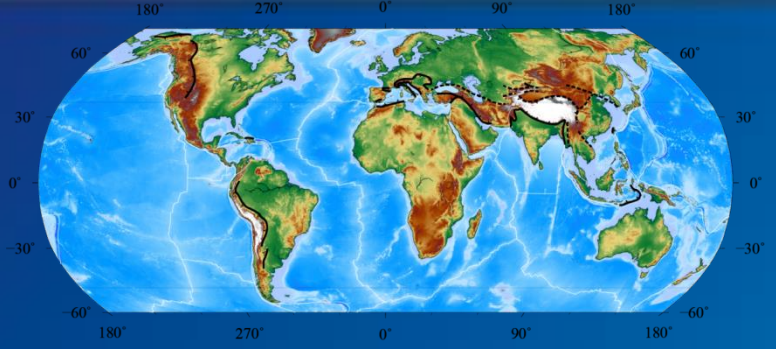

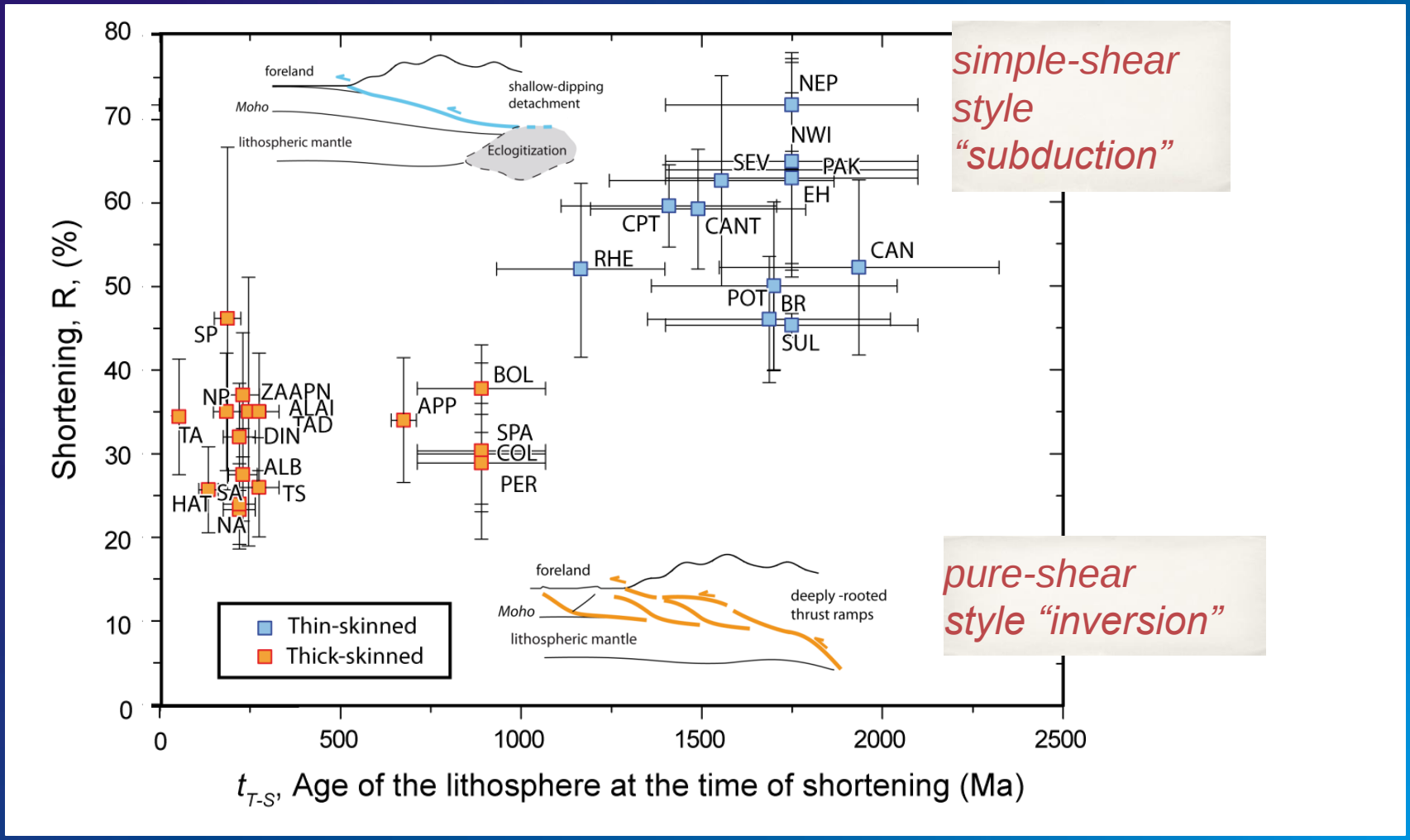

Young phanerozoic lithosphere
age = 50 Ma

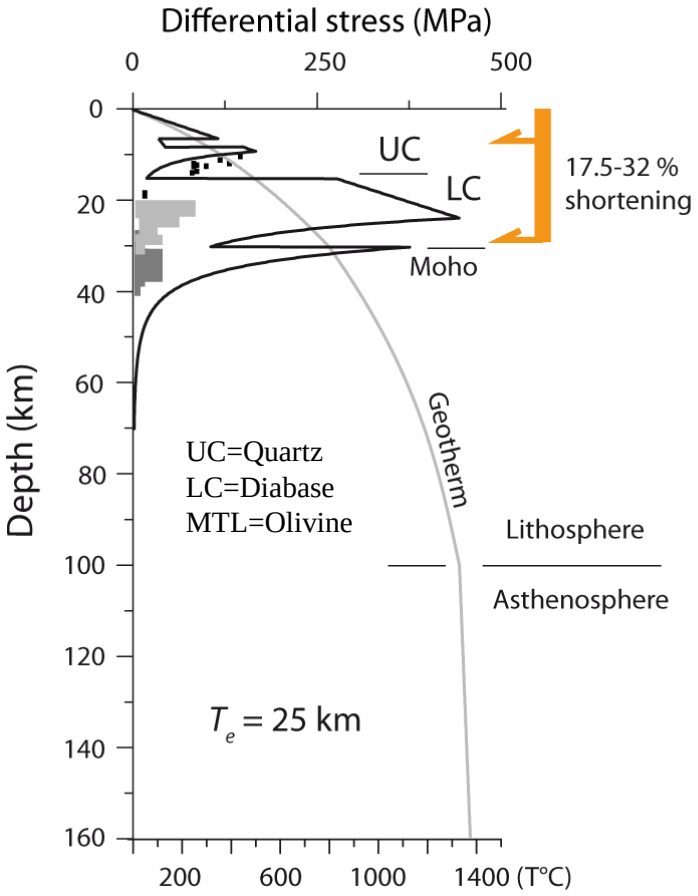

Shortening vs depth to décollement

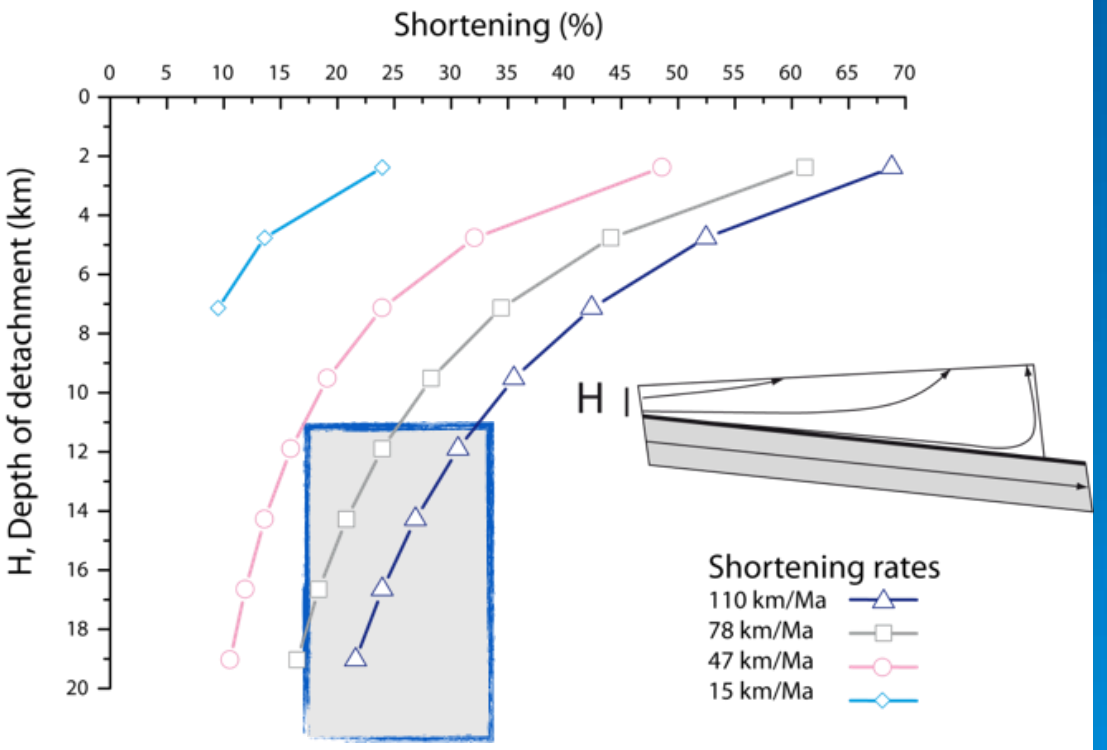

17.5-32 %

Young lithosphere

Mouthereau et al. (2013)

Cratonized lithosphere
age = 1 Ga

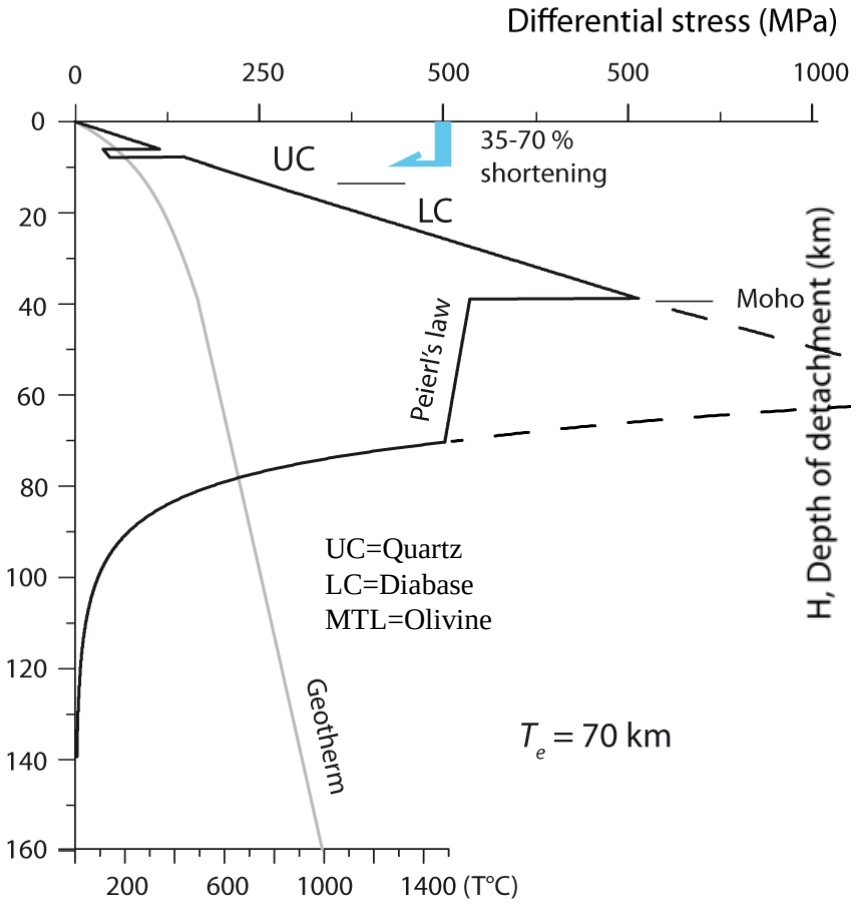

Shortening vs depth to décollement

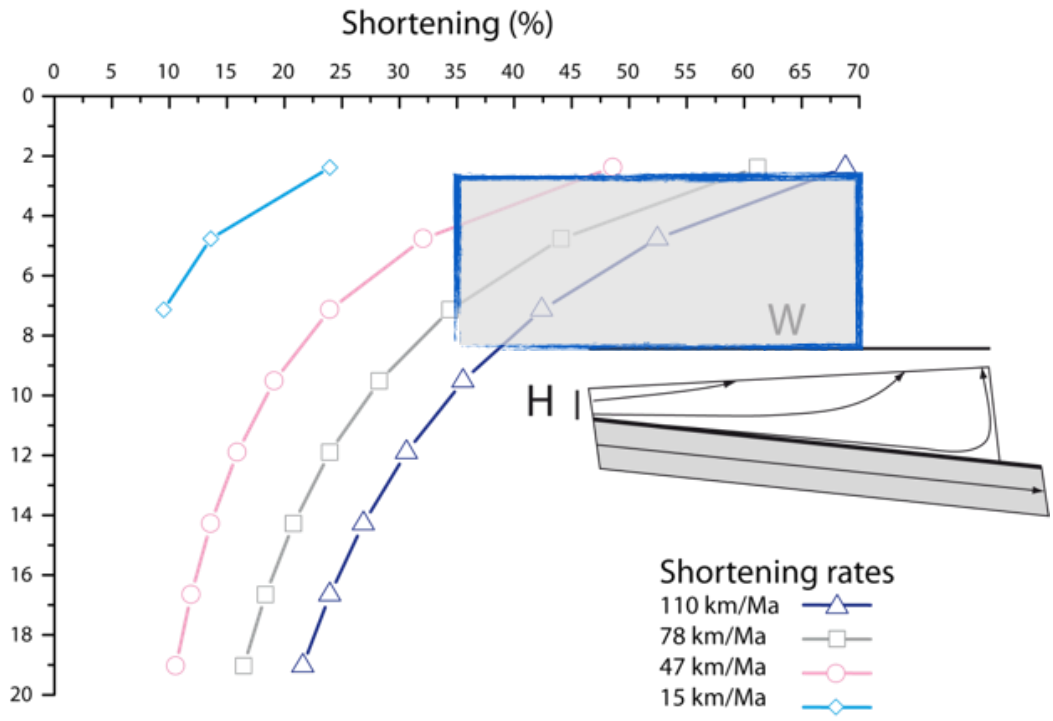

35-70%

Old lithosphere

Mouthereau et al. (2013)

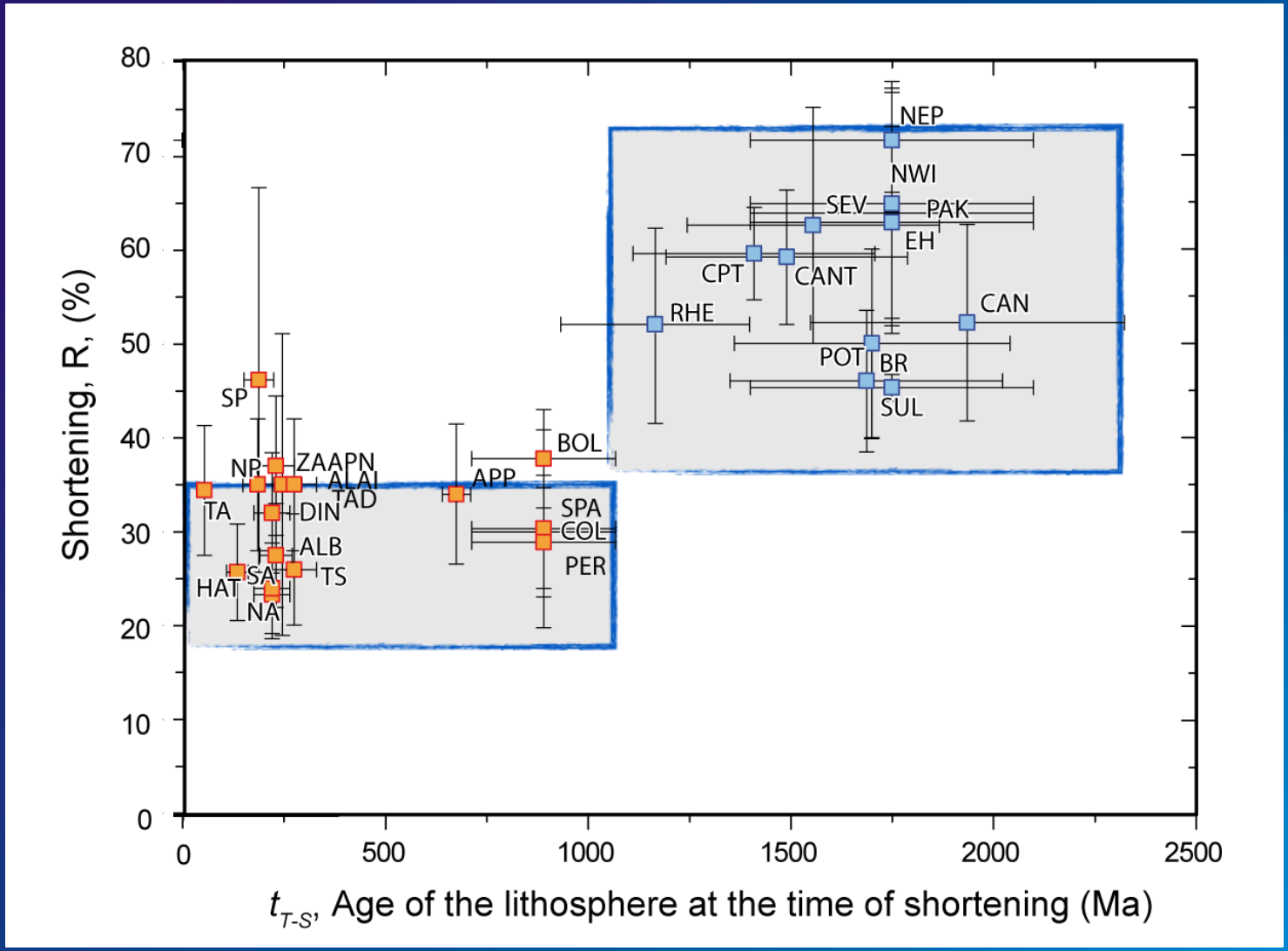
Shortening, R, (%)
$t_{T\text{-}S}$, Age of the lithosphere at the time of shortening (Ma)
0
10
20
30
40
50
60
70
80
0
500
1000
1500
2000
2500
NEP
NWI
SEV
PAK
EH
CPT
CANT
RHE
CAN
POT
BR
SUL
SP
NP
ZAAPN
ALAI
TAD
TA
DIN
ALB
SA
TS
HAT
NA
BOL
APP
SPA
COL
PER

Control by mantle strength ?

Thermal inheritance + *Mantle composition = f(age)*

Young margin

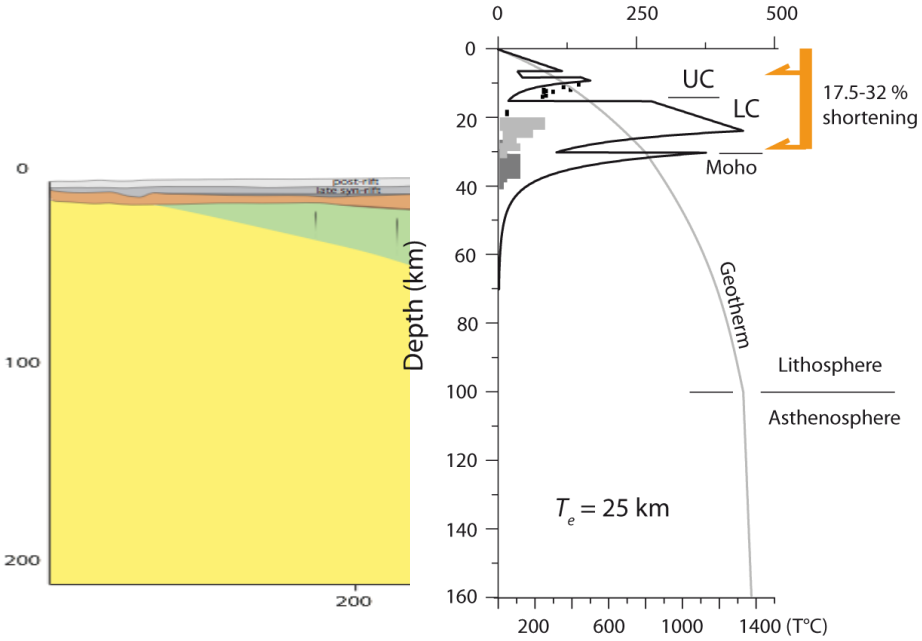

Old lithosphere

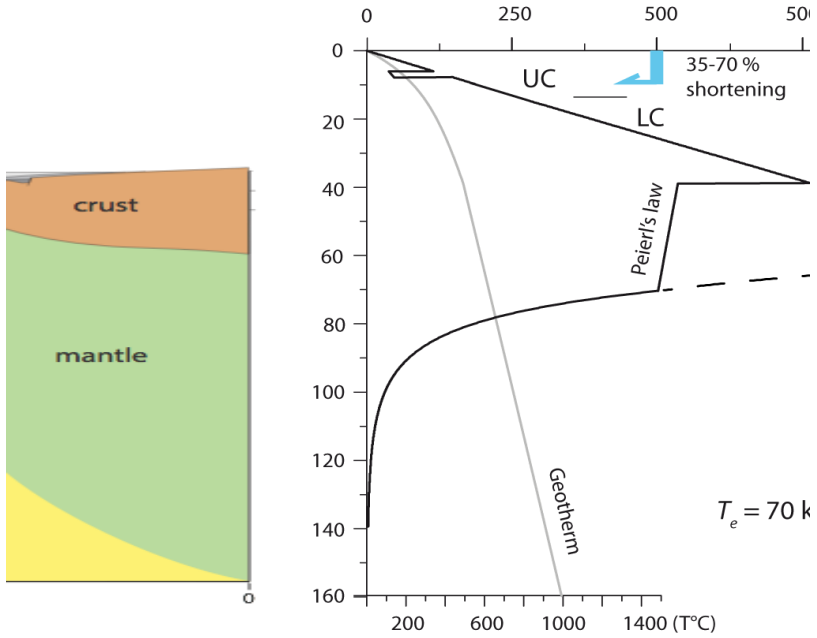

"Inversion" : Taiwan, Zagros

"Subduction" : Himalaya

Thank you
for your attention…

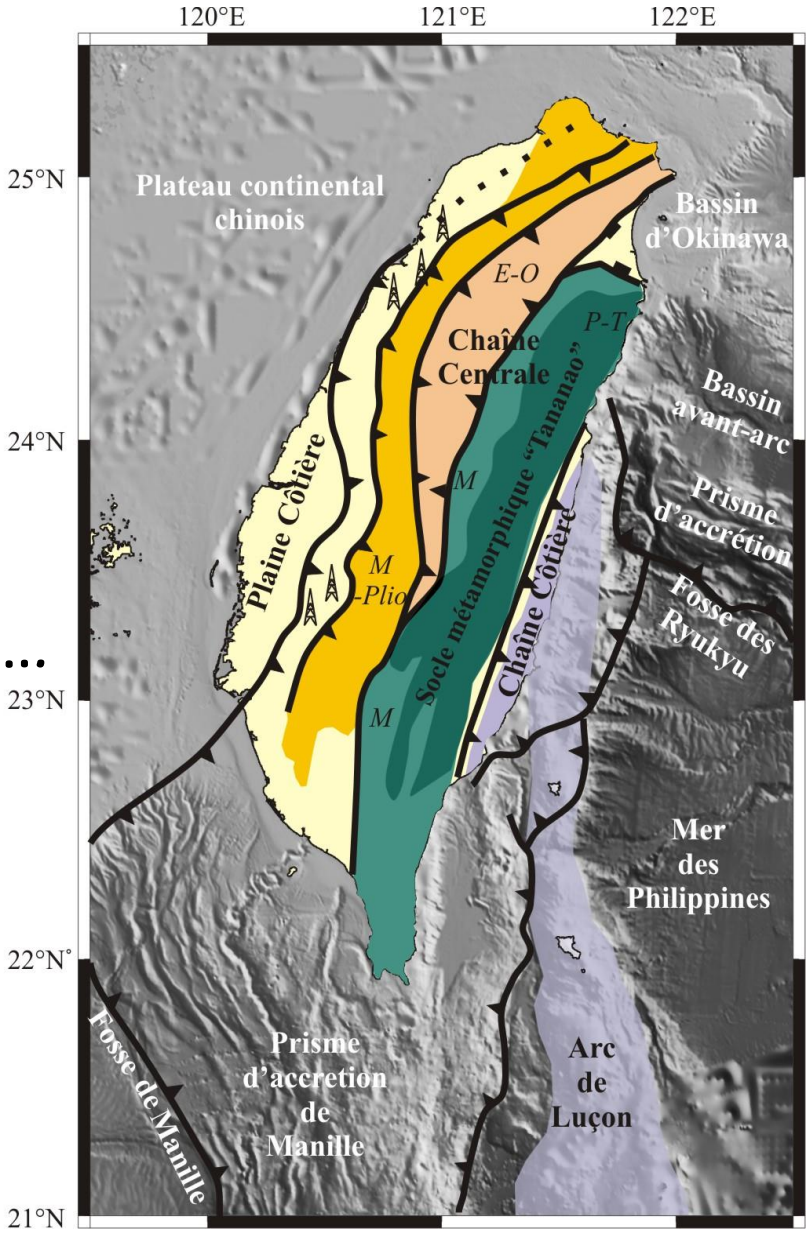

Suggested readings :

Lacombe O. & Mouthereau F., 2002. Basement-involved shortening and deep detachment tectonics in forelands of orogens : insights from recent collision belts (Taiwan, western Alps, Pyrenees). ***Tectonics****, 21, 4, 1030*

Mouthereau F. & Lacombe O., 2006, Inversion of the Paleogene Chinese continental margin and thick-skinned deformation in the western foreland of Taiwan, ***J. Struct. Geol.****, 28, 1977-1993*

Mouthereau F., Deffontaines B., Lacombe O. & Angelier J., 2002. Variations along the strike of the Taiwan thrust belt : Basement control on structural style, wedge geometry and kinematics. In Byrne T.B., and Liu C.-S., eds, Geology and Geophysics of an Arc-Continent Collision, Taiwan, Republic of China, Boulder, Colorado, ***Geol. Soc. Am. Spec. Pap.****, 358, chapter 3, 35-58*

Mouthereau, F.,Watts, A.B., & Burov, E., 2013. Structure of orogenic belts controlled by lithosphere age. ***Nature Geosciences****, 6 (9), 785-789*